AD-A169 165 JOINT SYMPOSIUM ON COMPATIBILITY OF PLASTICS/MATERIALS WITH EXPLOSIVES PR..(U) AMERICAN DEFENSE PREPAREDNESS ASSOCIATION ARLINGTON VA L R BARTRON ET AL. MAY 79 1/4

UNCLASSIFIED F/G 19/1 NL

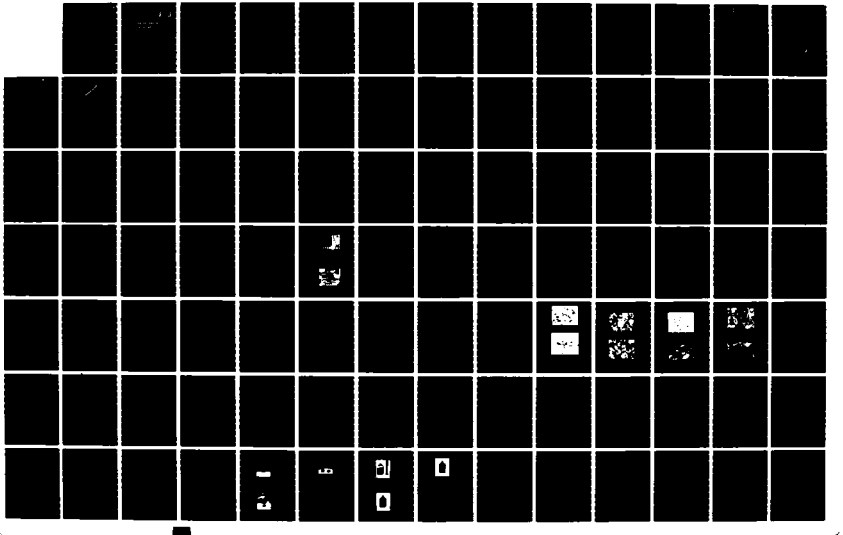

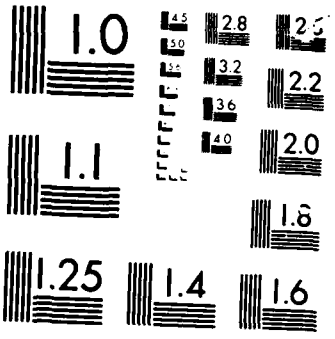
1.0
1.1
1.25
1.4
1.6
1.8
2.0
2.2
2.8
3.2
3.6
4.0
4.5
5.0

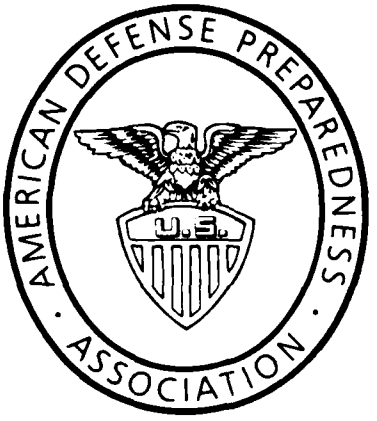

MEETING REPORT
JOINT SYMPOSIUM

COMPATIBILITY OF PLASTICS/MATERIALS WITH EXPLOSIVES PROCESSING EXPLOSIVES

May 15-17, 1979

Sandia Laboratories
Albuquerque, New Mexico

AMERICAN DEFENSE PREPAREDNESS ASSOCIATION
NATIONAL HEADQUARTERS:
Union Trust Building, Washington, D.C. 20005

PAPERS PRESENTED

at the

JOINT SYMPOSIUM

Entitled

COMPATIBILITY OF PLASTICS/MATERIALS WITH EXPLOSIVES

PROCESSING EXPLOSIVES

Sponsored by

MATERIALS & PROCESSES DIVISION

AMERICAN DEFENSE PREPAREDNESS ASSOCIATION

at

SANDIA LABORATORIES

Albuquerque, New Mexico

15-17 May 1979

Compiled by

Lester R. Bartron
Carlton L. Horine
Herman R. Leider

TABLE OF CONTENTS

Preface

The ADPA symposia respond to the need to bring together specialists from DOD research centers and industry in a forum to provide a thorough exchange of information on the current state of the art and of ideas that will advance the state of the art.

We anticipate that broadening the subjects covered from compatibility of plastics and other materials with explosives, propellants, and pyrotechnics to include the processing of explosives, propellants, and ingrediants will enlarge the forum to provide new insights and expand the scope of ideas.

We are most appreciative of the Sandia Laboratories' willingness to host this joint meeting of the Chemical and Plastics Materials Section of the Materials and Processes Division and the Propellants and Explosives Section of the Ammunition Technology Division. The cross-fertilization of ideas should stimulate all of us.

The success of a technical meeting is dependent on many things. Of utmost importance is the authors' willingness to pu' lish and present their work. Without such authors there could be no symposium. Additional required ingredients are (1) a willing and capable host, (2) a hard-working program committee, and (3) dedicated session chairmen. We are most appreciative of their efforts.

Lester R. Bartron
E. I. du Pont de Nemours & Co.
May ~~15, 1979~~

Symposium Committee

Chairman - Lester R. Bartron, E. I. du Pont de Nemours & Co.

Program Co-Chairman - Herman Leider, Lawrence Livermore Laboratory

Program Co-Chairman - Carlton Horine, United Technologies

Facilities Chairman - Thomas M. Massis, Sandia Laboratories

Publicity Chairman - Nicholas E. Berkholtz, Honeywell, Inc.

Government Laboratory Liaison - Harry Pebly, ARRADCOM

Industrial Laboratory Liaison - C. A. Zimmerman, Lockheed Missile and Space Company

Foreign Liaison - Geoffrey Hooper, British Embassy

ADPA Liaison - Lt. Col. Rudolph F. Rose, Jr., USAF (Ret.)

Advisor - Frank D. Swanson, Honeywell, Inc.

TATB DEVELOPMENT

by

T. M. Massis
Sandia Laboratories

Paper not available at time of printing.

A NEW TATB PLASTIC-BONDED EXPLOSIVE

James R. Humphrey and Harry F. Rizzo
Lawrence Livermore Laboratory, L-324, P. O. Box 808, Livermore, CA 94550

ABSTRACT

We describe a binder for use with the remarkably insensitive high explosive TATB that displays enhanced engineering properties for the compacted plastic-bonded explosive (PBX). The binder in the original TATB formulation was Kel-F 800; although this binder may be used to produce high density, mechanically stable billets of TATB that can be machined, repeated thermal cycling between -54 and 74°C causes permanent volume expansion (growth) of 1.5-2.0%. The debonding of binder from explosive that occurs during such growth reduces the mechanical strength of the material. It is shown that TATB also undergoes a secondary mechanical relaxation at about 30°C that coincides with an increase in the coefficient of thermal expansion (CTE) to a higher value than that measured at lower temperatures. Our new linear epoxy-type binder essentially eliminates growth, maintains strength after thermal cycling, suppresses the secondary mechanical relaxation, and lowers the CTE between ambient temperature and 74°C by about 25%.

INTRODUCTION

The remarkably good safety characteristics (ref. 1) of TATB [1,3,5-triamino-2,4,6-trinitrobenzene], are revolutionizing the design and deployment of nuclear weapons. The Department of Energy (DOE) is using TATB at a rapidly increasing rate, and the Department of Defense (DOD) has proposed its use on a much larger scale, particularly for highly specialized applications such as in the U.S. Air Force Hard Structure Munition (HSM).

Although commercial TATB contains 0.5-1.0 wt% of byproduct NH_4Cl trapped within the TATB crystals, several high-temperature tests (120°C), chemical-compatibility tests (ref.2), and long-term aging tests (32 mo at 100°C) (ref. 3) demonstrated that this impurity does not affect the properties or use of TATB. Commercial production of TATB for DOE has kept pace with increasing requirements.

Both Lawrence Livermore Laboratory (LLL) and Los Alamos Scientific Laboratory (LASL) use Kel-F 800 as a binder for TATB to produce plastic-bonded high explosives

(PBX). These high-density, mechanically stable billets can be machined into the required shapes. Unfortunately, all TATB/Kel-F 800 PBX formulations undergo a permanent and irreversible volume expansion (growth) when thermally cycled between -54 and 74°C.

Our objectives for developing a new TATB PBX were to eliminate growth during thermal cycling, improve the mechanical properties, and reduce the overall CTE. We therefore selected a binder with a glass transition point (T_g) greater than 74°C (the maximum expected temperature of the military stockpile) but low enough that the PBX could be formed in our conventional presses, which are currently limited to 120°C.

During thermal cycling, TATB crystals expand in an anisotropic fashion (ref. 4); the CTE values for unit cell axes of TATB single crystals measured between -54 and 107°C are $\bar{\alpha}_a$ = 8.3 X 10^{-6}/°C, $\bar{\alpha}_b$ = 20.9 X 10^{-6}/°C, and $\bar{\alpha}_c$ = 248 X 10^{-6}/°C.

The growth that occurs in TATB/Kel-F 800 samples resembles that observed in anisotropic polycrystalline ceramics such as graphite, boron nitride, and hafnium titanate. Because TATB lacks the solid-state bonding that binds ceramic materials together, the TATB particles must be embedded in a binder. If the T_g of the binder is too low, the binder softens at higher temperatures and fails to restrict TATB particle movement. The ideal polymer binder acts as a glass throughout the entire temperature range to which the material is exposed and exhibits the same properties throughout this range.

In this report, we compare the extent of growth, mechanical properties, and CTE values of the TATB/Kel-F 800 PBX presently used (RX-03-BB) with those of our new zero-growth TATB PBX (RX-03-CK).

BINDER SELECTION

After an extensive literature search to find such a binder material for testing, we selected an aromatic diamine-cured epoxy and seven thermoplastic binders with T_g values between 80 and 105°C. Figure 1 compares the growth observed for PBX formulations containing these binders with the TATB formulation used presently at LLL (RX-03-BB, 7.5% Kel-F 800) and pure TATB (ref.5). All of the formulations contained 7.5 vol% binder.

Eponol-55 and BAKELITE Phenoxy PKHJ (Phenoxy) are linear epoxy-type binders; the PS(90)/PPO(10) and PS(80)/PPO(20) binders are 90/10 and 80/20 wt% mixtures of polystyrene/polyphenylene oxide, respectively; ABS is acrylonitrile-butadiene-styrene; and ABS(90)/PPO(10) is a 90/10 wt% mixture of ABS and PPO. The formulations containing PPO produced compatible polymer blends that were expected to show improved mechanical properties. Kraton G 1650 block copolymer was selected because it has both high and low T_g values outside the normal cycling temperature range of -54 to 74°C. This latter PBX exhibits both a high CTE and lower compressive

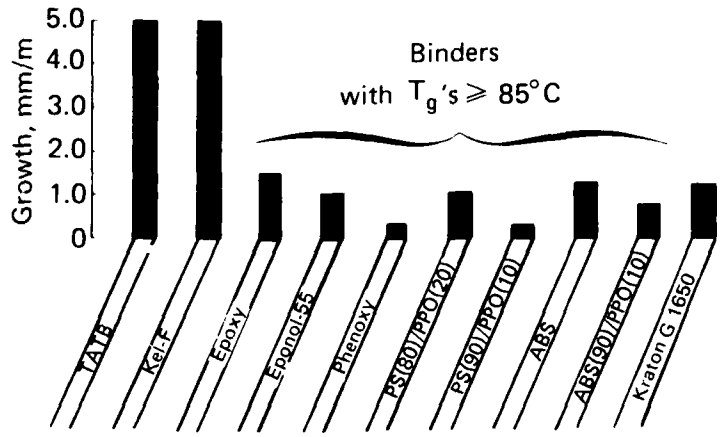

Fig. 1. Growth of TATB and TATB PBX formulations. Formulations containing binders with T_g greater than 85°C showed significantly less growth.

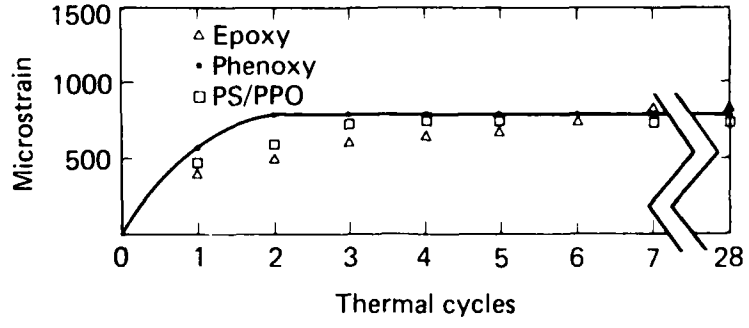

Fig. 2. Growth of TATB PBX forumlations containing 7.5 vol% binder (epoxy, Phenoxy, or polystyrene/polyphenylene oxide) during 28 thermal cycles between -54 and 74°C.

strength, which indicates that the polystyrene endblocks apparently control particle movement responsible for growth and that the ethylene-butylene rubber midblock dominates the mechanical response.

Figure 1 shows that the high-T_g binders reduce TATB growth at least five-fold. On the basis of this growth and the compressive strength data, we formulated, pressed isostatically, and tested three TATB PBX compositions; either an aromatic diamine-cured epoxy, 90/10-PS/PPO, or Phenoxy was used as the binder.

Figure 2 shows the growth for TATB formulated with 7.5 vol% aromatic diamine-cured epoxy, BAKELITE Phenoxy, and 90/10-PS/PPO after 28 thermal cycles between -54 and 74°C. All three formulations showed less than 1000 microstrain (1 mm/m) dimensional change after 28 cycles. This growth was far less than the growth noted for RX-03-BB under the same conditions. Growth of all of these high-T_g formulations ceased by the seventh thermal cycle. The two new thermoplastic binders did not, in fact, grow after the third cycle, and RX-03-CK (7.5 vol% Phenoxy) realized about 75% of its growth in the first thermal cycle.

These high-T_g binders apparently form strong films between TATB particles that severely restrict permanent displacement of the particles during thermal cycling.

The effectiveness of these high-T_g binders to hinder growth can be diminished, however, if the peak temperature of the thermal cycle exceeds the T_g of the binder or if the pressing temperature of the PBX is near or slightly below the T_g.

COMPARISON OF PROPERTIES OF RX-03-BB AND RX-03-CK

Composition

The TATB formulation (RX-03-BB) presently used at LLL as our main-charge high explosive (HE) contains 92.5/7.5 (vol%) of TATB and Kel-F 800 binder. Our improved formulation described in this report (RX-03-CK) contains 7.5 vol% of Phenoxy, a linear epoxy-type binder.

Growth

We measured changes of the axial length of isostatically pressed RX-03-BB and RX-03-CK rods (127 mm long, 12.7 mm o.d.) continuously during thermal cycling. We used a strain gage transducer containing four active elements and compensated for temperature. The CTE values were calculated simultaneously. Figure 3 shows the microstrain of RX-03-BB as a function of temperature when it was cycled from the ambient temperature to 74°C, to -54°C, and again to ambient once a day for seven days. We observed that growth of RX-03-BB continues for 22-24 cycles. To insure that all expected growth was achieved within this temperature range, we subjected the HE to a total of 28 thermal cycles (Fig. 4). We noted that the peak temperature had a greater effect on growth than the temperature range of the thermal cycle (ref. 5).

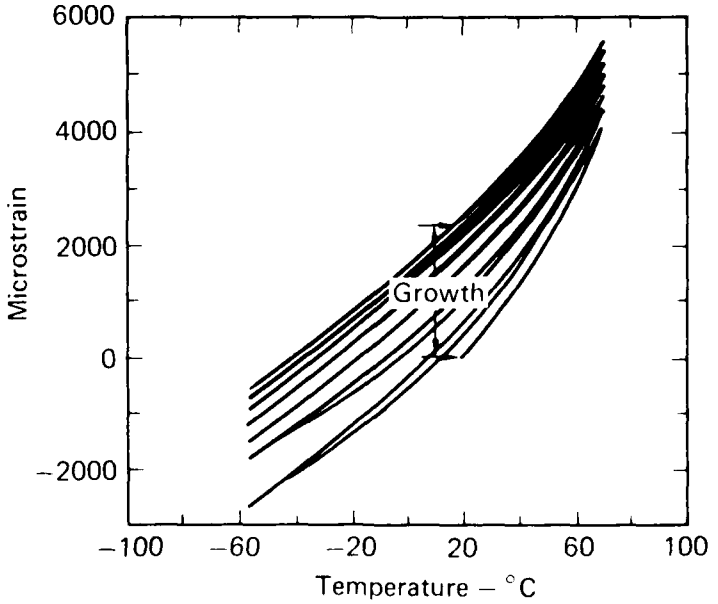

Fig. 3. Growth of RX-03-BB (TATB/Kel-F 800; 92.5/7.5 vol%) during seven thermal cycles between -54 and 74°C.

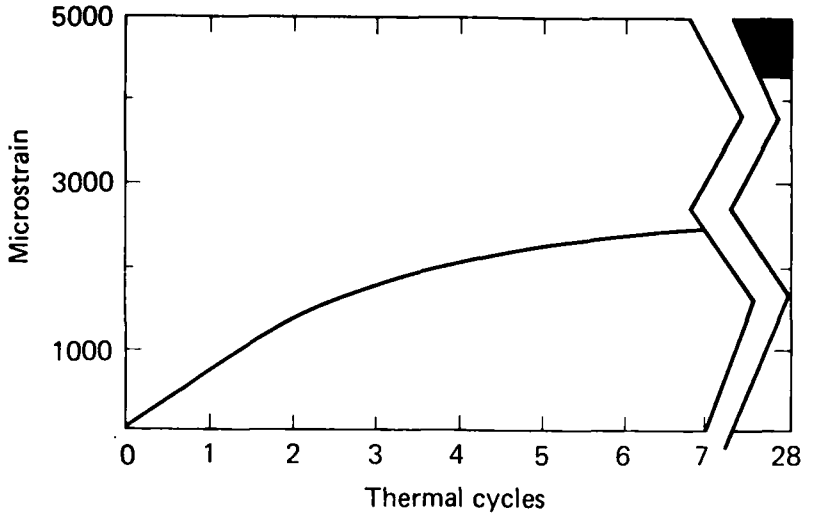

Fig. 4. Growth of RX-03-BB as function of number of thermal cycles between -54 and 74°C. After 28 thermal cycles, the range of microstrain values observed represents a volume change of about 1.5%.

The results given in Fig. 2 show that RX-03-CK completes the major portion of its growth in the first thermal cycle. Therefore, if a part made of this material is cycled once after pressing but before machining, it becomes essentially a zero-growth TATB PBX part for its entire stockpile life. Figure 5 plots microstrain vs temperature for 28 cycles. Comparison of these results for RX-03-CK with those for RX-03-BB after only seven cycles (Fig. 3) demonstrates that growth of RX-03-CK is substantially less than that of RX-03-BB.

Strength

We measured the maximum compressive stress and tensile strength of isostatically pressed RX-03-BB and RX-03-CK samples. Figure 6 shows that before thermal cycling, the compressive properties of RX-03-BB were very good compared to PBX formulations based on HMX (1,3,5,7-tetranitro-1,3,5,7-tetrazacyclooctane)(ref. 6). After several thermal cycles, however, the compressive strength of RX-03-BB decreased.

Figure 7 illustrates the good tensile properties of RX-03-BB and shows that thermal cycling dramatically reduced the tensile strength of RX-03-BB by about 45%. The loss in tensile strength was caused by debonding of the TATB particles from the Kel-F 800 binder.

The maximum compressive stress and tensile properties of RX-03-CK are shown in Figs. 8 and 9. The new formulation was stronger than RX-03-BB, and the mechanical properties were unaffected by thermal cycling between -54 and 74°C; compressive and tensile properties measured at -54 and 74°C were the same as those at 20°C.

Additional mechanical property data generated from a long-term aging study of RX-03-BB are shown in Figs. 10 and 11 (ref. 3). The compression and tensile strengths of RX-03-BB deteriorated noticeably after aging (a) isothermally at 40, 60, 80, and 100°C; and (b) during thermal cycles from -54 to 92°C repeated once

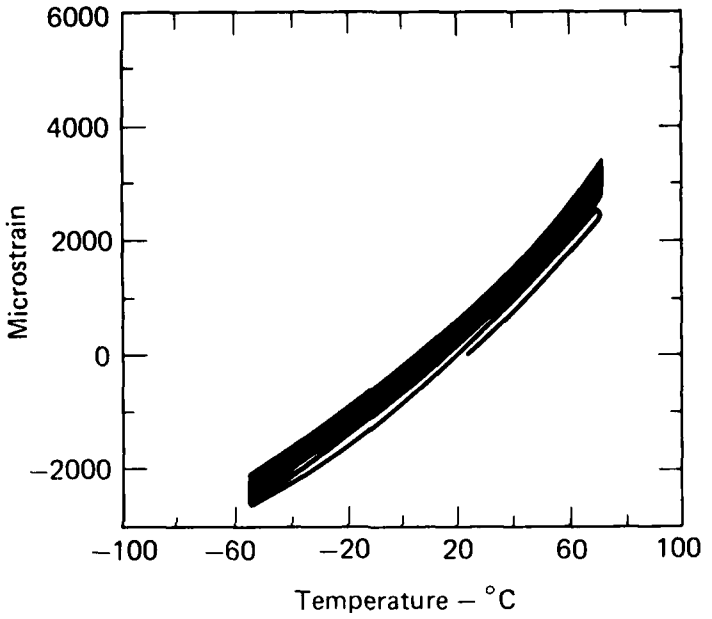

Fig. 5. Growth of RX-03-CK (TATB/Phenoxy; 92.5/7.5 vol%) during 28 thermal cycles between -54 and 74°C. Comparison of these results with those in Fig. 3 shows that growth of RX-03-CK is dramatically smaller than that of RX-03-BB.

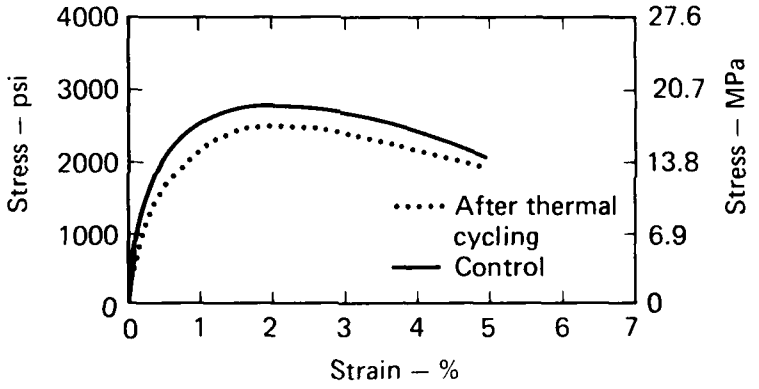

Fig. 6. Compressive properties of RX-03-BB before and after 28 thermal cycles between -54 and 74°C.

every 2.5 days for three months. The reduction of compressive and tensile strengths is generally attributed to the loss of density caused by growth. However, the decrease in maximum compressive stress observed when RX-03-BB was tested above 60°C for 500 days was greater than expected from a decrease in density caused by growth alone. It should also be noted that the 80 and 100°C isothermal tests are severe and that thermal cycling to 92°C instead of 74°C is excessive.

CTE

The CTE values for RX-03-BB and RX-03-CK were measured on the same rods used to measure growth. Figure 12 shows that the average CTE of RX-03-BB between -54 and 15°C was 40.4 X 10^{-6}/°C. Between 15 and 74°C, the average CTE increased to

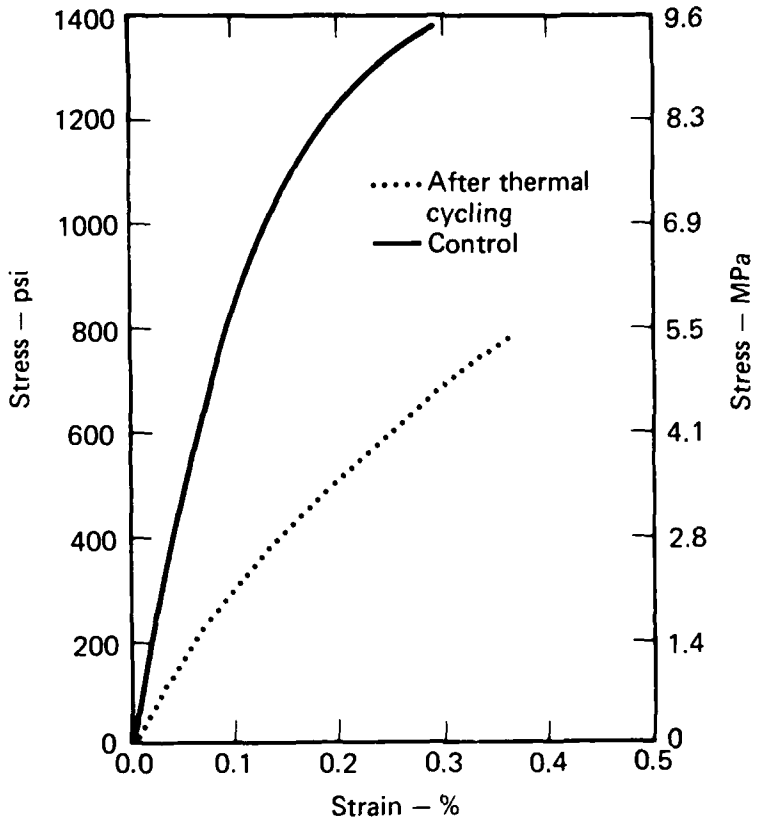

Fig. 7. Tensile properties of RX-03-BB before and after 28 thermal cycles between -54 and 74°C.

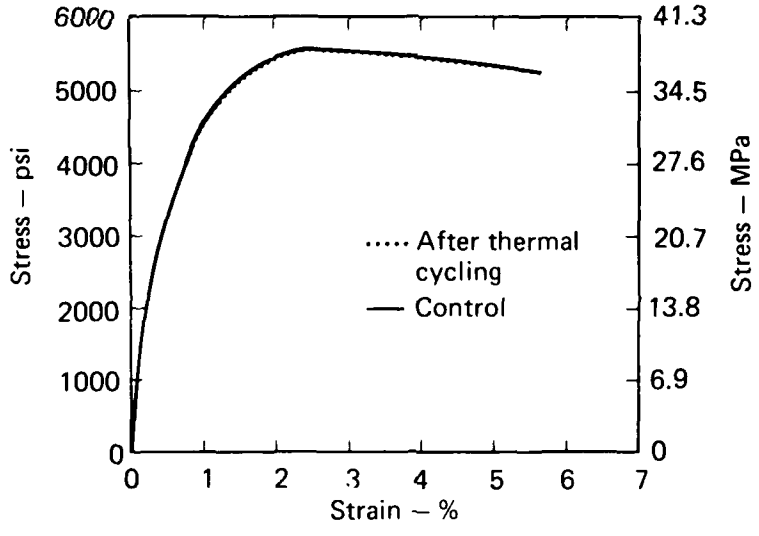

Fig. 8. Compressive strength of RX-03-CK before and after 28 thermal cycles between -54 and 74°C.

60.2 X 10^{-6}/°C. These CTE values were calculated after the RX-03-BB rods had been thermally cycled several times to insure that growth would not interfere with obtaining accurate values. Figure 13 compares the CTE of RX-03-CK and RX-03-BB; the overall CTE of RX-03-CK is notably less than RX-03-BB.

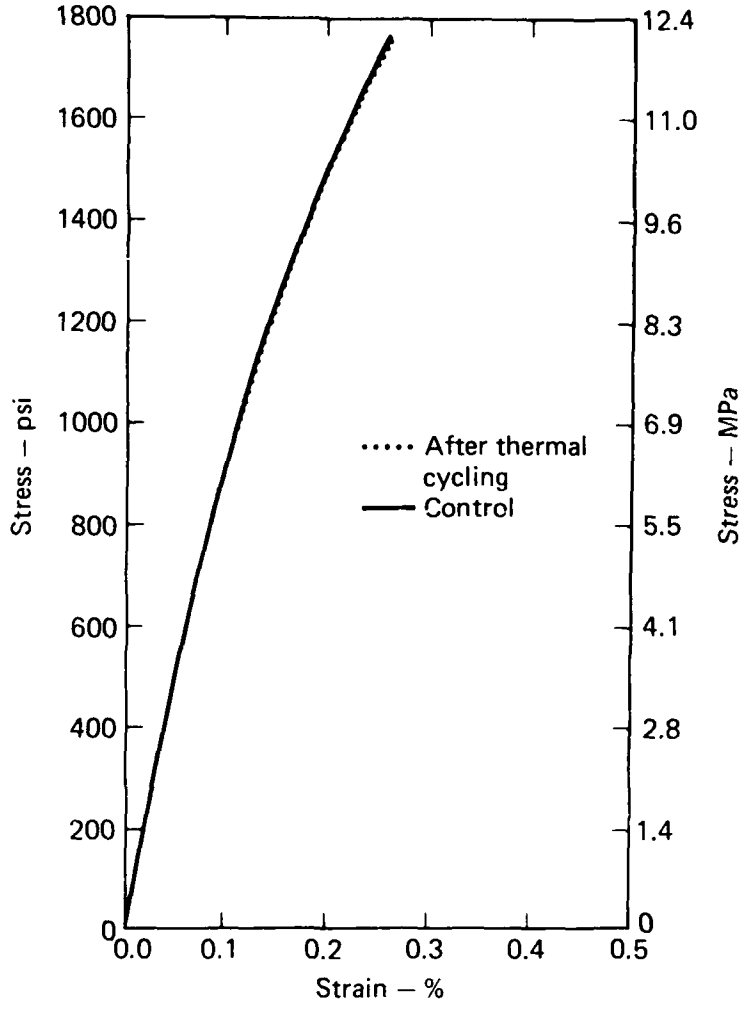

Fig. 9. Tensile strength of RX-03-CK before and after 28 thermal cycles between -54 and 74°C.

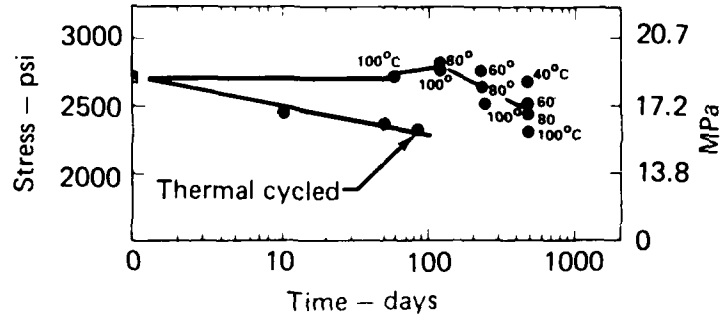

Fig. 10. Compression data of RX-03-BB aged under isothermal and thermal cycling conditions.

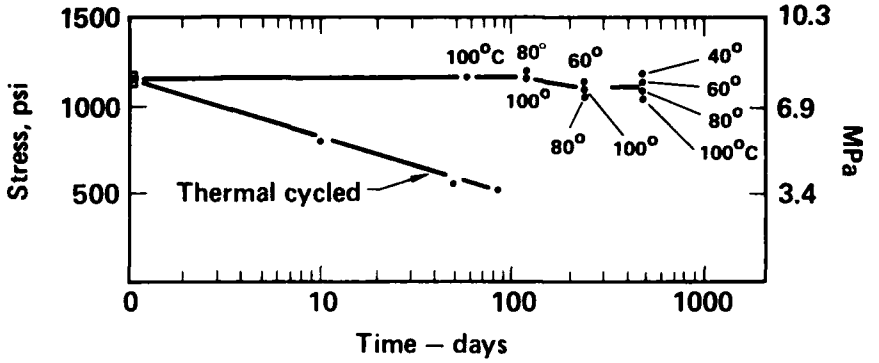

Fig. 11. Tensile property data of RX-03-BB aged under isothermal and thermal cycling conditions.

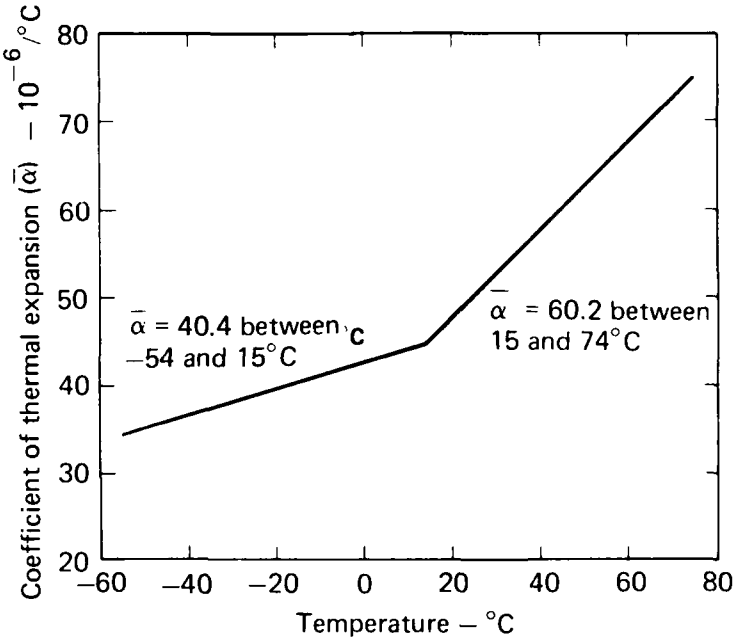

Fig. 12. Coefficient of thermal expansion ($\bar{\alpha}$) of RX-03-BB. The change of the slope at approximately 15°C results from a secondary mechanical relaxation that occurs in TATB at about 30°C.

Recent studies (ref. 5) have provided evidence that the change of the slope of the curves in Fig. 13 results from a secondary mechanical relaxation that occurs in TATB at about 30°C. Such mechanical relaxation results in greater molecular flexibility and hence greater expansion. Differential scanning calorimetry (DSC) and single crystal x-ray data indicated that this relaxation phenomenon is not a first- or second-order phase change.

Figure 14 shows the loss modulus of pure TATB measured with a Rheometrics Mechanical Spectrometer (RMS) at low frequency (0.1 Hz). The maximum in loss

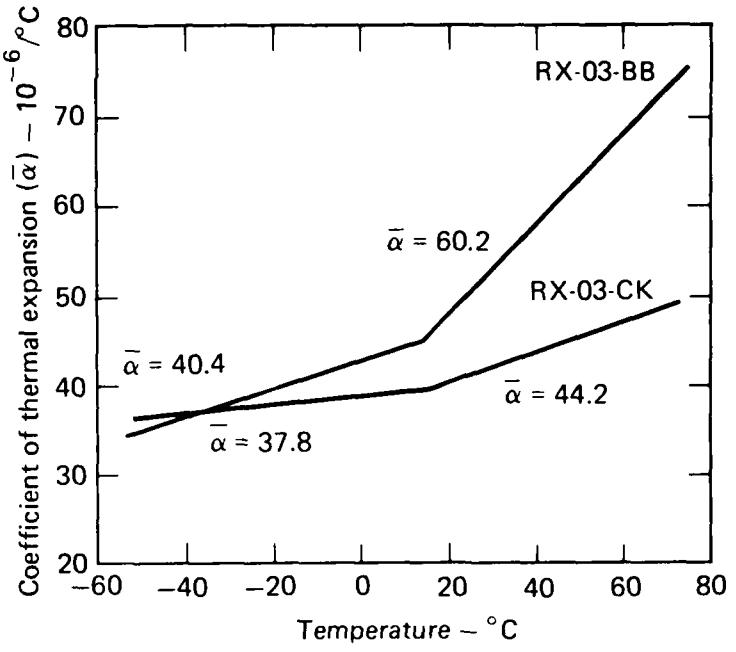

Fig. 13. Coefficients of thermal expansion ($\bar{\alpha}$) of RX-03-BB and RX-03-CK. The change of the slopes at approximately 15°C results from a secondary mechanical relaxation that occurs in TATB at about 30°C.

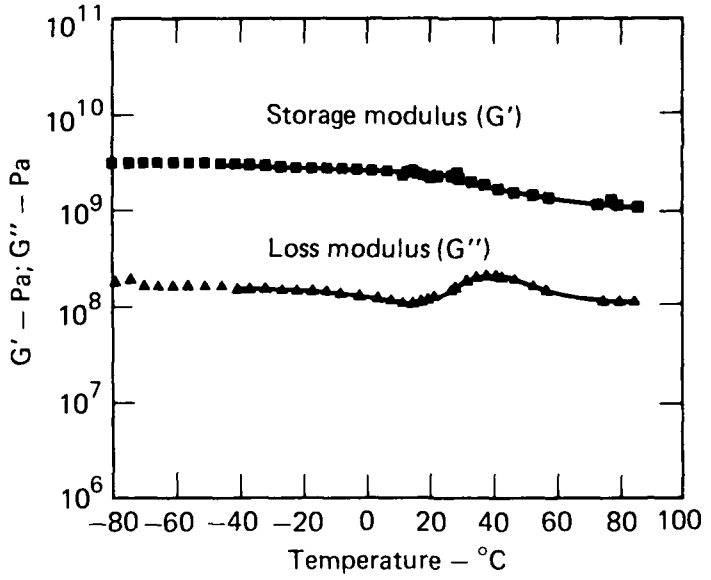

Fig. 14. Shear storage modulus (G') and shear loss modulus (G") of pure TATB as functions of temperature; samples were stressed at a constant frequency of 0.1 Hz.

modulus and the decrease in storage modulus of TATB between 20 and 40°C indicate that a secondary mechanical relaxation occurs between these temperatures, and the RMS data for RX-03-BB presented in Fig. 15 shows the same relaxation temperature as TATB. However, use of the high-T_g binder in RX-03-CK substantially minimized the deleterious effect of this secondary mechanical relaxation of TATB (Fig. 16). The reduced CTE of RX-03-CK may result from this suppression.

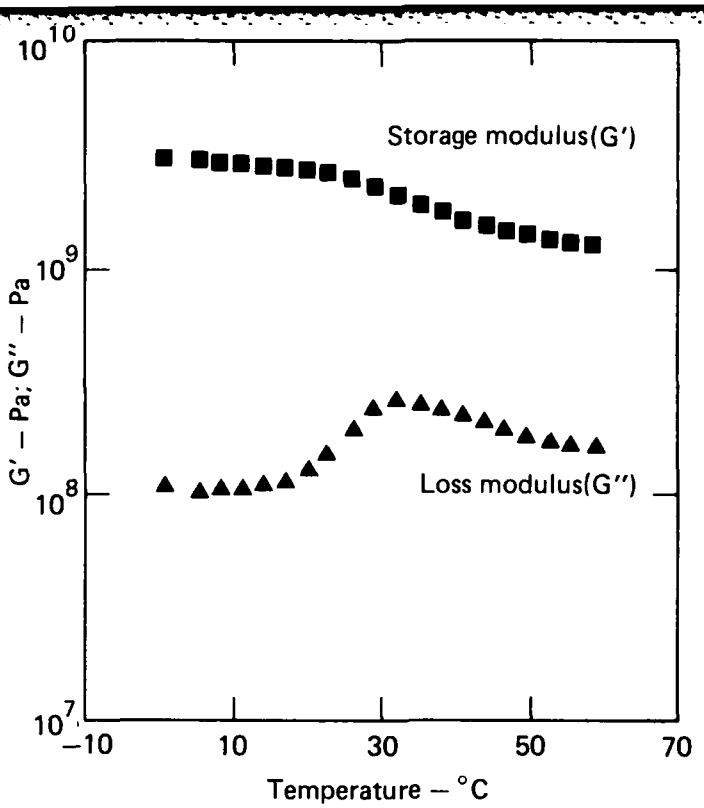

Fig. 15. Shear storage modulus (G') and shear loss modulus (G") of annealed RX-03-BB as functions of temperature; samples were stressed at a constant frequency of 0.1 Hz.

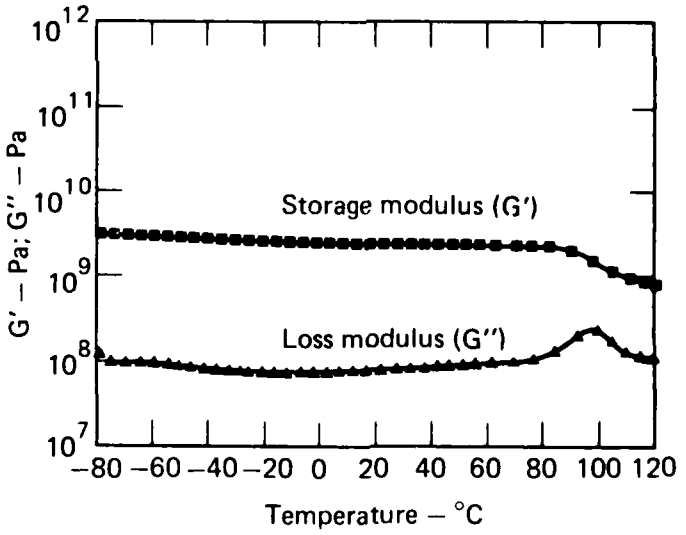

Fig. 16. Shear storage modulus (G') and shear loss modulus (G") of RX-03-CK as functions of temperature; samples were stressed at a constant frequency of 0.1 Hz.

Effects of Variations of Phenoxy Content and Temperature

We successfully restricted growth even when we reduced the amount of Phenoxy binder in the PBX to as little as 2.5 vol%. Figure 17 illustrates the variation of growth and maximum compressive strength of samples containing between 2.5 and 7.5 vol% Phenoxy. Figure 18 shows that reducing the Phenoxy binder content to 6 vol%

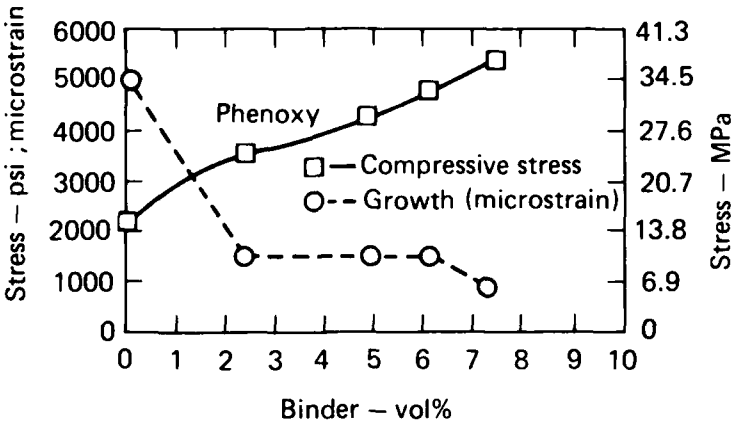

Fig. 17. Growth and compressive stress of TATB/Phenoxy compositions as function of the vol% content of Phenoxy binder.

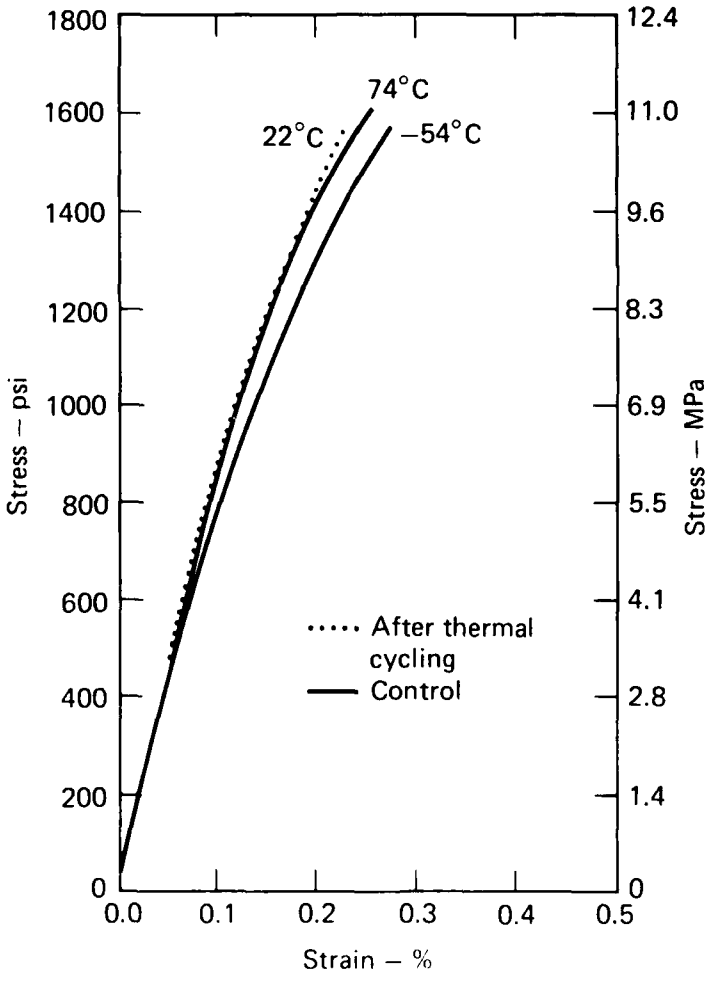

Fig. 18. Tensile strength of TATB/Phenoxy (94/6 vol%) before and after 28 thermal cycles; measurements were made on control samples at -54 and 74°C and on thermally cycled samples at 22°C, respectively. The tensile strength was not temperature dependent.

reduced the tensile strength of RX-03-CK by about 10%. Figure 19 shows that reduction of the binder content to 5 vol% further degraded the tensile strength of RX-03-CK. The data in Figs. 18 and 19 indicate that the tensile strengths of the Phenoxy-bonded PBX formulations tested at -54 and 74°C were not temperature dependent. These samples were not thermally cycled. Figure 20 shows that, in contrast, the tensile properties of RX-03-BB, which was also not thermally cycled, were highly temperature dependent. This temperature dependence of RX-03-BB also results in greater creep than that measured for TATB/Phenoxy (94/6 vol%). Table 1 lists the compliance data for TATB PBX samples under tension and compression at 74°C. This compliance data emphasizes the importance of selecting a binder with a T_g above the temperature range of the expected environment.

FABRICATION OF PHENOXY-BONDED TATB PBX SAMPLES

Phenoxy Binder

BAKELITE Phenoxy PKHJ resin is a very "tough" high-strength soluble linear epoxy polymer manufactured by Union Carbide and widely used in industrial surface

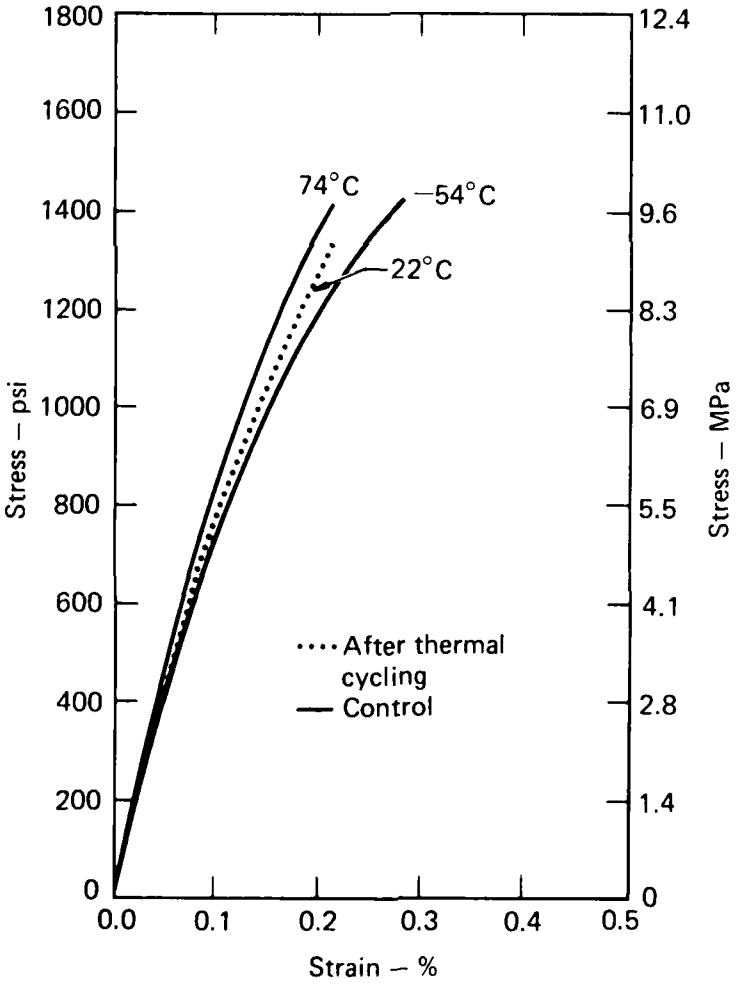

Fig. 19. Tensile strength of TATB/Phenoxy (95/5 vol%) before and after 28 thermal cycles; measurements were made on control samples at -54 and 74°C and on thermally cycled samples at 22°C, respectively. The tensile strength was not temperature dependent.

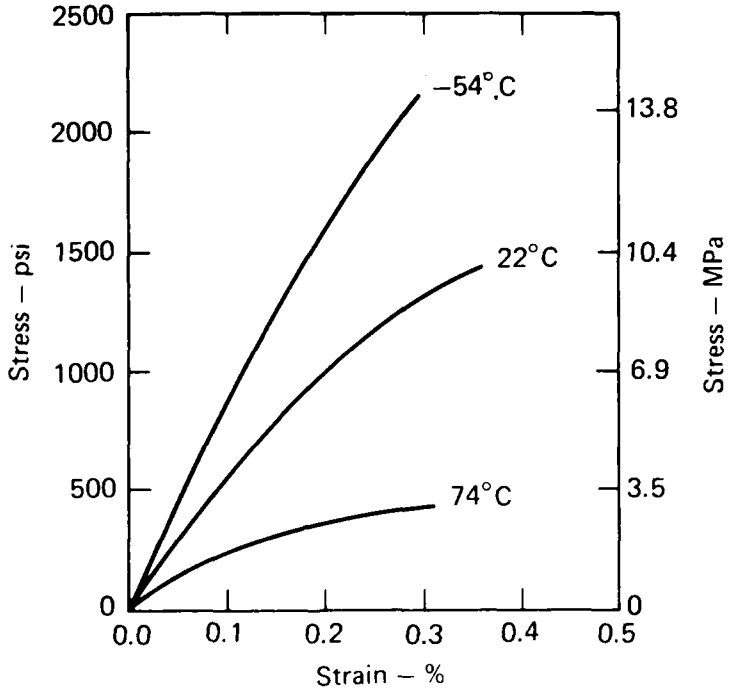

Fig. 20. Tensile strength of RX-03-BB at different temperatures.

TABLE 1.

Compliance data for RX-03-BB and TATB/Phenoxy (94/6 vol%)

		Compliance (J_t),[a]			
		time, h			
	Stress, psi	0	1	10	100
Tension					
RX-03-BB	250	2.4	5.6	10	---[b]
TATB/Phenoxy	250	1.2	1.5	1.8	2.0
	500	1.6	2.0	2.6	3.2
Compression					
RX-03-BB	250	2.4	3.6	7	11.5
TATB/Phenoxy	500	1.2	1.6	2.0	2.4

[a]Compliance $J_t = \epsilon_t/\sigma$, where ϵ_t is strain at time (t) and σ is stress. Measurements were made at 74°C.

[b]Sample failed after 11 h.

coatings; it is a copolymer of bisphenol A [2,2-(4'-dihydroxyphenyl)propane] and epichlorohydrin. Phenoxy has a high T_g (>85°C). No compatibility problems between the binder and TATB or between the binder and other weapon materials are anticipated. Test programs are in progress at LLL to verify the long term storage

stability and long term compatibility of the TATB/Phenoxy PBX. The availability of Phenoxy is not a problem.

Formulation

RX-03-CK and other TATB compositions containing as little as 2.5 vol% binder can be prepared using standard slurry techniques. To conserve energy during production of the molding powder beads, however, we did not use heat to evaporate the MEK-toluene (4:1) solvent from the Phenoxy-lacquer binder solution. We instead extracted the water-soluble MEK (2-butanone) by dilution of the PBX-lacquer slurry with water; because Phenoxy is insoluble in toluene, it precipitates onto the TATB crystals. We have also used the house vacuum as an air sweep to remove most of the lacquer solvent before dilution with water. Both processes worked equally well to produce high quality molding powder beads.

Pressing

All PBX formulations were pressed mechanically for preliminary test evaluations. The pressed rods were 25.4 mm long and 12.7 mm o.d. The molding powders and die were preheated to between 105 and 120°C (depending upon the binder), and the die was evacuated and pressurized to 207 MPa for 5 min; each part was pressed three times.

Only the best candidate formulations were pressed isostatically for final test evaluations because this is a costly and time-consuming operation. This pressing technique ensured that the compressed billets responded isotropically to thermal environments. Isostatically pressed parts were then machined to shape.

In both types of pressing operations, temperature was the most important variable. Figure 21 plots the density of TATB PBX compositions containing different amounts of Phenoxy as a function of the pressing temperature. The nearly linear response of density to pressing temperature in Fig. 21 was not observed in corresponding plots of growth vs pressing temperature or maximum compressive stress response vs pressing temperature. Instead, we noted a sharp decrease in growth and an increase in compressive strength when the pressing temperature exceeded the T_g of the binder. This indicated that the binder penetrated and flowed between TATB particles to produce strongly bonded pressed billets.

SUMMARY

We developed a new TATB PBX (RX-03-CK) that offers significant advantages over the presently used TATB/Kel-F 800 PBX formulations. After it has been subjected to only one thermal cycle over the military temperature range, RX-03-CK is essentially a no-growth explosive. This required thermal cycle can be easily performed after

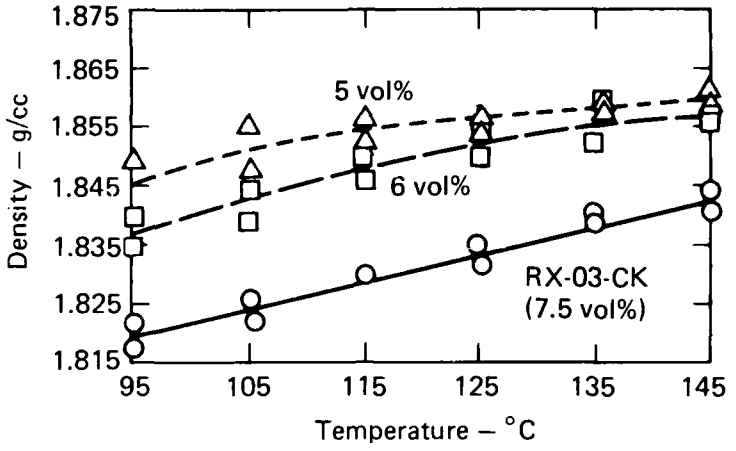

Fig. 21. Density of TATB PBX formulations containing different proportions of Phenoxy binder as function of pressing temperature.

pressing but before machining so that the finished parts maintain their final dimensions.

The CTE of RX-03-CK is about 25% lower than that of RX-03-BB. We showed that the tensile and compressive strengths of RX-03-CK were higher than those of RX-03-BB, the creep of TATB/Phenoxy (94/6 vol%) was lower, and, unlike RX-03-BB, thermal cycling of RX-03-CK did not reduce these responses. The Phenoxy binder used in RX-03-CK acts as an energy sink (i.e., absorbs explosive energy) compared to the Kel-F 800 binder used in RX-03-BB. Thus, RX-03-CK produces about 2-2.5% less energy than RX-03-BB. We are presently optimizing the PBX formulating and pressing techniques; we are also working to minimize the amount of Phenoxy binder required.

ACKNOWLEDGEMENTS

We wish to thank G.L. Moody for preparing the sample formulations, R.D. Breithaupt for the compression and tension measurements, C.V. Johnson III for the creep measurements, and D.M. Hoffman and J.R. Kolb for the secondary mechanical relaxation data.

REFERENCES

1 B.M. Dobratz, M. Finger, L.G. Green, J.R. Humphrey, R.R. McGuire, and H.F. Rizzo, The Sensitivity of Triaminotrinitrobenzene (TATB) and TATB formulations, Lawrence Livermore Laboratory, Livermore, Calif., UCID-17808 (1978).
2 R.H. Pritchard, Initial Compatibility Evaluation of TATB Plastic-Bonded Explosive, Lawrence Livermore Laboratory, Livermore, Calif., Preprint UCRL-77897 (1976).
3 R.D. Breithaupt, Mechanical Properties of Thermally Aged RX-03-BB Explosive, Lawrence Livermore Laboratory, Livermore, Calif., UCID-17871 (1978).

4 J.R. Kolb and H.F. Rizzo, The Growth of 1,3,5-Triamino-2,4,6-Trinitrobenzene (TATB). I. Anisotropic Thermal Expansion of TATB, Lawrence Livermore Laboratory, Livermore, Calif., Preprint UCRL-81189 (1978).
5 H.F. Rizzo, J.R. Humphrey and J.R. Kolb, The Growth of 1,3,5-Triamino-2,4,6-Trinitrobenzene (TATB). II. Control of Growth by Use of High T_g Polymeric Binders, Lawrence Livermore Laboratory, Livermore, Calif., UCRL-52662 (1979).
6 J.R. Humphrey, LX-14: A New High-Energy Plastic-Bonded Explosive, Lawrence Livermore Laboratory, Livermore, Calif., UCRL-52350 (1977).

"Work performed under the auspices of the U.S. Department of Energy by the Lawrence Livermore Laboratory under contract number W-7405-ENG-48."

Reference to a company or product name does not imply approval or recommendation of the product by the University of California or the U.S. Department of Energy to the exclusion of others that may be suitable

NO-ROLL PROCESSING OF COMPOSITE MODIFIED DOUBLE BASE EXTRUSION COMPOSITIONS

CRAIG E. JOHNSON

Naval Ordnance Station, Indian Head, Maryland

ABSTRACT

The No-Roll Process is a new method of manufacturing solventless double-base propellants suitable for extrusion. The process consists of slurrying fibrous nitrocellulose, energetic solids, and nitrate esters in a hydrocarbon medium. The liquid is then decanted from the slurry, and the remaining mix is dried and cured, and extruded into the final form.

Because the process can be carried out in commercially available equipment, and by remote control, it is safer and far less costly than conventional methods of manufacture. Also, it is possible to add energetic solids to the formulation.

By adding such energetic solids to the formulation, and using the No-Roll Process, it is possible to manufacture gun propellants with impetus levels equal to those presently available, but having lower flame temperatures.

This paper presents formulating data and test results of recent gun propellant formulations using nitrocellulose, plasticized with metriol trinitrate and triethylene glycol dinitrate, and loaded with RDX. Data are also presented on recent work to develop a solventless gun propellant based on nitrocellulose, nitroglycerine and nitroguanidine. This formulation is designed to approximate the ballistics of M30. Formulating data and test data are discussed.

INTRODUCTION

Extrusion is a low cost method of forming double-base solid propellants to a final shape. The extruded material must have a high enough viscosity to be able to hold its final shape without deforming during its operational lifetime. The mixing of the material to be extruded then becomes a problem, because the process of mixing is one of constant deformation and reformation of the propellant mass.

The high viscosity mixture has been handled two ways: One method uses heavy duty rolls to knead and mix the material; the other method dilutes the material with a solvent to reduce the mixture viscosity. The first method known as the solventless rolling method involves multiple handling steps and specialized equipment; the second method known as the solvent method produces a product that shrinks as the solvents dry out and causes environmental pollution problems.

The No-Roll Process was developed to avoid both of these problems and mix the materials for solventless formulations (ref. 1). The process is adaptable to making solids loaded compositions or so called composite modified double-base compositions (ref. 2) that can be extruded using slightly modified conventional extrusion presses. The Process consists of the following steps:

1. Slurry water-wet fibrous nitrocellulose in heptane; add the solids to the slurry; add the liquid plasticizers. Continue to slurry the materials together until the solids have deagglomerated and plasticizer has coated all of the solids. Decant the heptane.
2. Dry the propellant to remove the remaining heptane and complete the plasticization of the nitrocellulose.
3. Place the material in a vacuum type solventless press and extrude the material to its final size.

It is known that by adding energetic solids such as RDX or nitroguanidine to a double-base formulation it is possible to achieve greater impetus in gun propellants without increasing the flame temperature. These solids are commonly added to solvent-type formulations, but processing difficulties arise because of the shrinkage due to solvent evaporation after extrusion. Some limited success was obtained by Picatinny Arsenal (ref. 3) with the solvent-solventless method, but this involved a multiplicity of handling steps. Standard solventless rolling techniques are unsuited for energetic solids loaded formulations because of the potential safety hazards involved.

The No-Roll Process can mix solventless double-base formulations containing large amounts of solids (up to 60%) in a dilute slurry.

EXPERIMENTAL

Standard double-base formulations have roughly a 50/50 ratio of plasticizer to nitrocellulose. This produces a material which can easily be extruded at or below 10,000 psi. As solids are added, the resulting materials increase in hardness and are even more difficult to extrude. We wanted to add more solids, but avoid the concommitant difficulties in extruding the material. We found that we could do this, using the No-Roll Process and adjusting our formulations to give the binder a lower viscosity as the solids level increases. Thus, the ratio of nitrocellulose to plasticizer decreases as the solids level increases. Figure 1 shows this relationship. We also found that the number of nitrate groups on the nitrocellulose was important in solids loaded formulations. A 12.0% N nitrocellulose was found to give much better extrusion results than a 12.6% N nitrocellulose. Within the usual military blends, the viscosity of the NC did not seem to have much effect.

The original formulation work using a solids loaded gun propellant composition was done using RDX, nitrocellulose, metriol trinitrate and triethylene glycol dinitrate. At this time the intent was to duplicate the flame temperature of the usual gun propellants but increase the impetus. As shown in Table 1 we achieved impetus of 395,000 ft. - lb./lb. at a flame temperature of 3052°K. Later we changed the approach in this program to decrease the flame temperature while keeping the impetus level of the usual gun propellant. The formulations resulting from this program are shown in Table 2.

One of the more favorable aspects of the No-Roll Process is the ability of the process to disperse the ingredients and deagglomerate any particle clusters. We have always used the standard Class 5 (Class E) RDX in our formulations. We do not feel it is necessary to grind the RDX below this size of about 10 to 20 microns. As is shown in figure 2 we feel that we have achieved a reasonable burning rate/pressure slope. The closed bomb data indicates a slope of 1.059 for a formulation using 40% RDX and 1.123 for a formulation using 55% HMX.

In addition to the solids loaded formulations using RDX, we developed some using nitroguanidine. We wanted to create a solventless variation of M-30, which has been used by the Army for many years. Its composition and ballistic

properties are shown in Table 3. As it is conventionally manufactured, the M-30 must be processed with solvents, owing to its high viscosity. As was mentioned briefly in the introduction, this means that solvents must be added to the formulation so the material will be extrudable. However, after extrusion, the solvent evaporates, and the propellant strands do not remain in the desired size or shape. An additional drawback is that residual solvents which remain in the propellant strands can affect its ballistic properties over a period of time, or in various physical surroundings. Hence, the desirability of a solventless formulation which could circumvent these problems.

In our tests using the No-Roll Process, we found that we could achieve a very close approximation of the M-30 impetus, and flame temperature. The compositions shown in Table 3 represent these nitroguanidine loaded solventless formulations.

The compositions were processed normally and extruded through a 0.290 inch die with seven pins. Because of our die configuration, some of the compositions did not receive enough "working" in extrusion. These compositions did not show good consolidation and exhibited marginal strength. By reextruding the grains, good strands were obtained. Moisture data, extrusion data, safety data and heat of explosion for the solventless variations are shown in Table 4 and Figure 3.

FUTURE WORK

The formulations, with the exception of variation 1, processed nicely and the program can be considerate a success. However some further work should be done to optimize the formulations. The extrusion pressures are considered to be somewhat high for a production gun propellant. Reformulation to a slightly lower nitrocellulose to plasticizer ratio would alleviate the problem; the reformulating could include the minor adjustments necessary to match the ballistics of M-30 more exactly; a die design could be implemented to incorporate further working of the propellant in the extrusion process to avoid the double extrusion problems; and a processing variables study should be conducted to define the critical processing parameters and optimize the product. The process still awaits the necessary interest, funds, and projects to scale-up to an industrial sized processing capability for use in a large scope of work.

SUMMARY

The No-Roll Process is a new method of processing solventless double-base and composite solids loaded double-base formulations. The product can be directly extruded. The process offers significant safety and cost benefits over convential methods of manufacture. The results with RDX and NQ loaded formulations have been favorable.

REFERENCES

1 Johnson, C. E. and Dendor, P. F. "Method of Preparing Solventless Double-Base Formulations Suitable for Extrusion", U. S. Patent 4, 126, 497
2 Johnson, C. E. and Dendor, P. F. "Solids Loaded Solventless Propellant and Method for Making Same", U. S. Patent 4, 102, 953
3 Stack, J. S. "Investigation of High Energy-High Density Smokeless Nitramine Extruded Double-Base Propellants", Picatinny Arsenal, Dover, New Jersey, May 1970, Technical Memorandum No. 4047

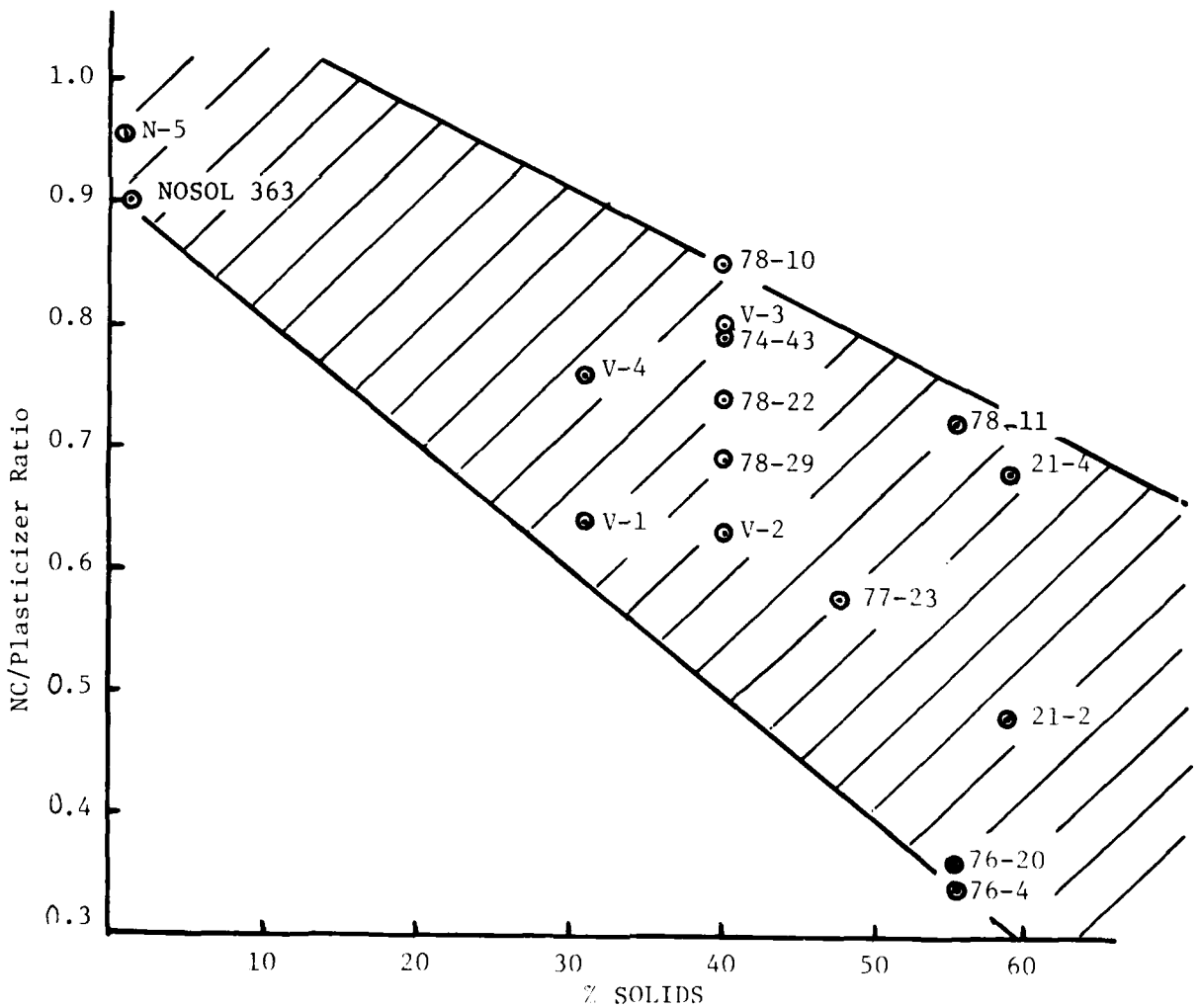

Figure 1. Effect of solids loading on binder composition

TABLE 1

Several Nitramine Loaded Formulations, Chemical Theoretical Data and Extrusion Data

	Formulation Number							
Ingredient	74-43	76-4	76-7	76-15	76-17	76-19	76-20	77-23
Nitrocellulose	26.4	8.8	8.8	6.0	8.0	5.0	11.9	19.2
Cellulose Acetate	---	9.9	9.9	9.9	9.9	8.9	---	---
Plasticizers	33.5	26.2	26.2	29.0	27.0	31.0	33.0	33.0
Additives	0.1	0.1	0.1	0.1	0.1	0.1	0.1	0.1
RDX/HMS	40.0	55.0	55.0	55.0	55.0	55.0	55.0	47.7
Extrusion Results	GS	GS PS	GS PS	RS PS	RS PS	GS PS	GS FS	RS FS
Impetus, Ft-lb./lb.	406K	---	---	392K	392K	---	396K	---
Flame Temp, ok	3310	---	---	3042	3063	---	3052	---
NC/Plasticizer	.79	.34	---	---	---	---	.36	.58

GS = Good Strand: PS = Poor Strength: RS = Rough Strand: FS = Flexible Strand: HPE = High Pressure Extrusion

Table 2

Several Nitramine Loaded Formulations, Chemical Theoretical Data and Extrusion Data

	Formulation Number				
Ingredient	78-10	78-11	78-19	78-22	78-29
Nitrocellulose	26.5	18.8	26.5	25.4	24.4
Plasticizers	33.4	26.1	33.4	34.5	35.5
Additives	0.1	0.1	0.1	0.1	0.1
RDX	40.0	55.0	40.0	40.0	40.0
Extrusion Results	HPE PS	HPE PS	PS ---	HPE GS	GS ---
Impetus, Ft.-lb./lb.	---	---	---	356K	---
Flame Temperature, °K	---	---	---	2652	---
NC/Plasticizer	.79	.72	.79	.74	.69

GS = Good Strand: PS = Poor Strength: RS = Rough Strand: FS = Flexible Strand: HPE = High Pressure Extrusion

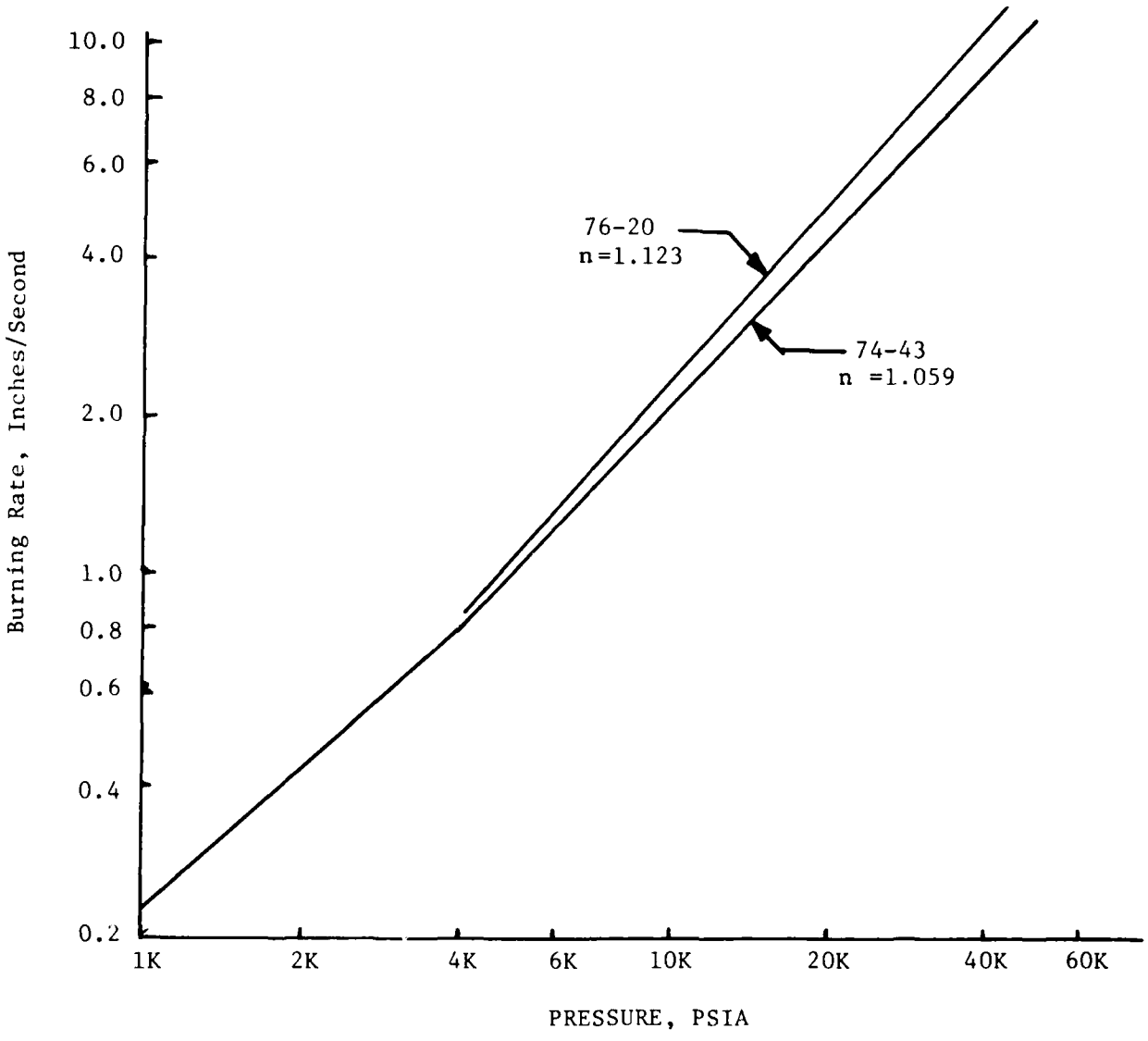

Figure 2, Burning rate data for nitramine loaded formulations

TABLE 3

M30 and Solventless Variations, Chemical and Theoretical Data

	Formulation Type				
Ingredient	M-30	Variation 1	Variation 2	Variation 3	Variation 4
Nitrocellulose	28.0	27.0	23.0	26.4	30.0
Plasticizers	24.0	42.4	36.4	33.0	39.4
Additives	0.3	0.6	0.6	0.6	0.6
Nitroguanidine	47.7	30.0	40.0	40.0	30.0
Impetus, Ft-lb./lb.	364,000	363,826	368,195	365,672	---
Flame Temperature,°K	3040	3028	3105	3087	---
NC/ Plasticizer	1.17	.64	.63	.80	.76

TABLE 4

Experimental Data on No-Roll Solventless M-30 Variations and NOSOL

Analysis	Formulation Type				
	Variation 1	Variation 2	Variation 3	Variation 4	NOSOL 363
Moisture, %	---	0.10	0.10	0.20	0.25
Extrusion (1) Pressure, psi	5400 to 9000 (2)	9000 to 10,000	9000 to 11,700	9000 to 10,350	4500 to 5400
Strand diameter, in.	---	0.301	0.298	0.294	0.291
Impact sensitivity, MM W/5Kg wt.	200	225	225	75	175
Friction sensitivity lb. at 8 Ft/Sec.	⩾980	⩾980	⩾980	⩾980	⩾980
Electrostatic sensitivity/joules	0.625	⩾12.5	⩾12.5	⩾12.5	⩾12.5
H.O.E., actual Cal/gm	---	972	949	1048	934
DDT test 12" X 2" diam.	Negative (pressure burst)	---	---	---	---
Density gm/cc	---	1.510	1.553	1.620	.1516

(1) .290 seven perf die 130 to 140°F
(2) Good strands not consistantly achieved

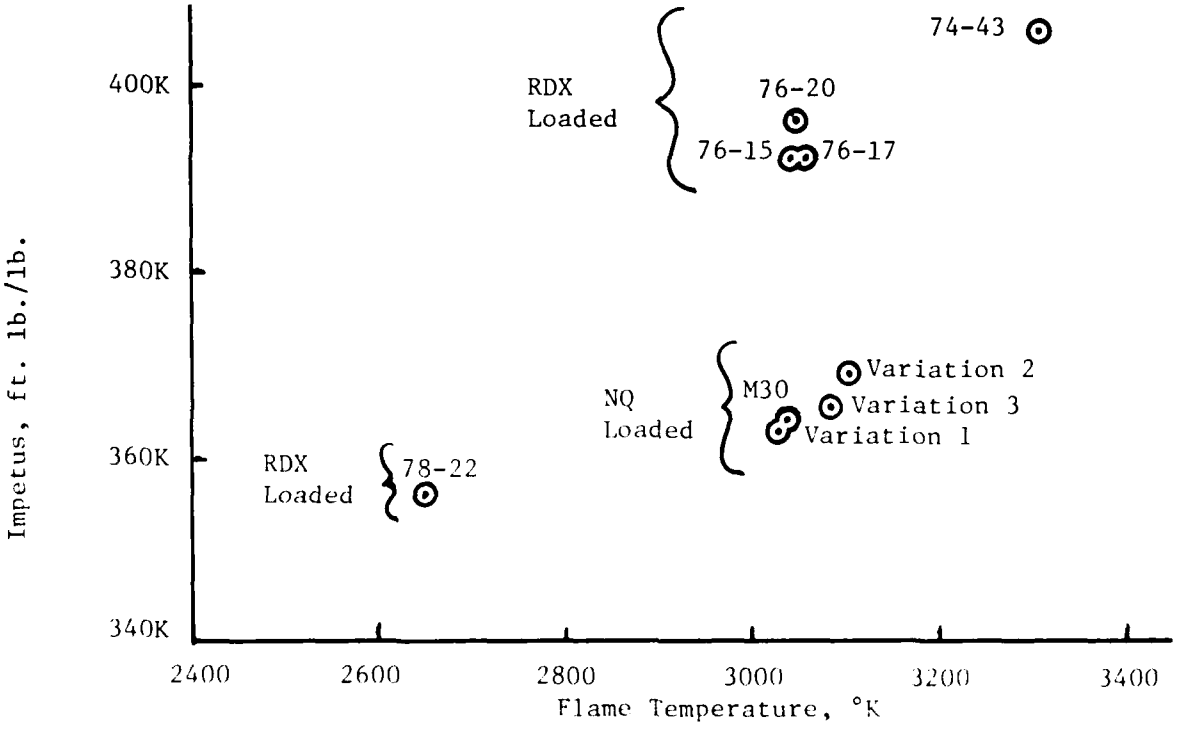

Figure 3. Theoretical Ballistics
Properties of several solids loaded formulations

UNIQUE PROCESS/DESIGN ASPECTS OF A MODERN MULTI-BASE PROPELLANT PLANT

J. P. ZEIGLER, Chief, Propellants and Explosives Division, Office of the Project Manager for Munitions Production Base Modernization & Expansion, Dover, New Jersey

ABSTRACT

A multi-year process development and facility design has been completed for a new continuous, automated facility for producing multi-base cannon propellant. These efforts have addressed many unique problems in processing energetic, nitroglycerin based propellants, incorporating latest DRC 385-100 safety requirements and interfacing DRC equipment design and Corps of Engineers (COE) facility design.

The new facility planned for construction in FY80 budget at an approximate cost of $100 million will expand our 1940-1950 technology labor intensive production base for multi-base cannon propellants by a dedicated process control system, offers substantial improvements in manufacturing safety, process/product quality, base readiness and adaptability to future requirements.

INTRODUCTION

This paper will trace the Army's achievement of its latest technological process for manufacturing multi-base cannon propellant. The culmination of the technology is scheduled to be the operation in 1985 of the Continuous Automated Multi-Base Facility, CAMBL, at Radford Army Ammunition Plant (RAAP), Radford, Virginia. The fifteen year cycle leading to the CAMBL's operation constitutes a $130 million program; $18 million for Manufacturing Methods & Technology (MM&T) process development, equipment design and facility design; $98.8 million for construction and $13 million for Prove-out and Acceptance.

Throughout development to date, many unique problems have been encountered and resolved both in the MM&T and facility design stages. These problems encompass achievement of technical breakthroughs in the continuous processing of multi-base cannon propellants, site unique design problems, special safety designs for provisions for explosive quantity distance, fire protection and personnel egress and lastly, intensive project management efforts throughout the life cycle.

The results of these efforts will be addressed in the following sections of this paper under five headings: Overview, Process Description, Facility Design, Advantages of CAMBL versus Batch Facility and Quantifiable Project Benefits.

RESULTS

Overview

The continuous automated multi-base line (CAMBL), Project 5802875, will be located at Radford AAP, Radford, Virginia. Total cost is $98.8 million. Of this amount, $66 million is for construction by the US Army Corps of Engineers (COE) and $32.8 million is for purchase of process equipment by DARCOM (Radford AAP). CAMBL will provide a capacity of 2.4 million pounds/month of multi-base cannon propellant. Construction, to be awarded in April 1980, will require 36 months to complete. An additional 18 months are required for prove-out and acceptance of the line.

The objectives of the project at RAAP are to accomplish two goals. First, the Army faces substantial shortfalls in capacity for multi-base cannon propellants. This shortfall greatly increased during the 1970's due to the introduction into the stockpile of new 105MM tank cartridges and new propelling charges for 155MM/203MM howitzers.

In addition, the CAMBL, by its incorporation of the latest technologies for both process equipment and dedicated process control systems, was developed to greatly enhance our readiness posture, provide compliance with safety, OSHA and EPA requirements, improve quality, provide our production base with capability to respond to changing operational reqirements beyond the Mid-80's and reduce the cost per pound of propellant produced. These objectives will be addressed in more detail later in this paper.

As is true in industry in technology developments, there is a cycle from development to full scale production capability which is determined by many factors. In our case, an eight year, $6.4 million manufacturing methods and technology (MM&T) program for the CAMBL propellant process was successfully completed prior to initiation of facility design. The pilot line used full scale equipment, operated in a continuous mode to eliminate future scale-up problems and was the basis for facility equipment specifications. These specifications were ultimately used to procure the equipment interface data; i.e., those equipment parameters such as size, weight and utilities, upon which the facility is physically sized and designed. The process parameters, including identification and resolution of operation problems, were established during this MM&T effort.

The pilot line was demonstrated in August 1976 with the successful ballistic test of continuously produced triple base propellant in the 105MM M-90 Tank Round. Based on this successful demonstration, facility design proceeded. Subsequently, work on the prototype line continued for broadening knowledge of process parameters.

An additional triple base pilot lot was successfully ballistically tested in September 1978 in the 155MM Howitzer M203 Propelling Charge. Smaller batches of double base propellant for the 152MM M411 Round were also successfully produced for laboratory evaluation.

During the MM&T effort, significant accomplishments were made in the development of the five major unit operations for multi-base cannon propellant; nitrocellulose dehydration, premixing, mixing, extruding and cutting. Throughout the development cycle on each piece of equipment and mode of material transfer, hazard analysis and anti-propagation tests were conducted with emphasis on exposures to nitroglycerin environments. The anti-propagation tests demonstrated that nitroglycerin solvent mix (NG, alcohol, acetone and ethyl centralite) can be transferred safely through three quarter inch I.D. rubber hoses; i.e., a detonation if it occurred would not be propagated through the hose. Additionally, the anti-propagation tests demonstrated that propagation of materials on conveyors could be averted by designing the conveyors with vertical gaps (drops) and right angle turns. During facility design and construction, a total System Hazard Analysis will have been completed for the CAMBL as a system, including all process equipment, COE support equipment and utilities.

Process Description

A process schematic and continuous mixer for the CAMBL are shown on Figure 1 and 2, respectively. In order to better understand the special design features and major problems resolved during facility design, a general process description is presented as follows:

Thermal Dehydration

Nitrocellulose (NC) slurry is fed to a continuous linear belt filter where the NC is filtered, dried by hot air, cooled and then sprayed with alcohol to provide a product having a nominal composition of 80% NC, 2% water and 18% alcohol. The capacity of each unit, approximately 340 pounds/hour of NC feeds one premix unit. The NC thermal dehydrator for CAMBL was a spin-off from the technology developed for the Continuous Single Base Propellant Facility. In addition, construction of a separate NC thermal dehydrator facility for the existing batch multi-base propellant lines at Radford AAP was completed this year.

Nitroglycerin and Solvents

Nitroglycerin (NG) is received from the NG area via an emulsion transfer system. At the solvent preparation building, the NG is separated from the emulsion and mixed with acetone, alcohol, and chemical additives in a btach mixing process. The resultant solvent mix is pumped by nitrogen pressure to a solvent feed tank in the green line complex (GLC) for use in premixing.

Nitroguanidine and Solids Preparation

The dry chemical ingredients are processed in chemical preparation buildings for subsequent addition to the premixing operation in the GLC. The operations consist of screening nitroguanidine (NQ), grinding cryolite, barium nitrate and potassium nitrate and blending the nitrates with graphite. The chemical preparation buildings for the NQ are on the CAMBL site to enable pulse feeding, via conveyor, to the GLC where it is added to the premixer. The other dry ingredients, constituting less than 2% by weight of propellant, did not economically justify new equipment, facilities or conveyor transfer to the GLC. Accordingly, once per shift, these ingredients will be prepared in an existing facility and manually transferred to the ingredient hopper at the premix.

Continuous Premixer

The dry chemical ingredients, solvent mix and the thermal dehydrated NC are continuously fed into a ribbon blender and physically blended to provide a homogeneous, uniformly wetted mixture for feed to the continuous mixing operation. The unit and associated feeding systems have a nominal capacity of 500 pounds/hour (dry weight basis). It is significant to note that the hazard sensitivity of the premix material on the CAMBL versus the existing batch line is substantially reduced due to the introduction of the NQ at this part of the process.

Continuous Mixer

The premix feed stock and additional acetone and alcohol, if required, are continuously fed to the continuous mixer. This mixer has twin screws and paddles configured to convey and intensively shear the premix as it traverses the lengths of the mixer barrel. Mixer screw speed and circulating water temperature are controlled to form a colloid which is forced through a multi-die plate and cut into pellets as feedstock for the continuous extruder. The mixer has a nominal capacity of 250 pounds/hour (dry weight basis). During the MM&T effort, the continuous mixer presented the most difficulty in establishing the design for producing acceptable multi-base propellant. The critical problem was the proper screw configuration to eliminate air entrapment with its consequent propellant porosity. After determining from the mixer manufacturer that there were no empirical design approaches which could be adapted from other industrial applications of their mixer, the MM&T initiated evaluation of a "segmented screw" configuration. In other words, in lieu of a monolithic screw with pre-located paddles for forwarding and backing, the paddles were constructed as individual units or segments. These segments were then evaluated in the mixer in varying arrangements until the final configuration, producing acceptable, porous free propellant was achieved. This segmented design also will provide flexibility when evaluating or changing production from one propellant formulation to another.

Continuous Extruder

The mixer output is fed continuously by conveyor to three inch vertical screw type extruders and extruded through multiple dies. The strands are then moved through a short plastic 90° angle tube onto a conveyor, cut by a shuttle cutter on the extruder and transferred to the continuous cutter.

The continuous extruder for multi-base cannon propellant was another significant technical accomplishment of the CAMBL MM&T effort and inquiries from the German government have already been received. The most significant problem encountered during equipment and process development was variation in hardness of the extruded strands as a function of propellant formulation and granulation. This hardness variation resulted in the cutter's smearing the cut ends (closing some of the propellant perforations) and in general, poor surface finish of the cut propellant.

This problem was overcome by providing two means to cool, or harden the strands before cutting with the shuttle cutter. First, the conveyor length between the extruder and the continuous cutter was doubled from approximately nine feet to 18 feet. Second, the conveyor was inclosed with an air cooled cover.

Continuous Cutter

The continuous cutter is a roll type cutter. It consists of two rotating cylinders in contact with each other. One of the cylinders has sharp blades spaced at the required grain length and the other is made of smooth, soft type material. As the cylinders rotate, propellant strands are continuously fed between them, resulting in grains cut to the proper length. Similar to the NC thermal dehydration, the CAMBL cutter was another technical spin-off from the continuous cutter technology development under a MM&T program for the Continuous Single Base Propellant Facility.

Traying

The cut propellant is conveyed from the GLC to the traying building for stacking into trays for subsequent transfer to the finishing area. The latter consists of the same processes and buildings for air drying through packing as are used for the batch operation.

Facility Design

Facility design was an intensively managed three-year effort requiring close coordination and cooperation between the Project Manager Office and the principle design agencies, Radford AAP (Hercules, Inc.), the Huntsville Division COE and the COE's Architect-Engineer (A/E). Of worthy mention are the special and innovative design features and procedures used to accomplish design. Additionally, several of the major design problems encountered due to topography, safety and process requirements required special emphasis.

The design features and procedures can be categorized into equipment and construction efforts with the equipment necessarily preceding the facility (construction). Of paramount importance, and a significant problem on past facility design and construction, are the specification and/or adequacy of the process equipment design interfaces. It is upon such interfaces that the COE designs the facility. Consequently, interface problems arising due to the unexpected equipment changes when the process equipment is delivered for installation will have significant schedule and cost impact on the construction effort.

To preclude these problems, design funds were needed to prepare detailed specifications for the process equipment developed under the MM&T effort. These specifications were then used to procure Corps Information Packages (CIPs) showing essential interface information (space envelopes, weights, utility requirements, installation specifications, etc.). The CIPs were provided to the COE for use in both facility design and the construction contract. In addition to the CIPs, the equipment specifications included requirements for fabrication, instrumentation, performance, source inspection, acceptance plans, warranties and an option price (including escalation clauses) to procure the equipment through 1980.

Total System Hazard Analysis and Reliability, Availability and Maintainability (RAM) Analysis is also being conducted by RAAP based on facility final design. This system approach is different from other facility projects in that the latter have generally stopped after analyses of individual pieces of equipment; i.e., total system integration was not affected.

Finally, RAAP has specified their requirements for Incremental Beneficial Occupancy Dates (BODs). Equipment deliveries can be coordinated with facility schedules and facility debugging/prove-out can proceed in a prioritized manner acceptable to RAAP. For example, by specifying the Control House and GLC 1 for early BOD, checkout of the Process Control System and the first process building can be initiated and continued while construction of the other buildings is in progress.

Human Factors Engineering will assume optimum man-machine interfaces for equipment installation, removal, transportability, maintenance and operation. The Standardization Analysis will assure, wherever practical, the commonality and interchangeability of parts. Finally, RAM analyses were used in the selection and design of the CE equipment. This analyses is being integrated into the Total System RAM Analyses to be performed by RAAP.

In addition to the System Engineering activities, Value Engineering (VE) studies were conducted by independent parties on both design criteria (preliminary design) and final design. The latter is ongoing and will be completed before initiation of construction in FY80.

Construction, or design check, models are also being made based on final design. These scale models are invaluable aids in identifying any errors in the final design,

especially in the areas of interferences. During construction, the models will be used at the job site for visual guides and planning tools. In the latter case, the piping contractor can actually pre-cut three to five percent of his pipes (at a cost savings to the government), based on the models.

Also, of worthy mention, are major design problems encountered in siting, facility safety features and the conveying system for the nitroguanidine (NQ). During design of the CAMBL, recognition was taken of the subsurface problems at RAAP. Prior to initiation of the concept design, the COE performed a detailed CAMBL site investigation including aerial photographs, borings and a seismic study. Building sitings were arranged to avoid weak areas noted during these investigations. Subsequent facility design included provisions for special foundations, supports and footings (estimated cost $8 million) to minimize future problems due to sink holes.

Major safety features addressed and resolved include TM Substantial Dividing Walls, Adjacent Bay Deluge Concept (ABDC) and safety egress for personnel.

The TM wall on the GLC provides Category 3 protection between each half of the GLC enabling this building to be sited based on 750 pounds versus 1,500 pounds of Class 1 material. Considering both the size of the GLC (approximately 120 feet long and 70 feet tall in the tower section) and the poor subsurface soil conditions, design of the required TM wall and its foundations were a major accomplishment.

The Adjacent Bay Deluge Concept for the GLC was a design approved by Safety Offices for maximizing our fire protection within rational constraints; i.e., a deluge trip in one area selectively trips only adjoining areas rather than the whole GLC. The latter would be very costly due to provisions for sizing of larger gutters and water disposal systems.

Safety egress on the GLC were also a significant problem due to the size of the building (height of the tower section) and the topography of the overall site. Although the GLC is unmanned during operation, both OSHA and DRC 385-100 (Safety Manual) require exits within 25 feet of any work station, including potential areas for maintenance and repair. To accomplish this phase of the design, a model of the GLC, including all chutes and external equipment, was fabricated. Based on this, design changes were effected. First, the safety chutes from the tower or high bay area were allowed to exit onto the roof of the low bay or extruder area with subsequent egress from the roof to the ground. To effect this change, the low bay roof was "hardened" to withstand the potential blast from the extruder bays (45 pounds/bay 6 bays) and to provide a firm foundation for the safety chutes.

The last major design problem to be addressed in this paper involves the Nitroguanidine (NQ) conveyor system from the Chemical Preparation Building to the GLC. Initially, the system consisted of a covered belt conveyor preceded by a bucket. The latter was required due to consideration of both conveyor elevation differences between the buildings and angle of repose for transporting the NQ. Additionally, due

the "fluffiness" of the NQ, the speed of the conveyor would cause the material to be blown off. To be sufficient to overcome this last problem, an air sweep, moving at the same speed as the conveyor, was used over the NQ to hold this material in place. Consequently, both this air sweep and the dusty nature of the NQ required wet separators for both pollution control and safety. In lieu of the original system just described, a zipper belt conveyor was designed for this application. The zipper conveyor, a patented commercial design, encloses the NQ in separated pulses by a "locking" mechanism at the input end in the Chemical Preparation Building.

At the GLC end, the "locked" conveyor is opened to discharge the NQ. The zipper conveyor therefore eliminated the need for the bucket conveyors and the air sweep and greatly reduced the pollution abatement requirements at the GLC.

Advantages of CAMBL versus the Batch Facility

The CAMBL facility will have many advantages, compared to the present batch operation in the areas of readiness, safety, OSHA and EPA requirements; process control and product quality, changing performance and regulatory requirements and operating costs.

Readiness

The ability to hire qualified labor (managerial, technical and blue collar) to move from a cold base to production status is generally the critical item over procurement of materials and components. The existing batch process requires 230 personnel as compared to only 35 for the CAMBL in the critical areas of mixing, extruding and cutting.

The above noted critical areas for batch operations are substantially more sensitive to acquired skills and judgments for operation, safety and the manufacture of a quality product. For example, operators acquire the experience to judge when, by visual or manual inspection of the in-process propellant, additional solvents must be added to the mixer, when and how the mixer is scraped down, when the mix cycle is complete, how much to adjust the feed rates on the press, etc. These skills have no counterpart in industry and, in a cold base, would be difficult or timely to acquire. Today's labor force, alerted by OSHA regulations, is becoming increasingly sensitive to the working environment. This could cause resistance to acquiring the needed labor force for the existing batch process due to its more hostile environment of nitroglycerin and solvent fumes. This environment is substantially reduced on the CAMBL due to its "closed" condition and limited manual operations.

On the CAMBL, the operating procedures, process control parameters, "cause-effect" relationships, etc, are programmed from prior facility operations. The stored program is immediately available on start-up from a cold base.

Safety, OSHA and EPA Requirements

The CAMBL facility incorporates the latest safety requirements for facility design, contains less in-process materials and more controls to reduce probability of a

catastrophic incident. The existing batch green line area, the area of most likely incident, was constructed in the 1940's and uses wood construction and 12 inch substantial dividing walls separating explosive quantities up to 625 pounds. These design features would not be permitted by today's safety requirements if these buildings were constructed from the ground up.

On the CAMBL facility, thorough hazard analysis of equipment designs has minimized the potential for initiation of materials in process. A dedicated process controller, programmed for shutdown before process parameters exceed fixed limits, greatly reduces the possibility of a "runaway reaction" which could result in a catastrophic incident. Full coverage by fast-acting deluge systems minimizes potential damage resulting from initiation by quenching fires quickly.

The continuous mixer contains less than 100 pounds of material versus 625 pounds for a batch sigma blade mixer. The continuous screw extruder contains only 10 pounds versus 120 pounds in the batch RAM press. Blocking, a potentially hazardous operation, is eliminated. Thus, the potential damage resulting from a catastrophic incident is reduced, with less loss or production.

The facility requires substantially less operating and supervision of pre-mixing, mixing, blocking, pressing, cutting and traying. Not only have the in-process quantities been substantially reduced, but the operator exposure on the CAMBL facility occurs during cleanup operations, when quantities are minimal and the potential for an explosion, rather than a fire, is virtually eliminated.

The CAMBL facility presents a "closed system" of equipment and substantial reduction in manual handling operations, greatly reducing the chance of contamination by foreign materials. Metal detectors, which will stop the equipment if activated, are provided at the most critical spot, the feeds to the extruders.

The CAMBL facility is controlled by a dedicated process controller which precludes those type of accidents that are caused by operator error. The process controller has pre-established limits for every control loop to prevent the operator from changing a setpoint at a level that could result in a hazardous situation.

Process Control and Product Quality

As in all chemical processes, environmental control, including temperature, pressure and humidity is essential for production output and production uniformity. The CAMBL facility, with dedicated process controller, permits a continuous flow of propellant between each green line operation without the holding periods or fluctuations in environment which are associated with the greater, exposed distances on the existing batch facility.

Any significant change in the process cannot be implemented without being authorized and programmed into the process controller. This eliminates unauthorized process variations being introduced by operators or supervisors on their own initiative.

The dedicated process controller with its alarm functions and ability for self-diagnostics, allows immediate notification of equipment failure so that redundant systems can be activated or monitored or repairs effected. Continuous control on the facility, by a dedicated process controller, does not rely on operator training, experience, judgment or frailty. Tolerance control and product uniformity are increased by holding the process within preset limits.

Since the automated process is designed to operate within close, preset tolerances, the production of scrap or rework material, a source of process variability and contamination on the existing batch line, is substantially reduced.

Changing Performance and Regulatory Requirements

The ability of the production base to meet expansion requirements for cannon propellants is severely limited. The only other existing batch line, at Sunflower AAP, was constructed in 1940, was modified to produce multi-base propellant in the 1950's and has been laid-away (along with support facilities) since 1958. The cost to rehabilitate this batch line, modernize a support facility and reactivate remaining support facilities, is in excess of $90 million. After investments to rehabilitate Sunflower AAP's batch line, the process would still represent a 1940 technology, labor intensive production capability without the offsetting benefits of the CAMBL facility.

Additionally, the trend in safety requirements has been for less operator and equipment exposures (category protection), more substantial construction (TM walls) and increased considerations of hardening for survivability. These trends, as well as more stringent requirements, can be anticipated in the future. The CAMBL facility being designed and constructed in accordance with the latest safety requirements, increased controls to reduce probability of catastrophic incident and reduced personnel requirements, is more suitable to meet future requirements.

OSHA, as well as State laws, are becoming stricter and are encompassing more materials. For example, OSHA is evaluating and setting new exposure limits for nitroglycerin and acetone. CAMBL's remote operation of the green line area represents substantial improvement in this regard and reduces the impact of further tightening of OSHA requirements.

As new weapon systems are developed or old systems improved, more stringent performance requirments can be placed on the propellant. Examples include both increased bulk density to improve shell loading and decreased temperature or pressure coefficients to improve characteristics at environmental extremes. The CAMBL facility is more adaptable than the existing batch to emerging performance requirements by its design of the green line complex as a "closed system" controlled by a dedicated process controller.

The facility, representing 1980 design and technology as compared to the existing batch 1940 design and technology is more adapatable to emerging technologies in

equipment and process controls during the next three decades. The technology of our production base will parallel, rather than lag, that of industry. The CAMBL facility parallels industry's lead to change from older operator dependent batch operations to continuous and more automated processes.

Operating Cost

A cost savings of $152/1000 pounds of propellant will accrue to CAMBL due to its significant reduction in direct high exposure labor as compared to that of the present batch line. These savings are equivalent to $365,000/month ($4.4 million/year) at full capacity. Intraplant transportation cost savings, included in the $152/1000 pound, are obtained by the elimination of material handling and trucking of ingredients and propellants. Material and labor savings would also accrue on the CAMBL due to substantial reduction of scrap or rework material.

Quantifiable Project Benefits

In conclusion, construction of $2.4 million pound/month CAMBL at Radford AAP, an active plant, will increase the Army's multi-base cannon propellant capability by 160% and will offer an expanded hot base for unexpected surge or mobilization requirements.

Personnel exposure to hazardous operations will be significantly reduced. A reduction of 56% will occur for the full workforce. However, a more dramatic reduction from 320 to 35 people, or 86% will occur in the direct labor for the most hazardous operations.

The quantities of hazardous materials in each operation are also significantly reduced. The three operations listed in this chart are key examples. The batch operations require manual charging or discharging of large quantities of propellant. Conversely, the CAMBL operation is automated and has much less propellant in residence. Furthermore, the CAMBL green line complex (Nitrocellulose, Thermal Dehydration, Premixer, Mixer, Extruder and Cutter) is sited per safety quantity-distance requirements.

Last but not least, the cost/pound of propellant is reduced by 10% or $152/1000 pounds ($4.4 million/year) at full capacity.

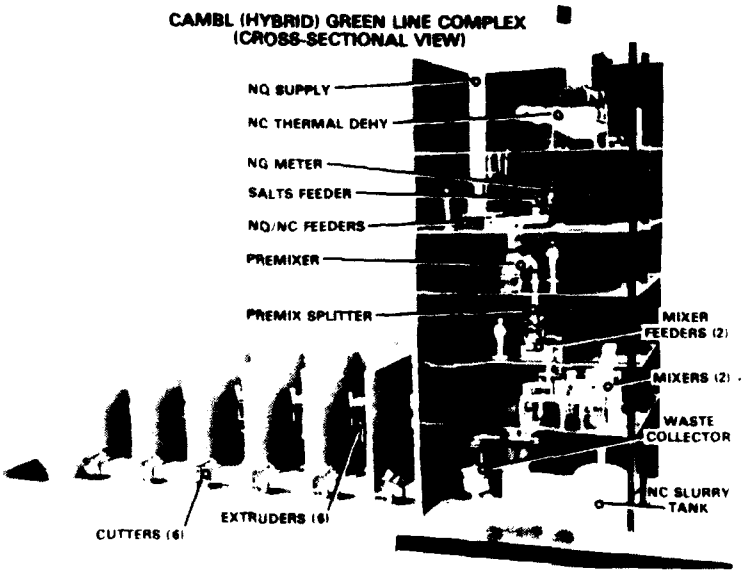

FIGURE 1

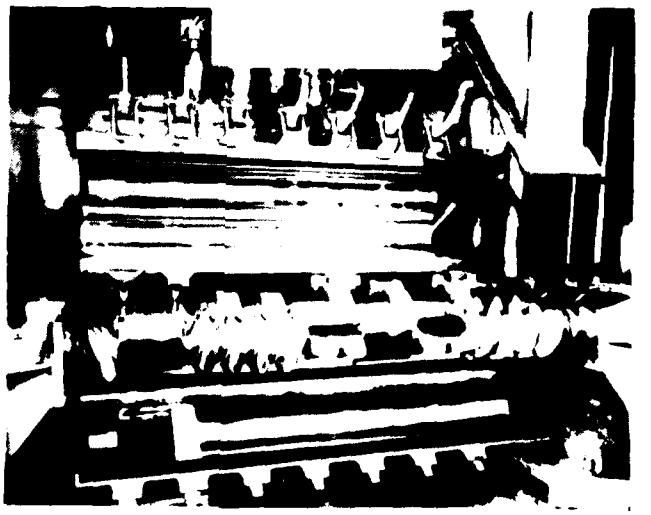

FIGURE 2

CRYSTAL GROWTH

IN

GROUND HMX, RDX AND TAGN

by

Capt D.C. Mann and SSgt A.D. Crews

United States Air Force Armament Laboratory

Eglin Air Force Base, Florida

Presented To

AMERICAN DEFENSE PREPAREDNESS ASSOCIATION

MATERIALS AND PROCESSES DIVISION JOINT SYMPOSIUM

COMPATIBILITY/PROCESSING EXPLOSIVES, PROPELLANT AND INGREDIENTS

Albuquerque, New Mexico

May 15 - 17, 1979

TABLE OF CONTENTS

PREFACE

This report is the result of research conducted by the Air Force Armament Laboratory, Armament Development and Test Center, Eglin Air Force Base, Florida, from January 1979 to May 1979.

References to specific manufacturers or supplies of scientific equipment used in this study is for the sole purpose of identification and does not constitute endorsement of these products by the United States Air Force.

The assistance of Captain M. Patrick, Environics Office, USAF Armament Laboratory, Eglin Air Force Base, Florida, who made all of the scanning electron microscope micrographs in this study, is gratefully acknowledged.

ABSTRACT

This is an interim progress report describing work initiated to determine effects that solvents and storage conditions have on ground HMX, RDX and TAGN. Changes in particle size were monitored as these materials were placed in various typical gun propellant processing solvents and storage solvents. The results indicate that ethyl acetate, as a processing solvent, has the least impact on the crystal growth of ground HMX, RDX or TAGN. Ground TAGN particle size changes were monitored during storage in isopropanol for 55 days. Agglomeration of the TAGN particles took place but normal gun propellant mixing operations will break up the agglomerates with little change in particle size weight median from the freshly ground material.

INTRODUCTION

The prime weapon system on the A-10 aircraft is the GAU-8 gun system. This gun system has demonstrated problems in muzzle flash and barrel erosion. Both these problems are functions of the high flame temperatures of the propellants now being used in GAU-8 ammunition. The Air Force is developing advanced nitramine gun propellants with lower flame temperatures and higher impetus levels than the conventional GAU-8 gun propellants. The lower flame temperatures will reduce both the muzzle flash and barrel erosion. The higher impetus levels of these nitramine propellants will provide greater ballistic velocities for improved operational performance of this gun system.

These advanced nitramine gun propellants consist of ground triaminoquadine nitrate (TAGN), and cyclotetramethylene tetranitramine (HMX) or cyclo-1,3,5-trimethylene-2,4,6-trinitramine (RDX), in a nitrocellulose binder system. TAGN, HMX and RDX are crystalline materials which must be ground to rigid specifications before they can effectively be used in gun propellant formulations. Past Air Force Armament Laboratory funded programs(Ref 1&2)have demonstrated that these materials must be ground to particle sizes of less than 10 microns within very narrow size distributions.

These materials are normally ground in two different types of grinder systems for gun propellant use. One is in a Sweco Grinding Mill. The sample material is placed in a "paint shaker" type of vibratory container along with grinding chips and a carrier solvent. Grinding time, chip size and carrier solvent determine the particle size and size distribution of the ground material. The second type is an air jet grinder system manufactured by several companies, the most frequently encountered within the propellant industry is called the Jet-o-mizer. This system introduces the sample into a chamber containing a high velocity air jet. The material is ground against itself with air speed and feed rate determining the final particle size and size distribution. This system requires dry material and uses no solvents. Sweco mills are often used for small scale research and developmental propellant mixes as even the small Jet-o-mizers require a minimum of approximately 25 pounds of material for each grind. Once ground by either method, these materials are known to "cake" or grow together within a short time. This has significant impact on ballistic performance as this crystal growth changes the particle size and the size distribution of the material as it is incorporated into gun propellant. This in turn can have an impact on the combustion properties of the gun propellant. The impact on combustion properties of large particle size changes, but not small changes, has been investigated (Ref 2&3).

This behavior of the ground materials, particularly in the research and development stages, causes problems in lot to lot reproducibility as the material added to the propellant mix may not be of the same particle size or size distribution measured after grinding. Solving these problems by grinding the material just prior to propellant manufacture greatly increases the cost of research, development and production efforts.

This report presents the interim results of current studies to monitor and characterize these changes in particle size and size distributions and their impact on ballistic performance. There are several periods in the life cycle of these ground propellant ingredients where crystal growth and/or agglomeration can take place. Crystal growth is used to describe the growth of an individual crystal or particle from material dissolved in a solvent and being deposited into the surface of the crystal or particle. Agglomeration is used to describe the process where adjoining independent particles are attached to each in some way forming a group or "clump" of two or more particles. These two processes can be occurring simultaneously in a container of ground material, and can actually cause two particles to grow together and become a new single particle.

The first opportunity for crystal growth and/or agglomeration is during grinding. This is of particular significance for the small scale development lots ground in a Sweco mill where the material is exposed to a solvent. Wherever a finely ground material is exposed to a solvent, even atmospheric humidity, there is opportunity for crystal growth. The second opportunity is during storage of the ground material. These materials are stored either dry or in a storage solvent. Storage in a solvent is preferred for safety reasons although it is more expensive. A third opportunity for crystal growth is during propellant mixing where these ground materials are exposed to the gun propellant processing solvents.

The first stage of this program was to examine ground material already on hand for crystal growth and to review scanning electron microscope (SEM) micrographs, also on hand, of ground material and finished gun propellants. This was done to build a comparative data base and to suggest possible fruitful areas and methods of investigation. The next step was to monitor the changes in particle size and size distribution in the time periods of possible crystal growth and/or agglomeration mentioned above. The last step of this program is to evaluate the effect of these changes on the ballistic performance of finished gun propellants. This report presents the results of monitoring the particle size changes of TAGN, HMX and RDX during processing operations.

Presented in this interim report are the initial results of a series of experiments to evaluate the effects of solvents on the crystal growth rates of these materials. To evaluate the effect of processing solvents encountered during propellant manufacture, ground TAGN, HMX, and RDX were placed in various standard processing solvent systems. As an initial evaluation of the life cycle of these ground materials a TAGN sample was monitored from grinding through 55 days storage in a storage solvent commonly used for TAGN. Work is continuing on this program and every effort will be made to make this data available to the propellant community in a timely manner.

METHODS AND MATERIALS

A. Preliminary Investigations

A preliminary investigation was performed by analyzing Scanning Electron Microscope (SEM) micrographs of ground TAGN and HMX that had been in storage for various time periods under solvent wet and dry storage conditions. SEM micrographs were also analyzed of finished gun propellants that contained ground TAGN and HMX.

The samples for SEM analysis were placed on colloidal graphite coated aluminum stubs and coated with 100% gold in an International Scientific Instrument PS-2 Sputter Coater. The ground TAGN and HMX were placed directly onto the stubs prior to gold coating. The gun propellant samples were prepared by first fracturing gun propellant grains with a razor blade at ambient temperature, then placing the propellant fragment onto the stub with the fractured surface face up. The samples were then examined in an International Scientific Instrument Super III A Scanning Electron Microscope at an acceleration voltage of 15 kV.

B. Particle Size Studies

The particle size studies can be divided into two major categories; Process Solvent Effects and TAGN Crystal Growth During Storage. These categories will be presented separately below.

A Quantimet Image Analyzer (QIA) was used to determine the particle sizes and size distribution of the samples evaluated. This computerized system is a new addition to the Air Force Armament Laboratory Propellant Formulation Laboratory.

As the QIA is a new sizing technique, a brief discussion of its operation is given. The QIA uses an optical microscope coupled through a high resolution vidicon camera tube to a data processing control console and computer. Samples are prepared on microscope slides and scanned by the vidicon camera. The microscopic image is converted to a series of light and dark (gray level) picture points. Adjacent picture points of differing gray level define a boundary. This information is passed through the control console and processed by a digital computer. The systen can provide reliable particle size data with three separate scans per slide within thirty minutes. The QIA records the number of particles, or defined boundary features, and the size of these features. All other data outputs are generated from this basic feature number and size data.

The QIA uses the control console to provide real-time observation of the particle being scanned and control of the data being evaluated. The QIA can measure virtually any feature, however, the one selected is the longest vertical chord (Feret diameter) of the particle detected. By controlling the gray level, minimum and maximum particle size accepted, type of particle shape, contours acceptable, and the degree a given particle deviates from a perfect sphere, the QIA can reduce data deviations due to odd shapes and particle agglomerates while providing a data display of each feature scanned and accepted. This provides the operator a great deal of flexibility in determining exactly the type and quality of the data produced. These features provide a significant advantage over other systems that must depend upon solvent dispersion techniques to limit errors due to nonspherical particles and particle agglomerates.

The QIA scans all detectable features in the field of view and compares the data generated with the variable input control parameters prior to final data processing. The scan during the tests being reported was limited to 3000 features. The QIA scans the first 3000 features detected in each run. Should one-third of these features be nonselected by the variable control parameters, the final data products will be from 2000 acceptable features detected. The data output is displayed as a histogram of the number of particles at each given size range. Calculated from the histogram and also output are the number mean, weight mean, number median and weight median. (The number mean is defined as the average particle size of the sample which the QIA has accepted as valid features. The number median is that particle size where 50% of the particles are smaller than that size. The weight mean is calculated from the number mean and defines the particle size which contains an average of the weight of all the particles accepted as valid features. The weight median is that particle size where 50% of the weight of the sample is contained in particles less than that size.) The histogram data is also input manually into a Hewlett-Packard 9830 calculator, plotter to produce a semilog plot of the cumulative percent of the total sample versus micron diameter.

The system does have some limitations that must be considered before the data can be properly interpreted and evaluated. The system has a depth of focus limitation due to the optical limitation of the microscope. This is reduced by using the lowest magnification required to scan the sample and, when possible, avoiding large particle size distributions. Another limitation of the system is the sample selection technique and dispersion of the sample on the microscope slide. Care must be taken to insure a truly representative sample is used. This is especially significant as small particles tend to demonstrate large static effects, especially in particles below 1 micron in diameter.

Another limitation is sample dispersion on the microscope slide. This is critical as the QIA must be shown a representative selection of the whole sample within the 3000 feature scanning limit. A new program is being written to open the scanning limit to 10,000 features. Solvents and wetting agents are used to reduce particle agglomeration and to achieve a uniform, representative distribution over the slide. Care must be exercised as the larger particles tend to settle out of the dispersion medium very rapidly. This effect is reduced by placing several small samples on a single slide rather than one large sample, and swirling these samples together in a uniform manner over the entire surface of the microscope slide. To avoid bubbles being included in the features detected, the slides are scanned dry with the dispersing medium removed by evaporation. The sample must be insoluble in this medium to avoid errors due to sample solvation and subsequent recrystallization upon solvent evaporation.

1. Process Solvent Effects

The effect of standard gun propellant processing solvents on ground HMX, RDX and TAGN was evaluated in the following manner. Small samples of each ground material were placed in various processing solvents for six days. While these materials would normally be exposed to the processing solvents for less than one day, the test period was extended to six days in the hope that minor trends or differences would show up with the longer time period. All the samples had been ground in a Sweco Grinding Mill and were then placed in storage for at least 30 days. The test samples were stored in the following solvent systems: ethyl acetate/acetone (2:1); ethyl alcohol/acetone (2:1); and ethyl alcohol/ ethyl acetate (2:1). The solvent level was approximately 1/4" above the sample level. One container for each material was kept dry as a control. Samples were stored in a laboratory and kept at 25°C for six days.

The sample preparation for the QIA was modified from the JANNAF MSA sample preparation method (Ref. 4). One drop of Tween 80 and 0.1 cc sample of the material to be used were placed on a glass plate and mixed. The mixture was then placed in a five milliliter test tube with heptane, shaken, and placed in an Electromation Components Corporation, Model 77 Ultrasonic Bath for two minutes. The sample was removed from the ultrasonic bath and shaken again. A micropipette was used to place and disperse the samples on a clean microscope slide. This procedure was used to obtain all the data presented in this report.

Each slide was scanned three times and each data point presented is the mean of those three scans. With this sample preparation technique for TAGN the number means and medians were equal to or less than $\pm 3\%$ and the weight medians and mean were approximately $\pm 15\%$. The weight mean

and median are calculated from the total number distribution. The weight median can be altered significantly by the incorporation of only one or two large particles in each scan. The weight medians are presented in this report as they are the conventional way of presenting particle size data generated from other sizing techniques. The difference between the number median and weight median can be considered as a measure of the size dispersion in the sample. However, such comparisons must be made with caution.

2. TAGN Crystal Growth During Storage

To determine the crystal growth of TAGN during storage, one lot of TAGN was monitored from grinding to storage after 55 days in isopropanol at 25°C. Isopropanol was chosen as it is used by several laboratories as a Sweco carrier solvent and as a long term storage solvent for TAGN. The TAGN was ground for six hours in isopropanol in a Sweco Mill. Samples were taken during the grinding operation to monitor the effects of grinding time on particle size. The sample taken after five hours of grinding (labeled 5HG) was then monitored for particle size changes within the first 80 hours after grinding. The lid for this container was not properly sealed and the sample dried out. Work with sample 5HG was terminated. The particle size of the four hour grind (4HG) sample was then monitored for storage effects during 55 days of storage in isopropanol.

RESULTS AND DISCUSSION

A. Preliminary Investigations

The results of the preliminary investigation is seen in the following SEM micrographs. The SEM micrographs in Figures 1 and 2 (see note below) show the bridging that typically occurs in these materials. Figure 1 shows crystal growth of TAGN within one week of grinding. Figure 2 shows TAGN that has been in outside storage for three months. Both samples were stored dry with an ambient temperature of 20°C. Figure 3 shows TAGN that has been ground for one hour in a Sweco Grinding Mill in isopropanol. The material has the appearance of "ground glass" with no bridging between particles. Note that these particles are not spherical but possess numerous irregular sharp edges. Figure 4 shows ground HMX that has been in storage for six months. This sample was stored dry with no solvent. Notice again the bridging and crystal growth. Figure 5 is a typical SEM micrograph of a HMX-TAGN gun propellant made from ingredients that had been in storage 90 days after grinding. This propellant contains 30% HMX and 45% TAGN in a nitrocellulose binder. Notice the lack of crystal agglomerates or bridges between the individual particles. Also note that the edges of the particles are somewhat rounded compared to Figure 4. Some of the questions generated by these SEM micrographs are: how different are the particle sizes in the finished propellant from the original, fresh ground material; why are agglomerates not seen in the finished propellant; what happens to these crystal "bridges" during propellant mixing; do the processing solvents solvate these materials enough to cause agglomeration during mixing so that several small particles are "welded" into one particle during the mix cycle?

The general lack of agglomerates or crystal bridges in finished propellants suggests that these particle networks are broken up during mixing and that the processing solvents "round off" the broken edges resulting from the fracture of the crystal bridges. This is not unusual

Note. The white bars on the bottom right of the SEM photomicrographs are size markers. The gap between the bars is 0.5 microns and the bar to the right is 5 microns long.

in that most organic materials normally described as insoluble in certain solvents are more accurately described as possessing extremely low solubilities in these solvents. These effects are not normally significant with oxidizers of large particle sizes, but are significant with particles in the micron and submicron ranges. This is of special consideration when the technique of "wicking" is used with the ground ingredients prior to adding these ingredients to the mixer. In wicking the ground particles are wet with the processing solvent for various time periods prior to adding them to the mix. As a result of evaluating this SEM data an in depth investigation of particle agglomeration and crystal growth was initiated.

B. Particle Size Studies

The results of the particle size studies can be divided into two major categories; Process Solvent Effects and TAGN Crystal Growth During Storage. These categories will be discussed separately below.

1. Process Solvent Effects

The results of placing ground HMX, RDX and TAGN in the various gun propellant processing solvent systems are presented and discussed starting with HMX.

Figures 6 and 7 show the change in particle size number median for HMX by day and by solvent system respectively. The significant feature of both these plots is that the particle size did not change significantly in any solvent system. Both figures show that the particle size number median for the dry sample on DAY 3 is a poor data point. Figures 8 and 9 show the particle size weight median by day and solvent system respectively. The weight median plots compared to the number median plots show the typical trend seen in most QIA data where the small changes in the number median plots are magnified in the weight median plots. The relative slope changes seen in the number median plot is the same as in the weight median plots with just the absolute values being different. Both weight median plots again show the DAY 3 dry sample data point to be in error. This was possibly due to poor sample dispersion on the slide. None of these number or weight median plots for HMX show any significant changes in particle size for these solvent systems.

Figures 10 and 11 show the RDX particle size number median change by day and solvent system respectively. The plots in both figures show little change in particle size for any solvent system. The weight median plots for RDX in Figures 12 and 13 are significantly different from the relatively simple RDX number median plots of Figures 10 and 11. This is

attributed to a few large particles in the RDX sample skewing the data. A few large particles will contain a significant percentage of the sample weight and yet may be less than one percent of the number of particles accepted by the QIA as valid features. This data would suggest that there is some crystal growth in both solvent systems containing ethyl acetate. The data from Figure 13 suggests that some crystal growth took place in all the solvent systems when compared to the data for the dry sample. The data is too scattered to make any positive assertions. This data does demonstrate a need for improvement in sample selection and dispersion methods for RDX. This is borne out by the almost two micron range for the dry sample weight median over the six day evaluation period.

Figures 14 and 15 show the change in the TAGN particle size number median by day and solvent system respectively. These plots again show data scatter for the dry control samples. The plot on Figure 14 of the TAGN particle size number median by day readily shows the rapid dissolution of the sample in the ethyl alcohol/acetone solvent system. The plot for the ethyl acetate/acetone system does not show such a rapid rate of particle size reduction. Both samples were completely solvated by DAY 6. These TAGN particle size number median plots show no significant changes for the other solvent systems evaluated. In these figures, as well as in Figures 16 and 17, the data scatter for the dry control sample is evident. Figure 16 shows that both solvent systems containing ethyl acetate had minimal effect on the TAGN. Conversly, the solvation of the TAGN in both systems containing acetone is readily seen in this weight median data as the particle size weight medians are reduced. Figure 17 again shows the stability of the ethyl acetate systems with TAGN.

This processing solvent study does show that the solvent effects for any solvent system are minimal within one day and that ethyl acetate has the least overall effect of any of the solvent systems investigated. The most pronounced event in the data is the total solvation of the TAGN samples in the solvent systems containing acetone.

The results of the data indicate some sample dispersion problems. The weight median dry control samples of each material vary as much as two microns during the six day test period. This is apparently due to the fact that each of the particle samples in solvent were already wet, and when mixed well with the Tween 80 resulted in a good dispersion of the sample in the heptane solvent. The dry materials apparently tended to agglomerate round droplets of Tween 80 when the sample was placed in the heptane rather than dispersing throughout the solvent. Similar results have been noted in subsequent testing and confirmed by visual observations of the prepared slides. While reducing the precision of the study, this effect did not mask major trends. The TAGN in both solvent

systems containing acetone can easily be seen reducing particle size as the samples are solvated.

2. TAGN Crystal Growth During Storage

One lot of TAGN was ground in a Sweco Mill to produce a fresh sample to monitor for crystal growth effects from grinding through storage. Figure 18 shows the results of the grinding time on particle size. After three hours there is no detectable significant change in the particle size with further grinding. Figure 19 shows the results of monitoring the TAGN particle size of the 5HG sample within the first 80 hours after grinding. Again the particle size does not change signifigantly.

Figure 20 shows the results of monitoring the TAGN sample for 55 days in isopropanol. While crystal growth is seen after 55 days, there is no appreciable change in the particle number or weight median. A possible explanation is that the freshly ground material, wet with solvent is coated with a "tacky" outer layer. Individual particles are very close together and are joined together by solvent bridges and possibly electrostatic charge forces. These bridges allow some flow of the crystalized material. Large solvent quantities are not required as this bridging is seen in TAGN ground in a jet pulverizer which uses no solvent. Atmospheric humidity or trace amounts of processing solvent remaining from the manufacture of the material may provide sufficient solvent for crystal growth. These bridges could allow flow of enough material to form additional bridges. As this process continues, a bridge network between all the particles is established. This process continues until a stage such as depicted in Figure 2 is reached. The resulting oblong particles would be somewhat smaller along the horizontal axis due to the movement of materia' used to make the bridge.

Figure 20 shows the change in the number and weight medians for the 4HG TAGN during storage for 55 days. Neither the number nor the weight median changed significantly during this time.

The data from the 55 day old TAGN would suggest that the effective particle size has not changed in the propellant. To test this hypothesis a sample of the 55 day old 4HG TAGN was placed in a test tube and vibrated in an ultrasonic bath for five hours. Figure 21 is the QIA plot of the number and weight medians. The data are also compared on Table 1. Apparently the ultrasonic bath broke up some of these bridges. The weight median is somewhat low but in line with the expected data.

Figures 22 and 23, the QIA number and weight median plots for 4HG on the day ground and after 55 days of storage, show no significant differences between each other on Figure 21. The data in Figure 21 are more scattered than for Figures 22 or 23. This is due to the few large particles, possibly from agglomerates that did not break up in the ultrasonic bath.

One significant problem with this data is determining the size distribution changes occurring during crystal growth. The rule appears to be that the small particles are "welded" onto the larger particles, thus reducing the overall surface area of the sample but having little impact on the weight median. This effect is counterbalanced by the growth of crystal bridges and their resulting fragments when broken during propellant mixing. More accurate techniques will need to be developed to evaluate the degree and significance of these size distribution changes. As particle size distribution effects are crucial to the combustion properties of advanced propellants, work will continue at AFATL to fully define processing solvent interaction with "as ground" and "as mixed" particle sizes.

TABLE 1

4HG TAGN PARTICLE SIZE GROWTH

	DAY 0	DAY 55	DAY 55 - 5 HOURS IN ULTRASONIC BATH
	Microns	Microns	Microns
Wt Mean	4.80	4.34	4.4
Wt Mean	4.05	3.39	2.98
No. Median	2.26	1.70	1.43

CONCLUSIONS

Ethyl acetate has the least solvent effect on ground HMX, RDX or TAGN during propellant manufacture. Ethyl acetate solvent systems should be used in the manufacture of gun propellants containing these ingredients where particle size and size distributions are important considerations.

Crystal growth and agglomeration occurs in ground TAGN stored in isopropanol. The agglomerates formed during storage are broken up during normal gun propellant mixing operations. The agglomeration effects do change the particle size number median, but have little impact on the particle size weight median of the sample.

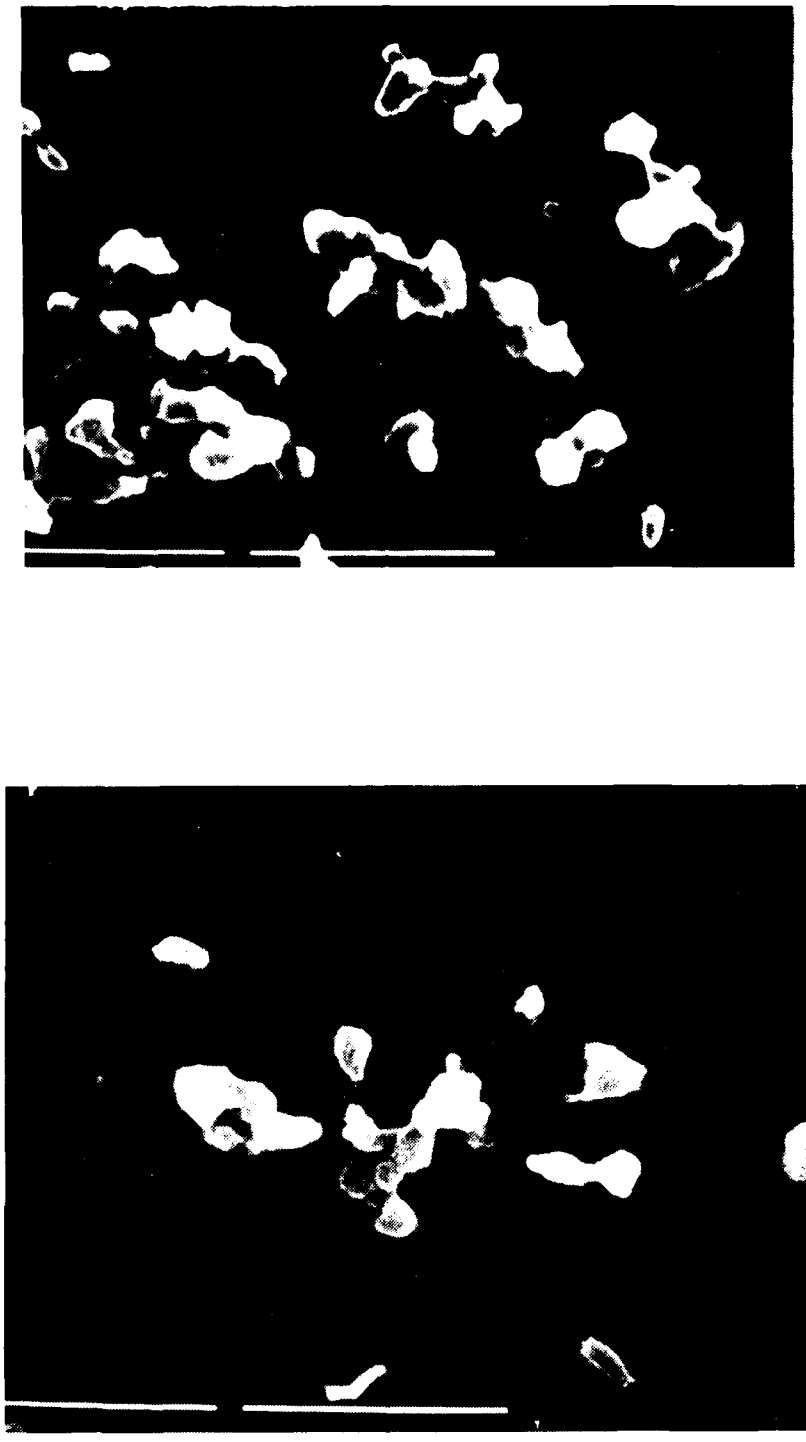

Figure 1. TAGN After One Week Storage in Isopropanol

Figure 2. TAGN Particles Showing Bridge Network

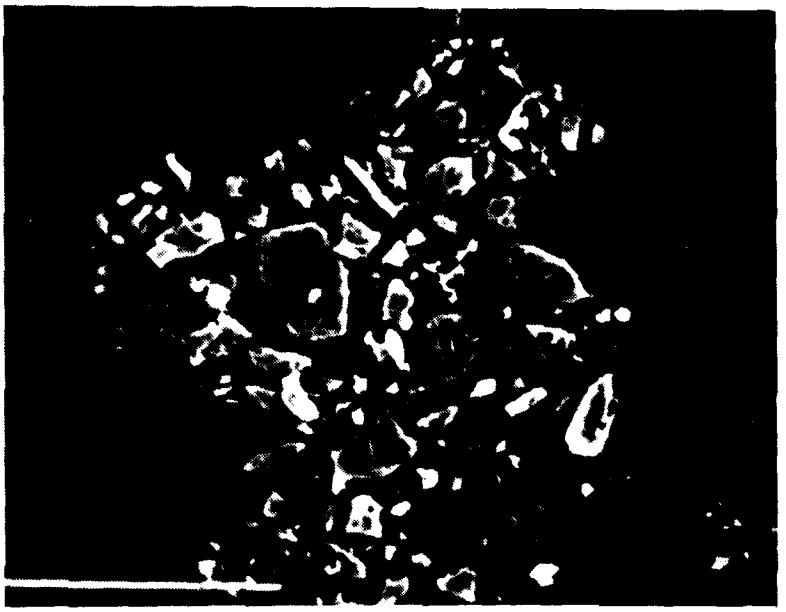

Figure 3. TAGN After Grinding One Hour in a SWECO Fluid Energy Mill with Isopropanol as the Grinding Solvent

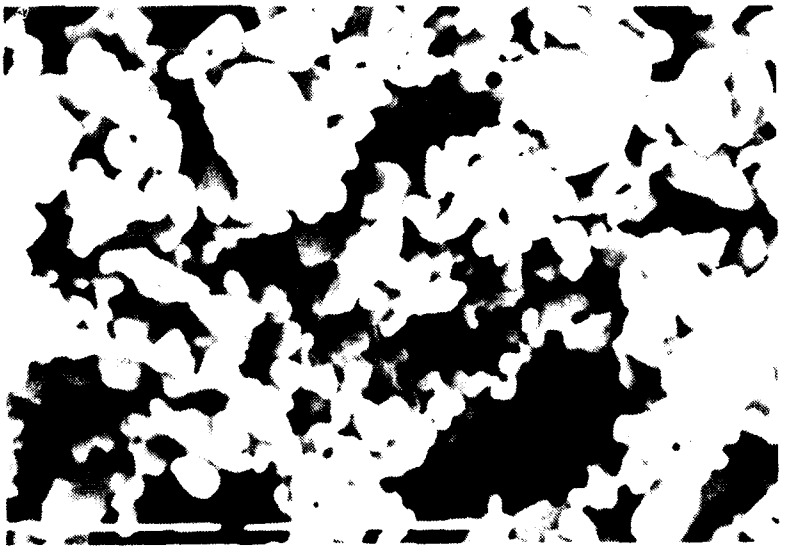

Figure 4. HMX Stored "Dry" After Six Months

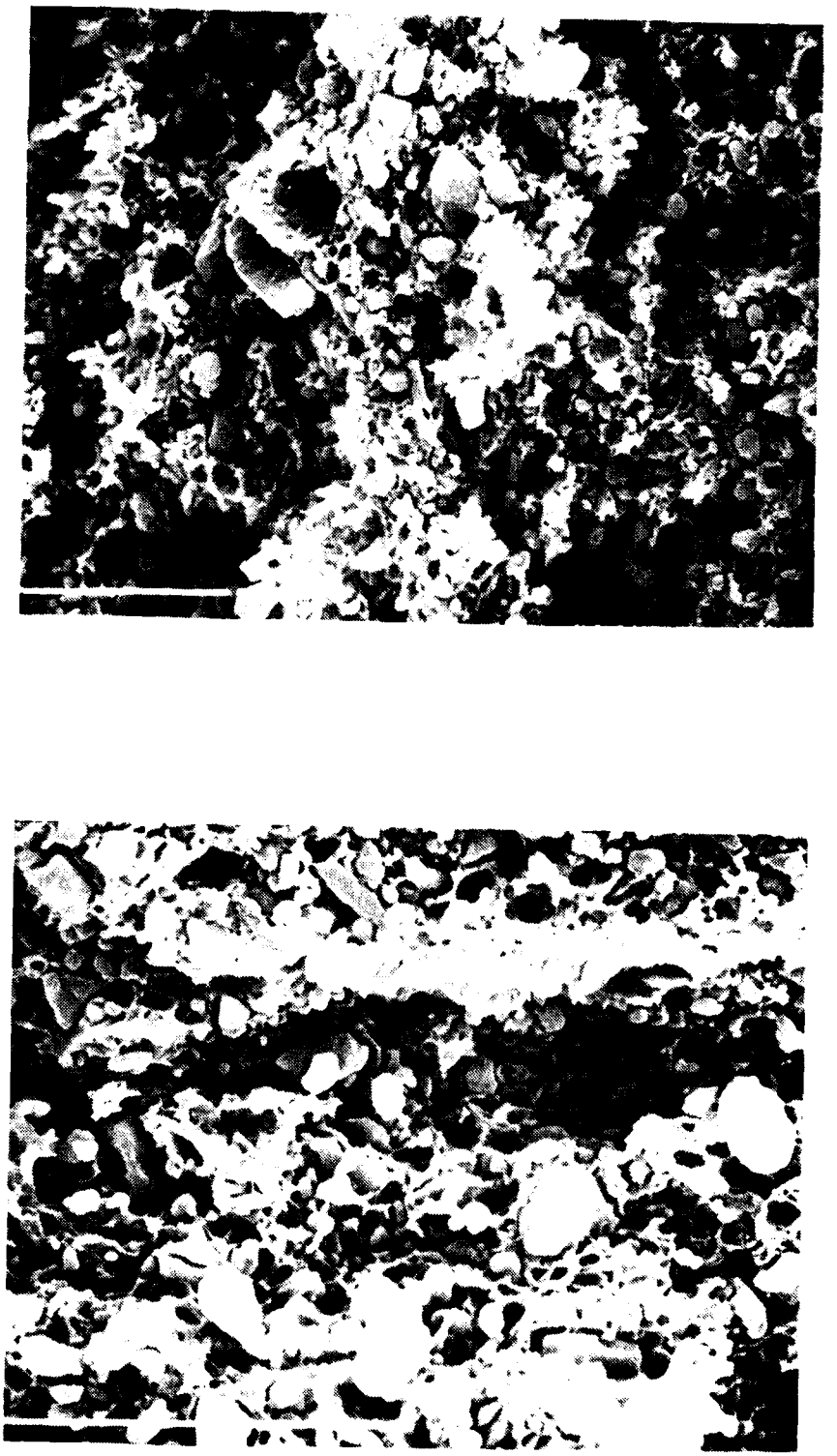

Figure 5. HMX/TAGN/NC Gun Propellant

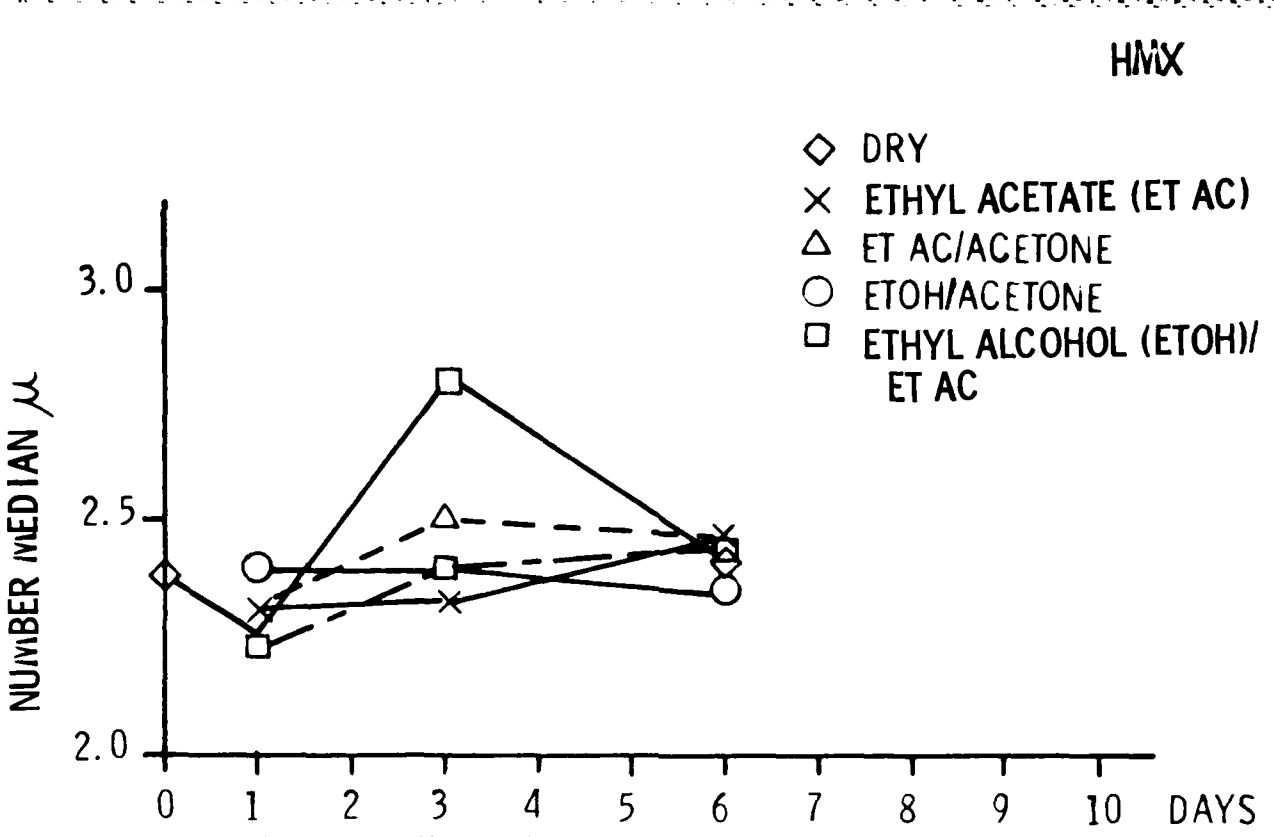

Figure 6. Change in HMX Particle Size Number Median by Day for Various Solvent Systems

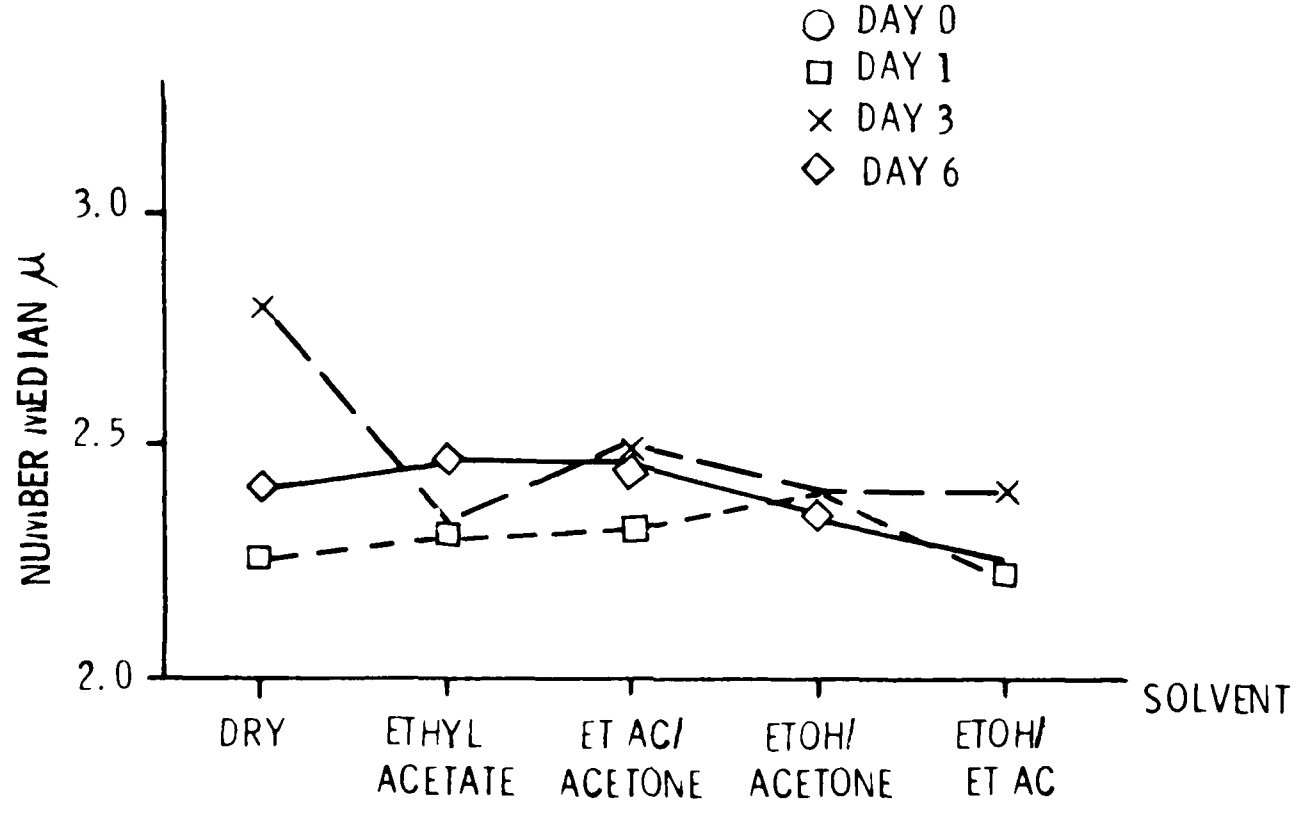

Figure 7. Change in HMX Particle Size Number Median by Solvent System for Each Day Samples were Taken

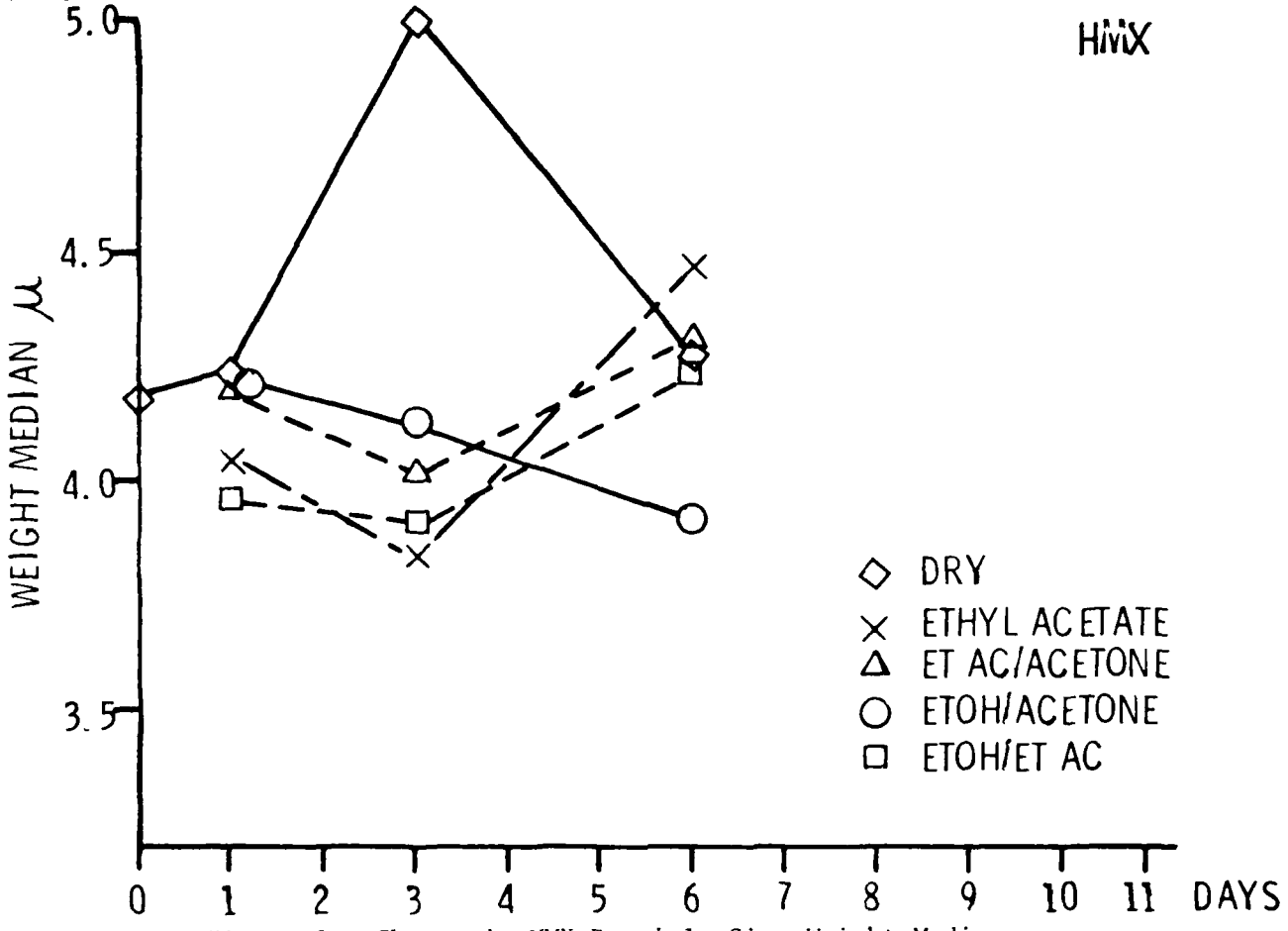

Figure 8. Change in HMX Particle Size Weight Median by Day for Various Solvent Systems

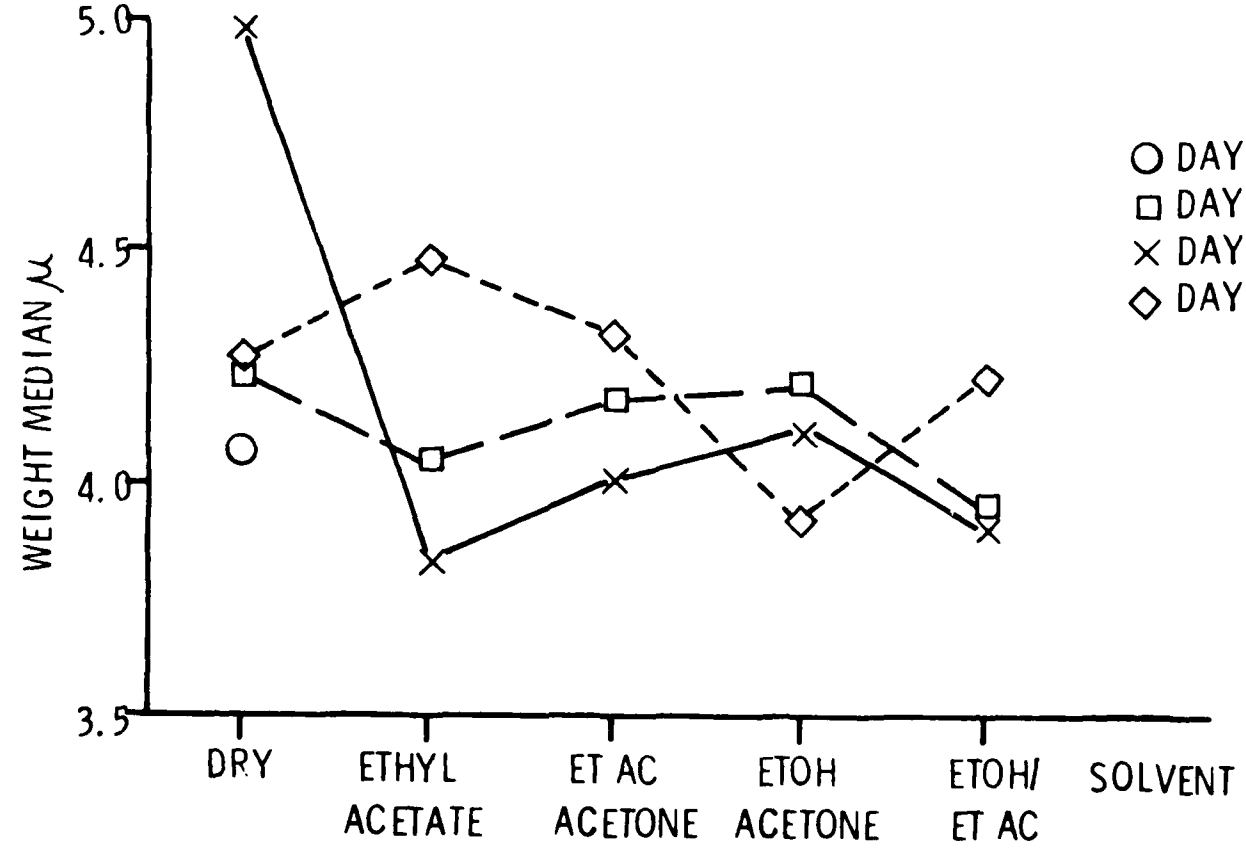

Figure 9. Change in HMX Particle Size Weight Median by Solvent System for Each Day Samples were Taken

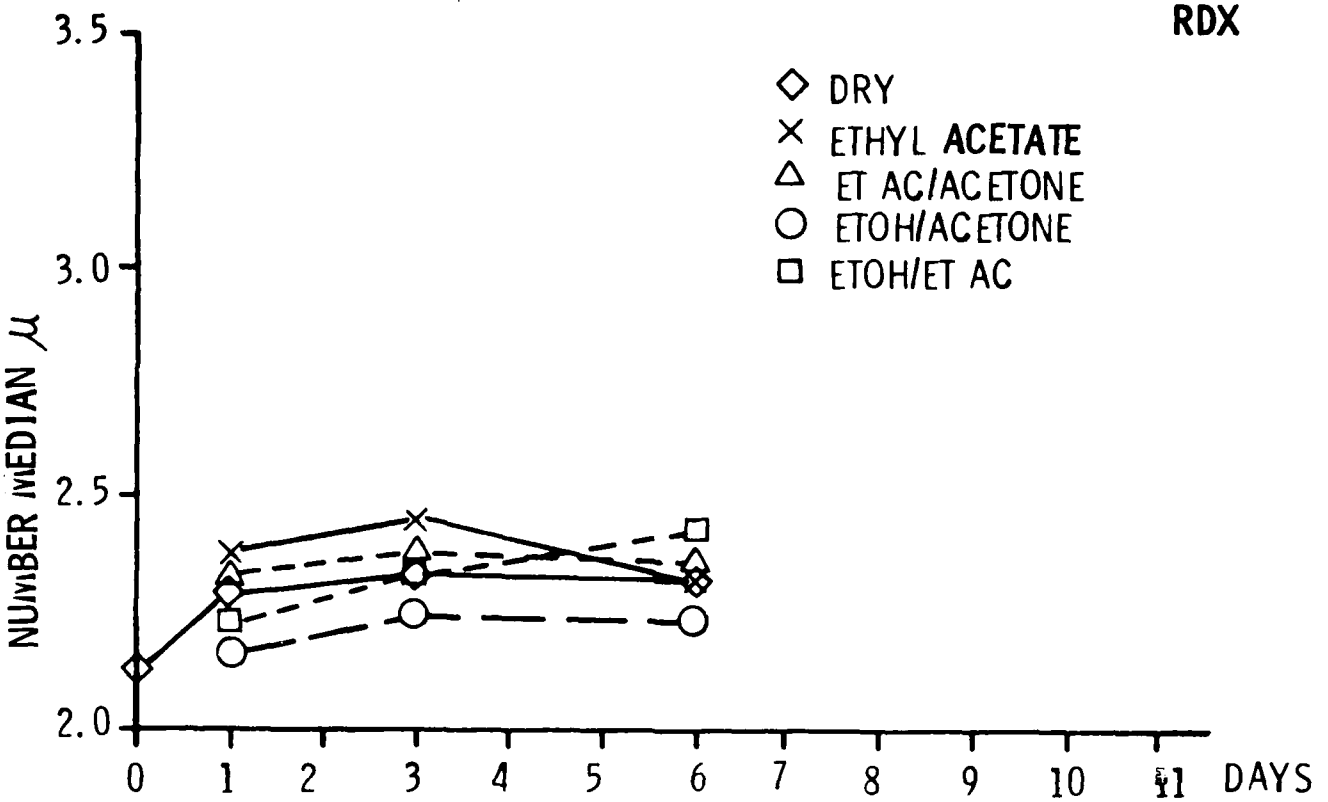

Figure 10. Change in RDX Particle Size Number Median by Day for Various Solvent Systems

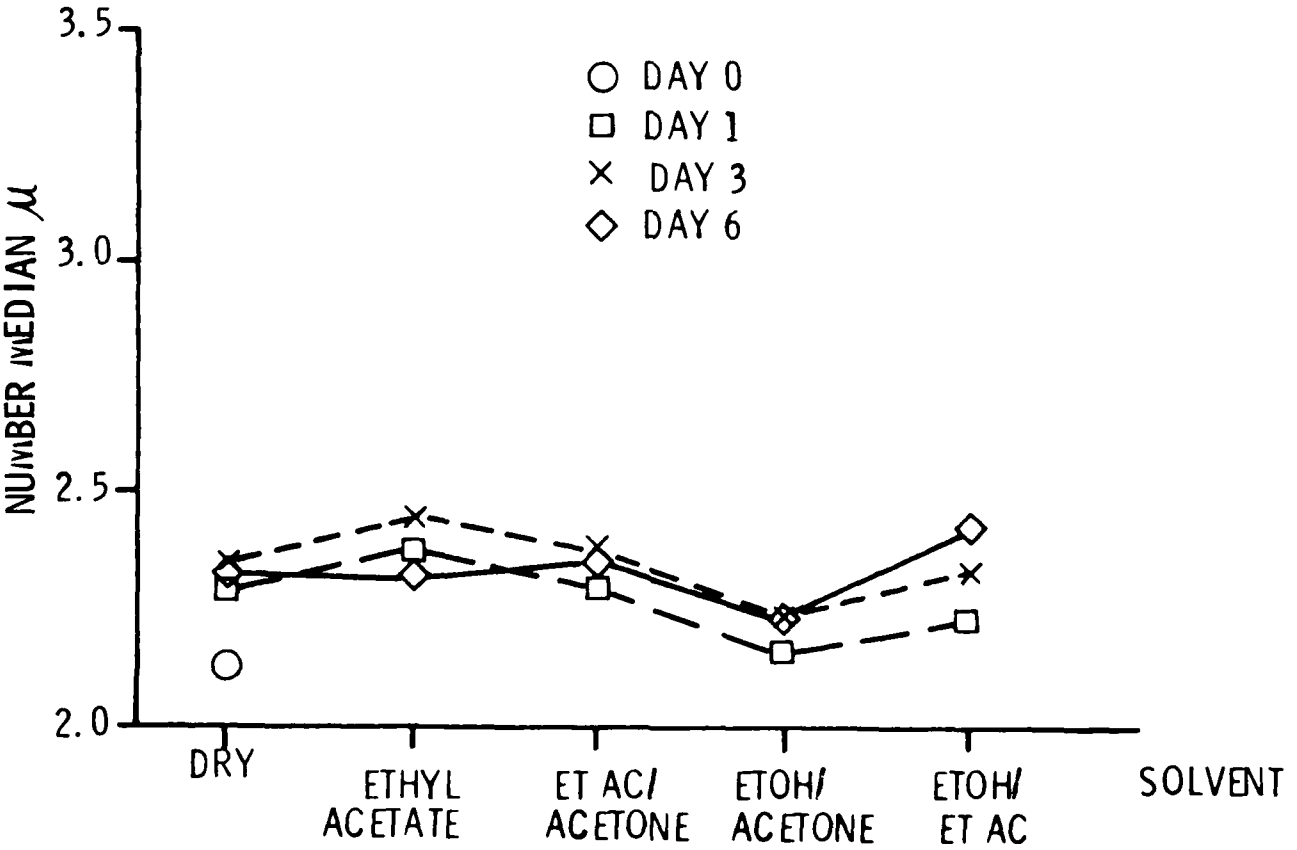

Figure 11. Change in RDX Particle Size Number Median by Solvent System for Each Day Samples were Taken

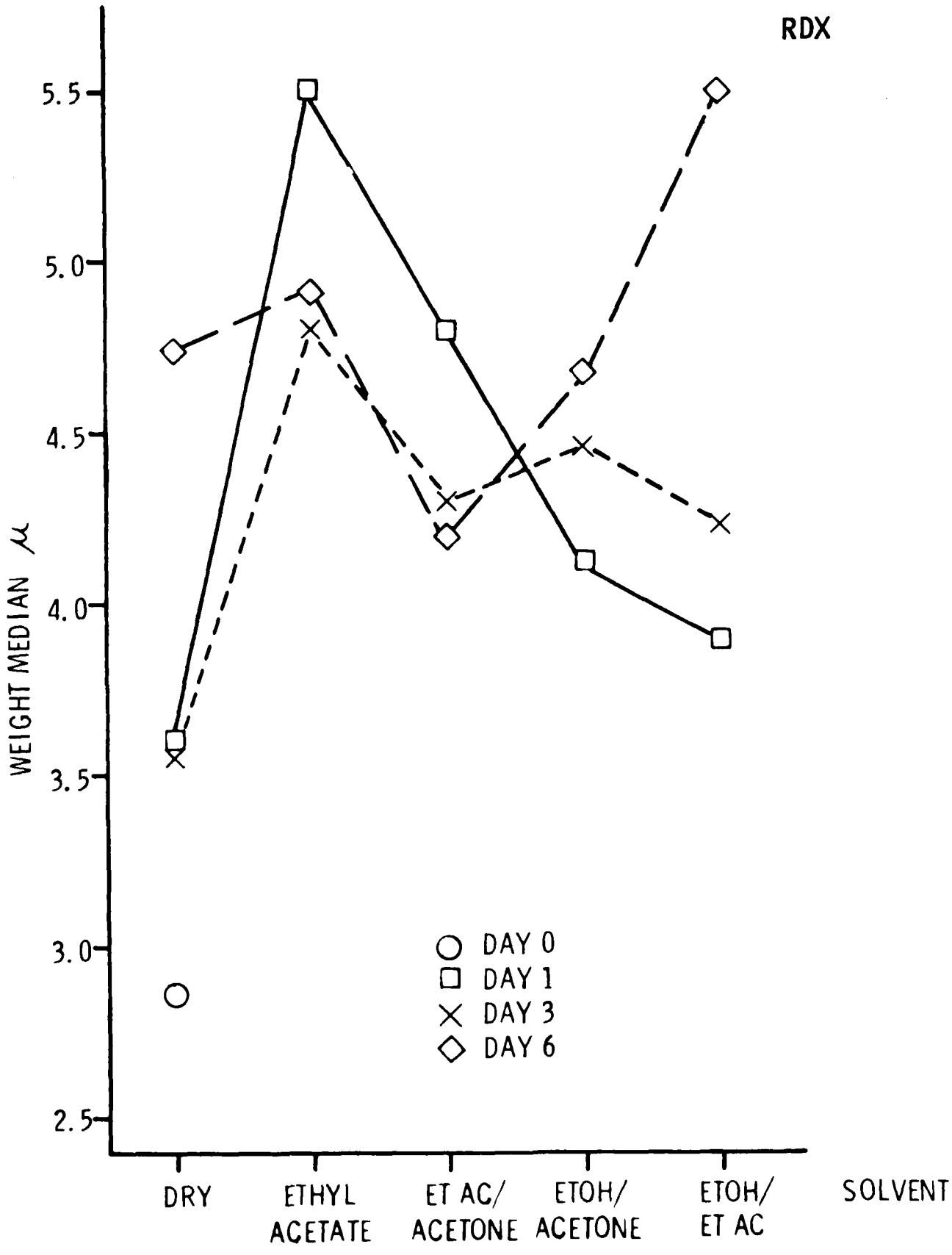

Figure 12. Change in RDX Particle Size Weight Median Solvent System for Each Day Samples were Taken

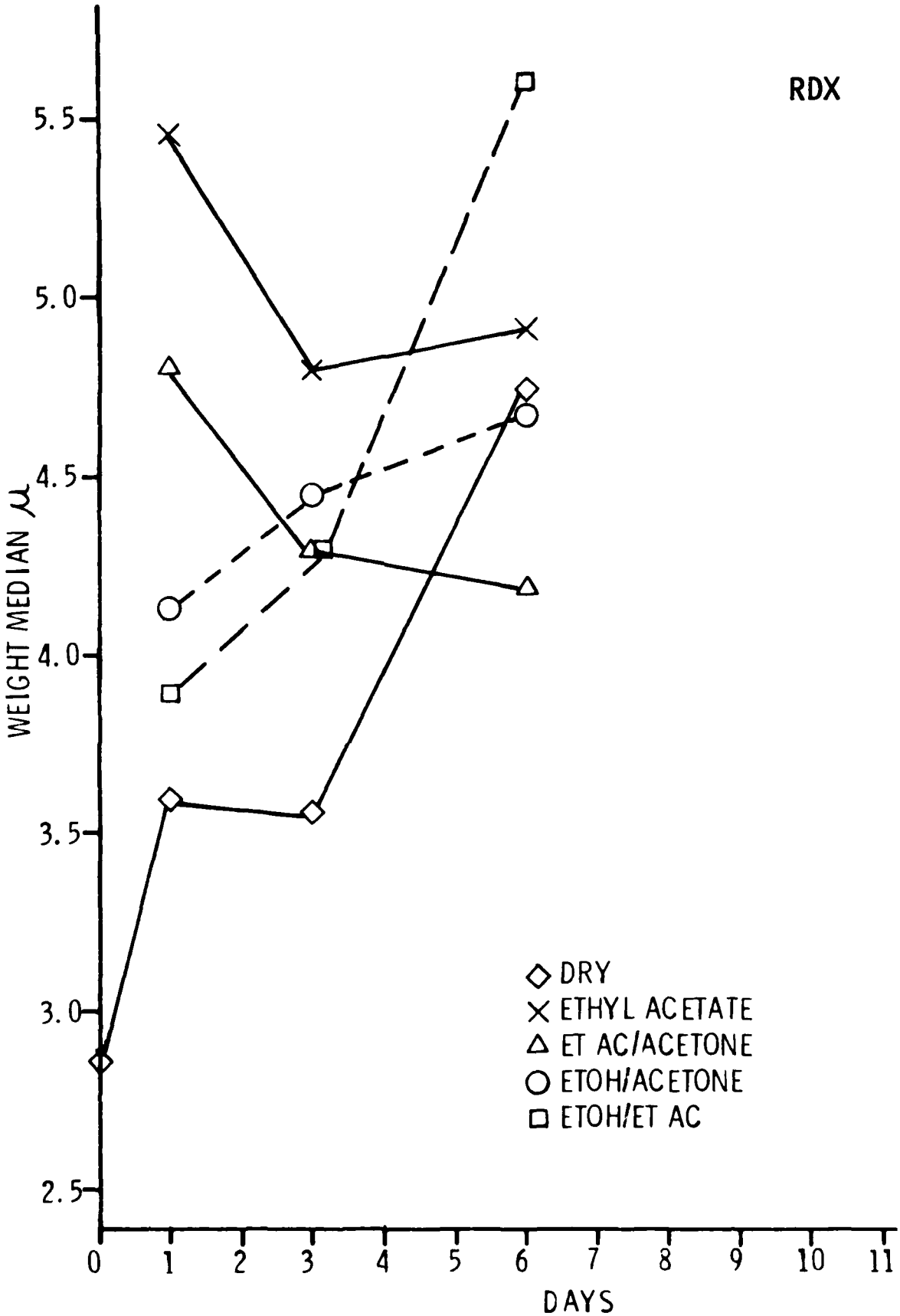

Figure 13. Change in RDX Particle Size Weight Median by Day for Various Solvent Systems

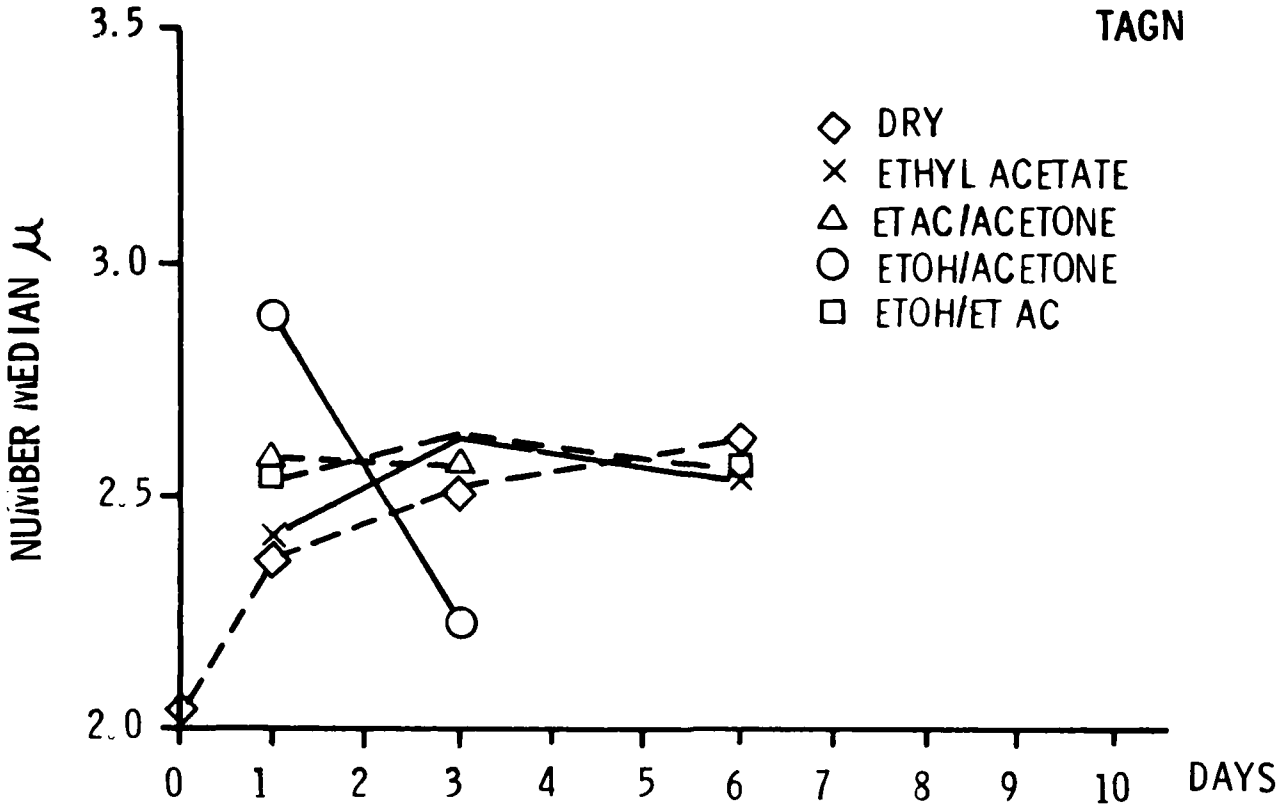

Figure 14. Change in TAGN Particle Size Number Median by Day for Various Solvent Systems

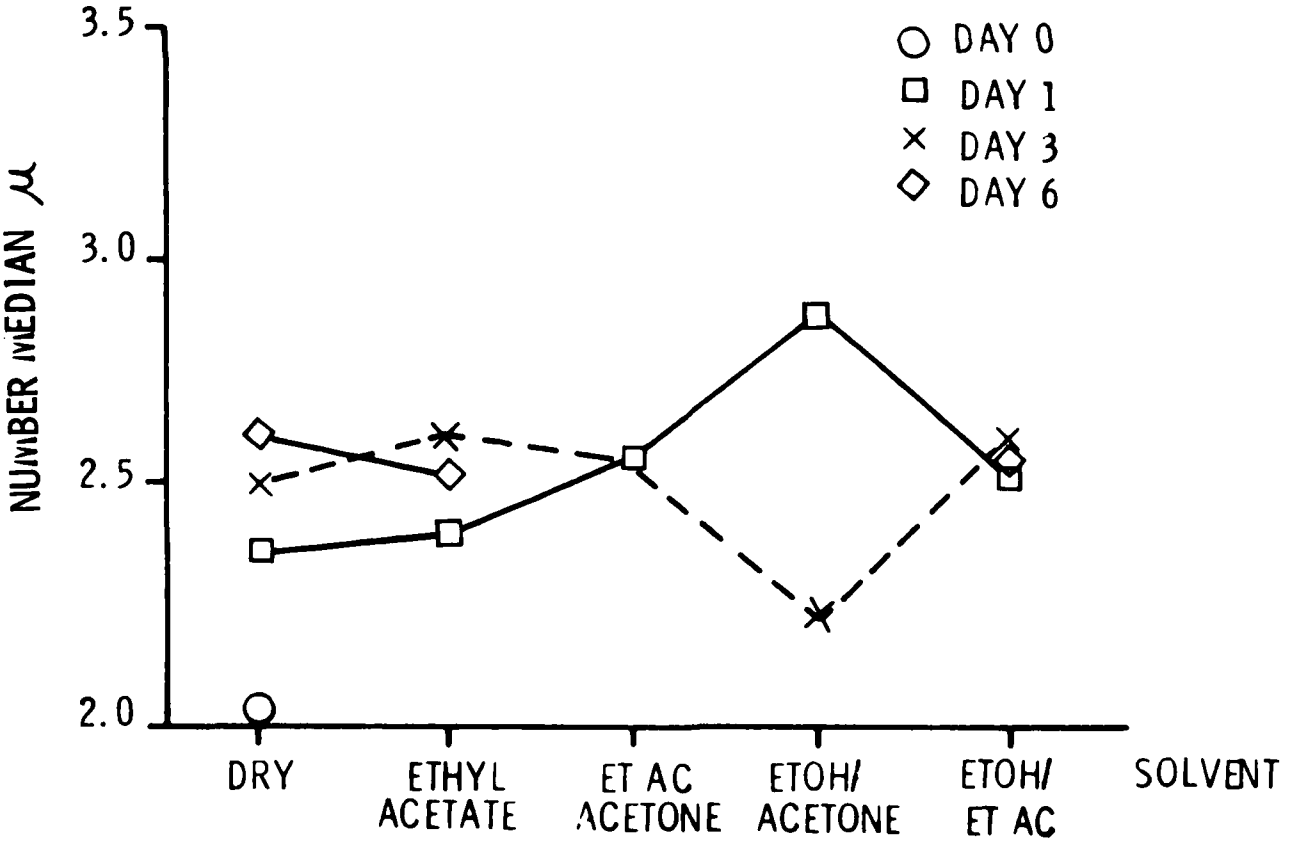

Figure 15. Change in TAGN Particle Size Number Median by Solvent System for Each Day Samples were Taken

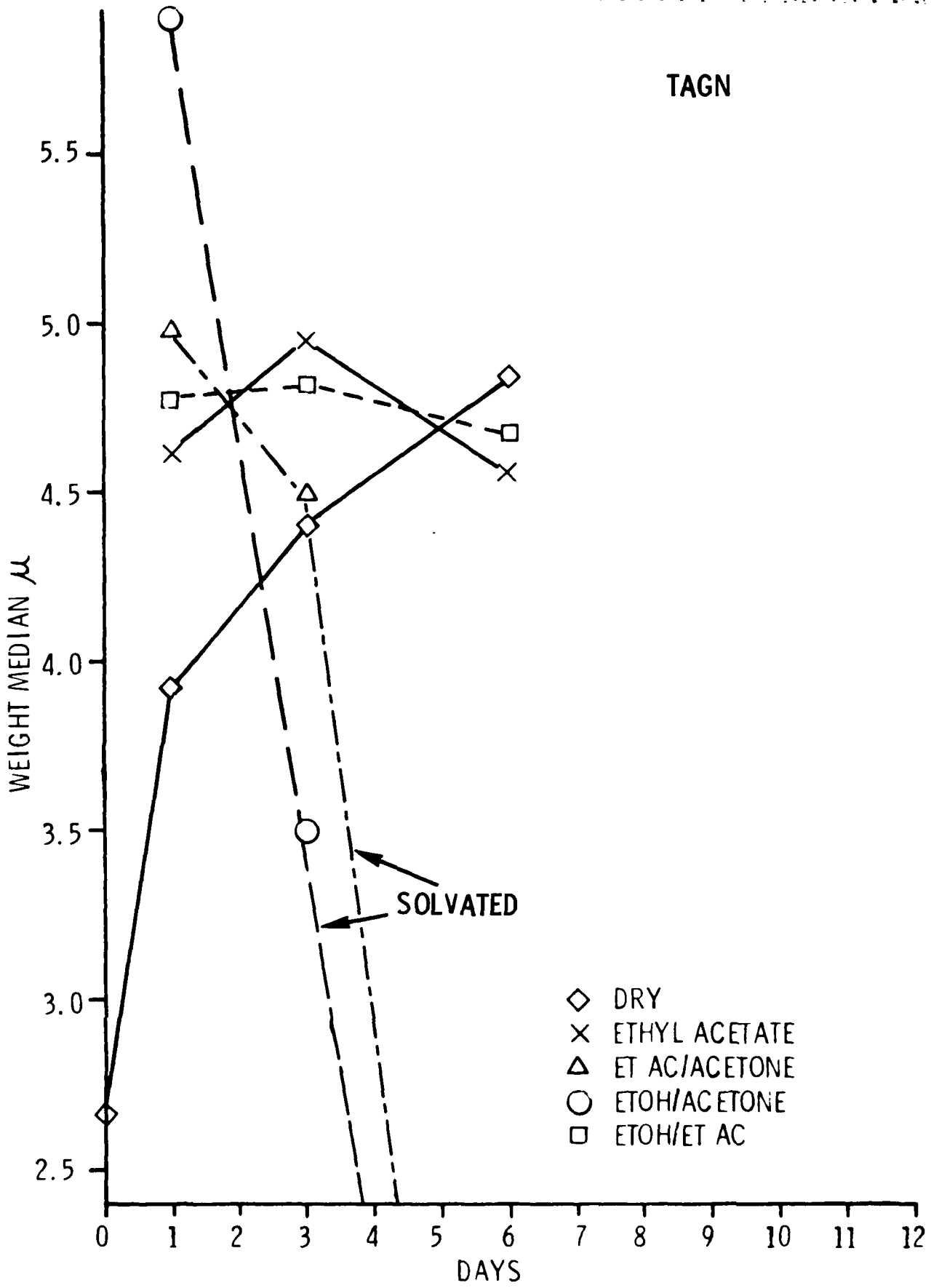

Figure 16. Change in TAGN Particle Size Weight Median by Day for Various Solvent Systems

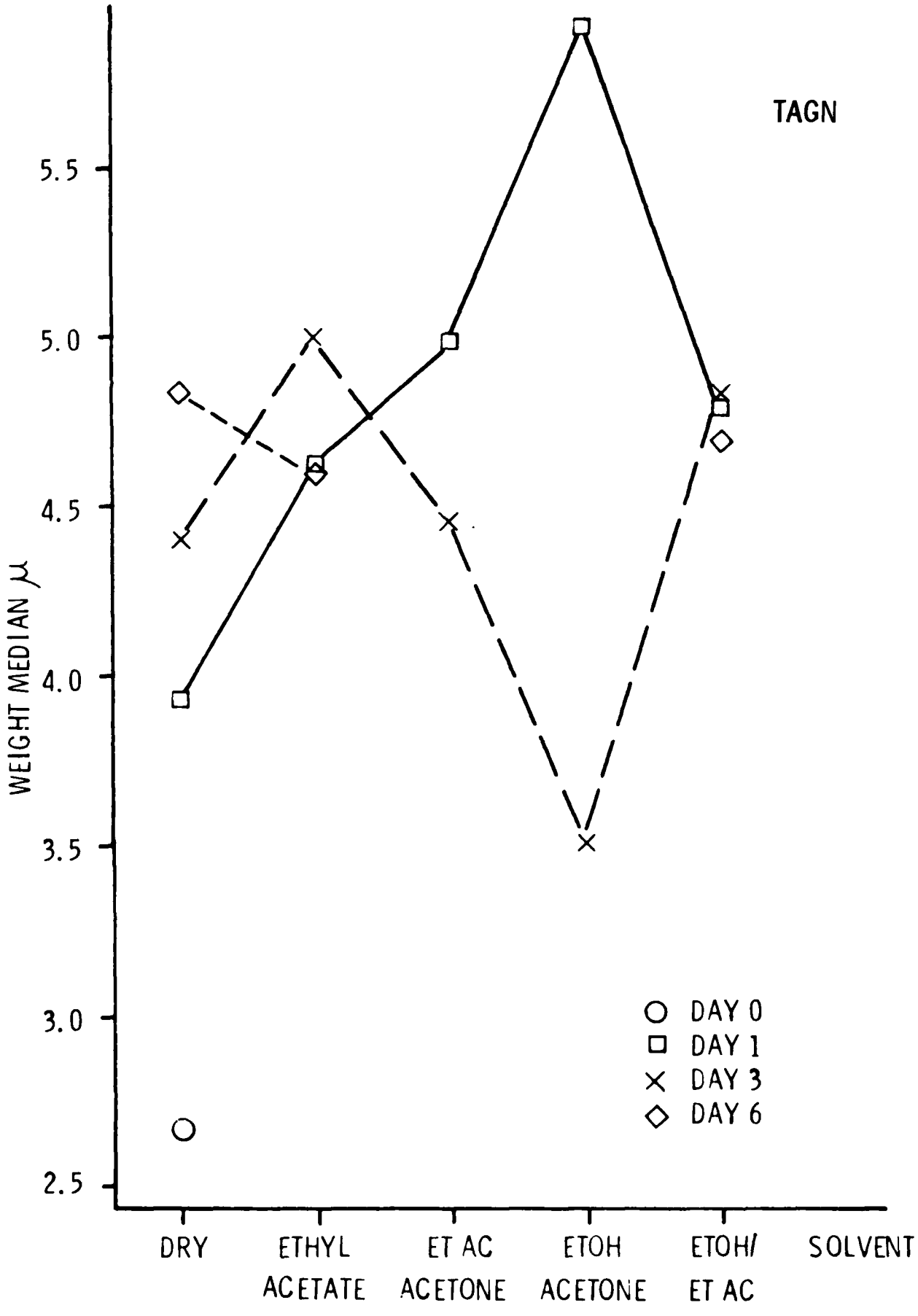

Figure 17. Change in TAGN Particle Size Weight Median by Solvent System for Each Day Samples were Taken

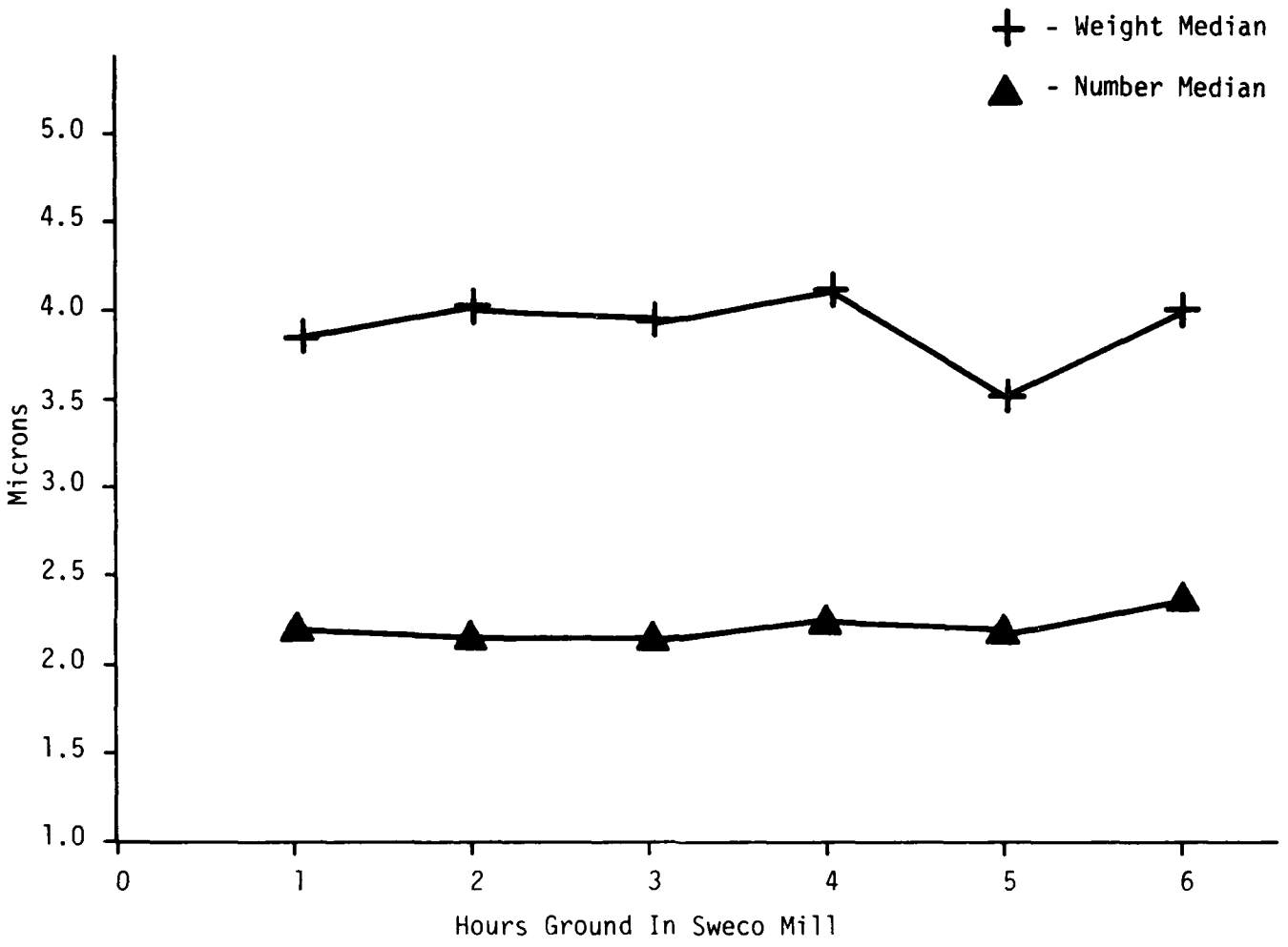

Figure 18. Change in 5HG TAGN Particle Size During Sweco Grinding in Isopropanol

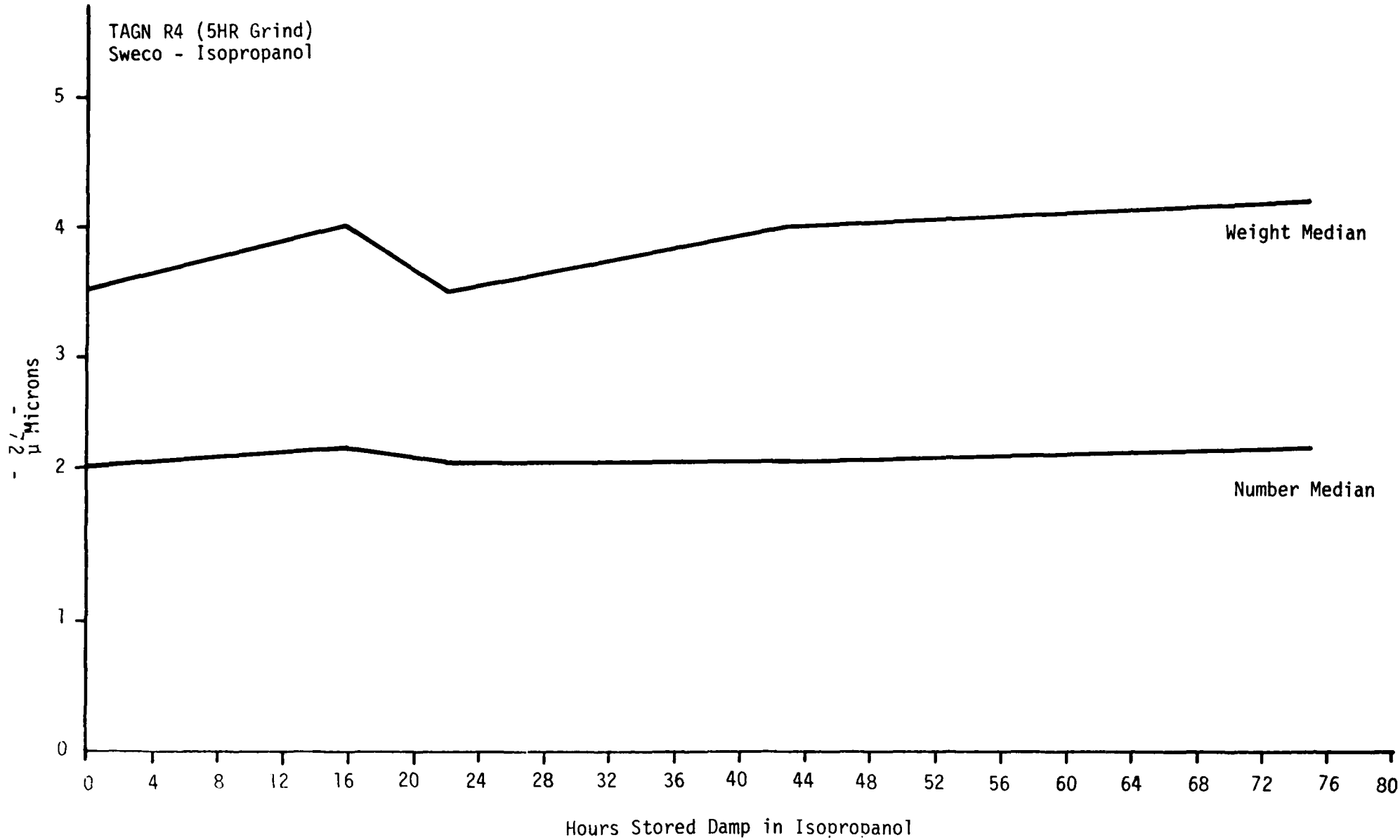

Figure 19. Change in Particle Size of 5HG TAGN Stored in Isopropanol for 80 Hours

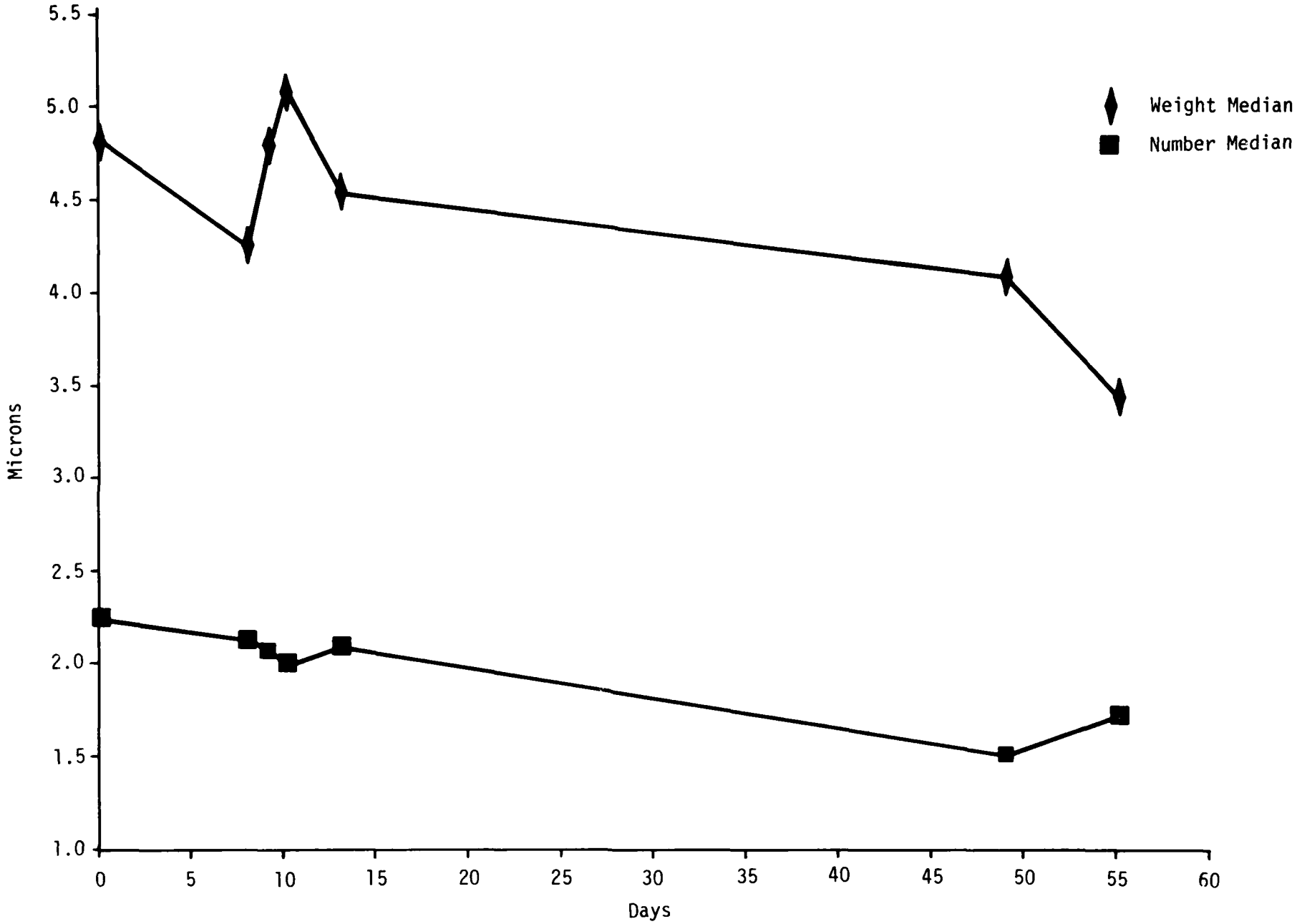

Figure 20. Change in 4HG TAGN Particle Size Stored 55 Days in Isopropanol

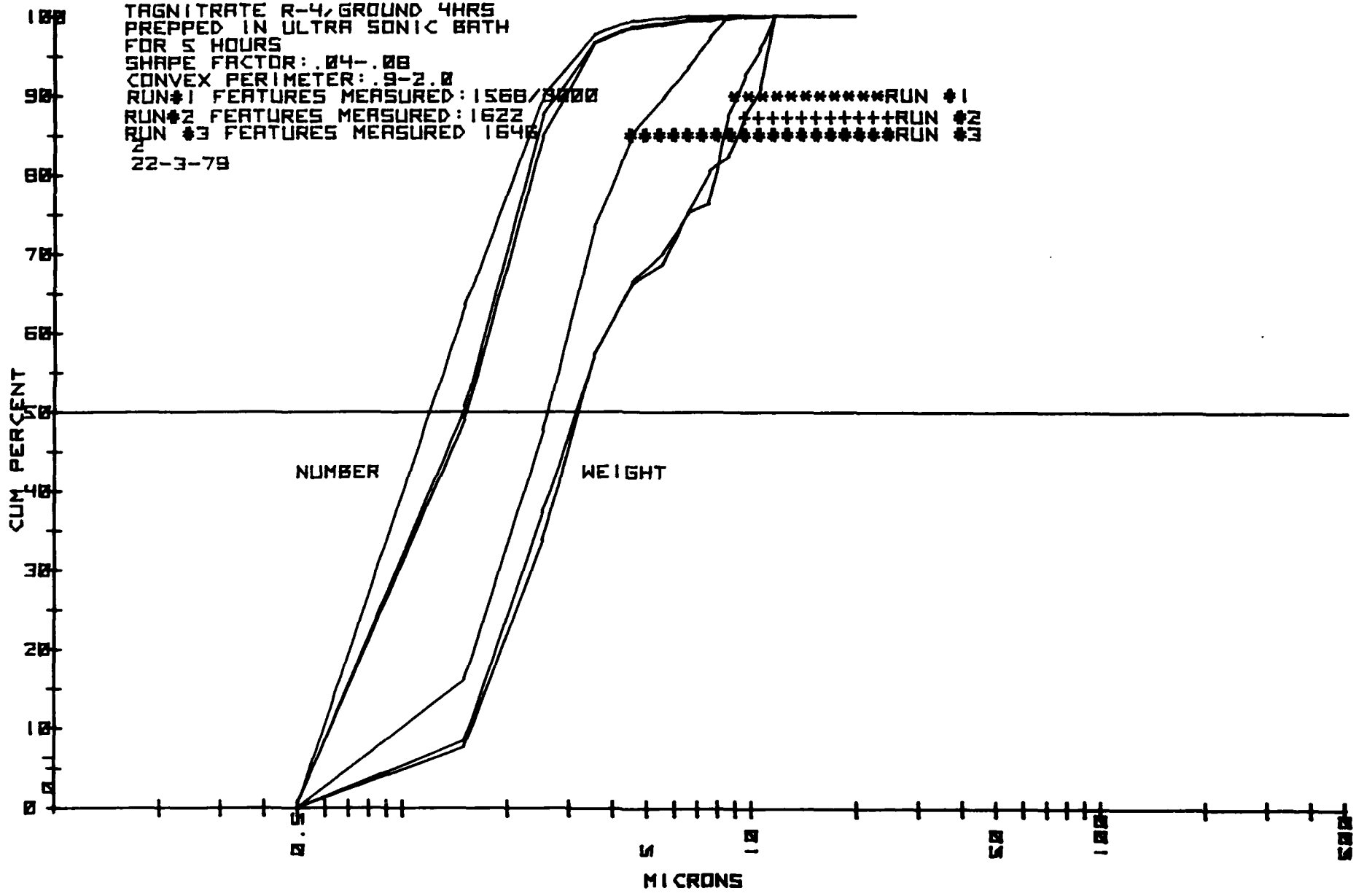

Figure 21. Semilog Plot of the Change in Cumulative Percent of the Day 55 4HG TAGN Sample by Particle Size Number and Weight Median

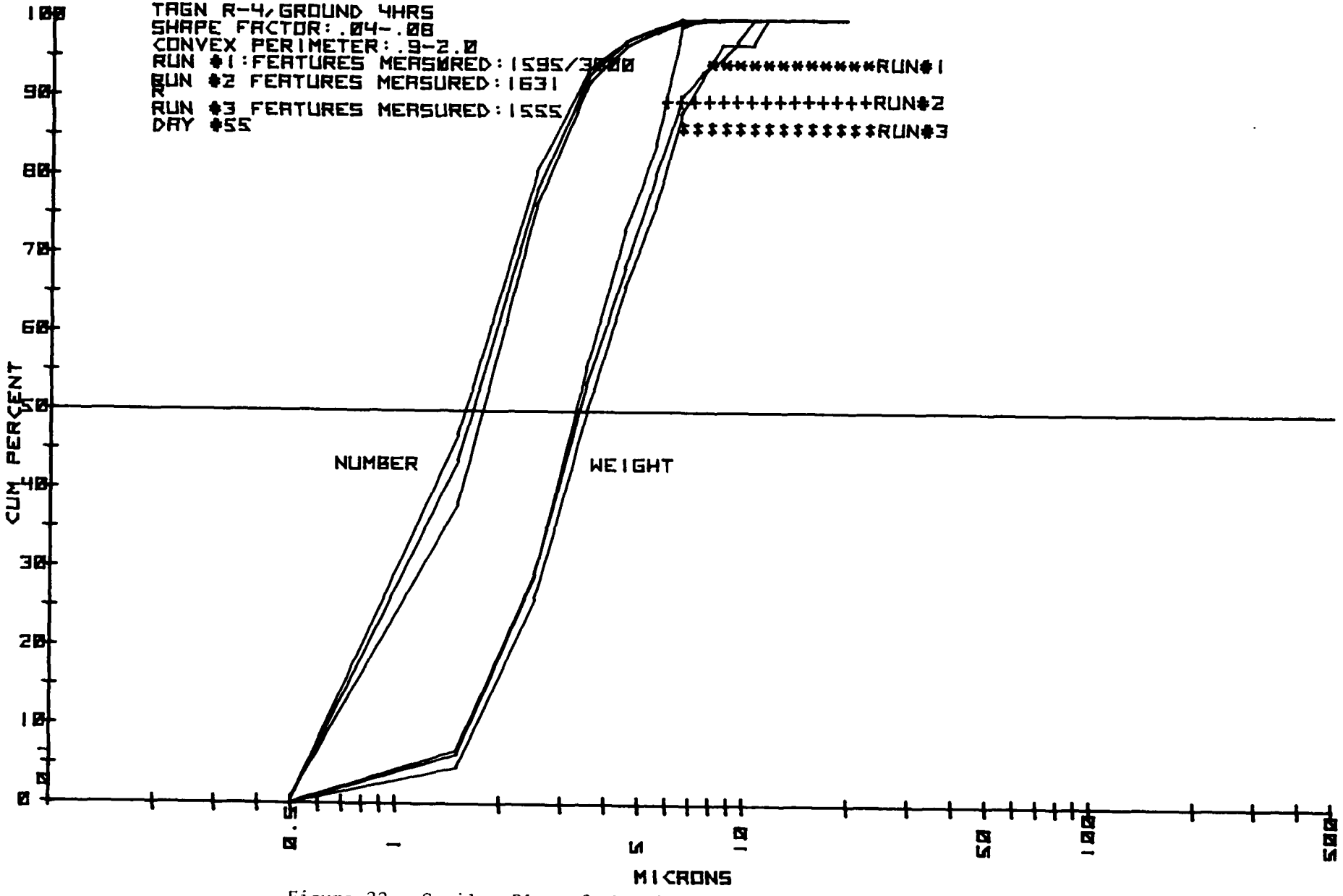

Figure 22. Semilog Plot of the Change in Cumulative percent of the Day 55 4HG TAGN Sample by Particle Size Number and Weight Median

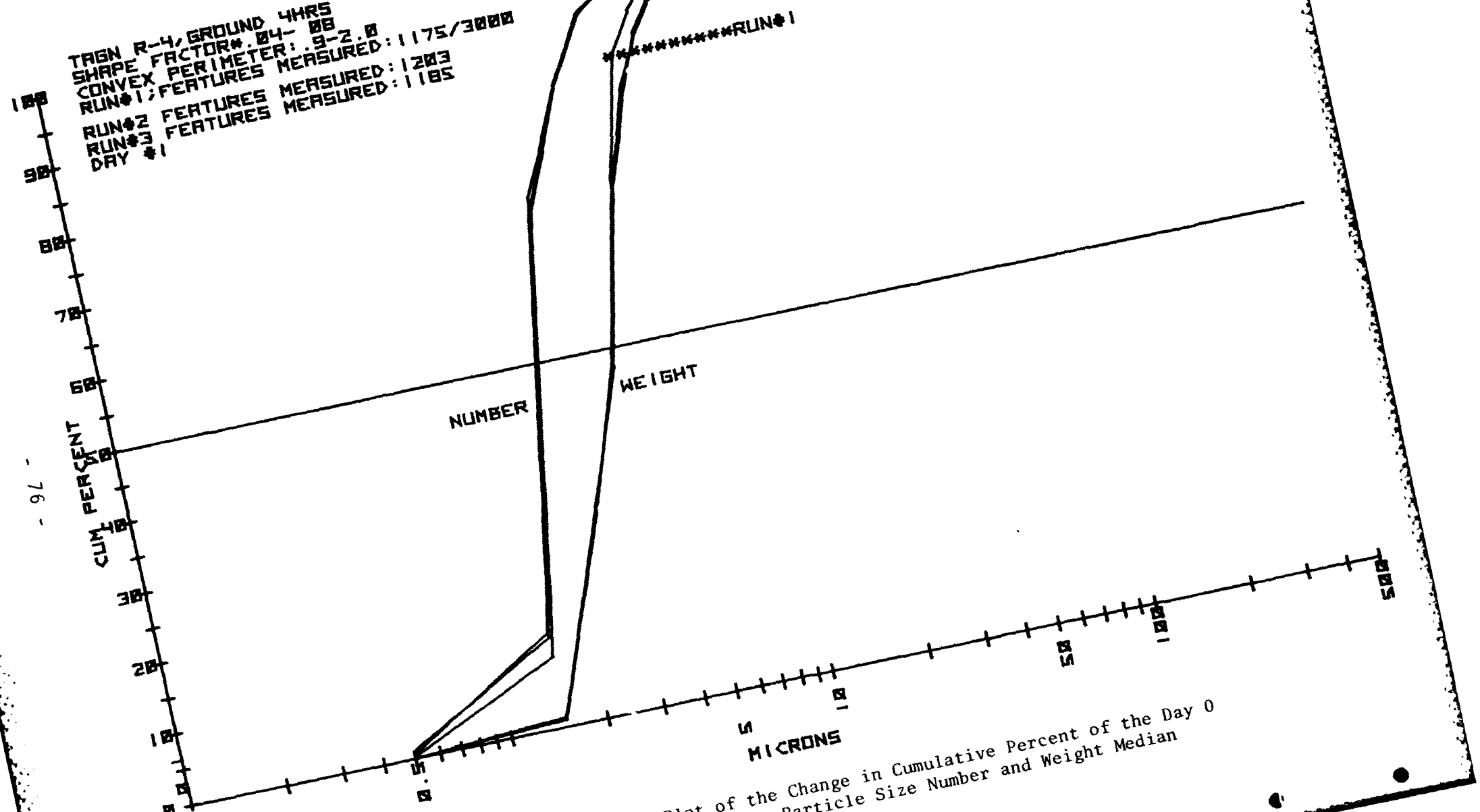

Figure 23. Semilog Plot of the Change in Cumulative Percent of the Day 0 4HG TAGN Sample by Particle Size Number and Weight Median

REFERENCES

1. Cohen, N.S., Combustion of Nitramine Propellants, Lockheed Propulsion Company, Redlands, California, Report No. 744-F, January 1979

2. Moy, B.K., Burning Rate Studies of HMX Propellants at High Pressures, AFATL-TR-75-53, March 1975.

3. Gray, J.C., Inhibited Cool Burning Solid Gun Propellant, Rocketdyne Division, Rockwell International, AFATL-TR-77-38, March 1977.

4. Oetjen, W. H., Interlaboratory Particle Size Characterization of Aluminum Powder, Eighth JANNAF Characterization Meeting, CPIA Pub. No. 289, pp 7-37, September 1977.

FLOWABILITY TECHNIQUES IN THE PROCESSING OF POWDERED EXPLOSIVES, PROPELLANTS, AND PYROTECHNICS

ALLEN J. TULIS
IIT Research Institute, Chicago, Illinois, U.S.A.

ABSTRACT

A very effective flowability additive developed by Dow Corning Corporation is obtained by converting a hydrophilic silica aerogel to a hydrophobic colloidal silica by reacting with hexamethyldisilazane. This additive has been used to prepare homogeneous powder mixtures with a minimum of mixing, to mil difficult materials, and to obtain amazing flow properties in troublesome powders. This hydrophobic silica has an exceedingly light bulk density of about 0.05 g/cc, and a particle size of about one millimicron. It can be premixed before milling and will allow milling of waxy materials. After treatment the powder becomes water repellant and the bulk density increases. Hydrophobic silica additive in amounts less than one percent by weight has often proven effective.

INTRODUCTION

A major problem in the processing of powdered formulations is agglomeration. This problem can be compounded when one or more of the powdered constituents are: (1) hygroscopic, such as ammonium perchlorate or sodium nitrate; (2) waxy or oily, such as nitroguanidine or TNT; or (3) unusually shaped, such as needle-type or flake particles. The agglomeration increases as the particle size decreases. In addition, moisture content directly increases agglomeration and leads to caking of the powder. Therefore, most fine-particled powders, and particularly those that are hygroscopic, oily, or oddly shaped, must be specially handled in all processing and handling operations. This means drying the powders at elevated temperatures, screening to break up or remove agglomerates, and dessicating to prevent moisture uptake.

Another, related problem is created by the milling of powdered formulations necessary to reduce particle size. Hygroscopic, waxy, and oddly shaped particles are difficult to mil except by extreme, and often very expensive, operations. For example, the milling of hygroscopic materials must be done under near-absolute dryness. As the particle size is reduced, the surface area increases and moisture

absorption becomes extensive. As another example, waxy materials can be milled only at reduced temperatures, so that the waxy particles "freeze" and become sufficiently brittle to fragment. Other techniques, such as milling under an appropriate liquid, have also been utilized.

This paper addresses these problems from the point of view of powder flowability. Flowability techniques are described that permit preparing homogeneous mixtures, particularly of explosive, propellant, and pyrotechnic powders, with a minimum of mixing, milling difficult materials, and obtaining amazing flow properties in troublesome powders.

POWDER CONDITIONING

Powder conditioning to overcome agglomeration problems generally involves the use of flow-conditioner additives. These are usually very fine powders of subsieve particle size and include various types of silicates, stearates, phosphates, diatomaceous earth, starch, magnesium oxide, talcum, and fatty amines (ref. 1,2). Calcium stearate and aluminum silicate have been utilized in the food industry where such additives have to conform to food legislation. The mode of action of these conditioners in inhibiting agglomeration and improving flowability has been explained in three ways (ref. 3):

(1) a solid barrier between the powder particles, reducing their attractive forces
(2) lubricants of the solid surfaces, reducing the friction between the particles
(3) neutralizers of electrostatic charges

For powders that are not destined to be consumed as foods, however, a potential solution to this problem was developed by Dow Corning Corporation (ref. 4). In their technique, a hydrophobic fumed silica powder is prepared from a hydrophilic colloidal silica by reacting the latter with hexamethyldisilazane. The effectiveness of this product has been shown in a dry-grinding process to prepare a free-flowing, readily dispersable powder of CN (tear gas), an oily, sticky solid with a low boiling point (ref. 5).

The advantages of this flowability conditioner are many:

- it has an exceedingly light bulk density, about 0.05 g/cc
- the particle size is about one millimicron
- the conditioner can be premixed before milling and will allow milling of waxy or oily materials
- the treated powder becomes water repellant, even if initially hygroscopic
- on a weight basis, less than one percent is often adequate
- the resultant powder generally has a higher bulk density after adding the conditioner
- it is chemically inert, even with sensitive propellants, explosives, and pyrotechnics

The powder is commercially available as Silanox™* or Tullanox™**. The silica aerogel is converted from the hydrophilic to the hydrophobic state by replacing the hydroxyl groups on the surface of the silica particle with siloxane groups:

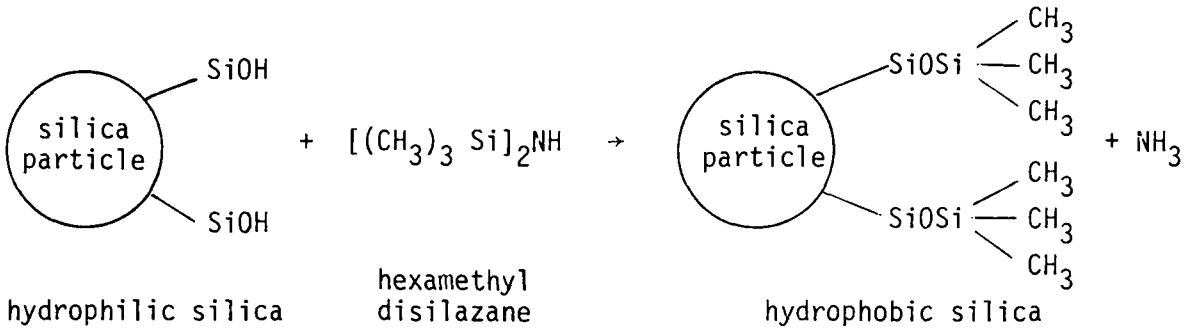

hydrophilic silica — hexamethyl disilazane — hydrophobic silica

It is the steric methyl field upon the particles that causes the particles to become hydrophobic.

POWDER PREPARATION

Moisture absorption by powders is an ever-present problem, not restricted to hygroscopic materials. The use of molecular sieves (ref. 6) for near-absolute drying of powders is an excellent procedure. (Molecular sieves are crystalline zeolites that have Angstrom-sized pores for selective and polar adsorption of gases and liquids.) Direct contact of molecular sieves with sensitive materials, such as explosives, however, must be avoided--the heat of moisture adsorption by molecular sieves is sufficiently great that it could cause ignition of sensitive materials.

In some situations, where the addition of an inert material will not degrade the system, the direct admixture of molecular sieves to a powder--particularly before a milling operation if size reduction is required--is advantageous. In the preparation of a water-ignitable pyrotechnic composition of boron and AgF_2, adequate size reduction of the AgF_2 was difficult even under the most sophisticated "dry" conditions. By adding various amounts of molecular sieves to the mixture before milling, however, the dryness of the AgF_2 powder was optimized. (The powders were dried under vacuum over P_2O_5 prior to milling, whether or not molecular sieves were used.) Subsequent ignition tests proved that the molecular-sieve additive system was much faster in ignition, with time delays reduced, for example, from 650 to 220 msec (ref. 7). Even after 24 hours the time delays remained low in the molecular-sieve additive system, actually decreasing to 200 msec. Some of these items were

*Silanox™ is manufactured by Cabot Corp., Boston, Mass., and is currently not available. It was, however, the hydrophobic silica used in the work described here.

**Tullanox™ 500 is a super-hydrophobic fumed silica manufactured under licensing arrangements with Cabot Corporation, Boston, Mass., by Tulco, Inc., North Billerica, Mass.

stored for several years and remained about as effective as the systems without molecular sieves were initially. (These latter systems did not function after such storage). The amount of molecular sieve additive in this example was 10 percent by weight, although much smaller amounts would have been adequate (ref. 7).

Molecular sieves can be obtained as fine powders. They readily absorb and hold up to 70 percent of their weight in moisture. It should be noted that when the molecular sieves are added to powders they simply transfer the moisture from such powders to themselves in an equilibrium process. Hence the moisture is not removed from the total system but simply from the powder. Their use in this manner is recommended only when a "continuous" drying action of very small amounts of moisture is desired, as in the AgF_2 milling operation. They can, however, be added to powders that are nearly dry and not sensitive to rapid temperature excursions in order to remove tightly bound moisture; they can then be removed by sieve separation. In this case molecular sieve pellets should be used rather than molecular sieve powder.

In certain milling operations we have found it advantageous to use both molecular sieves and hydrophobic silica: the molecular sieves achieve near-absolute dryness of the particles in the milling process so that, as the particles are fragmented, the hydrophobic silica instantly coats their surfaces. This minimizes subsequent absorption of moisture and greatly aids the milling action. This is particularly effective when one of the milled components is hygroscopic and the other is waxy; e.g., ammonium perchlorate and nitroguanidine.

The hydrophobic characteristic of powders treated with hydrophobic silica can be readily illustrated. Figure 1 illustrates ammonium perchlorate powder, with about 3 percent Silanox™ additive, floating on the surface of water. (Ammonium perchlorate is readily soluble in water.) Figure 2 illustrates how this ammonium perchlorate powder now repels water even when submerged under the water. Figure 3 shows two samples of ammonium perchlorate, one with Silanox™ added and the other untreated, after extended exposure to a humid atmosphere. There is no agglomeration in the Silanox™-treated sample, whereas the untreated sample is agglomerated badly.

The exceedingly high water repellency of powders conditioned with hydrophobic silica is attributed to air entrapment upon the surface of the powder particles. The water surface actually rests on the millions of points of the hydrophobic silica projections coating the surface of the powder particles. This same effect occurs in nature, with insects and foliage which repel water so efficiently that a sheen from the surface air film is observed when they are totally submerged under water. Such a sheen is also observed on the submerged powder in Figure 2. Hence both steric hydrophobicity and physical separation of the water surface from the powder particle surface by the air film combine to create a super-hydrophobic condition. This effect is fully described in a Tullanox™ product bulletin published by Tulco, Inc. (see footnote on page 2).

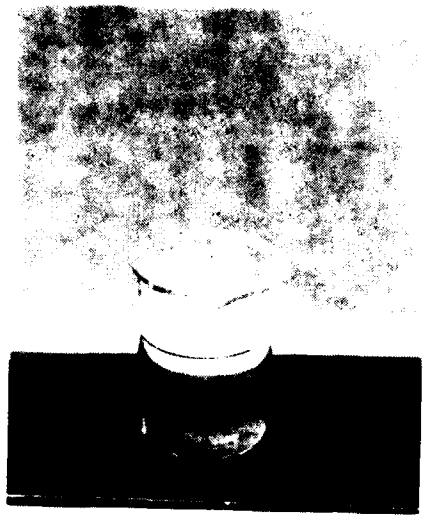

Fig. 1. Ammonium perchlorate powder floating on surface of water after being mixed with about three percent hydrophobic silica additive.

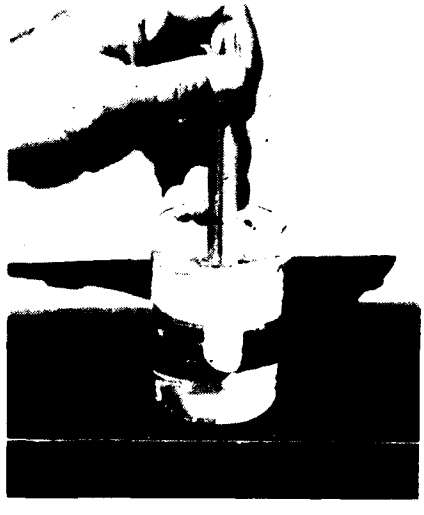

Fig. 2. Dry hydrophobic silica additive ammonium perchlorate powder submerged under water.

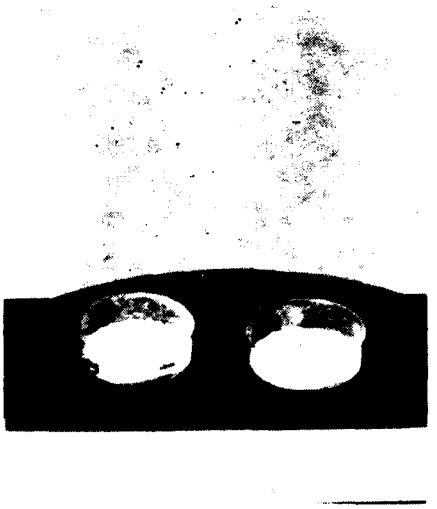

Fig. 3. Comparison of the effect of humidity on (left) ammonium perchlorate powder and (right) ammonium perchlorate powder with about three percent hydrophobic silica additive.

Figures 4 through 6 illustrate another advantageous characteristic of hydrophobic silica. The powder used was Borax. *In Figure* 4 approximately 6 liters (5905 g) of Borax is contained in the glass jar. The graduate contains 2 liters (100 g) of Silanox.™ In Figure 5 Silanox™ has been added to the Borax in the jar for a total of 8 liters material. However, after simple mixing (no milling) for about 15 minutes the overall volume for the mixture decreases to a volume less than that of the Borax alone initially, as illustrated in Figure 6. Depending on particle size and other factors, bulk-density increases of up to 50 percent have been obtained with additions of as little as 2 percent (by weight) of hydrophobic silica.

The combined lack of agglomeration and free-flowing characteristic of powders conditioned with hydrophobic silica is especially beneficial in preventing powder separation and the resultant air gaps in powder fills. We have successfully used 1 to 2 percent hydrophobic silica additive to pyrotechnic and composite explosive powders in the filling of 5 to 6 mm diameter tubes about 90 cm long. The hydrophobic silica additive not only allowed simple and rapid filling of the tubes but provided the compactness of filling and preclusion of air gap formation requisite for minimizing failure of reaction propagation over the length of the tube. Upon storing these tubes all powder settling, due to handling, etc., was evident at the top of the tube, thus allowing simple topping off of the tubes before use. Without the hydrophobic silica additive storage and handling caused a high degree of propagation failures due to powder separation within the tubes.

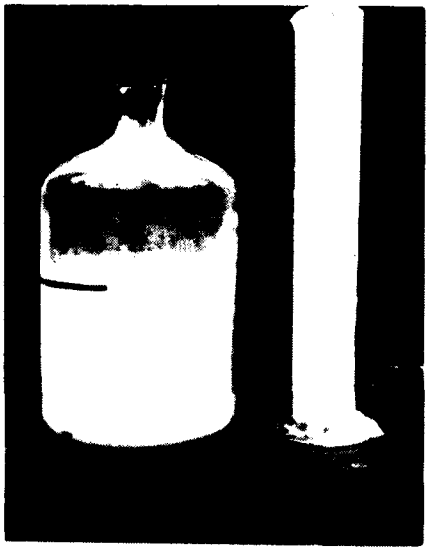

Fig. 4. Six liters Borax™ powder in a jar and two liters of Silanox™ in a graduate before mixing.

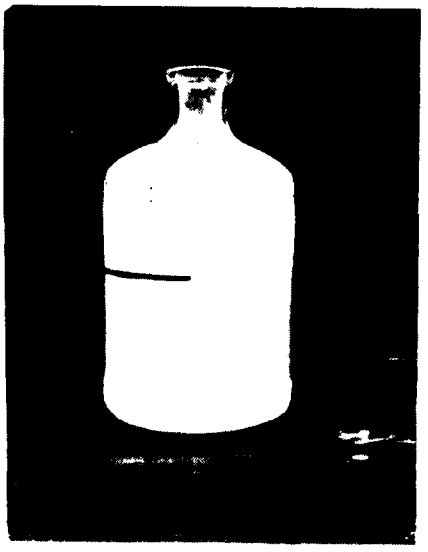

Fig. 5. Six liters Borax™ powder in a jar with two liters of Silanox™ poured on its surface.

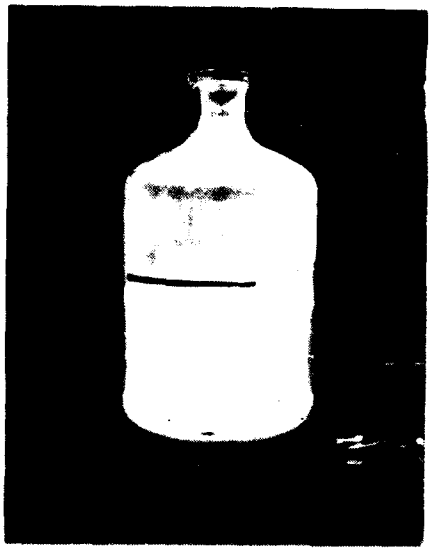

Fig. 6. Six liters Borax™ powder and two liters Silanox™ reduced to less than six liters total after simple mixing.

The fluidity of powder treated with hydrophobic silica is amazing. When agitated, it appears to be a liquid and gives the illusion that surface tension exists.

There is, however, one potential disadvantage, which is associated with the increased bulk density. The mechanism for this increase in bulk density is the fluidization of the individual particles--they flow and slip past each other readily so that they compact much better--hence, increased bulk density. If, however, this powder stands for an extended time, it acquires a thixotropic tendency--it is difficult to achieve instant motion. Once disturbed, the powder becomes "liquefied" as far as flowability is concerned, but the initial force required for movement is increased. This is no problem in the fluidization process, but for dispersal of powders that are initially tightly contained, this must be considered.

The question invariably arises: how much hydrophobic silica is required for optimum fluidity? This question cannot be readily answered as the optimum amount depends on many factors. The mechanism is a coating action in which the millimicron hydrophobic silica attempt to coat the much larger micron-sized particles. Incomplete coating will be effective, but not optimum. On the other hand, excess hydrophobic silica will not improve flowability appreciably and will in fact in many cases segregate from the coated particles, floating on the surface as a separate layer.

During milling, the hydrophobic silica will continuously coat fresh surfaces as long as excess hydrophobic silica is present. Once all hydrophobic silica has coated the particles, further milling will start to degrade the system. If the particles were initially waxy, the problem will recur and affect the milling action.

Adding more hydrophobic silica will allow further milling and reestablish the flowability. Hence, the amount of hydrophobic silica required depends on the material to be fluidized and its particle size. If the particle size is reduced, either by milling, by deagglomeration, or by another particle reduction technique, additional hydrophobic silica will be required.

SUMMARY

In summary, we have described a flowability additive or conditioner that can be utilized with most pyrotechnic, propellant, explosive, and other powder formulations where problems of hygroscopicity, agglomeration, poor flowability, and perhaps even low bulk density are prevalent. The additive is a hydrophobic silica; it is not new, has been utilized in powder technology for many years, and is commercially available. It has a bulk density of about 0.05 g/cc, a particle size of about a millimicron, and should be treated with caution for health and safety reasons as it is readily respirable. Because of its low bulk density, a very small amount--from 1 to 3 weight percent--is adequate in most cases. It can totally eliminate agglomeration problems, minimize hygroscopic problems, and improve the flowability of powders by many orders of magnitude. We have used it very effectively with explosive, propellant, and pyrotechnic powders to prepare homogeneous mixtures with a minimum of mixing, to mil difficult materials, and to obtain amazing flow properties in troublesome powders. It has proven effective in fluidization processes, particularly for the rapid dispersion of powders and powder elutriation.

REFERENCES

1 N. Burak, "Chemicals for Improving the Flow Properties of Powders," Chem. Ind., (1956), p. 844.
2 W. B. Pietsch, "Adhesion and Agglomeration of Solids During Storage, Flow and Handling," Trans. ASME, 5 (1969), p. 435.
3 M. Peleg and C. H. Mannheim, "Effect of Conditioners on the Flow Properties of Powdered Sucrose," Powder Tech., 7 (1973), p. 45.
4 L. A. Ranner and W. J. Maynard, "Hydrophobic Silica as a Grinding Acid," U.S. Patent 3,333,776, Aug. 1, 1967.
5 J. D. Wilcox and J. M. Klein, "A New Concept in Preparation Techniques of Powders," Powder Tech., 5 (1972), p. 19.
6 C. K. Hersh, Molecular Sieves, Reinhold, New York, 1961.
7 A. J. Tulis, J. L. Austing, C. K. Hersh, P. W. Cooper, and J. P. Weber, "Water-Ignition of Hypergolically Reactive Pyrotechnic Compositions," Proceedings Second (Int.) Pyrotechnics Seminar, July 1970, pp 347-378.

SLU-FAE ROCKET MOTOR: VOLUMETRIC CASTING AND CENTRIFUGAL CURING

J. R. WAGENER

Naval Ordnance Station, Indian Head, Maryland

ABSTRACT

The rocket motor for the SLU-FAE system (Surface Launched Unit-Fuel Air Explosive) requires exactly 12.00 $\pm$ .05 pounds of propellant covering the interior of a five-inch diameter tube over a length of about 48 inches to a thickness of only 0.30 inches.

The Naval Ordnance Station, Indian Head, has developed a method for precision volumetric casting of the required propellant weight and a technique for centrifugal curing to achieve the desired propellant web thickness. Initially, various crude methods were used to feed propellant into the motor tube and at least succeeded in proving that the task was possible. Finally, a volumetric propellant loader was designed and built which dispensed the required amount of propellant evenly over the 48 inch length. The original 12-grain centrifugal curing rack was superseded by a production prototype 24-grain rack. Effects of spin times and speeds on motor ballistic performance have been determined, and over 1700 grains have been processed.

INTRODUCTION

The SLU-FAE rocket developed by NWC, China Lake, consists of a five-inch diameter rocket which propels a larger diameter fuel-air-explosive (FAE) warhead in a surface-to-surface trajectory. Precise trajectory and range requirements require the propellant weight be controlled to 12.00 $\pm$ .05 pounds. The grain design calls for the propellant to cover the tube interior over a length of about 48 inches to a thickness of only 0.3 inches.

The rocket motor and its complete processing will be briefly described, then the evolution of the two primary processing steps, volumetric casting and

centrifugal curing, will be described.

PROCESSING REQUIREMENTS

Outline of Total Process

The steps required in SLU-FAE motor processing are: degreasing, fairing installation, fairing sealing, propellant injection, propellant spreading, spin-curing, static curing, motor loading, testing, painting, and packout. Spin-curing was dictated by the propellant weight tolerance. Variations within motor tube tolerances alone would preclude forming the grain with a conventional mandrel arrangement.

Description of Processing

The complete processing of SLU-FAE rocket motors includes the following: The motor tube interior and the fairings are degreased and dried. As the tube is rotated 360 degrees, bonding compound is injected at the proper location near the forward end of the tube. A forward fairing is inserted in the tube and pushed to the correct position. An aft fairing is inserted in the tube and bonding compound is applied about 5.5 inches from the aft end. The fairing is then drawn back to its final position. The bonding compound cures overnight at room temperature, then a small additional amount of freshly mixed material is applied to seal the knife-edge of both fairings and is also cured overnight. The motor tube is not primed or lined. The prepared motor tubes are serialized, weighed and delivered to the casting area preheat oven. The propellant mix is delivered to the casting building in the mixer bowl which is fitted with a follower plate and pressure lid. The mixer bowl is positioned and its discharge valve is attached to a volumetric propellant loader. After priming the loader, it dispenses 12.0 pounds of propellant into each motor tube along the 48 inch distance between the fairings. The tube is removed from the loader to a scale for verification of the propellant weight. Propellant may be added or removed with a spatula as required. Meanwhile, the tube is manually rotated 360 degrees at a net speed of about one revolution per minute so the propellant flows around the tube interior. The entire bonding surface must be wet with propellant at this

time, or bare spots will remain in the finished grain. End adapters are fitted to the tube and it is clamped in the spin cure rack, which is in a 150°F oven. The rack rotates the motors slowly until all motors are installed, then the speed is increased to 250 rpm for two hours. Then the speed is reduced to 100 rpm and spin-curing continues for a total of 18 hours. The motors are removed from the spin racks and cured horizontally at 135°F for a total cure time of five days.

Cured motors are inspected, weighed and have the propellant thickness measured with an eddy current device. The nozzle-igniter assembly is installed and the motor is leak tested and X-rayed. The igniter circuit resistance is verified and the motor is painted, stenciled and crated for shipment to a loading depot where the complete round is assembled.

EARLY CASTING AND SPIN-CURING WORK

The goal of the volumetric casting operation is to meter 12.00 pounds of propellant into the motor tube and dispense it evenly along the 48 inch distance between the fairings. If this is done properly, simply rotating the tube slowly will allow the propellant to spread around the interior surface of the tube. The spin cure at 250 rpm takes care of smoothing the propellant and removing voids.

Manual Methods

The earliest experimental casting at the Naval Weapons Center, China Lake, California was accomplished by scooping propellant into the end of a motor tube held at about a 45° angle. When the correct propellant weight was reached and the propellant spread down the length of the tube, the tube was rotated to spread the propellant. The spin curing was on a roller device functionally identical to a drum roller.

When the experimental motors showed promise of success, the Naval Ordnance Station was asked to process larger numbers of motors. The first casting method tried was based on a motor tube lining technique: The propellant was dispensed from a casting pot onto a long TFE paddle about three inches wide. The paddle was inserted into the motor tube and inverted. The propellant stuck to the paddle, so a scraper was inserted in an attempt to coax the propellant to fall off.

The stickiness of the propellant turned this into a slow, messy operation, although some motors were successfully made this way. The first spin cure rack was an existing spin lining/curing rack which was modified to grip the motor tube at the forward end and support the aft end on idler rollers. Difficulties with this twelve-motor rack were the time required to engage and secure the motors in the drive hub and the unsettling tendency of the unbalanced motors to bounce on the idler rollers until the propellant was evenly distributed inside the tube.

Propellant Injection

After the extreme difficulties with the paddle-loading technique, a propellent injector was assembled from existing casting hardware, see Fig. 1.

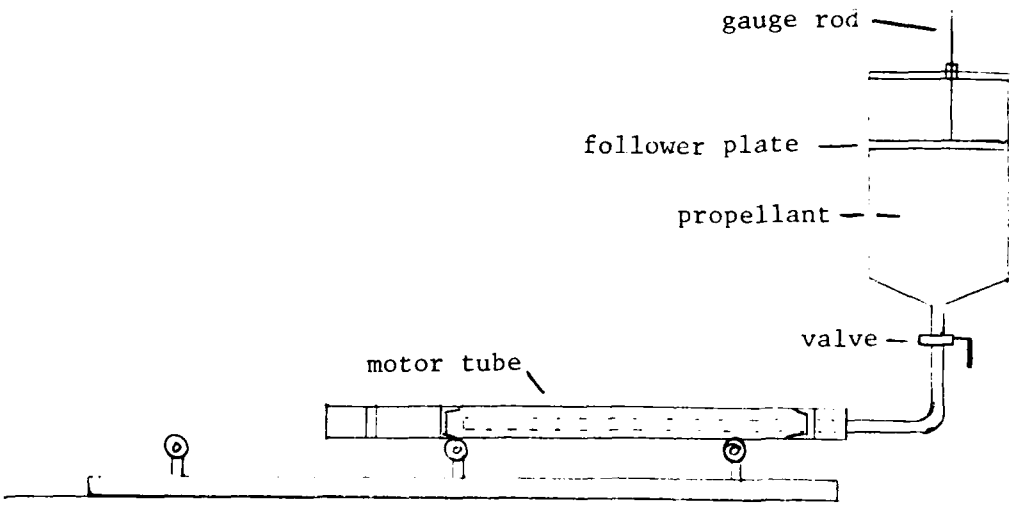

Fig. 1 Propellant Injection Apparatus

The propellant flowed smoothly out the injection tube and gradual withdrawal of the motor tube spread the propellant along the length of the tube. To meter the correct weight of propellant, we determined that 1.75 inches of follower plate travel expelled 12 pounds of propellant. This distance on the gage rod was divided into sixteen parts and the injection tube was marked with sixteen three-inch increments. In practice, one operator monitored the gage rod and called out each scale division movement to a second operator who moved the motor tube. At the sixteenth division, the first operator closed the propellant valve and the second parted the propellant ribbon at the end of the injection tube. He gave the motor tube a quarter-turn to start the spreading process as the

motor was removed to a scale. A batch of twelve motors could be cast with this technique in about one hour, since propellant expulsion time at 25 psi was about 3.5 minutes. Over 700 motors were cast with this equipment during the rocket motor development program.

THE VOLUMETRIC CASTING MACHINE

Increasing the number of motors produced from one propellant batch required faster propellant dispensing and more accurate control of the weight dispensed. The casting pot arrangement had proved itself, within its limitations, so the "SLU-FAE loader" was designed as an automated version of the same device, but using a small diameter volumetric dispensing cylinder for increased accuracy. Fig. 2 outlines the device. The old casting pot becomes the 30-gallon mixer bowl, a volumetric cylinder is added, and the propellant dispensing tube remains the same. These three components meet at a three-port rotating plug valve. With the valve in the "re-load" position, propellant flows under 50 psi nitrogen pressure from the mixer bowl into the volumetric cylinder, pushing back the TFE piston and the hydraulic cylinder. When the valve is shifted to the "cast" position, the straight-through passage is opened from the volumetric cylinder to the propellant tube. When the loading handle is pulled, hydraulic oil flows to the hydraulic cylinder to drive the piston to the left, expelling the propellant. Now volumetric propellant casting machines are not unheard of, but the requirement to dispense the propellant over a 48 inch length adds a new twist. The number-calling operators are replaced by a chain attached to the tail rod of the hydraulic cylinder. Sprockets at the extreme right end multiply the 16.3 inches of piston travel to 48 inches travel of push rod which pushes the motor tube toward the left along the outfeed rollers. Some details of the loader may be interesting:

a. The central valve is made by the Ladish Company, Tri-Clover Division. The tapered plug is covered with Buna-N, and functions like a large laboratory stop-cook. We lubricate it with R-45M, the propellant binder prepolymer. The valve works flawlessly, but with a high effort once propellant gets in the lubricated space.

AD-A169 165 JOINT SYMPOSIUM ON COMPATIBILITY OF PLASTICS/MATERIALS WITH EXPLOSIVES PR..(U) AMERICAN DEFENSE PREPAREDNESS ASSOCIATION ARLINGTON VA L R BARTRON ET AL. MAY 79 2/4

UNCLASSIFIED F/G 19/1 NL

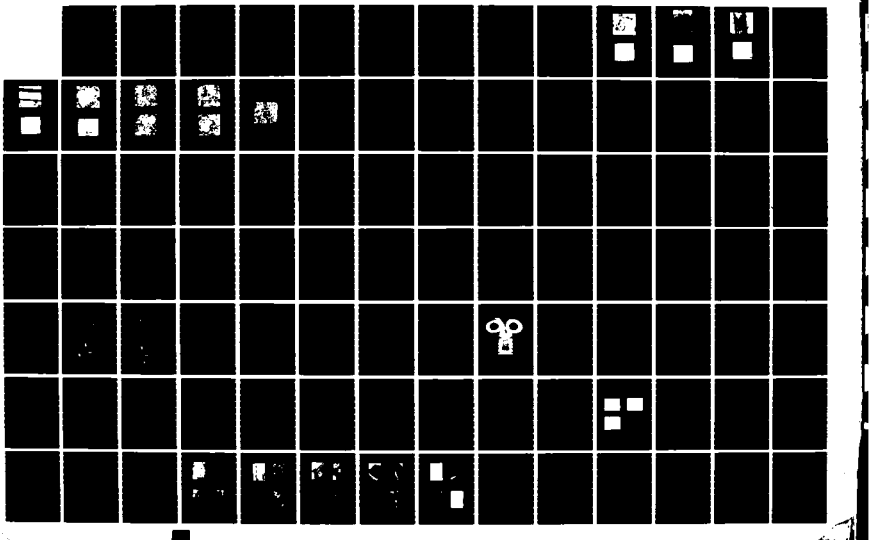

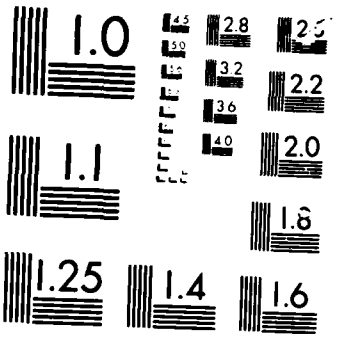

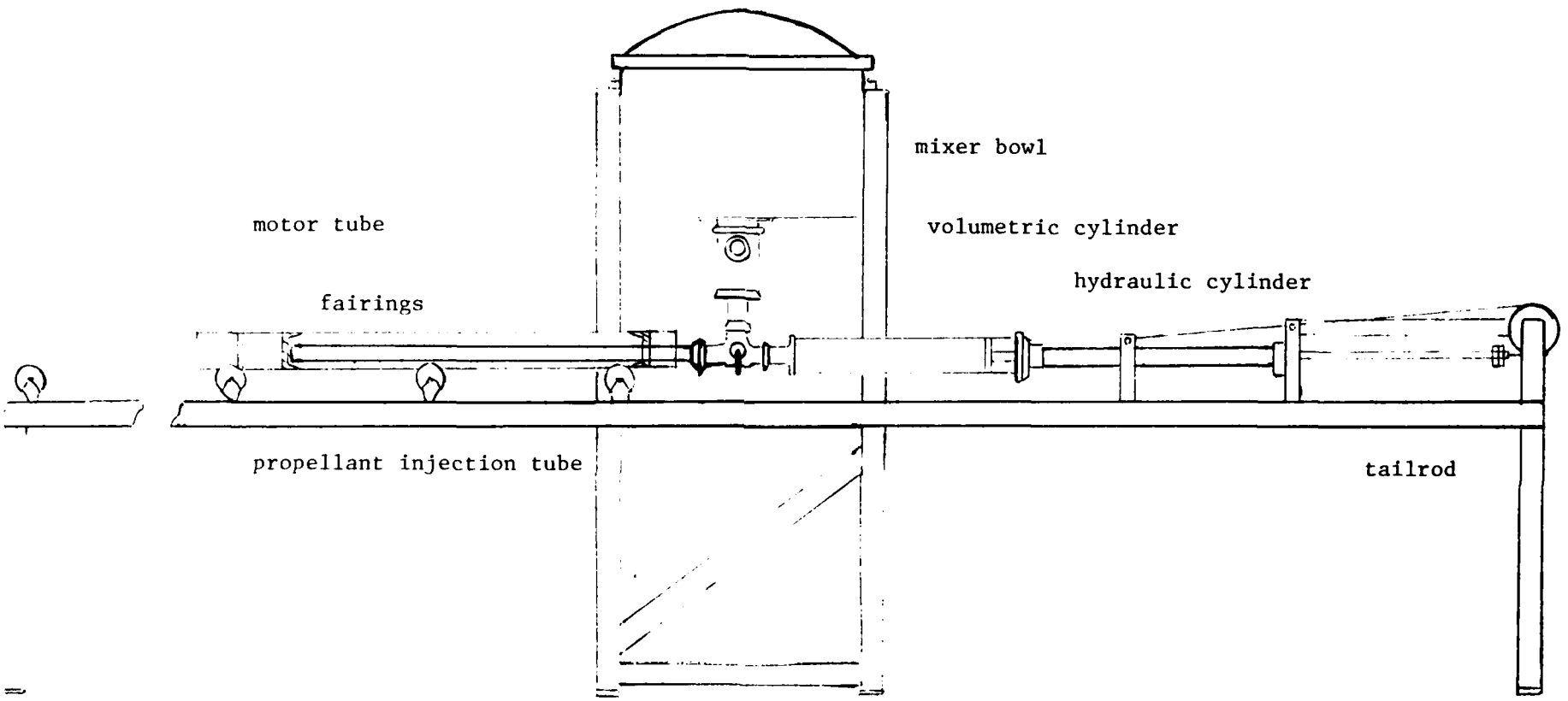

Fig. 2 SLU-FAE Volumetric Propellant Loader

b. Bleeding of air from the system during the initial charging of the volumetric cylinder is accomplished with a vent opening plugged with a wad of glass fiber. Air escapes, but propellant reaching the plug is stopped. Air in the injection tube is not a problem, as the propellant initially flowing out the tube is in plug flow, although slower at the tube wall, so no air is trapped.

c. The volume of propellant accepted by the cylinder is limited by a stop at the end of the hydraulic cylinder tailrod.

d. The volume of propellant expelled is fine-tuned by controlling where the hydraulic cylinder stops at the end of its expulsion stroke. This is done by turning a large "nut" on the tailrod which alters the stopping position of the cylinder.

e. The volumetric cylinder is stainless steel and the piston is TFE with two o-rings.

f. Pressure on the propellant is limited to 50 psi maximum, during both the re-load and casting cycles.

Reloading takes about one minute and casting about 1 minute, 10 seconds, although each total cycle time increases two seconds per cycle as the propellant viscosity increases. End-of-mix viscosity is 4 kilopoise but transportation and set-up take an hour, by which time viscosity is 8 KP. Actual casting time for 23 motors is 55 minutes, by which time viscosity is 11.5 KP. About 30 minutes later, the propellant viscosity reaches 14 KP, and will no longer spread around the tube interior to wet the surface.

The first motor ever cast received 11.98 pounds of propellant, but overall, about half have required manual adjustment of the propellant weight. Correct operation of the volumetric loader is contingent on its receiving void-free propellant, so we lower the mixer bowl slowly at the end of the mix to avoid air bubbles as the mixer blades pull out of the mix. Probably the major source of inacurracy in dispensing the precise amount of propellant is that we still must manually part the propellant ribbon at the end of the injection tube when casting is complete. We feel that addition of an automatic cutoff would increase loading precision such that almost all motors would meet the weight requirement

without adjustment.

THE SPIN-CURING RACK

When designing a piece of production prototype equipment to replace the 12-motor spin rack, the prime considerations were increasing capacity to 24 motors, fitting in a 15 foot wide bay, holding motors securely at both ends, and facilitating fast loading and unloading. A drawing of the resulting design is too complex to be instructive, but an exploded schematic representation of one station is shown below.

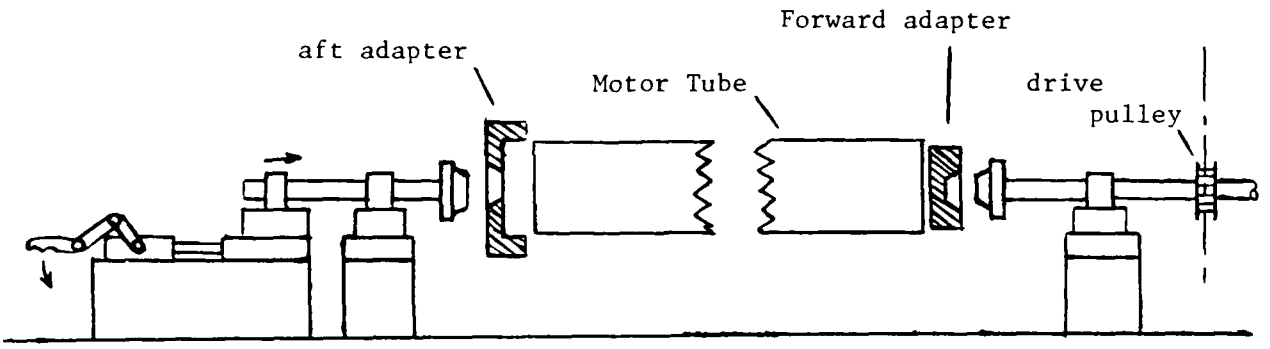

Fig. 3 Schematic of spin-cure setup

When viewing the rack from the front, the layout is six stations high and two deep. Rather than dwell on the details of the design, suffice it to say that the device works but some lessons have been learned: Avoid a high clamping force. Apply the clamping force in line with the long axis of the motor, rather than offset. Make the design more tolerant of tube dimensional variations - in our design a slightly longer tube created higher clamping forces. Do not trust a setscrew to hold a hub on a shaft - back it up with a snap ring. Provide for leveling and alignment of each motor station at fabrication, so that only leveling of the machine's base is required at installation. Ensure that installation and removal of the end adapters is fast and easy. Provide a direct reading permanently mounted tachometer, not intermittent use of a hand-held device.

The volumetric loader and 24-motor spin rack have been used for casting 981 motors.

EFFECTS OF SPIN TIMES AND SPEEDS

Based on results with motors from the 12-motor spin rack, which had poor speed control, we suspected the propellant was being centrifugally separated to varying degrees. An experiment was set up to evaluate the effect of spin speed on motor performance. Four motors were cast from one mix and two were spun 2 hours at 250 rpm (5 g's on the propellant) and two were spun at 350 rpm, which produces 10 g's on the propellant. The remainder of the cure was completed and the motors were assembled and fired. Results are shown in Table 1.

TABLE 1

Effect of spin speed on motor performance

Motor No.	Spin Speed (rpm)	Action Time (msec)	Peak Thrust (lb)	Impulse (lb/sec)
793	250	320	8900	2594
796	250	358	8700	2605
794	350	310	9800	2603
795	350	312	9600	2608

The extra centrifuging creates a faster burning rocket motor which hits a higher peak thrust, so spin speed must be closely controlled. Also, temperatures during casting and curing, which affect viscosity, must be constant from mix to mix.

The effect of spin time was examined by casting eight motors from a mix and spinning all at 250 rpm, for different lengths of time, then slowing to 100 rpm and continuing all for a total of 18 hours. After static cure was completed, the motors were assembled and fired. Results are shown in Table 2. There was no discernable effect of the spin time on motor performance. (Note: The action times of all these motors are longer than those of the motors in Table 1 because the ground oxidizer used in these motors was coarser.)

TABLE 2

Effect of fast spin time on motor performance

Motor No.	Spin Time (min.)	Action Time (msec)	Peak Thrust (lb)	Impulse (lb/sec)
785	30	384	7800	2588
786	30	380	7870	2589
787	60	369	8116	2594
788	60	360	8300	2595
789	120	388	7649	2585
790	120	366	7840	2608
791	120	382	8370	2593
792	120	378	7880	2597

FUTURE WORK

The Naval Ordnance Station has been funded by the Army to design production prototype equipment to produce 1600 units per month. This would mean casting about 100 units per day instead of our current 22. Given the limited propellant pot life and the limitation on propellant pressures, the answer was a four-station loader to be fed propellant from our 150-gallon mixer. The main innovations are an automatic shutoff on the end of the propellant injection tube and a custom sliding plug valve, really four valves ganged together.

The spin cure racks will each hold 24 tubes, arranged six units high by four deep. Adapters screw into each end of the tube and it is placed in a cradle just below the actual spinning position. As the aft end support is pushed in by hand and locked, tapered hubs center and engage the motor to the slowly rotating drive. When all tubes are loaded, the hydraulic motor drive speed is increased as required.

Added refinements include an eight-tube slow speed holding rack which rotates the tubes at 1 rpm after casting and a cart on which rotation can be continued as tubes are transported to the spin cure area.

MORPHOLOGICAL CHANGES IN $KClO_4$: A SENSITIVE INDICATOR OF POTENTIAL CORROSION PROBLEMS IN Ti/$KClO_4$ LOADED DEVICES*

D.H. HUSKISSON, T.M. MASSIS and J.T. HEALEY
Sandia Laboratories,† Albuquerque, New Mexico 87185 (U.S.A.)

ABSTRACT

Extensive corrosion has been observed on the header pins (Alloy 52) and bridgewires (Tophet C) of an actuator loaded with a Ti/$KClO_4$ pyrotechnic blend. A number of these devices have been opened and subjected to microscopic and chemical analysis. Particular attention has been focused on the interfaces between metal parts of the header (pins and bridgewires) and the pyrotechnic material. Upon separation of the powder from the header surface, impressions of the header pins and bridgewire remained in the pyrotechnic pellet allowing examination of both header and pellet surfaces with a 1:1 location correlation. The scanning electron microscope and energy dispersive x-ray analysis of the header surfaces revealed extensive chlorine-related corrosive attack on both the Alloy 52 pins and Tophet C bridgewire. Examination of the corresponding pyrotechnic surface revealed a major change in the appearance of the $KClO_4$ powder that was adjacent to the corrosion regions. No morphological alteration of the pyrotechnic powder was observed away from the pin interfaces or in uncorroded actuators. The degree of morphological alteration proved to be a sensitive indicator of potential corrosion problems, and accurate predictions of corrosion could be made prior to the actual observation of corrosive attack. Selective chloride ion electrode analysis of the pyrotechnic revealed significantly higher chloride ion concentrations in the morphologically altered areas as compared to areas remote from the pin surfaces in corroded units or within any areas in noncorroded units. The increased chloride content was indicative of decomposition of the $KClO_4$.

---

*This work was supported by the United States Department of Energy under Contract DE-AC04-76-DP00789.
†A U. S. Department of Energy Facility.

INTRODUCTION

Pyrotechnic components such as actuators and igniters are used in numerous Sandia Laboratories applications. These devices must have high reliabilities and shelf-lives in excess of twenty years. These requirements place stringent compatibility constraints on the various materials in the devices, both with respect to the corrosion properties of the header materials and to the decomposition characteristics of the pyrotechnic blend.

One pyrotechnic actuator has exhibited serious compatibility problems resulting in corrosion of the pins and bridgewire during early production, although earlier development studies had indicated there were no materials compatibility problems. In addition, a number of other pyrotechnic devices containing many of the same materials as this actuator had been in production for over ten years with no apparent compatibility problems. In order to determine the source of the compatibility problems encountered during production, a series of aging studies were initiated on loaded and sealed headers.

EXPERIMENTAL PROCEDURES

The header pin material in the actuators was Alloy 52 (nominally 50 weight percent Fe and 50 weight percent Ni), and the bridgewire material was Tophet C (57 to 60 weight percent Ni, 14 to 18 weight percent Cr, and balance iron). The pyrotechnic blend was a $Ti/KClO_4$ mixture (33/67 weight percent), and the header seal material was Corning 9010 glass.

The pyrotechnic charge was loaded into the actuator bodies at a relative humidity of approximately 50 percent to reduce static ignition hazards. Following loading, a closure disk of 21-6-9 stainless steel was welded to the output end to ensure a hermetically sealed environment. Aging of the actuators was conducted for various times up to 16 months at room temperature, and as long as 120 days at 60°C. After aging, the actuators were opened by machining away the closure disk and charge holder regions of the header. Examination for materials degradation was performed shortly after opening and removal of the pyrotechnic charge. Prior to examination the opened actuators were stored in a desiccated chamber to minimize any atmospheric effects.

The actuators were examined after opening by scanning electron microscopy and energy dispersive x-ray analysis. Surfaces of the pins and bridgewire were examined to determine the presence and elemental composition of any corrosion products on these materials. In addition, the technique used to open the components resulted in a clean separation

of the pyrotechnic charge from the header such that impressions of the header pins and bridgewires were easily observable on the pyrotechnic pellet surface. These impressions permitted a direct 1:1 location correlation to be made between the pyrotechnic charge and that of the pins and bridgewire. The examination of the pyrotechnic charge was performed to determine whether any alteration or decomposition of either the fuel or oxidant powders had occurred.

Following the scanning electron microscope examinations of the pyrotechnic powder surfaces, a small amount (< 5 mg) of the Ti/$KClO_4$ powder was removed from the areas of the pin impressions and also away from the pins(i.e., in the bulk). These powders were then treated with water and the solution analyzed using a specific ion electrode procedure to determine total free chloride content. These free chloride contents of material adjacent to the pins were then compared to the free chloride analysis of the bulk sample. The presence of a free chloride ion content above that in the bulk would indicate decomposition of the $KClO_4$. The observed changes in chloride ion content provided insight into the possible mechanisms involved in the corrosion problem.

RESULTS

Examination of the pins and bridgewire surfaces showed extensive regions of corrosive attack on the pin surfaces along with isolated areas of corrosion on the bridgewires. Figure 1A shows a scanning electron micrograph, along with the corresponding energy dispersive x-ray spectrum, of one of the pin areas exhibiting corrosive attack. Of particular interest is the associated energy dispersive x-ray spectrum which indicates the presence of chlorine in the absence of potassium. The absence of potassium eliminates the possibility that the chlorine-containing product is merely some oxidant powder ($KClO_4$) which has transferred to the metal surface. The morphology of the chloride-containing corrosion product regions is best described as typical "mud-cracking," as exemplified in Figure 1A. Figure 1B is a scanning electron micrograph of an uncorroded pin surface. Figure 2A shows one of the isolated regions of corrosive attack present on the Tophet C bridgewire along with the associated energy dispersive spectrum. This bridgewire was taken from the actuator whose pin surface is shown in Figure 1A, aged 16 months at room temperature. Again, chlorine is observed in association with the nickel, iron, and chromium from the Tophet C wire. The corrosion of the bridgewire was far less extensive than that on the pin surfaces and was observed only on

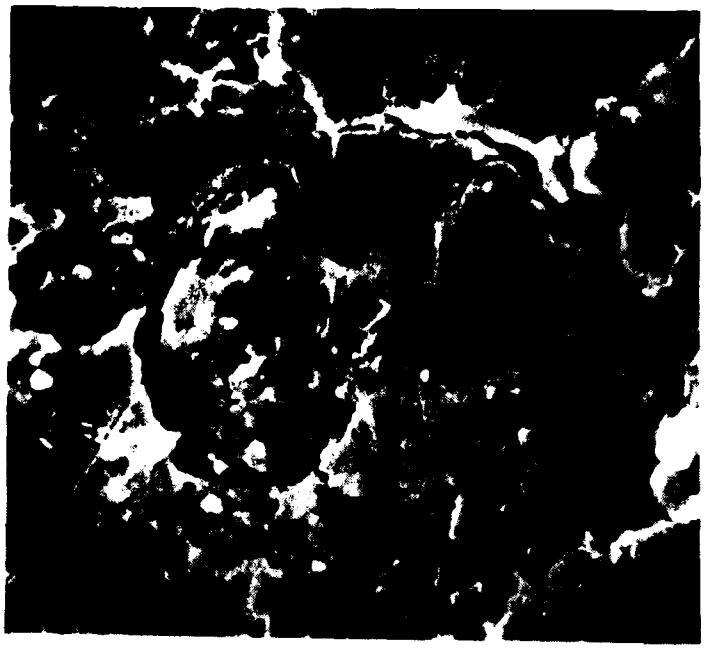

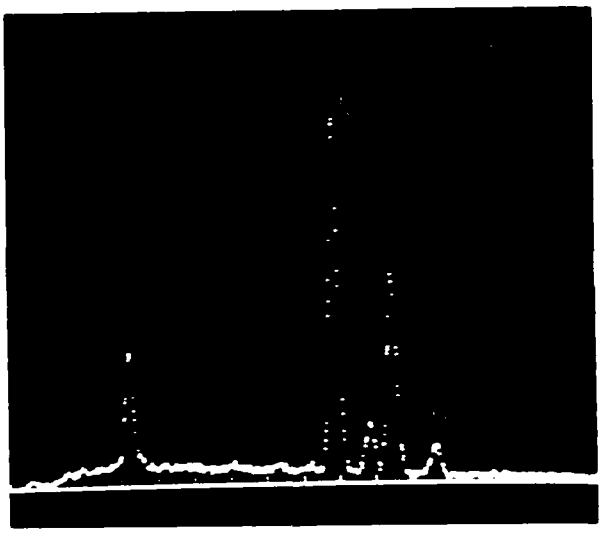

Fig. 1A. Micrograph of pin area showing corrosive attack on actuator aged 16 months at room temperature, along with the associated energy dispersive x-ray spectrum.

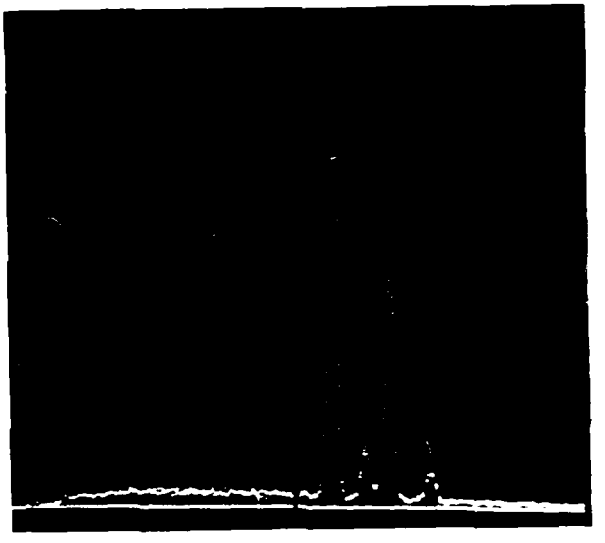

Fig. 1B. Micrograph of the pin area of an uncorroded actuator with its corresponding energy dispersive x-ray spectrum.

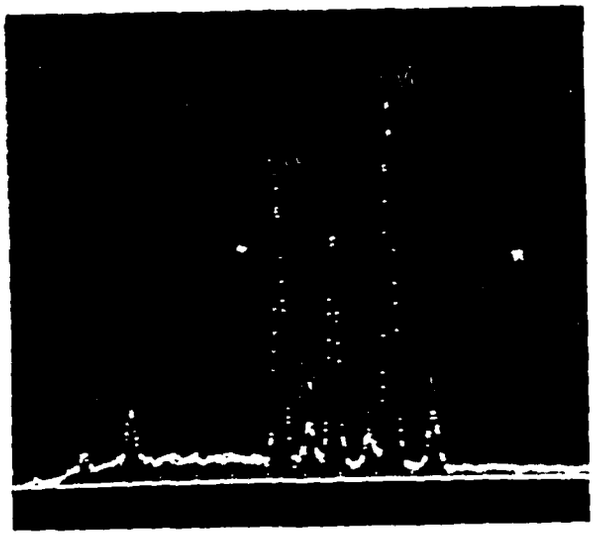

Fig. 2A. Micrograph of one of the isolated areas of corrosion present on the bridgewire of the actuator from Fig. 1A and the corresponding energy dispersive x-ray spectrum.

those actuators where extensive corrosion of the pin surfaces was present. Figure 2B shows the typical appearance of an uncorroded bridgewire along with its corresponding energy dispersive x-ray spectrum for comparison.

Examination of the corresponding pyrotechnic powder surfaces showed two relevant characteristics. First, directly opposite the area shown in Figure 1A was the structure shown in Figure 3. From the presence of iron and nickel in the energy dispersive x-ray spectrum shown in Figure 3, it is apparent that the products of pin corrosion had transferred to the powder surface. The second feature of note was a morphological alteration of the $KClO_4$ particles. Figure 4A shows the appearance of the pyrotechnic interface in areas away from the pin surfaces and Figure 4B in areas adjacent to the pin surfaces. The unaltered $KClO_4$ powder in areas away from the pins had an appearance which is typical of ball milled material, with sharp cleavage facets and rounding of corners. The average particle size was approximately 8 μm diameter. The altered $KClO_4$ particles observed in areas adjacent to the pin surfaces appear to result from a fusing together of larger amounts of the oxidant powder, giving the material a cratered or "swiss cheese" appearance. In the worst case, as shown in Figure 5, the alteration of the $KClO_4$ powders occurred over the entire pin interface area. In the proximity of corroded pin material transfer, examination of the $KClO_4$ powder by energy dispersive x-ray analysis revealed an increase in the Cl/K ratio near the surface of the particles.

Examination of the pyrotechnic surfaces after only short aging times at room temperature revealed only very minor indication of the $KClO_4$ morphological alteration, primarily in the form of cratering and minor fusion of the particles as would be expected during the early stages of this process. On some short-term aging samples, the alteration of the $KClO_4$ particles was observed without the attendant corrosion of the pin and bridgewire; however, examination of similar actuators after longer periods of aging revealed the actual corrosion of the pins and bridgewires along with more extensive alteration of the $KClO_4$ as previously described.

Analysis of the pyrotechnic surfaces for free chloride ion content by the specific ion technique showed an increase in the free chloride ion content at the pin-powder interface. Table I gives examples of the total free chloride ion content both in the altered pin-powder interface region and away from the interface for both corroded and noncorroded actuators. It can be seen from these chloride ion contents

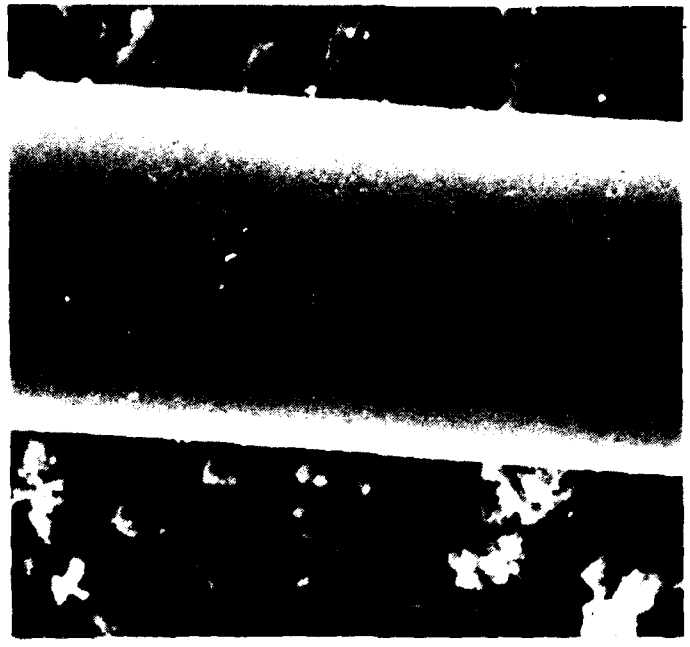

Fig. 2B. Micrograph and energy dispersive x-ray spectrum of uncorroded bridgewire of actuator shown in Fig. 1B.

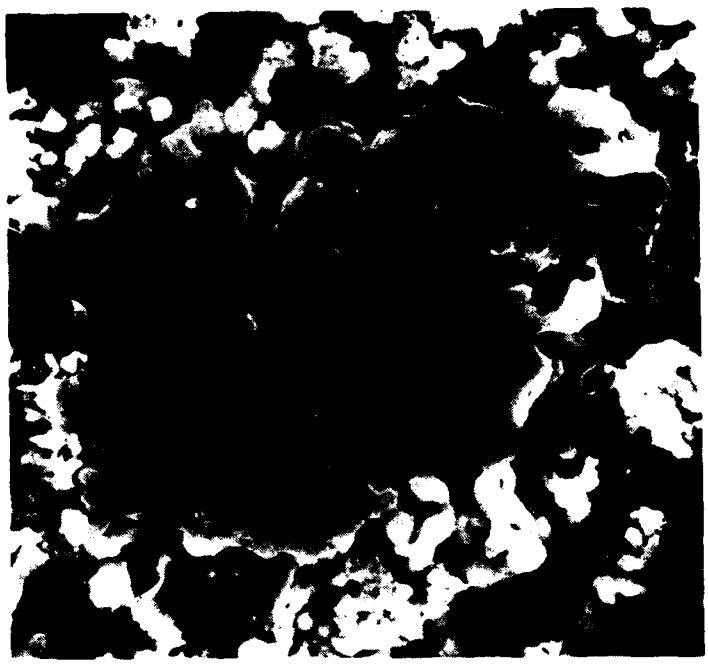

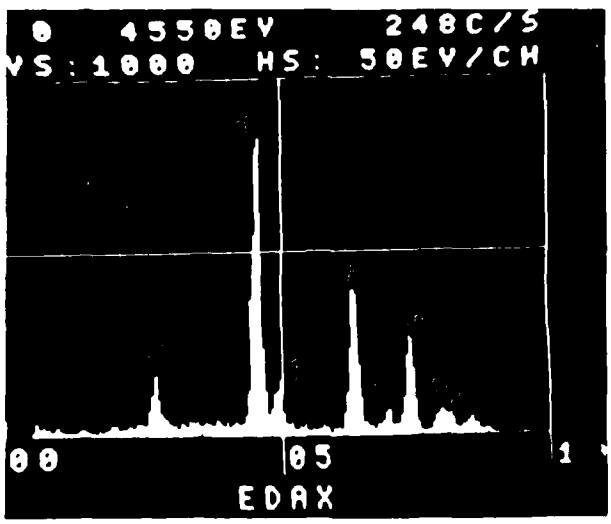

Fig. 3. Pyrotechnic powder surface of area directly opposite the corrosion shown in Fig. 1A. The energy dispersive spectrum shows transfer of pin material.

Fig. 4A. Appearance of the pyrotechnic interface remote from the pin surface, from actuator aged 16 months at room temperature.

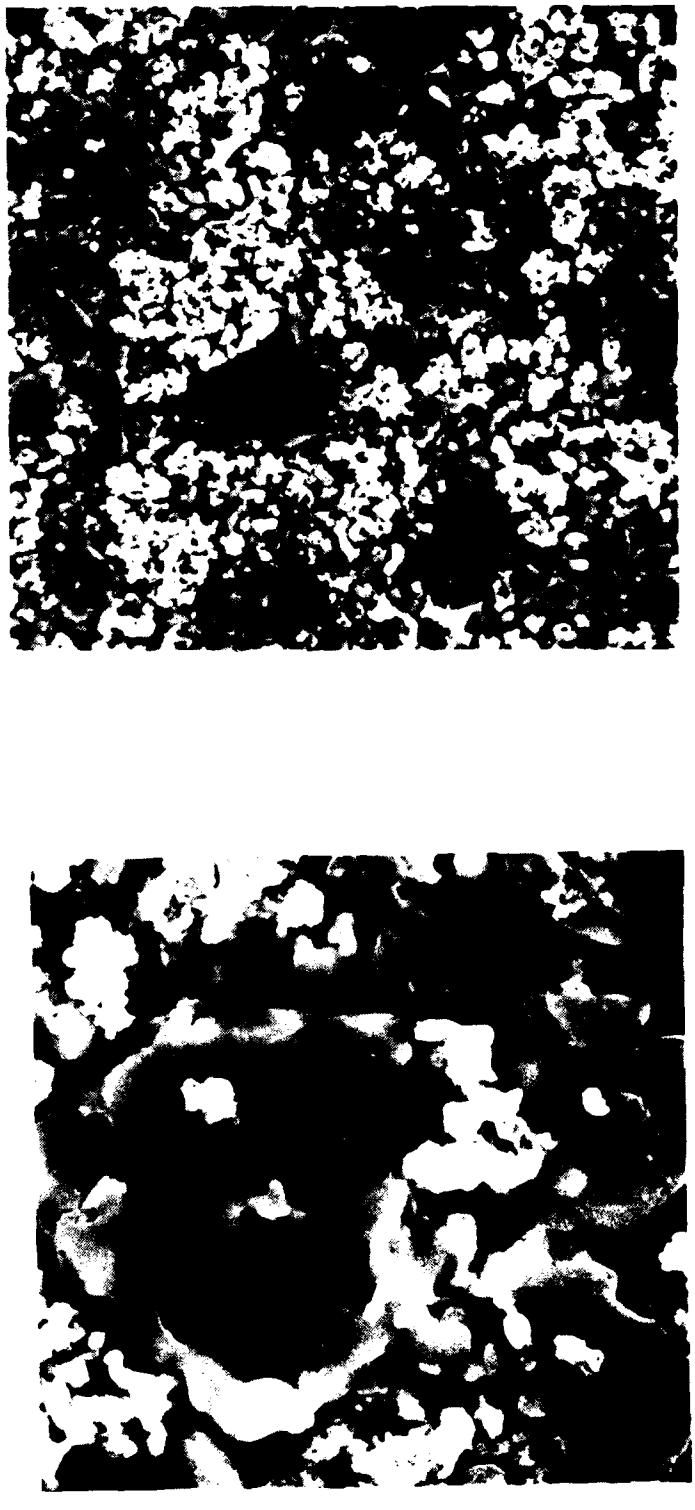

Fig. 4B. Appearance of pyrotechnic interface in areas adjacent to the pins from same actuator as Fig. 4A.

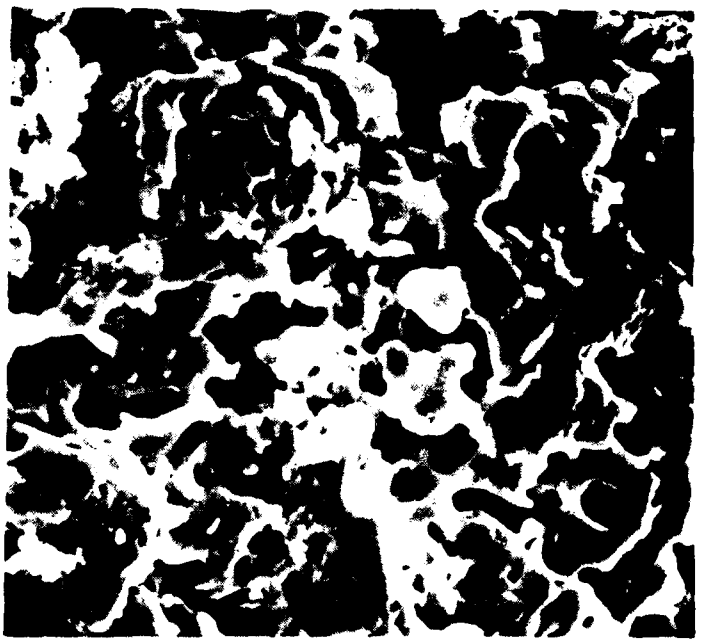

Fig. 5. Worst case type of alteration of the $KClO_4$ particles demonstrating cratering and "swiss cheese" morphology.

that a significant increase was observed in the pin interface areas of the corroded units. The noncorroded units examined for comparison do not show a similar increase in chloride ion content at the pin-powder interface.

TABLE I

Free Chloride Ion Content in Pyrotechnic Powder Interfaces

Actuator No.	Chloride Ion Content at interface ppm Cl^-	Chloride Ion Content bulk ppm Cl^-
Corroded Unit #1793	305	145
Corroded Unit #1826	482	140
Corroded Unit #1904	314	200
Noncorroded Unit G31-5	200	160
Noncorroded Unit G31-14	200	185

NOTE: The bulk samples are accurate to ± 20 ppm whereas the interface samples are accurate to ± 50 ppm.

DISCUSSION

The results of these examinations have shown that a direct correlation exists between the corrosion observed primarily on the Alloy 52 pins, the occurrence of the morphological alteration of the $KClO_4$ particles, and the measurement of $KClO_4$ decomposition to chloride. The degree of the perchlorate alteration increases with increasing corrosion of the actuator pin surfaces. The regions of most extensive morphological alteration of the perchlorate particles occurred in areas where corrosion of the Alloy 52 resulted in transfer of pin material to the pyrotechnic surface. In actuators that display very little or no corrosion, only isolated small areas of the $KClO_4$ morphological alteration have been observed. The fact that the alteration of the perchlorate powders has been observed in those units where corrosion of the pins was in its early stages, and that the alteration was present even when corrosion could not be identified unequivocally, indicates that the presence of this perchlorate morphological alteration would serve as a sensitive indicator of the presence or future occurrence of corrosion on the pin surfaces.

The free chloride ion analysis presented in Table I shows a definite increase in chloride ion content on those units displaying the alteration of the perchlorate particles. The most probable source of the increase in free chloride ion concentration is the decomposition of the perchlorate. An increase in the Cl/K ratio was observed on the surface of some of the altered $KClO_4$ particles during energy dispersive x-ray analysis of "worst case" particles, which is another indication

that decomposition of the perchlorate particles is partially responsible for the alteration process. The decomposition and fusion of the perchlorate particles are indicators of incipient but still observable corrosion. This process is also a contributor to further corrosion as the decomposition of the potassium perchlorate will provide a continuing source of free chloride ions.

SUMMARY

1. The morphological alteration of the potassium perchlorate has been shown to occur in conjunction with and adjacent to the corrosion of the pins.
2. The alteration of the potassium perchlorate serves as a sensitive indicator of potential future corrosion on uncorroded units.
3. Free chloride ion analysis has shown that the alteration is accompanied by a decomposition of the potassium perchlorate.

ACKNOWLEDGEMENTS

The authors wish to thank Raymond Merrill of Sandia Laboratories for performing the selective ion chloride analyses.

STABILITY AND COMPATIBILITY STUDIES OF PYROTECHNIC AND EXPLOSIVE MATERIALS BY MODULATED BEAM MASS SPECTROSCOPY

by

John W. Reed
Monsanto Research Corporation
Mound Facility

ABSTRACT

A modulated molecular beam quadrupole mass spectrometer has been assembled with an appropriate sample handling system to study gas producing reactions of pyrotechnics and explosives in temperature regions of consequence in compatibility studies. Limits of sensitivity of the system, noise problems and applications to specify systems are discussed.

The detection limit for water at mass 18 at a 1:1 signal to noise ratio is approximately 10^{-13} moles sec^{-1}. Detection limits for other species with less background signal are appropriately lowered.

Results are presented for a series of survey determinations on a number of energetic materials. Data covers the temperature range of interest for stability and compatibility as well as temperatures well into the region of initiation and decomposition.

USE OF WEIBULL DISTRIBUTION STATISTICS IN ASSESSING LONG TERM COMPATIBILITY OF PROPELLANTS WITH POLYMERIC MATERIALS

NATALIA PETRIANYK and DAVID W. LEVI

Applied Sciences Div., DRDAR-LCA-CA, Dover, NJ 07801

ABSTRACT

The long term compatibility of propellants with polymers may be evaluated by statistical means. The Weibull distribution function was used in an effort to provide a more accurate means of estimating the effect of aging of the inert material in contact with the propellant.

This method was applied to several systems exhibiting different degrees of compatibility. Exposure at 140°F of the RTV 680 rubber with M30 propellant in the XM735 projectile displayed no apparent adverse effects. Distribution analysis supported the conclusion that the RTV 680/M30 system is compatible at ambient temperatures. Another silicone displayed an initial decline in mechanical properties followed by a period of stability when stored with M30 at elevated temperatures over a period of 12 months.

A fair amount of incompatibility was displayed by 30% glass filled nylon which had been exposed to a double base propellant WC870 for an extended time. The Weibull distribution plots indicate that the propellant exerts a damaging effect on both Nylon 12 materials, particularly at elevated temperatures.

Thermal aging may contribute to the ultimate failure of a polymer, as well as direct contact with an energetic. This is illustrated in the case of the M205 non-metallic cartridge case used in the projectile of a 152mm round, with M26E1 propellant. Although it is difficult to separate the effect of these variables upon the lifetime of the system, Weibull statistics provide some measure of prediction.

INTRODUCTION

In an earlier report (1) it was shown that a Weibull distribution function was useful in evaluating compatibility data for a polypropylene in contact with M9 and M26 propellants. Although usually there was some difficulty in evaluating the data due to a pronounced scatter, it was shown statistically that there was essentially no

difference* between control and with-propellant data.

In the present work we extend this type of treatment to several polymer-propellant systems showing varying degrees of compatibility (or incompatibility).

RESULTS AND DISCUSSION

The Weibull distribution is a statistical distribution that has been shown to have wide applicability, especially in treating mechanical property results (2,3). The cumulative distribution function may be written (2,3)

$$\log \log \left[\frac{1}{1-F(X)}\right] = \log \alpha + \beta \log (X-\gamma) \qquad (1)$$

where F(X) is the distribution function, i.e., the fraction of samples showing a mechanical property value of X or below. α is the scale parameter (y-intercept), β is the slope and γ a location or threshold parameter. A plot of the left hand side of Equation (1) vs. log $(X-\gamma)$ should give a straight line of slope β and intercept α, γ may be selected on an iterative basis by making trial plots. In the present work satisfactory results were obtained by taking $\gamma=0$ and thus using a two parameter distribution.

Weibull differential distribution curves may be calculated by using the equation

$$f(X)=\frac{b}{a}\left(\frac{X}{a}\right)^{b-1} \exp\left[-\left(\frac{X}{a}\right)^{b}\right] \qquad (2)$$

where the parameters a and b are related to those in Equation (1) by $\beta=b$ and $\alpha=-b \log a - 0.36$. Constant a and b in Equation (2) are calculated in each case from the least squares values of α and β in Equation (1).

Case I

Generally the most desirable case is one of complete compatibility. This would correspond to the situation where the mechanical property for the controls and for the polymer after storage with propellant are statistically the same. Exposure of the silicone RTV-680 with M30 propellant appears to fit this case. The silicone was stored in the propellant at 150°F for 18 months and silicone samples were tested (tensile strength and elongation) at 3,6,9,12 and 18 months. Controls were treated in exactly the same way except that they were not in contact with propellant. Figures 1 and 2 show the linear plots according to Equation (1). The correlation coefficients are shown in Table 1. One very wild point in the control tensile strength was not

*For tensile and elongation properties.

used in the correlation (see Figure 1). An illustrative differential distribution plot according to Equation 2 is shown in Figure 3. Figures 1 through 3 show that difference between controls and exposed samples are very small.

An independent test for any significant differences between the populations was also performed. The Wilcoxon Sum of Ranks (4) is simple and convenient for this purpose. This test involves ranking the data in order of increasing values and numbering accordingly. The smallest sum of ranks is compared with appropriate tables and the probability (P) of getting the two sets of data in the actual order is determined. Usually anything greater than one chance in 20 (i.e., P=5%) is taken to mean that there is no difference. For the system under consideration it turns out that P > 10%. It seems reasonable to conclude that there are no statistical differences between the populations.

Since after 18 months at 150°F the RTV 680 - M30 system showed no statistically adverse effects, one could reasonably conclude that this system is compatible and could be expected to have a long lifetime under ambient conditions.

Case II

A second case involves fundamental incompatibility with a progressive decrease in mechanical properties with time. Some studies of two commercial Nylon 12-30% glass-filled specimens with WC870 propellant for the 30mm Plastic Cartridge Case program fall in this category. The studies were accomplished at 140°F and tests were made after contact times of 6, 12, 18 and 24 months. The tensile strength versus time curves are shown in Figures 4 and 5 and the linear Weibull plots are given in Figures 6 and 7. Correlation coefficients for the Weibull lines in Table 1 indicate that this treatment is adequate. It is noteworthy that the mechanical properties fall off slowly at first with propellant exposure time and then the drop appears to accelerate, with some levelling off at the longer exposure times. The decrease in Weibull slope with exposure time is indicative of a greater data scatter as the propellant interacts with the Nylon 12.

The foregoing would indicate that Nylon 12 should not be used with this type of propellant. Indeed, any nylon should be tested thoroughly before use with WC870 or related propellants.

Case III

A third case involves some degree of incompatibility as evidenced by an initial sharp decline in mechanical properties upon exposure to propellant. However, this reduction is followed by a period of stability in which the properties remain essentially constant. A good example of this situation involves the system Silgan silicone potting compound with M30 propellant. Figure 8 shows the comparison of the controls with polymer exposed to M30 for 3 months at 140°F and for 12 months at 150°F.

Data for the two storage periods are indistinguishable. However, the exposed population has much lower strength values than the controls. Such a system could be cautiously used if the reduction in properties is tolerable under use conditions. Under ambient applications the life would be much larger than under the accelerated testing conditions.

Case IV

In this case there is a decrease in mechanical properties, followed by a levelling off as in Case III. At longer temperature accelerated times there is a further decrease in properties. This may be due to further polymer-propellant interaction, to thermal aging of the polymer, or to both. Where there are multiple effects the situation may be quite complex. Such a case is illustrated by the M205 nonmetallic cartridge case in contact with M26E1 propellant (5). The averages and data value ranges are shown in Figure 9. Although there might be a slight downturn at the highest storage value for the ambient controls, the data overlap indicates that probably there is no change.

In the case of the accelerated tests, the downturn (Figure 9) both for the controls and for the propellant treated would seem to indicate that changes are occurring between 25 and 30 months. Figure 10 perhaps gives a better indication of the magnitude of these changes. In this Figure the experimental points are omitted in order to reduce the clutter. An idea of the goodness of fit in each case can be obtained from the correlation coefficients in Table 1.

From Figure 10 it is hard to draw definitive conclusions. It does appear that both thermal and compatibility effects contribute to the strength reduction at the longest exposure times. However, from the data in hand it does not seem possible to quantitatively separate these effects. It is interesting to note that the reduced strengths after storage are higher than those required by the item in field use. Thus this combination could well be acceptable for use in a temperate zone. Indeed, this item has been in the field for several years and has been reported to be mechanically satisfactory (5).

MATERIALS AND METHODS

RTV 680 is a two component silicone rubber (available from General Electric), which was studied as a potential replacement for the polyurethane seal in the 105mm XM735 projectile. The M30 propellant used in this system has the following formulation (in percent):

Nitro cellulose (12.6% N)	28.0
Nitroglycerin	22.5
Nitroguanidine	47.7
Ethyl Centralite	1.5
Graphite	0.1

Tensile bars made from the RTV 680 elastomer were stored at 66°C (150°F) in direct contact with the M30 propellant in a closed glass container. The samples were periodically removed at intervals of 3, 6, 9, 12 and 18 months and mechanically tested. Tensile strength was determined according to ASTM-D412 "Tension Testing of Vulcanized Rubber" using an Instron Universal testing machine at a rate of 5 inches/minute.

Silgan silicone was also evaluated as a candidate for the aft seal in the XM735 projectile. Silgan (SWS Silicones Corp) long-term compatibility with M30 propellant was evaluated using the same procedures as described above for the RTV 680 silicone.

Commercial Nylon 12 containing 30% glass filler (Hüls and Polymer Research) was evaluated for long-term stability with WC870 double base propellant at intervals of 6, 12, 18 and 24 months. This system was considered for the 30mm plastic cartridge case. The WC870 propellant composition (in percent) is:

Nitrocellulose (13.15%N)	79.0
Nitroglycerine	10.0
Dinitrotoluene	0.5
Diphenylamine	1.0
Dibutyl Phthalate	7.0
Calcium Carbonate	0.6
KNO_3	0.7
$Sn\ O_2$	1.0
$Na_2\ SO_4$	0.1
Volatiles and Moisture	1.0

The tensile strength of the nylon samples was measured on the Instron machine at room temperature with a crosshead speed of 0.2 inch/minute.

The M205 non-metallic cartridge case is used in conventional 152mm ammunition. The propellant charge for such ammunition is a double base M26E1 propellant whose formulation is (in percent):

Nitrocellulose (13.15% N)	68.7
Nitroglycerine	25.0
Ethyl Centralite	6.0
Graphite	0.3

The cartridge case has the following nominal composition (in percent):

Nitrocellulose (12.6% N)	55.0
Kraft Fiber (cellulose)	9.0
Acrylic Fiber (fibrillated)	25.0
Polyvinyl Acetate Resin	10.0
Diphenylamine	1.0

The cartridge case was stored[5] in the form of tensile specimens at 122°F in contact with the M26E1 propellant. After storage for various time intervals the specimens were subjected to tensile stress at a crosshead speed of one inch/minute until failure.

All the control samples (those not exposed to propellant) were treated in the same manner as the test specimens.

ACKNOWLEDGEMENTS

The authors wish to thank Mr. Robert Bonk for supplying the compatibility data for Nylon 12 and silicones, and Mr. Joseph Gulbierz for the Silgan silicone data.

REFERENCES

1. J. Rubin, R.B. Bonk and D.W. Levi, "Compatibility Evaluation of Polymers with Propellants Based Upon the Technique of Linearization of Data, In Proceedings ADPA Symposium on Compatibility of Plastics and Other Materials with Explosives, Propellants and Pyrotechnics, Held at Naval Ordnance Station", April 1976, II-E-1.
2. C.A. Moyer, J.J. Bush and B.T. Ruley, "The Weibull Distribution Function for Fatigue Life", Mater. Res. Stand. 2, (1962) 405.
3. FH Steiger, "Practical Applications of the Weibull Distribution Function", Chem. Tech. 1971, 225.
4. R. Langley, "Practical Statistics", Dover Pub, NY 1971, pp 166-178.
5. S. Axelrod, "Effect of M26E1 Propellant on the M205 Nonmetallic Cartridge Case and the EPDM Elastomeric Barrier Bag for 152mm Conventional Ammunition, PA Tech Rept 4749, 1975.

TABLE 1

Correlation Coefficients for the Linear Weibull Distribution Plots

System	Correlation Coefficient
RTV-680 Controls Tensile	0.995
RTV-680-M30 Tensile	0.968
RTV-680 Controls Elongation	0.984
RTV-680-M30 Elongation	0.989
Nylon 12 (Huls) Controls	0.949
Nylon 12 (Huls)-WC870 6 Mo.	0.963
Nylon 12 (Huls)-WC870 12 Mo.	0.946
Nylon 12 (Huls)-WC870 18 Mo.	0.888
Nylon 12 (Huls)-WC870 24 Mo.	0.986
Nylon 12 (Nylatron) Controls	0.975
Nylon 12 (Nylatron)-WC870 6 Mo.	0.982
Nylon 12 (Nylatron)-WC870 12 Mo.	0.990
Nylon 12 (Nylatron)-WC870 18 Mo.	0.938
Nylon 12 (Nylatron)-WC870 24 Mo.	0.951
Silgan Controls	0.970
Silgan-M30	0.960
M205 Case Controls 1-25 Mo.	0.974
M205 Case-M26E1 1-25 Mo.	0.943
M205 Case Control 30 Mo.	0.944
M205 Case-M26E1 30 Mo.	0.964

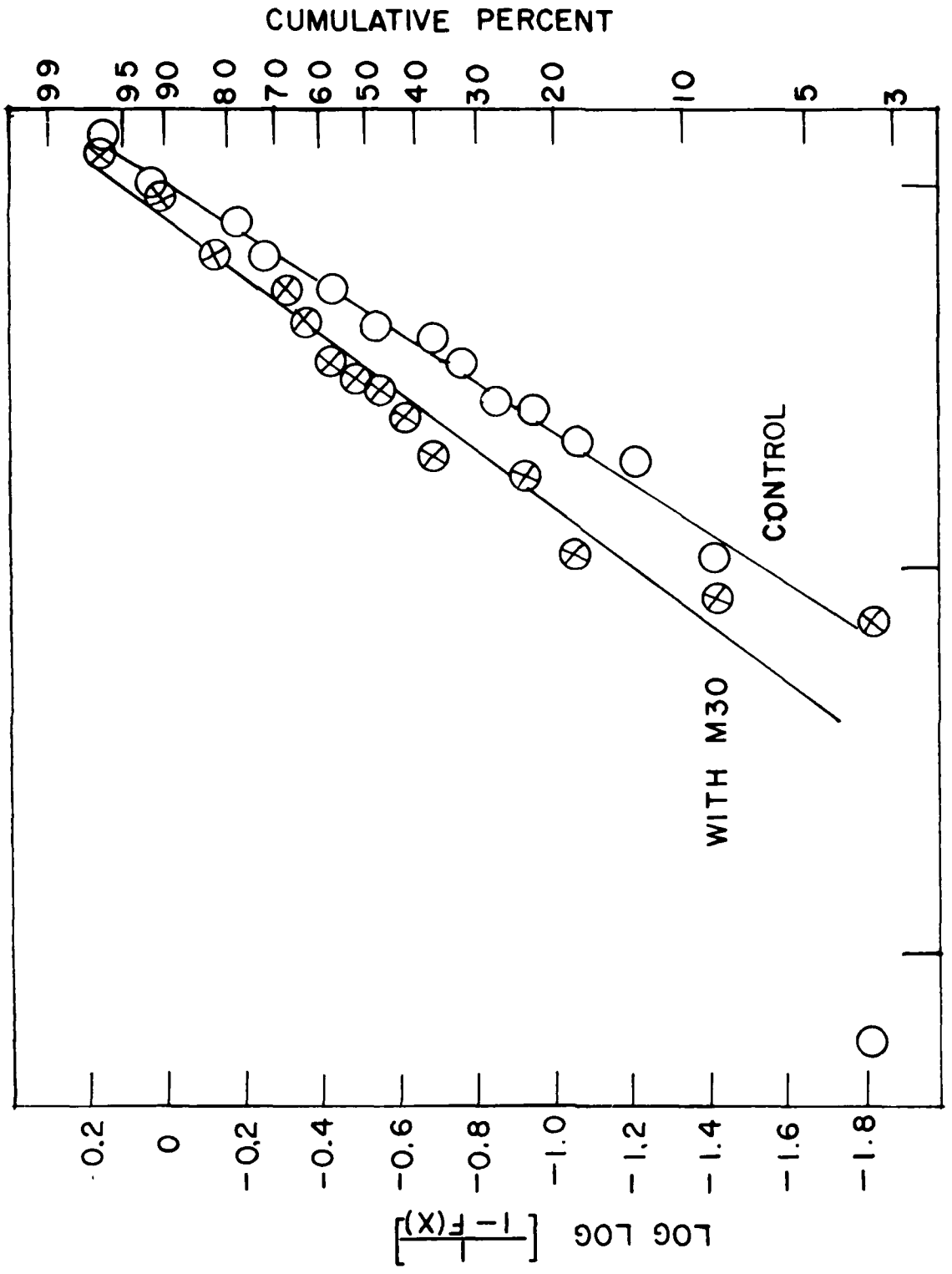

FIG. 1 LINEAR WEIBULL DISTRIBUTION PLOTS FOR CONTROL AND FOR M30-TREATED RTV-680 DATA.
X = TENSILE STRENGTH.

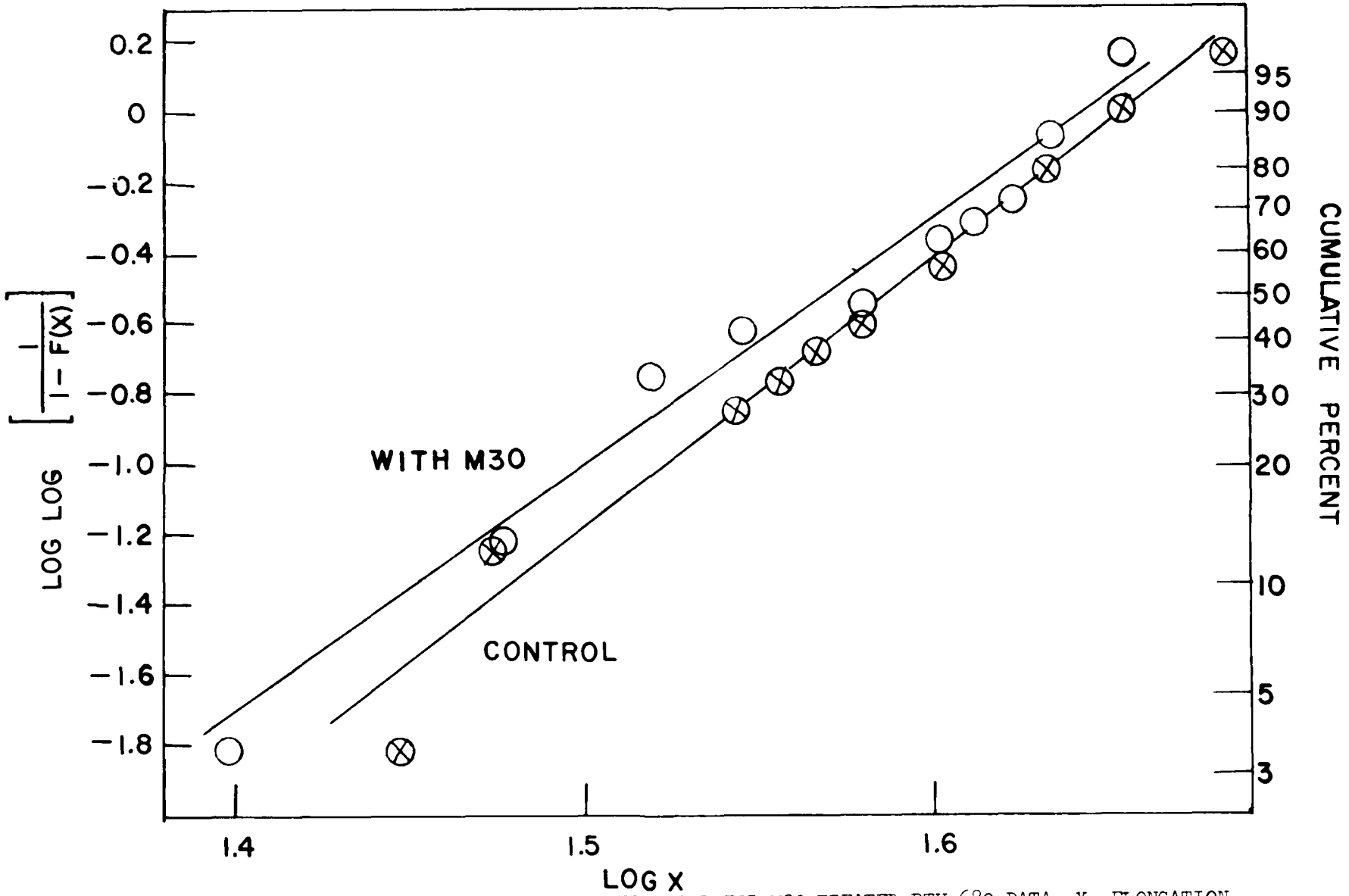

FIG.2 LINEAR WEIBULL DISTRIBUTION PLOTS FOR CONTROL AND FOR M30-TREATED RTV-680 DATA. X= ELONGATION.

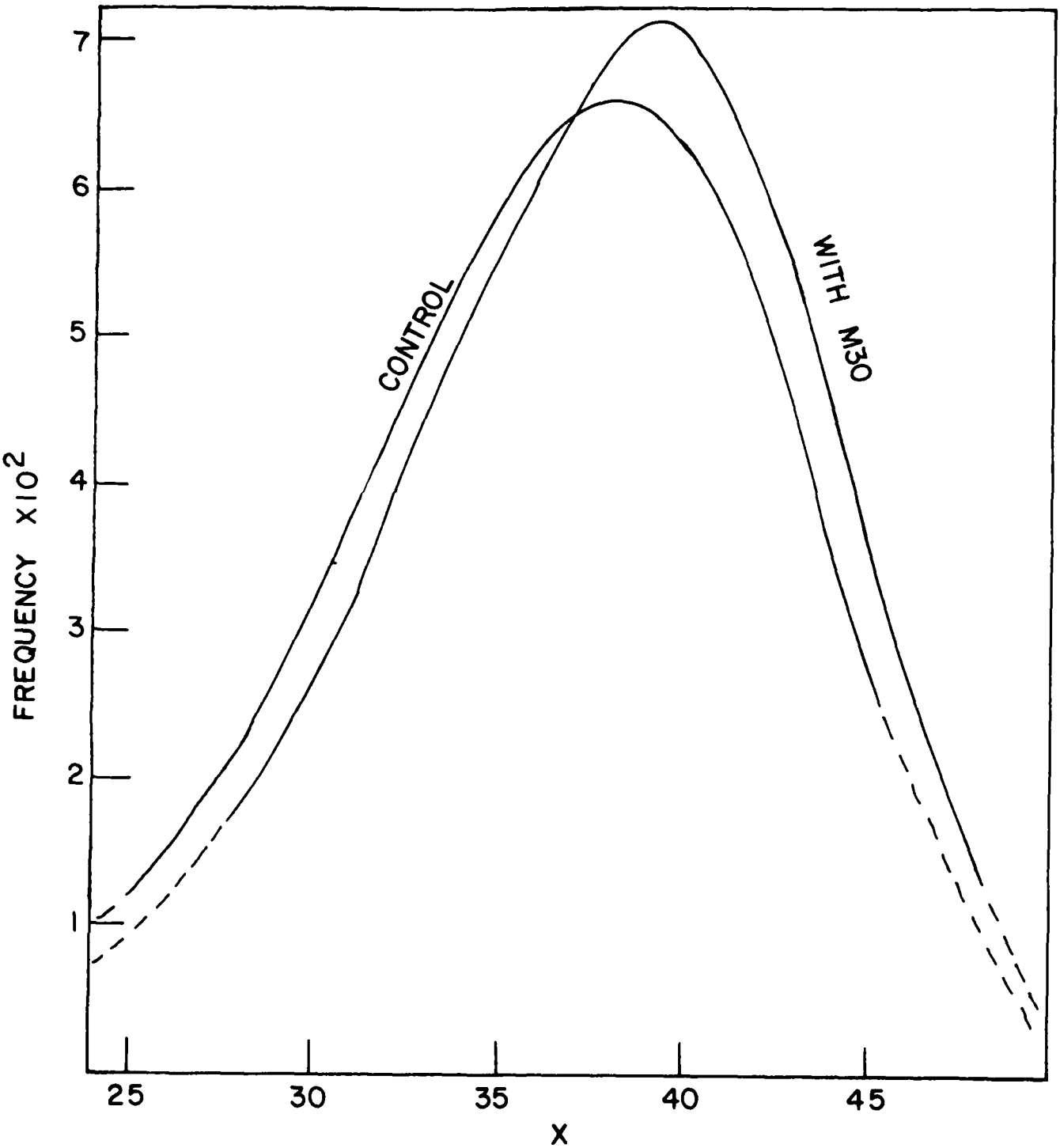

FIG. 3 DIFFERENTIAL WEIBULL DISTRIBUTION CURVES FOR CONTROL AND M30 TREATED RTV-680.

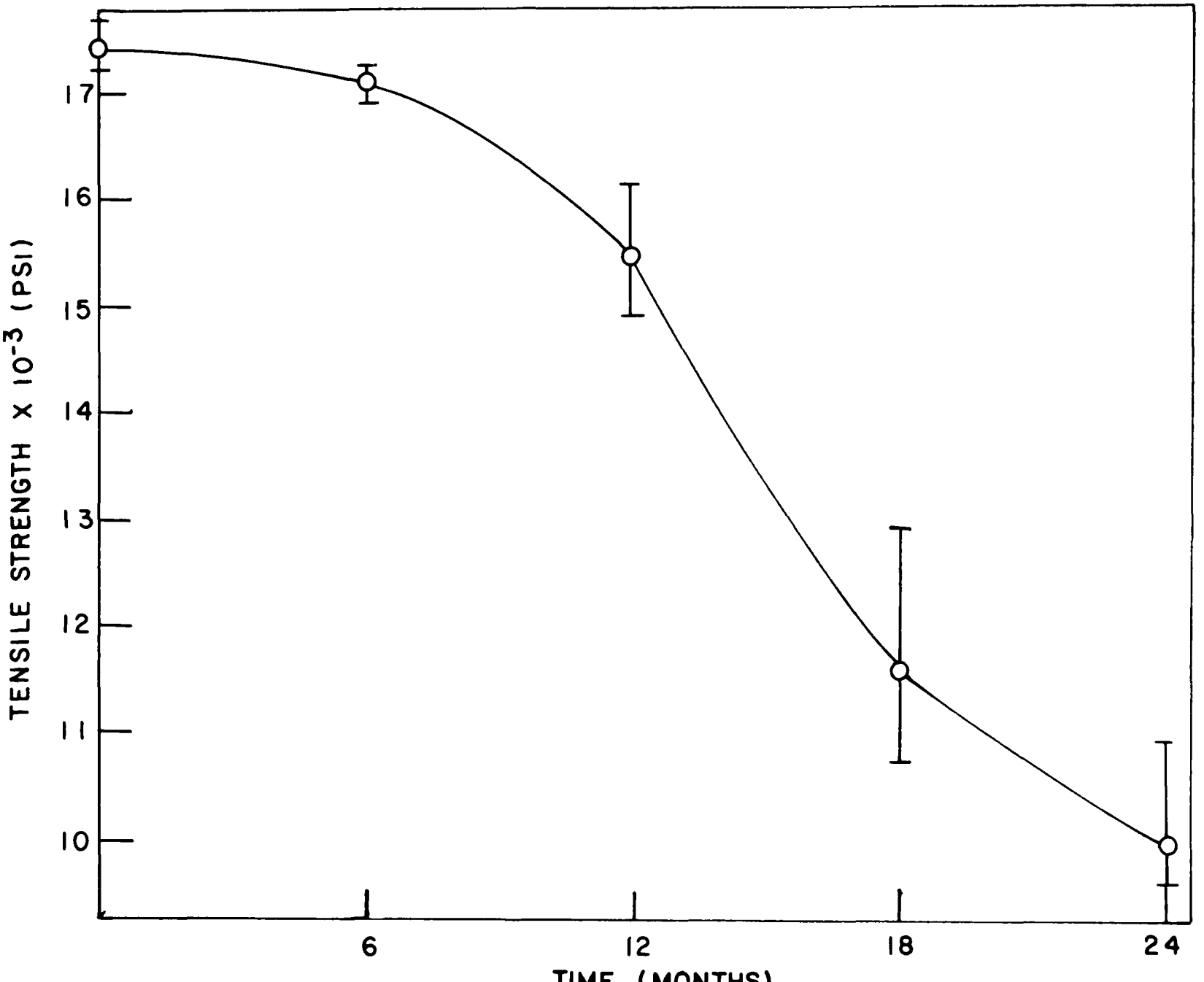

FIG.4 STRENGTH VS. STORAGE TIME AT 140°F WITH WC870 FOR NYLON 12 (HULS)-30% GLASS.

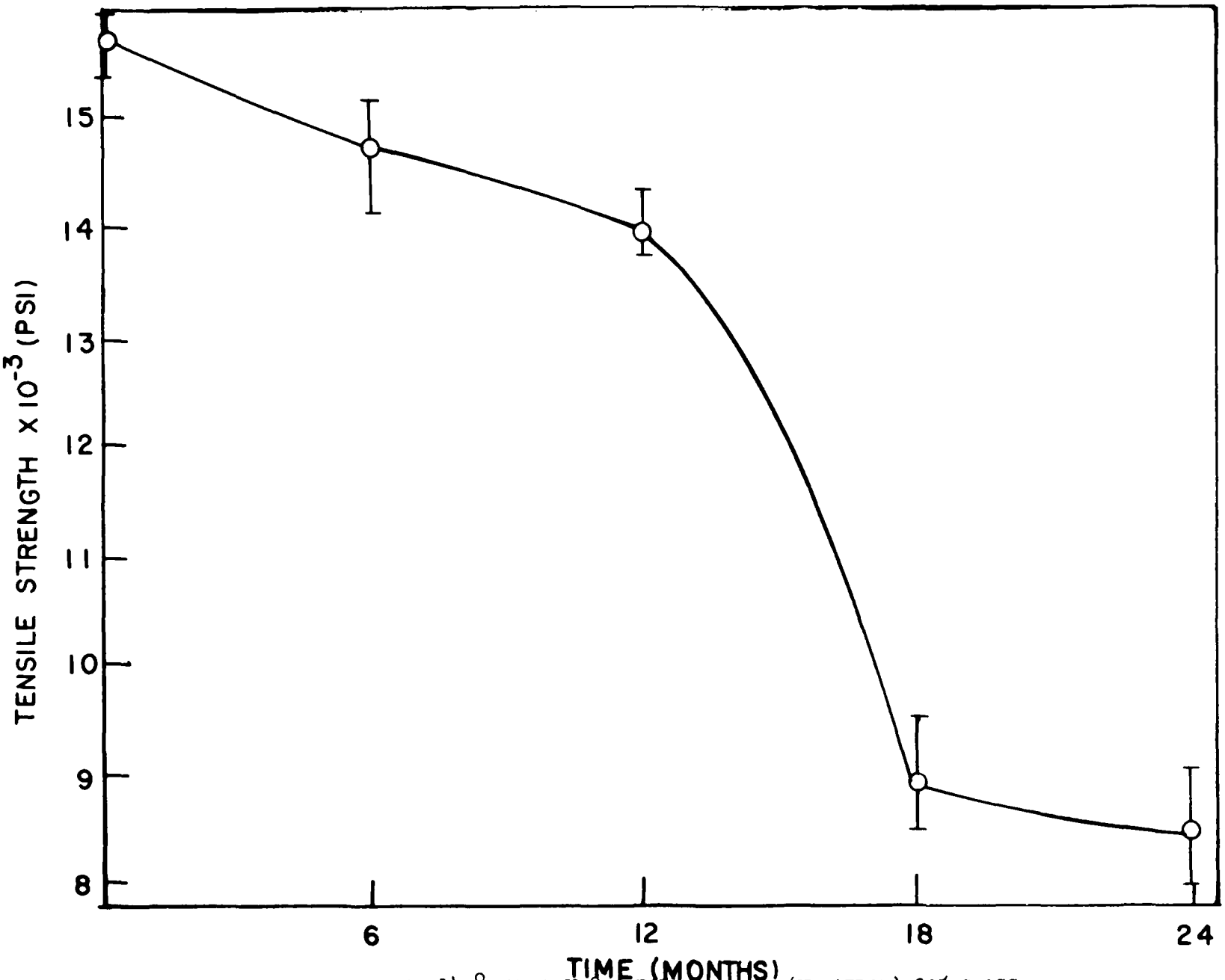

FIG.5 STRENGTH VS. STORAGE TIME AT 140°F WITH WC870 FOR NYLON 12 (NYLATRON)-30% GLASS.

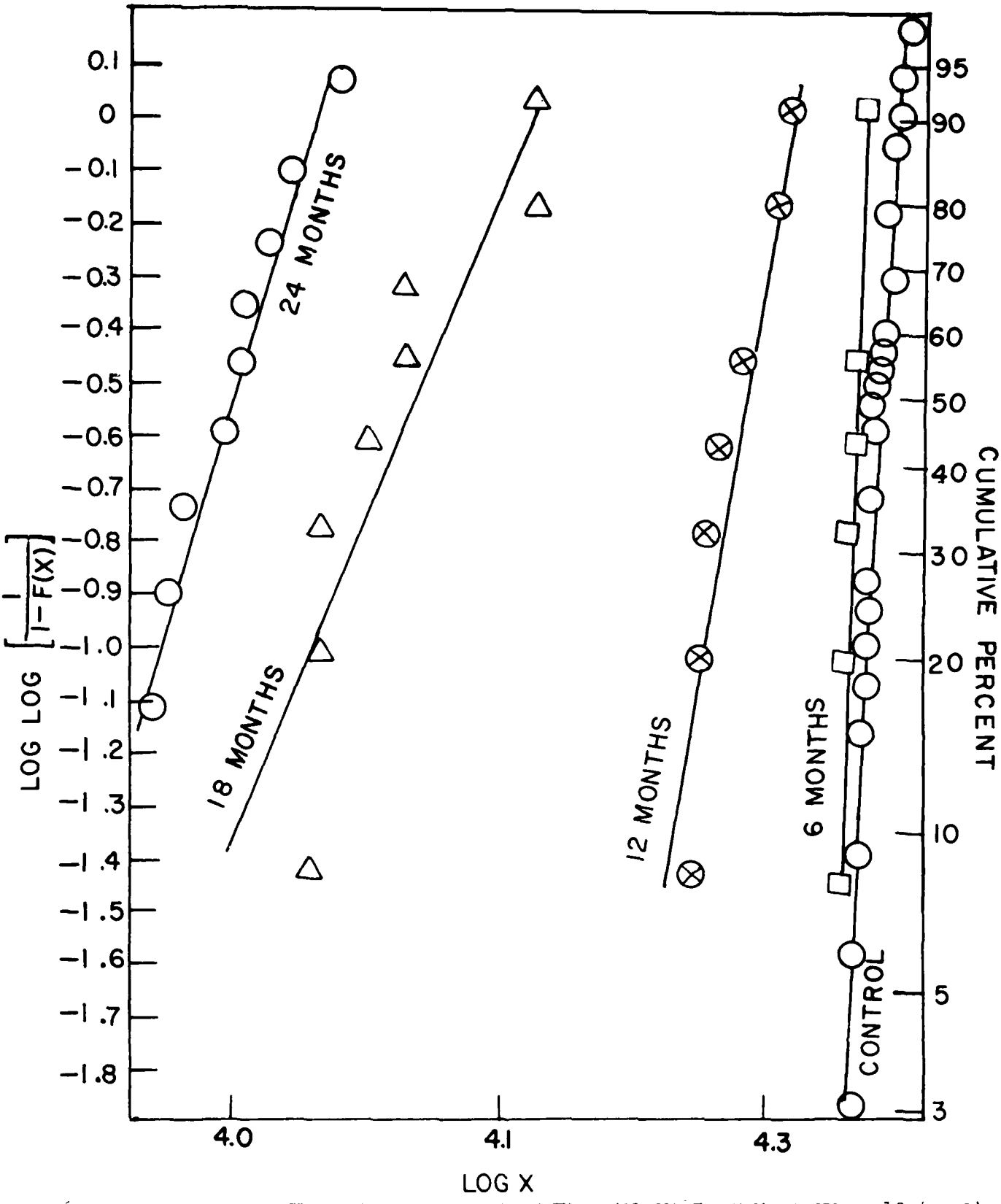

FIG. 6 LINEAR WEIBULL DISTRIBUTION PLOTS FOR CONTROL AND WOMO-TREATED NYLON 12 (HTS)-30% GLASS. X= TENSILE STRENGTH.

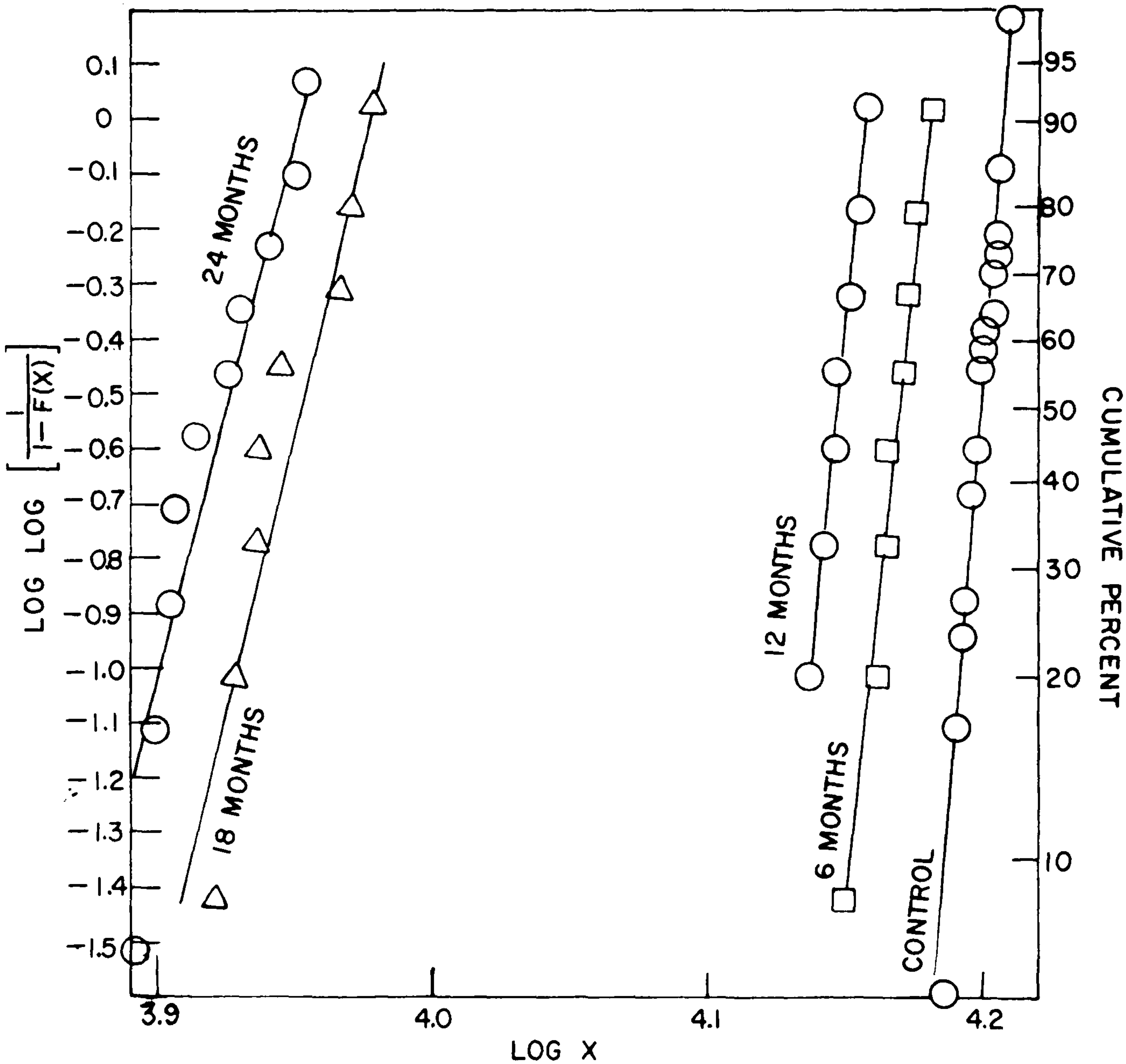

FIG. 7 LINEAR WEIBULL DISTRIBUTION PLOTS FOR CONTROL AND WC870-TREATED NYLON 12 (NYLATRON)-30% GLASS. X = TENSILE STRENGTH.

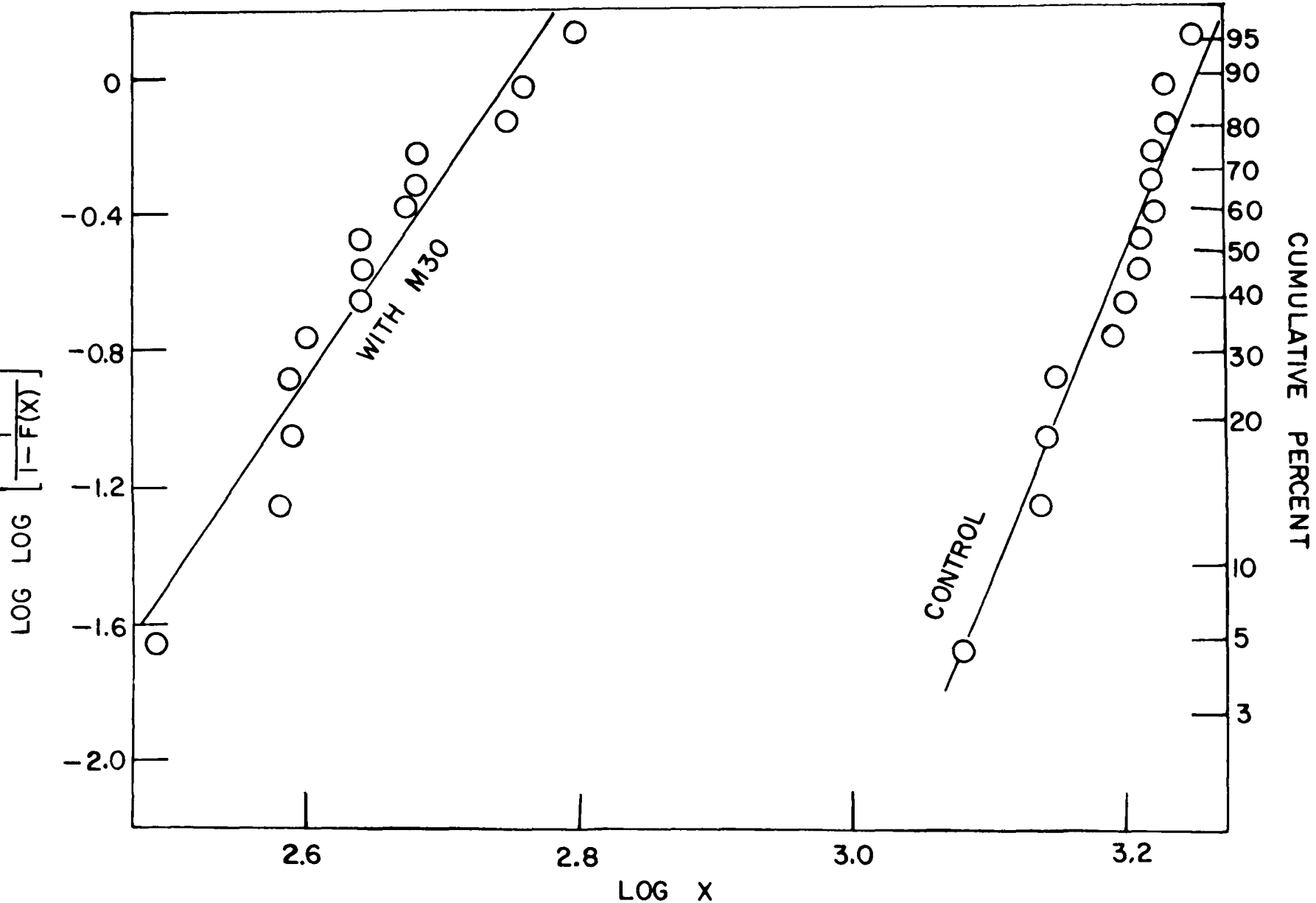

FIG. 7 LINEAR WEIBULL DISTRIBUTION PLOTS FOR CONTROL AND FOR M30-TREATED SILGAN SILICONE. X= TENSILE STRENGTH.

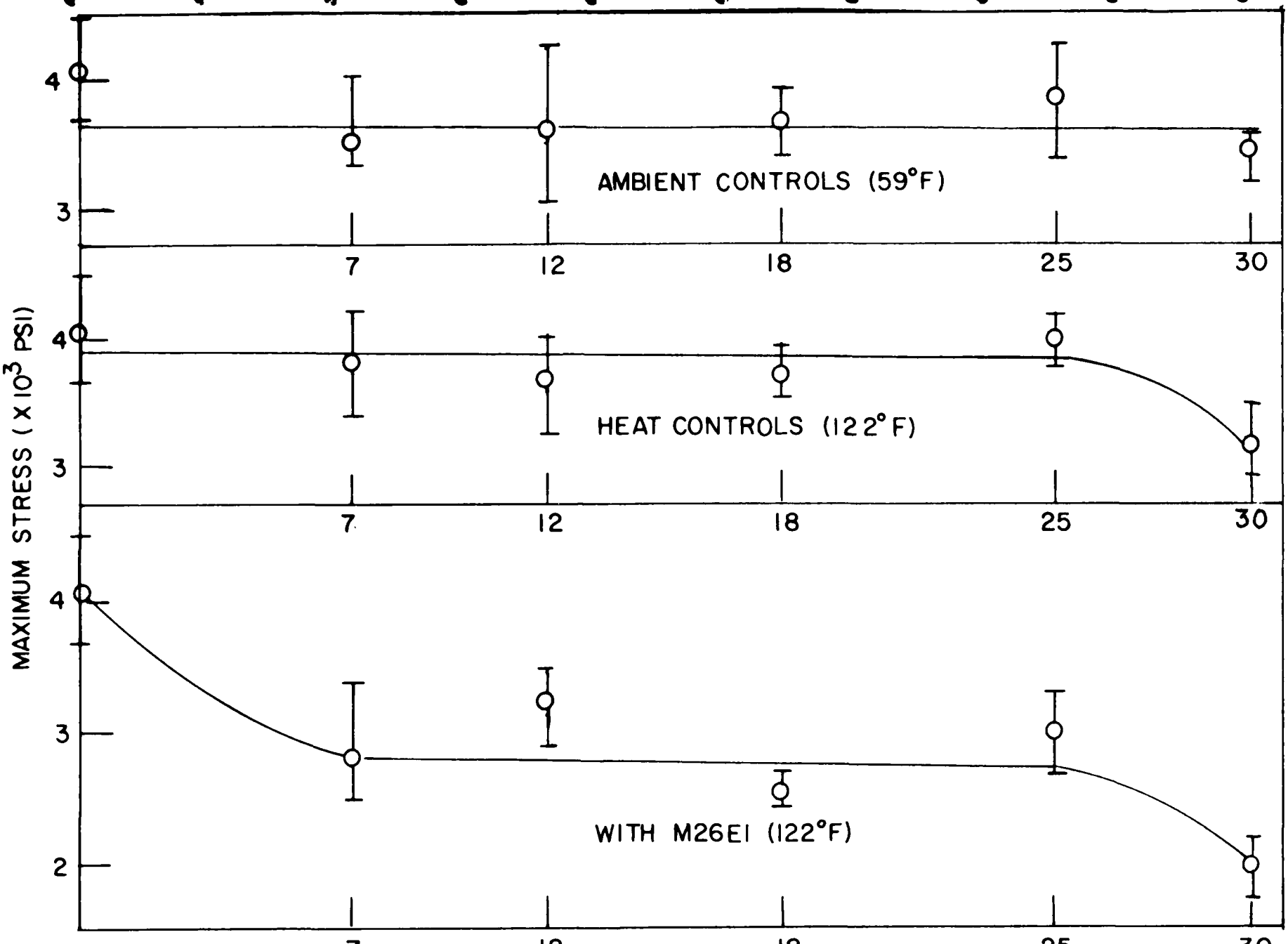

FIG. 9 EFFECT OF STORAGE OF M205 CARTRIDGE CASE WITH M26E1 PROPELLANT

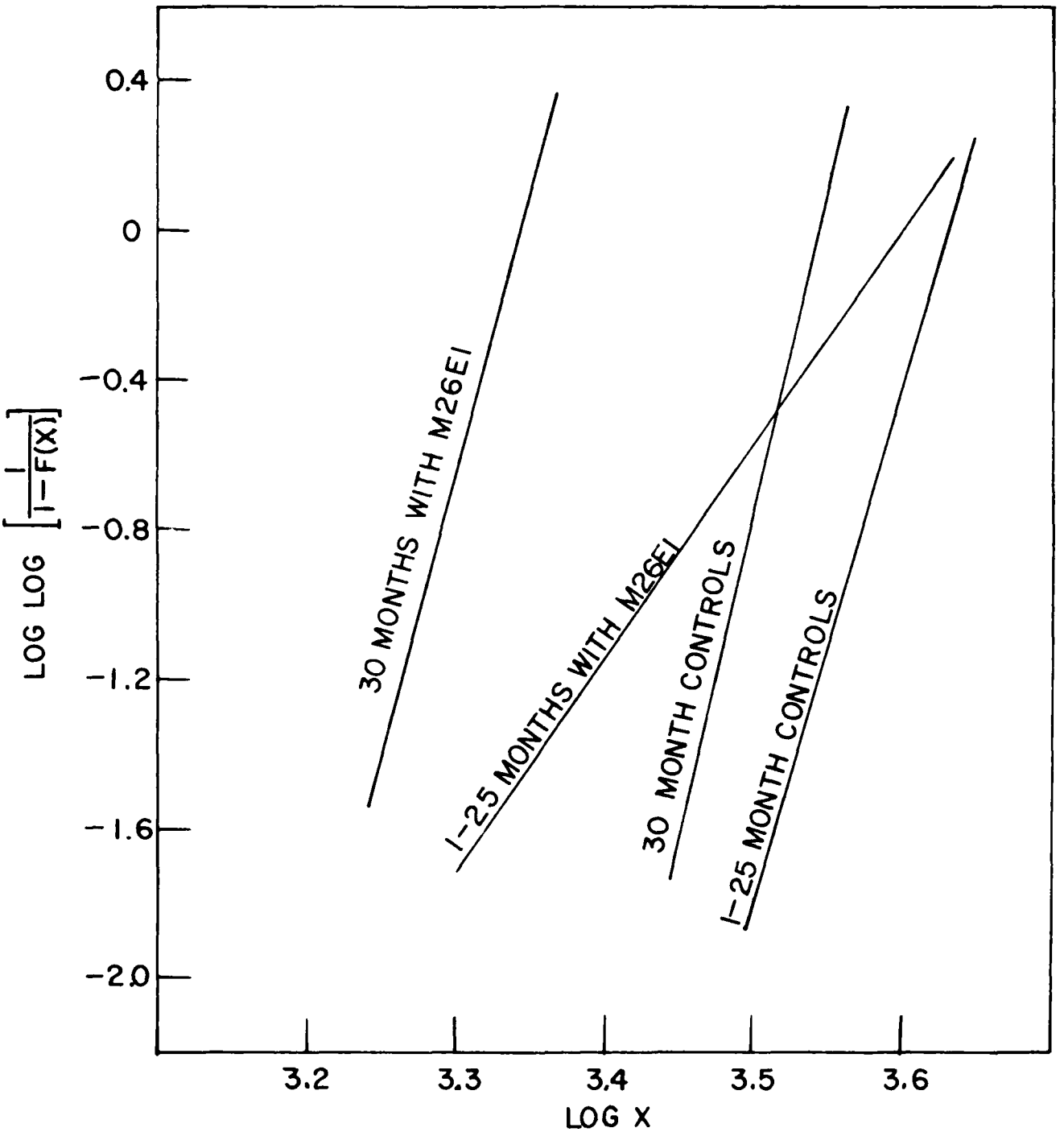

FIG. 10. EFFECT OF STORAGE TIME AT 122°F ON TENSILE STRENGTH OF THE M205 CASE.

LABORATORY TESTS AT ELEVATED TEMPERATURES FOR THE PREDICTION OF THE RATES OR PRESSURE RISE IN HYDRAZINE TANKS AT NORMAL STORAGE TEMPERATURES

CLIFFORD R BENNETT, DOUGLAS R B SAW and DEREK SUTTON

Procurement Executive, Ministry of Defence,
Propellants, Explosives and Rocket Motor Establishment,
Westcott, Aylesbury, Buckinghamshire, UK

ABSTRACT

Various types of laboratory equipment have been used to measure the rates of gas evolution from liquid phase decomposition of hydrazine and from surface decomposition at elevated temperatures. In general the rates were found to be independent of time after the first few days on test and the surface rates obeyed the Arrhenius relationship with respect to temperature, hence enabling extrapolations to be made to normal storage temperatures. Good agreement was obtained between the measured rate of pressure rise in a 32 litre, titanium alloy tank at 70°C and that predicted on the basis of samples tested in laboratory equipment at the same temperature. A procedure by which rates of pressure rise can be converted to rates of hydrazine decomposition, taking into account the solubilities of nitrogen and ammonia, is given.

1. INTRODUCTION

The internal volume of a hydrazine tank should be large enough to contain the maximum load of propellant at the highest anticipated storage temperature together with sufficient ullage to limit the pressure rise due to hydrazine decomposition to an acceptable level throughout the storage life of the system.

Calculation of the minimum ullage, and from it the minimum size of tank, requires a knowledge of the rates of decomposition of hydrazine both in the liquid phase and in contact with the internal surface of the tank at the storage temperatures of interest. In practise the rates of decomposition are often quite slow and difficult to measure with accuracy at normal storage temperatures and over short experimental times unless very careful control of test temperature is maintained and sensitive pressure measuring devices are used. However, even

these slow rates can lead to considerable rises in ullage pressure over extended storage times, such as ten years, and methods for assessing the ullage requirements at the start of a project without recourse to sophisticated control and measuring equipment is desirable. The use of test temperatures in the range 60-90°C rather than the normal storage temperatures of 10-30°C produces rates of hydrazine decomposition that are typically 10 to 50 times higher. This data can then be extrapolated to the lower temperatures of interest providing that the rates of decomposition are not varying with respect to time and providing that they obey the normal Arrhenius relationship with respect to temperature (logarithm of rate proportional to reciprocal of absolute temperature). This enables relevant data to be obtained in much shorter times and reduces somewhat the need for very accurate control and measuring equipment.

Various types of laboratory test equipment that have been used to determine the rates of gas evolution from the liquid phase and from surfaces over a range of temperatures are described and examples of the data obtained are presented. Laboratory data obtained at 70°C is used to predict the rate of pressure rise in a 32 litre, titanium alloy tank and the measured rate at 70°C is compared with that predicted.

A procedure by which rates of pressure rise under given conditions can be converted into rates of hydrazine decomposition is given in an appendix. This makes allowance for the effects of the differing solubilities of nitrogen and ammonia in hydrazine and the effect of temperature on these solubilities is included. Data regarding the rate of pressure rise for a system with a known fraction of ullage can be converted into rates of pressure rise for any other fraction of ullage at that temperature.

2. TEST EQUIPMENT AND PROCEDURES

This section contains details of the different types of test equipment used at PERME to measure rates of gas evolution from hydrazine and includes cleaning procedures, calibration and filling procedures and methods of temperature control.

The hydrazine used in all the tests was purchased to conform with the US Military Specification MIL-P-26536C[1] and chemical analysis during the course of the tests confirmed this requirement. This specification requires the content of hydrazine to be above 98% w/w.

2.1 Pressure Measurement by Mercury Manometer (Equipment A)

The first type of equipment tested was made entirely from glass and had a ground joint which was greased connecting the tube containing hydrazine to the mercury manometer 'U' tube. Problems of sealing this joint at elevated temperatures resulted in a change to the equipment shown in Fig. 1 which employs a screwed joint to squeeze a PTFE wrapped silicone rubber washer between the two

glass surfaces. Figure 2 includes a section through this type of joint. The taps have PTFE keys to avoid the use of greases. The glass bulb and tap attached to the left-hand limb of the mercury manometer serves a dual purpose. The tap is closed during an experiment to isolate the mercury manometer from the effects of changing atmospheric pressure and the size of the bulb (30 cm^3 approx) is sufficient to ensure that movement of the mercury column due to gas generation makes virtually no difference to the volume and hence pressure of the air that is locked above the left-hand limb. The volume of ullage between the hydrazine and the right-hand limb (30 cm^3 approx at 70°C) is also sufficient to minimise changes on that side of the manometer.

The internal volume of the equipment to the right of the manometer was determined by filling with water and weighing, the glassware then being cleaned by filling with concentrated nitric acid at 50°C for at least one day, washed out with deionised water and then filled with anhydrous hydrazine and heated for several days at 70°C. After [illegible] this initial filling of hydrazine about 85 cm^3 of the hydrazine [illegible] tube and the exact quantity determined by [illegible] heated in an oven controlled at the temperature [illegible] fitted with an "over-temperature" cut-out [illegible] test temperature for safety. The automatic control [illegible] was usually sufficient to reduce "drift" to about ±0.3°C, [illegible] being checked by use of the manual controls. [illegible] equipment was attaining the oven temperature the position [illegible] was controlled by adding a little nitrogen to the left-hand [illegible] meter the test being started with the mercury meniscus near the top [illegible] attached scale that was 3 cm long and graduated in millimetres.

The position of the mercury meniscus was read twice daily until the mercury column (left-hand side) had risen to near the top of the scale, further runs could then be carried out by readjusting the position of the mercury column by means of the taps. When sufficient data had been obtained to enable a value for the rate of pressure rise to be calculated, the test temperature could be changed and the procedure repeated.

This equipment can also be used to determine the rate of gas generation on the surface of samples added to the hydrazine when the rate of gas generation in the absence of the sample is subtracted from that with the sample added at the same temperature. Measurement of the rate of gas generation after removal of the sample indicates whether contamination of the hydrazine from the sample has occurred resulting in a change in decomposition rate. A typical type of sample would be a metal or plastic strip about 7.5 cm x 1.25 cm. Some details of the equipment are listed in Table 1.

2.2 Pressure Measurement by Transducer (Equipment B)

Equipment A has a number of disadvantages. It is fragile, it is difficult to control the position of the mercury column during "warm-up", it occupies considerable space in the oven, the range of pressure measurement is limited, the mercury column tends to stick and hydrazine becomes trapped within the column producing gas bubbles and breaks within the column. For these reasons the use of pressure transducers was investigated and the first type of equipment developed is shown in Fig. 2 (details in Table 1). A stainless steel pressure transducer is mounted above an aluminium alloy connector which attaches to the screwed joint at the top of the sample tube. The connector is provided with a stainless steel relief valve. The transducers were designed for use over the pressure range of 0-2 bar absolute and had a full scale output of 25 mv, they were calibrated against an accurate mercury manometer (vacuum type) before use and checked at intervals between tests. The transducers and other metal parts were given an initial cleaning in an ultrasonic bath containing an aqueous solution of a mild detergent, the glass tube was cleaned by the procedure outlined in Section 2.1. The internal volume of the equipment was determined before cleaning by filling with water and weighing.

About 85 g of hydrazine was weighed into the equipment and after placing in the oven at the set temperature the output of the transducer was monitored on a digital voltmeter twice daily until sufficient data had been obtained to define the rate of pressure rise or the pressure limit (2 bar) had been reached. Excess pressure could then be released through the valve and the process repeated or the experiment carried out at a different temperature.

2.3 Pressure Measurement by Inverted Transducer (Equipment C)

The rates of gas generation measured in Equipment B were found to be about three or four times as high as those measured in Equipment A, presumably due to the decomposition of hydrazine on the metal surfaces of transducer, connector and valve. This would limit the use of Equipment B to the role of providing blanks for added samples and even here the size of the blanks would limit the accuracy with which the net rate due to the sample could be assessed. One possible solution is to replace the stainless steel transducer with one made from titanium alloy that joins directly to the screwed joint, pressure relief being provided by a glass/PTFE tap joined to the top of the sample tube below the joint. Titanium alloy is more compatible than stainless steel (see Section 3.4) but is considerably more expensive. An alternative approach is shown in Fig. 3 (details in Table 1) and this constitutes the present state of development of this type of equipment. The stainless steel transducer is now inverted and filled with mercury to prevent contact of hydrazine with the metal surface, pressure relief being from a glass/PTFE tap. Rates of gas generation with this

type of equipment are similar to those found with Equipment A without the accompanying disadvantages. Procedures for measuring the internal volume, cleaning and for monitoring tests have been described previously. It is likely that this type of equipment or the modification of Equipment B using titanium alloy transducers will probably be used at PERME in the future for measuring either homogeneous or heterogeneous rate of decomposition.

2.4 Aluminium Lined Pressure Container (Equipment D)

The rates of decomposition on some materials were sufficiently high to limit the useful experimental time available with the types of equipment described previously. The form of equipment shown in Fig. 4 (details in Table 1) was used for these materials. An aluminium (S1B) lined stainless steel pressure vessel was provided with a lid containing a stainless steel relief valve and a 0-10 bar stainless steel pressure gauge (Bourdon tube). A PTFE seal made the system pressure tight and a PTFE sample holder could be inserted into the container. The sample holder had room for two strip samples (15 cm x 1 cm) and prevented contact between the samples and the wall of the vessel.

The container was cleaned by first degreasing with isopropyl aclohol, filling with 50% nitric acid for two hours at room temperature and then washing out with deionised water. The data from the first filling with hydrazine was rejected if the rate of pressure rise was abnormally high, the cleaning procedure then being repeated until the usual rate was obtained (0.10 to 0.15 bar/day at 70°C). The test procedure was similar to that described earlier, a blank rate first being obtained in the absence of the samples, the rate in the presence of the samples then being determined and finally a post blank rate being determined. The ullage space above the liquid was flushed free from air using argon gas when an analysis of the gases produced by decomposition was required.

2.5 Titanium Alloy Vessel (Equipment E)

The rate of decomposition on strip samples of titanium alloy (Ti6A14V) was too low to measure with confidence using Equipment A or C and it was therefore decided to fabricate a small vessel from this alloy to facilitate measurements. The vessel was in the form of a cylinder (11.45 cm diameter x 17.3 cm) with a wall thickness of about 0.64 cm. A circumferential weld was located near the top of the vessel and a tube (0.63 cm OD) of Ti6A14V was welded to the centre of the flat top of the vessel and protruded about 15 cm above it. The capacity of the vessel was determined by accurate measurement and confirmed by filling with water. Some details of the vessel are given in Table 1. Polythene tubing was used to connect the top of the vessel to a mercury manometer, the vessel being mounted vertically and completely immersed in a water bath at 70°C whilst on test. A total of 1238 g of hydrazine was accurately added to the vessel and the

ullage space was filled with argon. The rate of gas evolution was measured with the manometer over a period of about ten days, the excess gas vented through a two-way tap on top of the manometer, and the procedure repeated seven times. A sample of the gas was taken for analysis by chromatography. The amount of hydrazine in the vessel was then reduced to 413 g and the rate of gas evolution re-measured (average of six determinations). Finally the amount of hydrazine was reduced to 159 g and the procedure repeated.

2.6 Stainless Steel Vessel (Equipment F)

An almost identical vessel to the one made in titanium alloy (Equipment E) was made from stainless steel (S 130). Details are given in Table 1. Experimental procedures were similar to those described above except that 1200 g of hydrazine was added and experiments were carried out at temperatures of 30, 40, 50, 60 and 70°C.

2.7 Titanium Alloy Tank (Equipment G)

A 32 litre spherical titanium alloy tank (Ti6A14V) was manufactured as part of an ESRO programme[2] and was available for compatibility tests. The tank was designed for positive expulsion and had a hemispherical, elastomeric diaphragm made from a modified EPDM rubber (a terpolymer of ethylene/propylene/diene monomer). Details are given in Table 1.

The tank was evacuated, about 24 kg of hydrazine was weighed into the tank and then nitrogen gas at atmospheric pressure was introduced on the gas side of the diaphragm which was connected to a mercury manometer. The tank was immersed in a water bath maintained at 70°C and the rate of pressure rise was monitored over a period of 28 days. A sample of hydrazine taken from the tank at the end of the test period was checked for gas evolution rate in Equipment A and a sample of ullage gas was checked for hydrogen content.

3. RESULTS AND DISCUSSION

3.1 Presentation of Data

Many different units have been used to tabulate data obtained by various workers for rates of gas evolution, rates of pressure rise or rates of hydrazine decomposition and there are arguments both for and against any particular system adopted depending on the context of the work and the use to which the data is to be applied. There is no doubt that the most fundamental units are those that refer to the rate of hydrazine decomposition (e.g. mg of hydrazine decomposed per unit time) but units that refer to rates of pressure rise or rates of gas evolution are of more immediate value to the designer who is concerned with the amount of ullage to leave in a tank. Because the present work is intended to be used in this context rather than that of the chemical kineticist the data is

presented in terms of rates of gas evolution. In some instances the rate of gas evolution was measured directly (Equipment E and F) whilst in others it was calculated from a knowledge of the rate of pressure rise and the volume of the ullage (Equipment A, B, C and D). The rate of gas evolution is expressed in standard cubic centimetres (SCC) per unit time, which is the volume of gas reduced to standard conditions of $0^{o}C$ and 1 atmosphere pressure. This rate is divided by the weight of hydrazine in the case of gas evolution from the liquid phase or by the surface area involved in the case of heterogeneous decomposition. The tabulated rates of gas evolution at a particular temperature can be used to calculate rates of pressure rise for systems having ullages that occupy between 10 and 40 per cent of the tank volumes and at temperatures up to $90^{o}C$ without introducing errors greater than 10 per cent into the calculation. However for ullages smaller than 10% the increasing fraction of nitrogen that remains dissolved in the hydrazine and for ullages over 40% the increasing fraction of ammonia that is released to the ullage introduce progressively greater errors into the calculation. A method by which account can be taken of the solubilities of nitrogen and ammonia is given in the Appendix which relates rates of gas evolution to the more fundamental units of rates of hydrazine decomposition. Gas analysis of the products of decomposition of the liquid phase and of the decomposition on stainless steel or titanium alloy have shown that only small quantities of hydrogen are produced (typically 1%) and the stoichiometry of decomposition at temperatures up to $90^{o}C$ can be represented by

$$3N_2H_4 = N_2 + 4NH_3$$

2.24×10^{4} scc of nitrogen are therefore produced by the decomposition of 96 g of hydrazine.

3.2 Processes Contributing to Hydrazine Decomposition

Hydrazine may decompose homogeneously in the liquid phase and the vapour phase or heterogeneously on surfaces both below and above the liquid level. However the rate of homogeneous vapour phase decomposition at the temperatures of interest can be shown to be negligible by extrapolation of data obtained at high temperatures[3]. One question that the present work was designed to answer was the relative contributions of the surface decomposition above and below the liquid level and the tests with Equipment E were planned to give an answer to that question.

3.3 Liquid Phase Decomposition (Equipment A)

Decomposition of hydrazine in the liquid phase is not easy to measure due to the fact that most container surfaces contribute to the overall rate of gas generation. The Equipment A was designed to minimise surface decomposition but it was necessary to demonstrate that the surface contribution was indeed small.

This was done in two ways. The rate of gas generation from a sample of hydrazine in the Equipment A was first measured at 70°C and then a large number of glass rods of small diameter were introduced and the rate was remeasured. Although the surface area of glass had been increased by a factor of four the rate of gas generation was almost unchanged. In a second series of experiments the amount of hydrazine in the tube of Equipment A was reduced in stages and the rate of gas generation (corrected for gas solubility) was calculated for each stage. It was found that the rate of gas generation per unit weight of hydrazine was approximately constant. These two sets of measurements confirm that the contribution of the glass, PTFE and mercury surfaces in Equipment A can be neglected. Other workers[4,5,6] who have used mercury manometers have not noticed any signs of incompatibility with hydrazine.

Samples of hydrazine conforming to MIL-P-26536C but taken from five different drums were tested at temperatures of 70, 80 and 90°C in Equipment A. The rates of gas evolution were found to be steady after the first few days and are shown in Fig. 5 where it is seen that there is considerable sample to sample variation between different drums and that even from one drum successive samples also show considerable scatter. One reason for this scatter is probably contamination from the atmosphere during transfer because it was not appreciated at the time that these experiments were carried out that traces of carbon dioxide, for example, can cause changes in the rate of decomposition. Future work will employ glove box procedures for filling sample tubes. The data has been treated as a single set for the pruposes of extrapolation to lower temperatures and the assumption made that the Arrhenium relationship can be applied. Further work over a wider range of temperature is required to confirm this assumption. The slope of the line yields an activation energy of 66.3 kJ $mole^{-1}$ (15.8 kcal $mole^{-1}$). It should be emphasised that hydrazine manufactured to a different specification will probably yield different rates of gas evolution and different values for the activation energy. The present work indicates that decomposition in the liquid phase is catalysed by impurities and that the true homogeneous rate of pure hydrazine may be considerably lower than those measured here.

3.4 Decomposition on Surfaces

3.4.1 Aluminium lined pressure vessel (equipment D)

The aluminium lined pressure vessels (Fig. 4) minus the PTFE sample holder were used to determine the rate of gas evolution from 99.5% aluminium (S1B). A total of nine vessels was used at temperatures up to 90°C and the results are shown in Fig. 6. A sample of hydrazine taken from one of these containers and tested in Equipment A confirmed that less than 5% of the gas evolved came from the liquid phase. The rate of gas evolution has been divided by the total internal surface area of aluminium to yield a rate per unit area rather than by the

area beneath the liquid surface. The reason for this will be explained in the next section. The data in Fig. 6 show that there is considerable variation from vessel to vessel but the data has been treated as a single set and obeys the Arrhenius expression. The activation energy is 61.1 kJ $mole^{-1}$ (14.6 kcal $mole^{-1}$). The reason for the variation from vessel to vessel is not known but may be associated with differences in surface finish (true surface area), differences in the hydrazine purity (a glove box was not used for filling) or variable contribution to the gas generation rate from the stainless steel pressure gauge and relief valve. Average data is also presented in Table 2.

3.4.2 Titanium alloy vessel (equipment E)

The rate of gas evolution for three different quantities of hydrazine was measured at 70°C and using the method given in the Appendix was converted to a rate of nitrogen formation. Analysis of a sample of gas from this vessel had shown only traces of hydrogen and the assumption regarding the stoichiometry of the reaction made in the Appendix was therefore valid. The data is shown in Fig. 7 and it is seen that there appears to be a linear increase in rate with the quantity of hydrazine present and that extrapolation of the data to zero quantity of hydrazine yields a positive intercept for the rate of formation of nitrogen.

A sample of hydrazine was taken from the vessel when the ullage was being increased from 10 to 70% and a further sample when the ullage was increased from 70 to 88% at room temperature. These two samples were tested in Equipment A and gave a mean value for the rate of nitrogen formation due to homogeneous decomposition of 9.8×10^{-4} scc g^{-1} day^{-1} at 70°C. This value accounts for the whole of the increase in rate of nitrogen formation that was measured with respect to the fraction of the vessel filled with liquid. Indeed if one assumes that the whole of this increase is due to homogeneous decomposition it yields a calculated rate of 9.2×10^{-4} scc g^{-1} day^{-1} at 70°C (Fig. 7). The rate extrapolated to 0% filled must be due to surface decomposition and the fact that the total rate at 100% filled can be interpreted as the sum of the rate at 0% filled and that due to homogeneous decomposition suggests that within experimental error the surface rate is independent of the position of the liquid level. This implies that the rate on the titanium surface above the liquid is the same as that below and this conclusion is not unreasonable when it is recognised that condensation of hydrazine vapour due to minor variations in temperature may be regularly wetting the surface.

The calculated rate for nitrogen formation on the titanium alloy surface is shown on Fig. 7 and Table 2 and is the lowest value found for a metallic surface.

3.4.3 Stainless steel vessel (equipment F)

The total amount of gas evolved per day from the stainless steel (S 130) vessel is plotted on Fig. 8 against temperature which ranges from 30°C to 70°C. The Arrhenius relationship is obeyed and the activation energy is 50.6 kJ $mole^{-1}$ (12.1 kcal $mole^{-1}$). These rates were divided by the total internal surface area of steel to give the data presented in Table 2. The rates presented in Table 2 may be 10 to 15% too high due to the contribution from liquid phase decomposition which was not separately measured in Equipment A at the time of these tests.

3.4.4 Various surfaces

Samples of various types of metal in the form of strips were tested in Equipment D whilst samples of rubbers were tested in Equipment A. The results are given in Table 2 and it is seen that rates of gas evolution vary considerably with the material on test. In general it was found that austenitic stainless steels containing titanium as an additive (e.g. S 526) gave higher rates than those containing niobium (e.g. S 527 or S 130) and furthermore the rate on a sample of S 526 increased during the first 20 days on test and then maintained its higher value during the next 40 days. Exposure of stainless steel samples to the atmosphere whilst wet with hydrazine caused marked increases in the rate of decomposition on subsequent immersion (rates as high as 1 scc cm^{-2} day^{-1}) and this was probably due to the absorption of carbon dioxide and the formation of carbazic acid[7]. The effect of carbazic acid on the decomposition of hydrazine on a steel surface has been noted[8] at Jet Propulsions Laboratory, Pasadena. It is therefore apparent that contact with the atmosphere must be avoided when materials are wet with hydrazine especially in the case of steels.

Another significant result of the tests is that rubbers which have a silica filler are much more compatible than those containing the more usual carbon filler.

3.4.5 Titanium alloy tank (equipment G)

The rate of pressure rise in the ullage of the tank when on test at 70°C was compared with that predicted on the basis of tests in laboratory equipment. Table 3 contains details of this comparison. Analysis of a sample of ullage gas at the end of the test showed only a trace of hydrogen which confirms checks made from laboratory equipment.

The predicted contributions of liquid phase, titanium alloy surface and rubber diaphragm surface are listed in Table 3, the sum of these leading to a predicted rate of pressure rise that is close to the one actually measured. It is seen that for this size of tank (32 litre) made from the most compatible materials tested (Table 2) the majority of the gas evolved results from liquid phase decomposition. However for much smaller tanks (e.g. 1-5 litres) with higher

ratios of surface to volume and especially if constructed from somewhat less compatible materials (e.g. stainless steel) then the surface rates of decomposition may predominate.

4. SUMMARY AND CONCLUSIONS

Various types of laboratory equipment have been used to measure the rates of gas evolution from liquid phase decomposition of hydrazine and from surface decomposition at elevated temperatures. In general after the first few days on test the rates of gas evolution were found to be independent of time and the surface rates varied with respect to temperature in accordance with the Arrhenius relationship. This gives confidence that the surface rates determined at elevated temperatures can be extrapolated to normal storage temperatures and used to predict rates of pressure rise in hydrazine systems over extended periods of storage. Further work is required before the homogeneous rates can be extrapolated with confidence. The rate of pressure rise in a titanium alloy tank at 70°C was predicted on the basis of laboratory tests on the hydrazine, the titanium alloy and the rubber diaphragm, good agreement being obtained with the rate found whilst the tank was on test.

Tests in a titanium alloy vessel at 70°C and containing various quantities of hydrazine indicate that the rates of gas evolution from the surface above the liquid level is the same as that below. This implies that when predictions are made regarding the rate of pressure rise in closed systems the whole internal surface of the system must be considered and not just that part below the liquid surface.

The importance of avoiding contamination with carbon dioxide is apparent from tests with stainless steel samples and the superior compatibility of rubbers having a silica filler rather than a carbon filler was noted.

5. REFERENCES

1 "US Military Specification, Hydrazine", MIL-P-26536C, 23/5/1969.

2 I.M. Gibbon and A.L. Stokoe, "Design, manufacture and test of a positive expulsion propellant tank", Proceedings of international conference on "Properties of hydrazine and its potential applications as an energy source" held at Poitiers, 22-25 October 1974, p.413-442.

3 I.J. Eberstein and I. Glassman, "The gas phase decomposition of hydrazine and its methyl derivatives", Tenth Symposium on Combustion, 1965, p.365-374.

4 E.T. Chang and N.A. Gokcen, "Compatibility of alloys with hydrazine containing freon", Report SAMSO-TR-76-34, 1976.

5 T.F. Seamans and J. Kahrs, "Hydrazine azide as an additive for mono-propellant hydrazine", J. Spacecraft and Rockets Vol. 8, No. 10, 1971, p.1080-1083.

6 J.P. Young, V.A. Lamb, G.I. Reid, J.F. Berkeley and W. Ng, "Electroplated coatings on maraging steel for retarding catalytic decomposition of hydrazine rocket fuel", Plating, Vol. 57, 1970, p.921-926.

7 H. Greer, "Vacuum start up of reactors for catalytic decomposition of hydrazine", J. Spacecraft and Rockets, Vol. 7, No. 5, May 1970, p.522-528.

8 L.R. Toth, W.A. Cannon, C.D. Coulbert and H.R. Long, "Propellant/material compatibility program and results", JPL Technical Memorandum 33-799, August 1976.

TABLE 1 DETAILS OF TEST EQUIPMENT

Designation	Type	Internal Volume cm^3	Internal Surface Area cm^2	Weight of Hydrazine added g	% Ullage at Ambient Temperature, Approx
A	Mercury Manometer	120 approx (sample side of manometer)	170 approx	85 approx	30
B	Transducer	105 approx	150 approx	85 approx	20
C	Inverted Transducer	110 approx	160 approx	85 approx	23
D	Aluminium lined Vessel (without sample holder)	232	267	186	20
E	Titanium Alloy Vessel	1313	677	1238 413 159	10 (including manometer) 70 (" ") 88 (" ")
F	Stainless Steel Vessel	1294	672	1200 approx	10 (" ")
G	Titanium Alloy Tank	32×10^3	2400 (Ti6A14V) and 2400 (EPDM rubber)	24.05×10^3	25

TABLE 2 RATE OF GAS EVOLUTION FROM DECOMPOSITION OF HYDRAZINE ON SURFACES

Material	Measured rate of gas evolution, 10^{-3} scc cm^{-2} day^{-1}								Equipment Used (see Table 1)
	90°C	80°C	70°C	60°C	50°C	40°C	30°C	20°C	
Titanium Alloy (6A1.4V)			0.7 (from Fig 7)						E
Aluminium Alloy DTD 5080			<3						D
Aluminium, S1B	31	17	9.6	4.9	2.5	1.2	0.55	0.24	D
Stainless Steel (Niobium stabilised) S527, S130			6.8, 9.6	4.1	2.4	1.3	0.7		F, D
Stainless Steel (Titanium stabilised) S526			68 → 130						D
Inconel 600		66	45						D
Radiometal 50 (50% Fe, 50% Ni)		160	93						D
Tungsten Carbide (polished) (94% WC, 4% Co)			120						D
Butyl Rubber (Carbon filler)			40						A
Butyl Rubber (Silica filler)			5						A
Ethylene/Propylene Rubber (Carbon filler)			88						A
Ethylene/Propylene Rubber (Silica filler)			3						A
Modified EPDM Rubber (Silica filler)			0.15						A

TABLE 3 MEASURED AND CALCULATED RATES OF PRESSURE RISE IN THE TITANIUM ALLOY TANK (G) AT 70°C

Tank Data

Weight of hydrazine	=	24.05×10^3 g
Volume of ullage at 70°C	=	7.03×10^3 cm^3
Surface area of titanium alloy exposed to hydrazine	=	2.4×10^3 cm^2
Surface area of EPDM rubber exposed to hydrazine	=	2.4×10^3 cm^2

Test Data

Measured rate of gas evolution from liquid phase sample at 70°C (equipment A)	=	1.41×10^{-3} scc g^{-1} day^{-1}
Therefore calculated rate from 24.05×10^3 g	=	34.0 scc day^{-1}
Measured rate of gas evolution from titanium alloy at 70°C (equipment E)	=	0.67×10^{-3} scc cm^{-2} day^{-1}
Therefore calculated rate from 2.4×10^3 cm^2	=	1.6 scc day^{-1}
Measured rate of gas evolution from EPDM rubber at 70°C (equipment A)	=	0.15×10^{-3} scc cm^{-2} day^{-1}
Therefore calculated rate from 2.4×10^3 cm^2	=	0.4 scc day^{-1}
Total calculated rate of gas evolution	=	36.0 scc day^{-1}
Calculated rate of pressure rise in ullage of 7030 cm^3 at 70°C $= \frac{36}{7030} \times \frac{343}{273} \times 1.013$	=	6.52×10^{-3} bar day^{-1}
Observed rate of pressure rise at 70°C	=	6.71×10^{-3} bar day^{-1}

APPENDIX CALCULATION OF RATES OF HYDRAZINE DECOMPOSITION FROM RATES OF PRESSURE RISE

A1. INTRODUCTION

At normal storage temperatures and at the elevated temperatures (e.g. up to 100°C) used to accelerate compatibility/stability tests liquid anhydrous hydrazine decomposes either homogeneously or heterogeneously to yield mainly nitrogen and ammonia as products. Nitrogen gas is only sparingly soluble in the liquid phase but ammonia is appreciably soluble and in order to relate the rates of pressure rise in the ullages of the closed systems under test to rates of hydrazine decomposition in a quantitative manner it is necessary to take account of the solubilities of these two gases. The fraction of the gas produced by decomposition that is released to the ullage is a function of the relative size of the ullage and liquid phases as well as a function of the solubility of the gas which itself varies with temperature.

In the first part of the Appendix an expression is derived which enables the fraction of the gas released to the ullage to be calculated and data for nitrogen and ammonia at ullages of 0-100% and temperatures of 20, 40, 60, 70 and 80°C are tabulated. In the second part the way in which this data can be used to calculate rates of hydrazine decomposition from rates of pressure rise is illustrated.

A2. PARTITION OF GAS BETWEEN ULLAGE AND LIQUID HYDRAZINE

Let W = weight in g of gas dissolved in hydrazine
M = molecular weight of the gas
T = temperature in °K

At this temperature T

Let V_H = volume of hydrazine in cm^3
V_U = volume of ullage in cm^3
D = density of hydrazine in g cm^{-3}
K = mole fraction of dissolved gas in liquid hydrazine in equilibrium with a partial pressure of 1 atmosphere of the gas

Now moles of gas dissolved in hydrazine = W/M
and moles of hydrazine (mol.wt.32) = $V_H D/32$

Therefore mole fraction of dissolved gas = $\frac{W/M}{V_H D/32 + W/M} = K$

for partial pressure of 1 atmosphere.

Therefore for this condition, moles of dissolved gas, $W/M = \frac{KV_H D}{32(1-k)}$ ... A

Also for this condition, moles of gas in ullage = $\frac{V_u}{22,400} \times \frac{273}{T}$ ..... B

Therefore the fraction of the gas in the ullage (i.e. $\frac{B}{B+A}$)

$$= \frac{\frac{273\ V_u}{22,400T}}{\frac{273\ V_u}{22,400T} + \frac{KV_H D}{32(1-K)}}$$

$$= \frac{V_u}{V_u + \frac{2.564\ KV_H DT}{(1-K)}} \quad .$$

In the above equation the actual values of V_H and V_u can be substituted by % hydrazine and % ullage without changing the numerical value obtained for the fraction of gas in the ullage.

A2.1 Data for Nitrogen

Values of K for nitrogen from Journal of Physical Chemistry Vol. 72, No. 2 p.638, February 1968:

Extrapolation of values to higher temperatures tabulated below.

Temperature ^{o}C	Temperature T ^{o}K	$\log_{10}K$	K	D	$\frac{2.564K\ DT}{1-K}$
20	293	-5.161	6.902×10^{-6}	1.008	5.227×10^{-3}
40	313	-5.055	8.810×10^{-6}	0.990	7.000×10^{-3}
60	333	-4.958	1.102×10^{-5}	0.972	9.146×10^{-3}
70	343	-4.921	1.225×10^{-5}	0.963	1.038×10^{-2}
80	353	-4.870	1.349×10^{-5}	0.953	1.164×10^{-2}

% Hydrazine	% Ullage	Fraction of gas in ullage = $\frac{V_u}{V_u + \frac{2.564\ KV_H DT}{1-K}}$				
		20°C	40°C	60°C	70°C	80°C
99	1	0.659	0.591	0.525	0.493	0.465
98	2	0.796	0.745	0.691	0.663	0.637
97	3	0.855	0.815	0.772	0.749	0.727
95	5	0.910	0.883	0.852	0.835	0.819
90	10	0.955	0.941	0.924	0.915	0.905
80	20	0.980	0.973	0.965	0.960	0.956
60	40	0.992	0.990	0.986	0.985	0.983

A2.2 Data for Ammonia

Values of K for ammonia taken from RPE Tech Memo 611, PERME, Westcott, UK, and extrapolated to higher temperatures below.

Temperature ^{o}C	Temperature T ^{o}K	$\log_{10}K$	K	D	$\frac{2.564K\ DT}{1-K}$
20	293	-0.958	1.102×10^{-1}	1.008	93.79
40	313	-1.208	6.194×10^{-2}	0.990	52.46
60	333	-1.426	3.750×10^{-2}	0.972	32.33
70	343	-1.524	2.992×10^{-2}	0.963	26.12
80	353	-1.619	2.404×10^{-2}	0.953	21.25

% Hydrazine	% Ullage	Fraction of gas in ullage = $\frac{V_u}{V_u + \frac{2.564\ KV_H DT}{1-K}}$				
		20°C	40°C	60°C	70°C	80°C
80	20	0.0027	0.0047	0.0077	0.0095	0.0116
60	40	0.0071	0.0125	0.0202	0.0249	0.0304
40	60	0.0158	0.0278	0.0443	0.0543	0.0659
20	80	0.0410	0.0709	0.110	0.133	0.158
10	90	0.0877	0.146	0.218	0.256	0.298
5	95	0.168	0.266	0.370	0.421	0.472
3	97	0.257	0.381	0.500	0.553	0.603
2	98	0.344	0.483	0.602	0.652	0.698
1	99	0.514	0.654	0.754	0.791	0.823

A3. CALCULATION OF RATES OF HYDRAZINE DECOMPOSITION FROM RATES OF PRESSURE RISE

It is assumed that the rate of pressure rise in atmospheres per unit time $\frac{dp}{dt}$ at a given temperature T (^{o}K) and the volume of the ullage V_u (cm^3) at that temperature are known. Also the total volume of the system is known. The rate of pressure rise is first converted to a rate of gas generation in standard cubic centimetres (scc) per unit time.

$$\text{Rate of gas generation} = V_u \times \frac{dp}{dt} \times \frac{273}{T} \text{ scc/unit time.}$$

It is next assumed that the decomposition proceeds according to

$$3N_2H_4 \longrightarrow 4NH_3 + N_2$$

(96 g) $(4 \times 22.4 \times 10^3$ scc) $(1 \times 22.4 \times 10^3$ scc)

Let us assume that b (scc) of nitrogen are being generated per unit time.

By use of the tabulated data (for temperature T) the fraction of this nitrogen that is released to the ullage (for the % ullage of the system at temperature T) can be estimated.

Let this fraction be f_{N_2} .

Similarly the volume of ammonia being generated per unit time is 4b (from chemical equation above) and the fraction released to the ullage if f_{NH_3}, therefore

$$4b\ f_{NH_3} + bf_{N_2} = \frac{273\ V_u}{T} \times \frac{dp}{dt}$$

from which the value of b can be calculated.

This can then be converted to weight of hydrazine decomposed per unit time since 96 g (N_2H_4) yields 22,400 scc (N_2).

APPENDIX

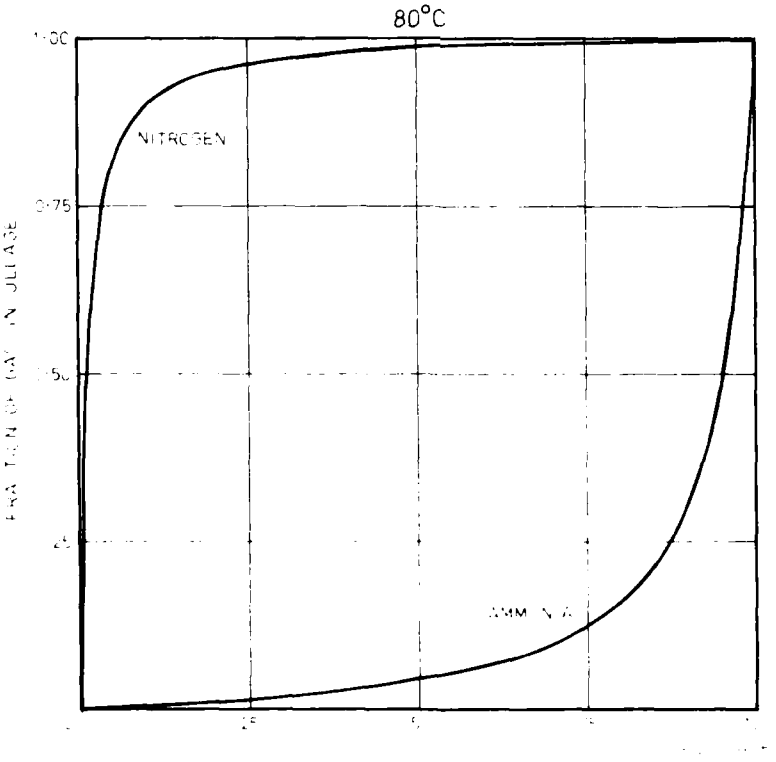

ANHYDROUS HYDRAZINE - PARTITION OF GAS
BETWEEN LIQUID PHASE AND ULLAGE

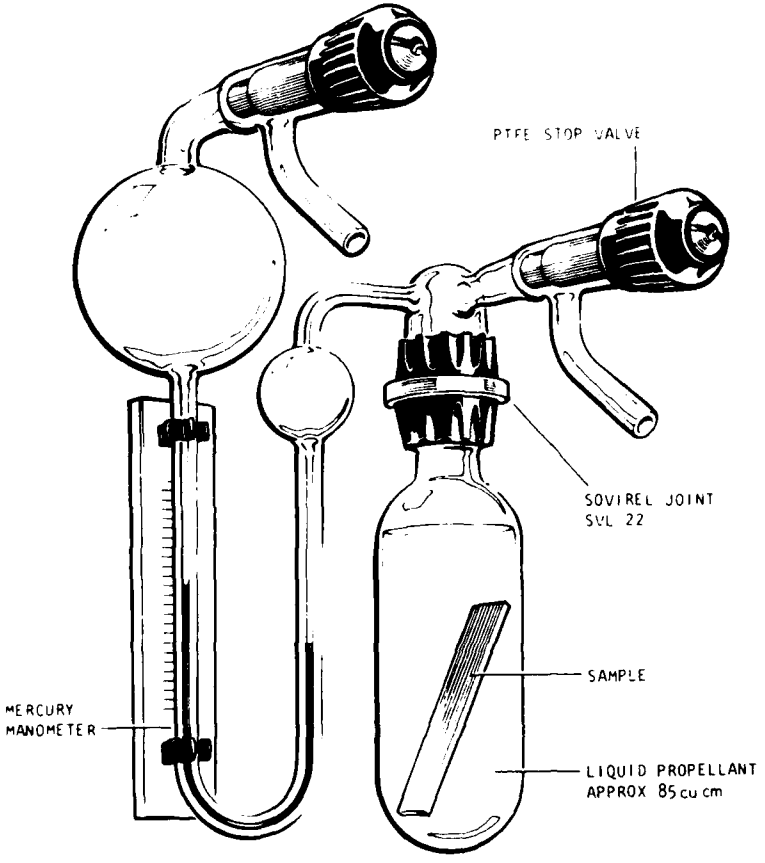

FIG.1 PRESSURE MEASUREMENT BY MERCURY MANOMETER – EQUIPMENT A

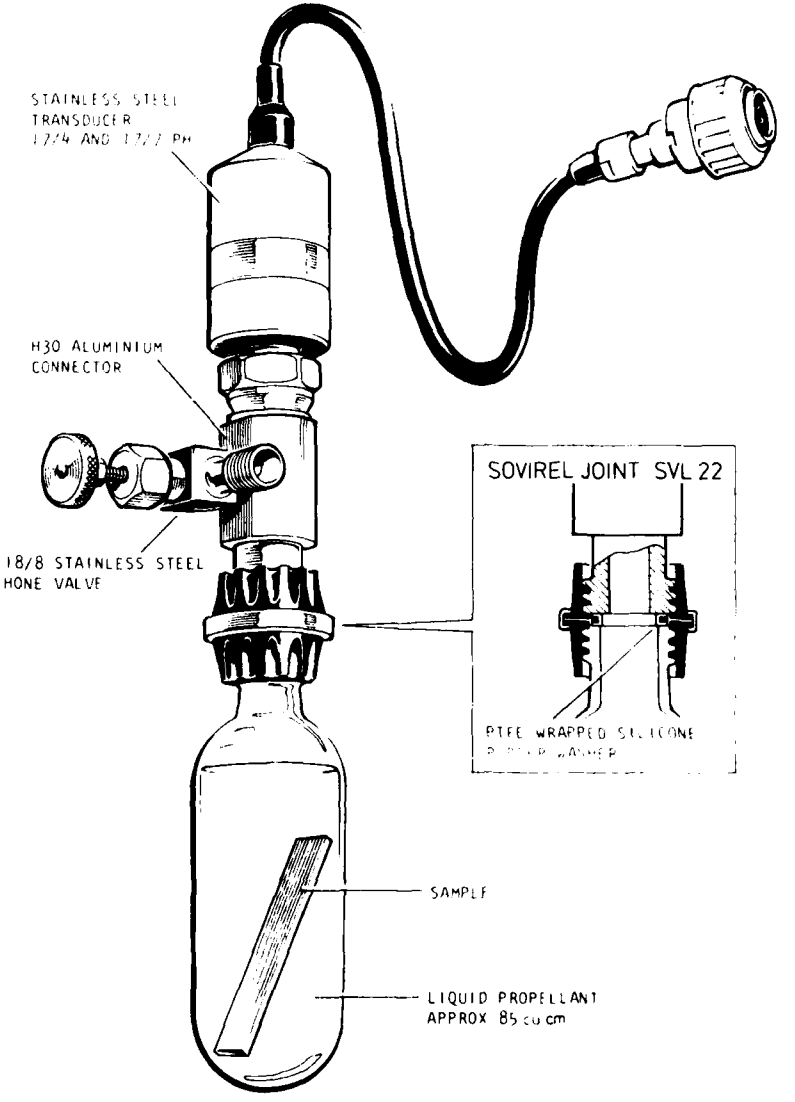

FIG.2 PRESSURE MEASUREMENT BY TRANSDUCER – EQUIPMENT B

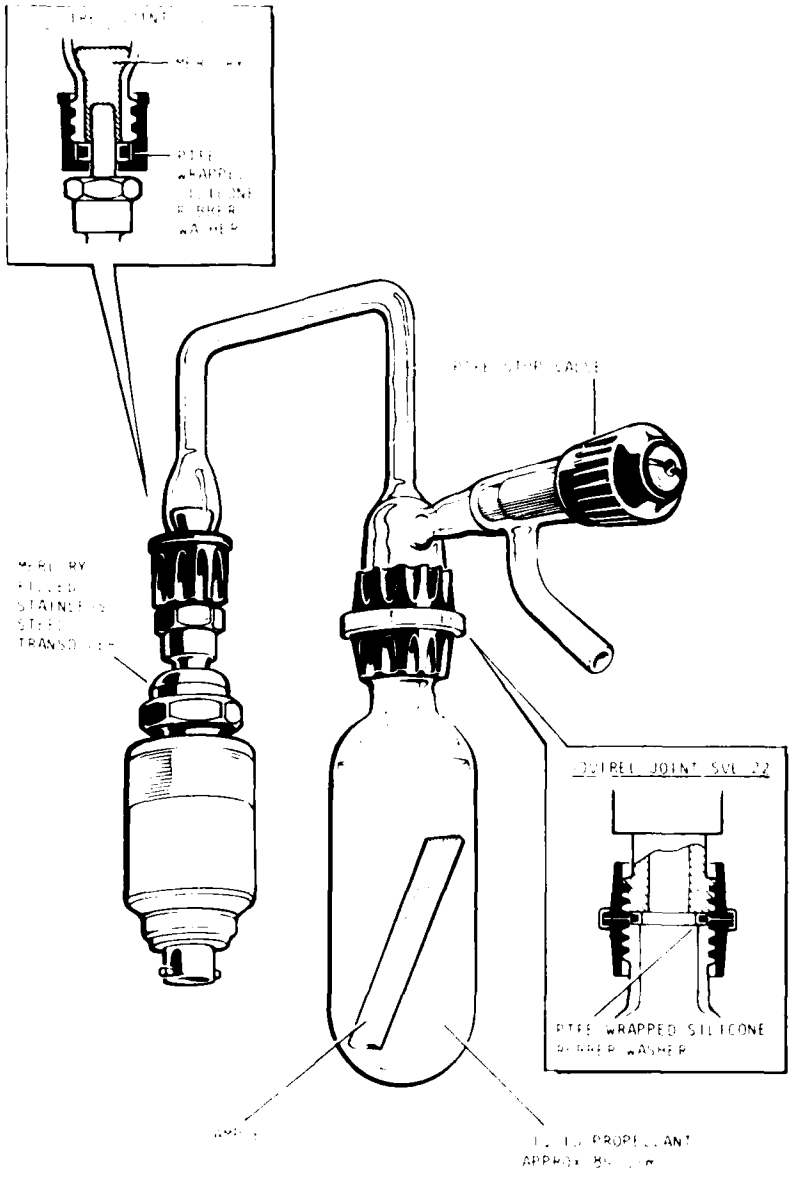

FIG. 3 PRESSURE MEASUREMENT BY INVERTED TRANSDUCER – EQUIPMENT C

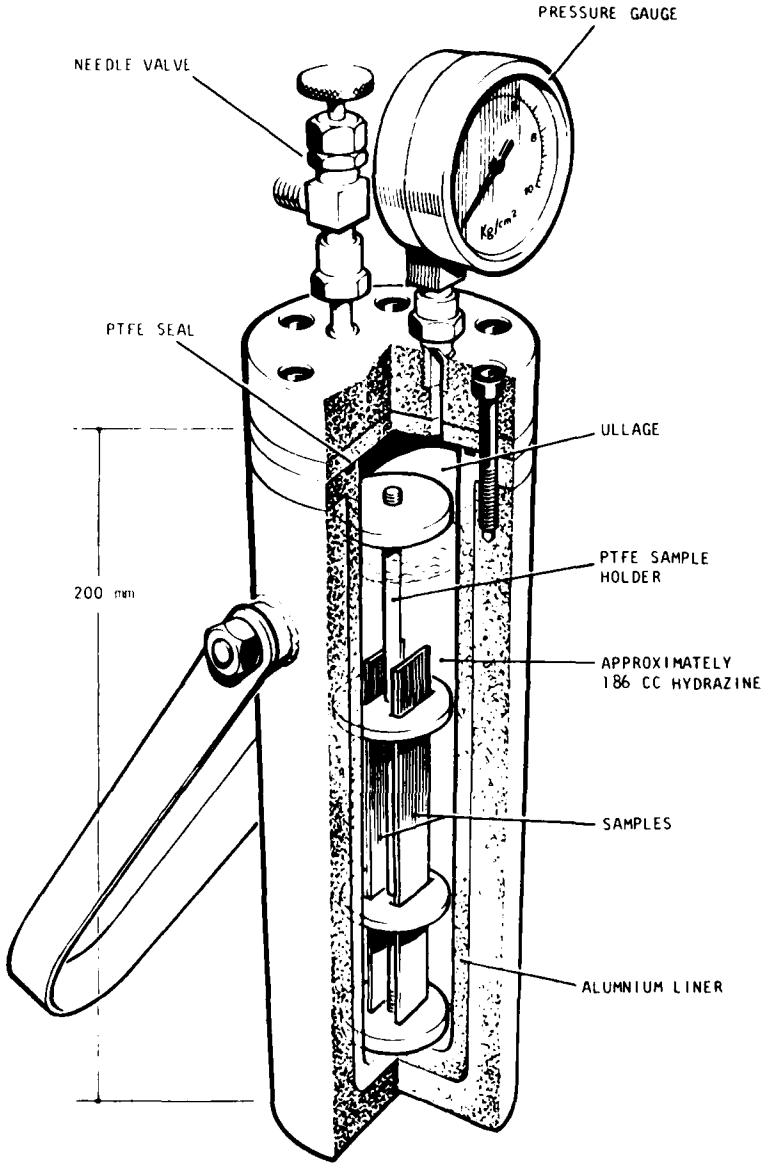

FIG. 4 ALUMINIUM LINED PRESSURE CONTAINER – EQUIPMENT D

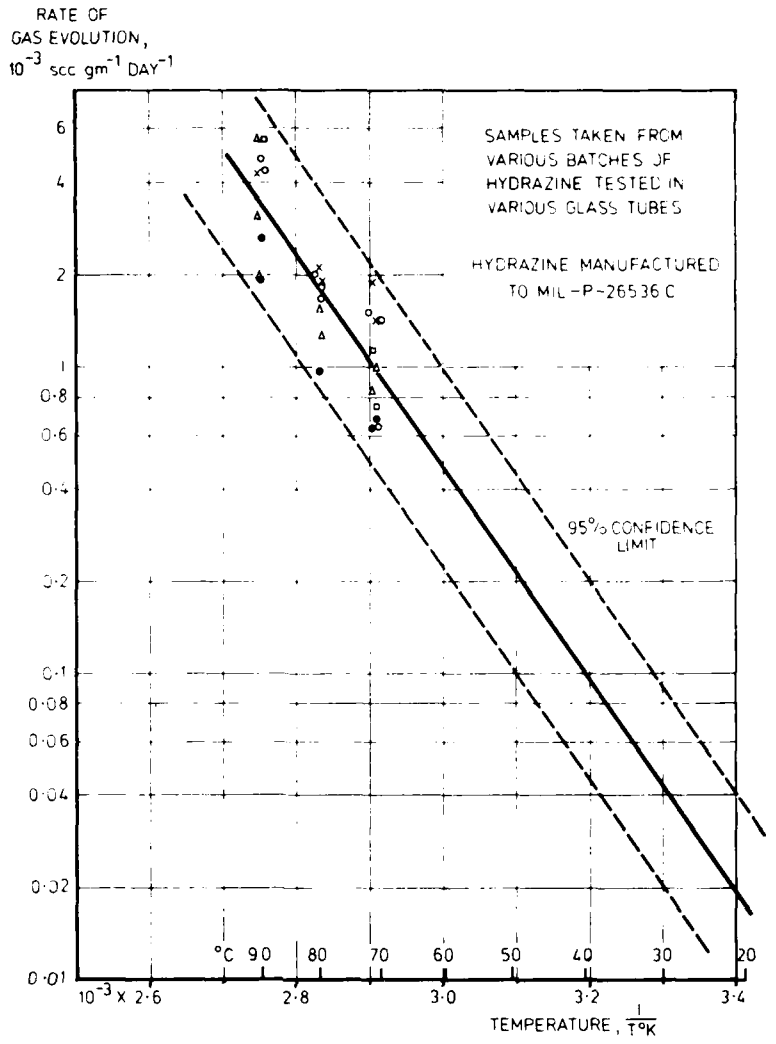

FIG.5 RATE OF HOMOGENEOUS DECOMPOSITION OF HYDRAZINE IN GLASS – EQUIPMENT A

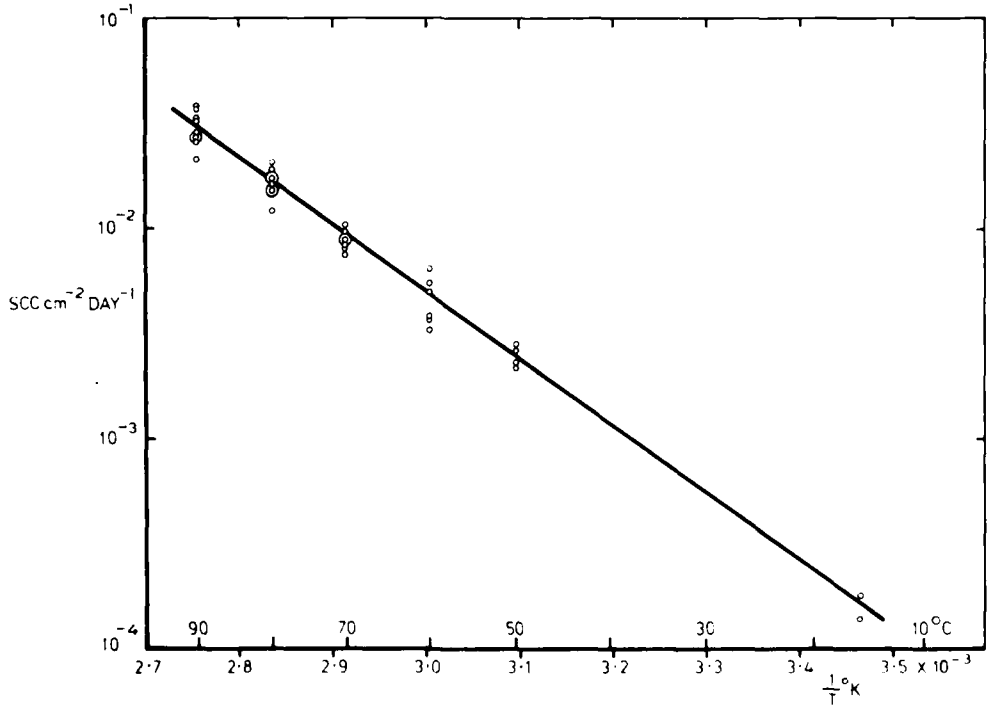

FIG.6 GAS EVOLUTION RATE FROM ALUMINIUM LINED VESSEL – EQUIPMENT D

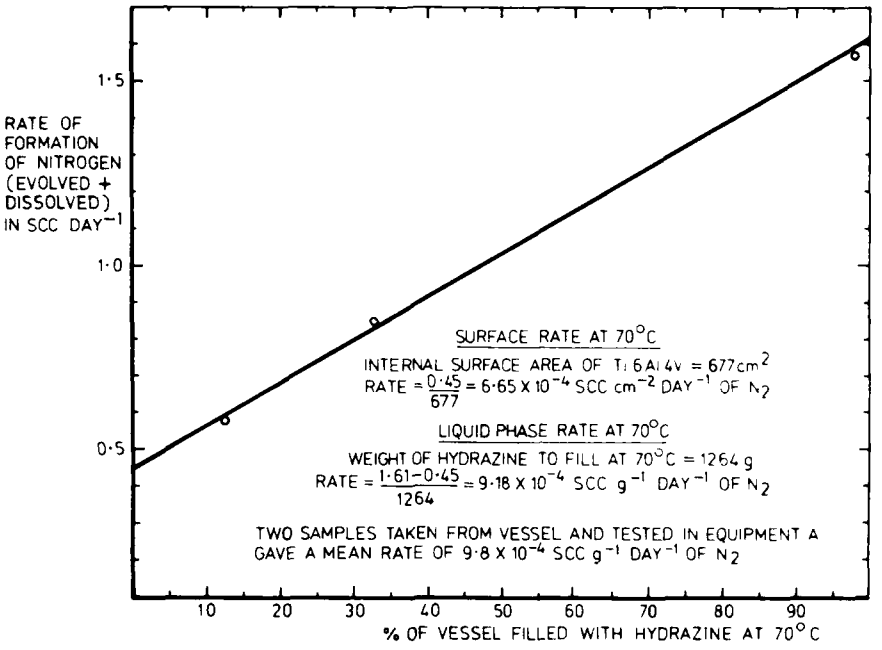

FIG.7 DATA FROM TITANIUM ALLOY VESSEL – EQUIPMENT E

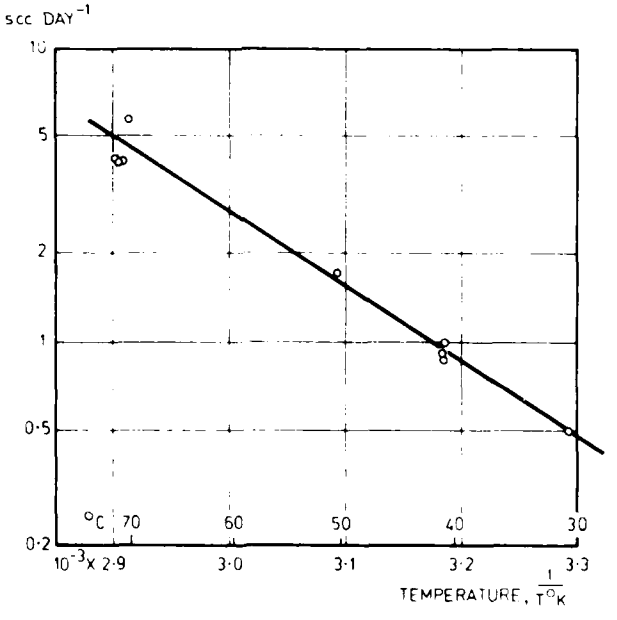

TOTAL INTERNAL SURFACE AREA OF STAINLESS STEEL VESSEL = 672 cm^2

WEIGHT OF HYDRAZINE ADDED = ~1200 g

FIG.8 PLOT OF GAS GENERATION RATE AGAINST TEMPERATURE FOR STAINLESS STEEL VESSEL – EQUIPMENT F

AGING EFFECTS ON THE DETONATION VELOCITY OF XTX-8003.*

H. GOLOPOL, N. HETHERINGTON, and K. NORTH
Lawrence Livermore Laboratory, Livermore, CA 94550

ABSTRACT

In this work we measured the effects of time and temperature on the detonation velocity of XTX-8003. We found an initial increase in velocity, followed by a total decrease of 2% after 48 months at the highest temperature. At the lower storage temperatures, the changes in velocity were only slight. Five batches of XTX-8003 were used in the study and each batch was significantly different in a statistical sense. However, all five batches performed satisfactorily. This data was best described by H. Eyring's model for uncased charges, which also can give us calculated values for h, an effects parameter. In general, with increasing exposure in the time-temperature matrix, h initially decreases up to about two years then increases non-linearly in the logarithmic time domain. Projections from our response surface analysis predict that the batches would function after storage of more than 30 years at room temperature (20°C). We established an empirical relationship between service life and storage temperature (°C):

$$\text{Service life (years)} = 147\ e^{(-.0268)x\ (T°C)}.$$

INTRODUCTION

XTX-8003 is a Los Alamos Scientific Laboratory (LASL) extrudable explosive composed of 80 wt% of pentaerythritol tetranitrate (PETN) and 20 wt% of Dow Corning Sylgard 182, a silicone resin. It is prepared by first mixing the dry PETN with the silicone resin/curing agent mixture and then it is processed through a three-roll point mill for 25 passes.

The purpose of this test was to establish the aging characteristics of this explosive formulation. As a measure of its aging characteristics we studied the change in detonation velocity as a function of track width. Our ultimate goal is to mathematically describe the data using a model that has a theoretical basis. This model could then be used as a prediction tool for new production batches.

---

*Work performed under the auspices of the U. S. Department of Energy by the Lawrence Livermore Laboratory under contract #W-7405-Eng-48.

RESULTS

Experimental Design

Since the response we wished to measure in this test was the detonation velocity, we designed a special velocity block (Fig. 1). Made of polycarbonate, it is 12.5 mm (0.5 in.) thick, 127 mm (5 in.) wide by 254 mm (10 in.) long, and contains four

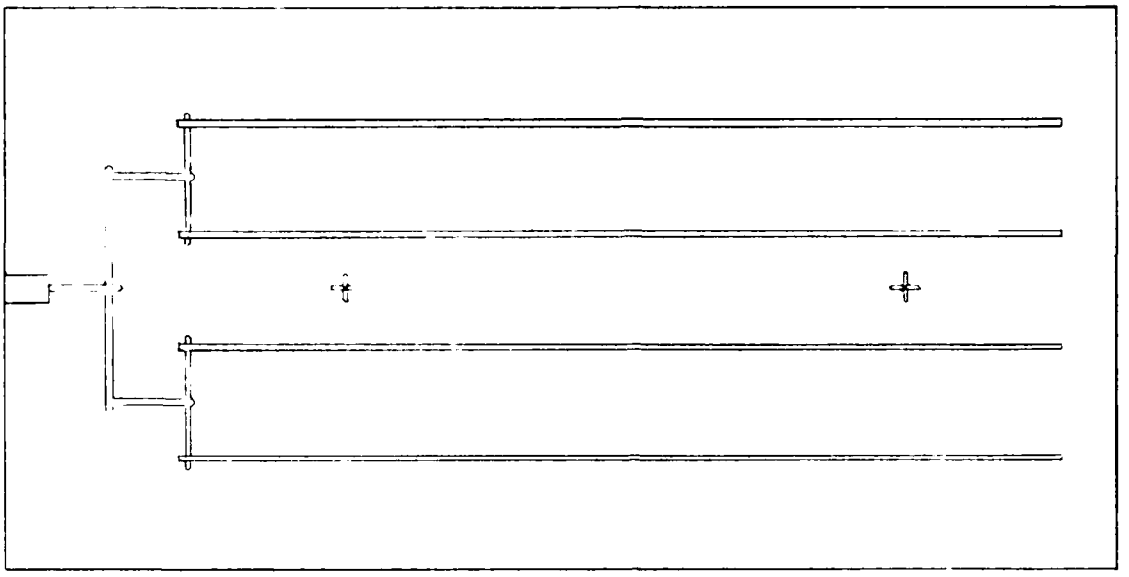

Fig. 1. Velocity test plate.

parallel square channels with widths of 0.38 mm (.015 in.), 0.508 mm (.020 in.), 0.889 mm (.035 in.), and 2.032 mm (.080 in.). The four parallel channels are connected by an 0.889 mm channel as shown in Fig. 1. The spacing between the channels on the block is sufficient to prevent shock interaction between adjacent channels. These blocks were loaded with the XTX-8003 by extrusion through an orifice plate. Sixty blocks were loaded for each of the five batches, giving us a total of 300 blocks. After loading and curing, each block was wrapped in aluminum foil for exposure to isothermal storage. Our test matrix for this study, Table 1, included three temperatures at six periods; three blocks were fired for each data point.

Table 1. Experimental matrix.

Temp. (°C)	Time, mos.						
	0	3	6	12	24	38	Total
20	15	3	3	3	3	3	30
50		3	3	3	3	3	15
70		3	3	3	3	3	15
			60 x 5 (batches)				300

For test fire, a switch plate containing eight ionization switches spaced one inch apart along each tract was clamped to the surface (Fig. 2). A single detonator

simultaneously initiates all four channels. As the detonation velocity proceeds down the track, each swtich is successively shorted and the time is recorded on an oscilloscope.

Data Reduction

After studying the time-distance data, we concluded that we should assume a constant velocity down the track. There were numerous instances where we found a switch reporting very late and usually this was followed by a very early switch. We believe that this is due to an electronic problem. When this occurred in the middle of the track it was readily apparent. However, at either end of the track interpretation was more difficult. To resolve these problems we first estimated the detonation velocity from the slope of a least squares (LSQ) fit to the time-distance data. We found that the LSQ value usually agreed with the average velocity determined by measuring the elapsed time between the second pin switch and the seventh pin switch.

Another problem in reducing the data was due to a change in the firing procedure during the four-year test period. All of our test fire data was normalized to 20°C. Initially, we fired these blocks in an indoor facility with a known, controlled temperature. Firing was subsequently transferred to an outdoor firing table. The blocks were placed in styrofoam boxes to maintain a constant temperature, but their temperatures were not recorded. This procedural change was discovered in reviewing the 24-month data. For the 48-month test fire samples, we installed thermocouples and so determined the firing temperature. The net effect is that there is an uncertainty of ∿2% in the temperature corrections for the 6-, 12-, and 24-month data. This temperature correction proved to be significant only for the 12-month data. The overall test error is also 2%.

Discussion

The average velocities with their 95% confidence limits (n = 4) for each channel diameter, representing each point in the time-temperature matrix, are present in Table 2 and Figs. 3-6. Figures 7 and 8 are plots of velocity vs. 1/W, the reciprocal of the channel width at 0 and 48 months, to show the channel size effect on the detonation velocity. H. Erying's[1] model for an uncased charge, which adequately describes the data, is:

$$\frac{D}{D_i} = 1 - \frac{a}{W} \qquad (1)$$

where D is the measured velocity, D_i is the infinite track width velocity, a is a reaction zone length, and W is the track width. We also tried to fit the data to the modified Eyring equation[2] which is given by:

Fig. 2. Detonation velocity block test fire assembly.

Table 2. Average detonation velocity of XTX-8003.

Channel diam	T°C	Time (mos.) 0	3	6	12	24	48
		V (mm/μsec) 95% C.L.*	V (mm/μsec) 95% C.L.	V (mm/μsec) 95% C.L.	V (mm/μsec) 95% C.L.	V (mm/μsec) 95% C.L.	V (mm/μsec) 95% C.L.
2.03 mm	20	7.284 ± .025	7.292 ± .023	7.285 ± .007	7.281 ± .020	7.296 ± .013	7.290 ± .069
	50		7.298 ± .017	7.297 ± .023	7.289 ± .027	7.305 ± .025	7.305 ± .045
	70		7.310 ± .035	7.313 ± .023	7.288 ± .023	7.255 ± .020	7.166 ± .075
0.89 mm	20	7.261 ± .019	7.265 ± .025	7.261 ± .010	7.254 ± .008	7.270 ± .008	7.269 ± .037
	50		7.269 ± .023	7.267 ± .016	7.258 ± .023	7.280 ± .026	7.257 ± .050
	70		7.282 ± .022	7.288 ± .017	7.257 ± .018	7.220 ± .029	7.112 ± .082
0.51 mm	20	7.219 ± .030	7.223 ± .013	7.222 ± .034	7.211 ± .019	7.232 ± .024	7.223 ± .098
	50		7.217 ± .031	7.213 ± .042	7.207 ± .034	7.234 ± .044	7.217 ± .067
	70		7.235 ± .021	7.257 ± .033	7.218 ± .011	7.162 ± .052	7.029 ± .143
0 ' mm	20	7 046	7.191 ± .025	7.192 ± .052	7.170 ± .039	7.196 ± .041	7.196 ± .133
	50		.171 ± .069	7.170 ± .092	7. 9 ± .067	7.197 ± .065	7.192 ± .076
	70		203 ± .032	7.237 ± .029	7.182 ± .015	7.104 ± .080	6.937 ± .141

..L. = cor ..er.. limit

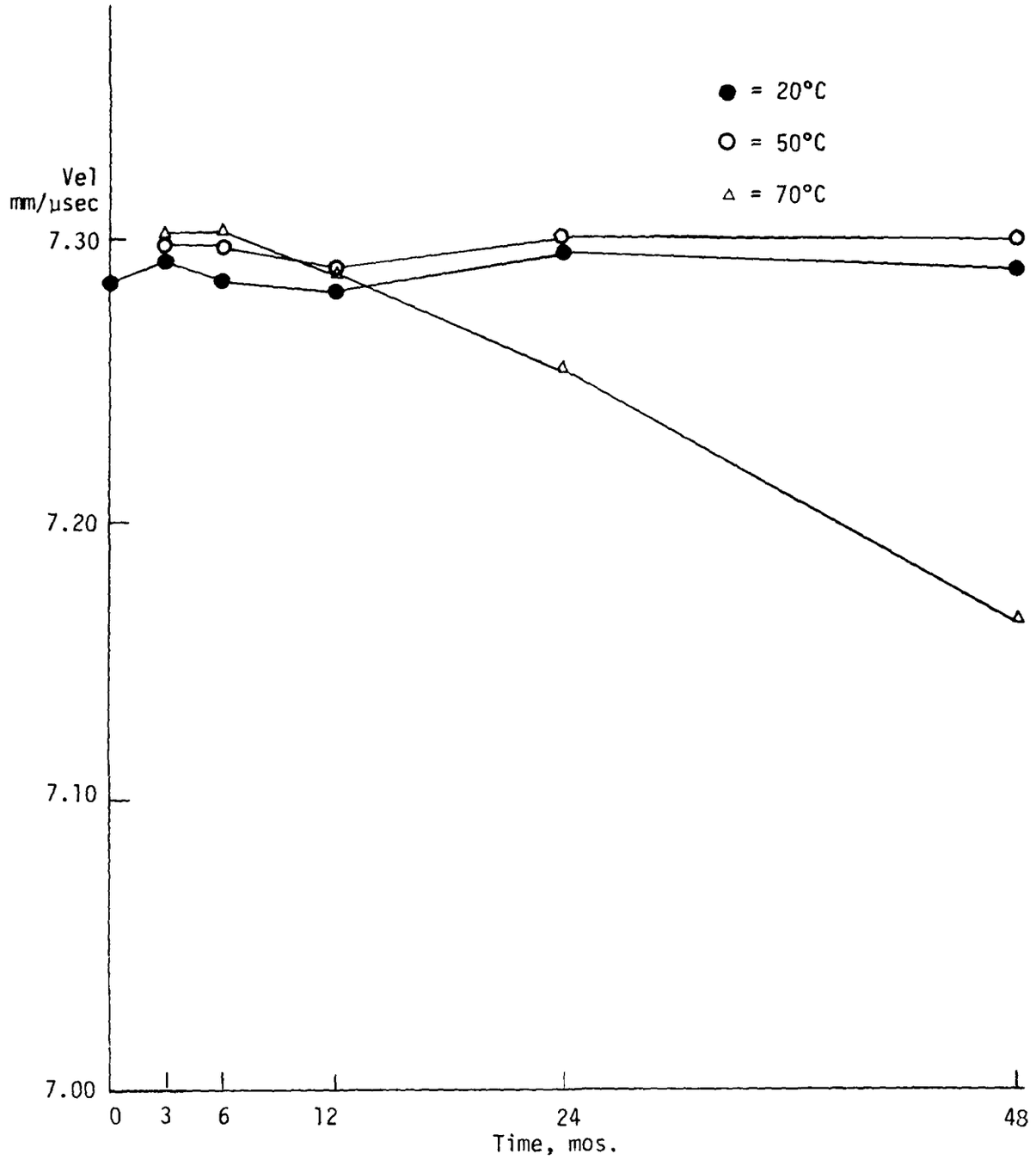

Fig. 3. Detonation velocity in 2.03 mm track.

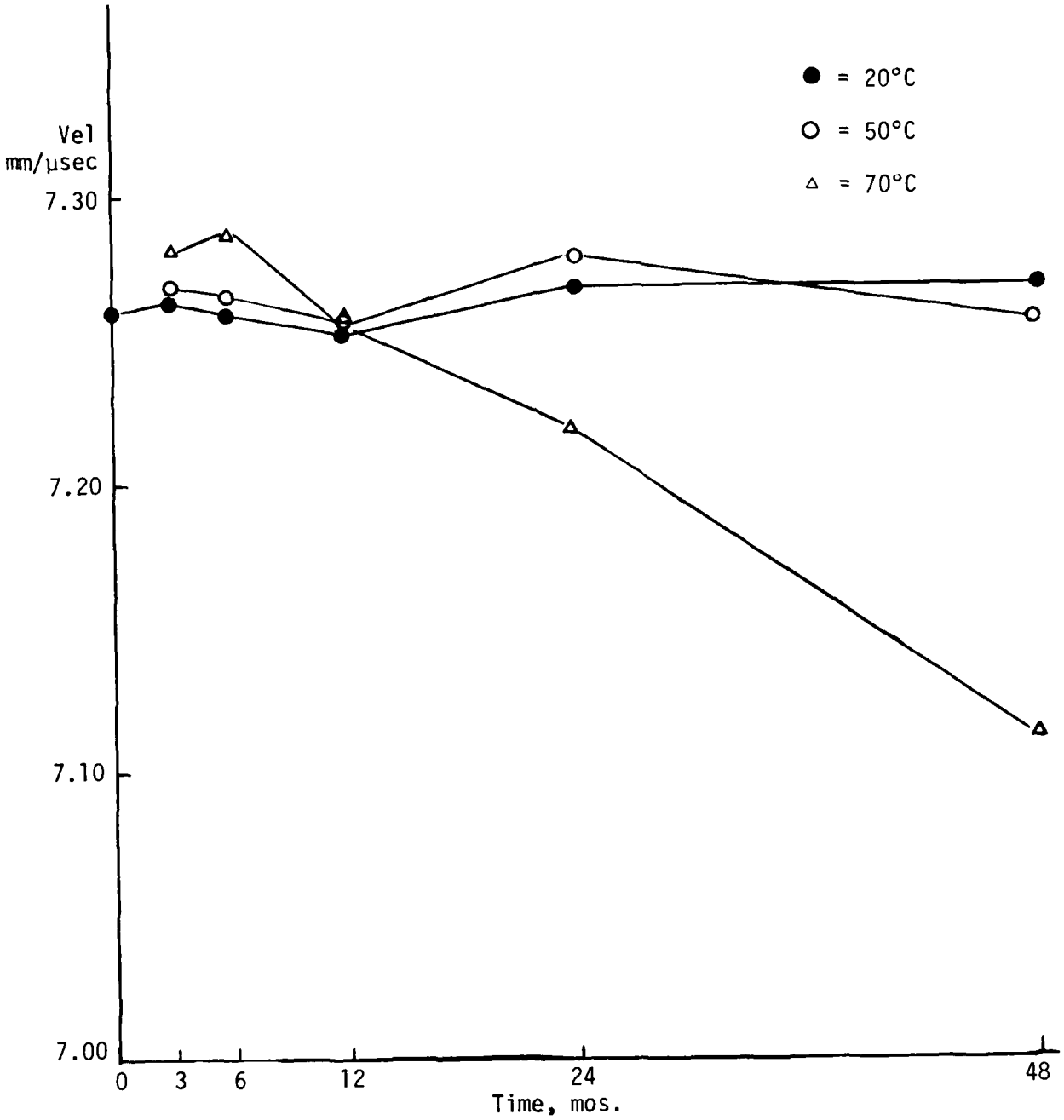

Fig. 4. Detonation velocity in .89 mm track.

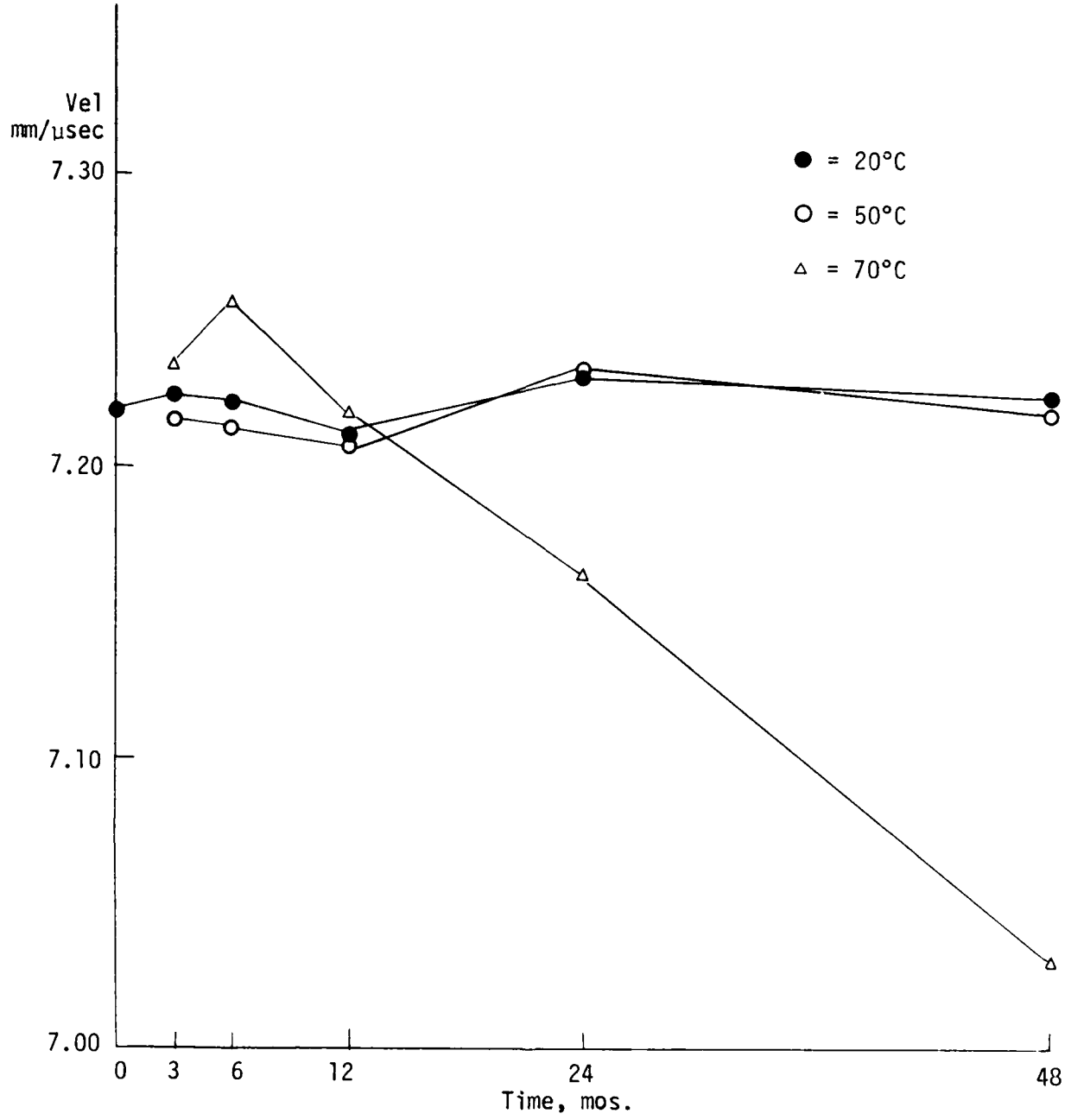

Fig. 5. Detonation velocity in .51 mm track.

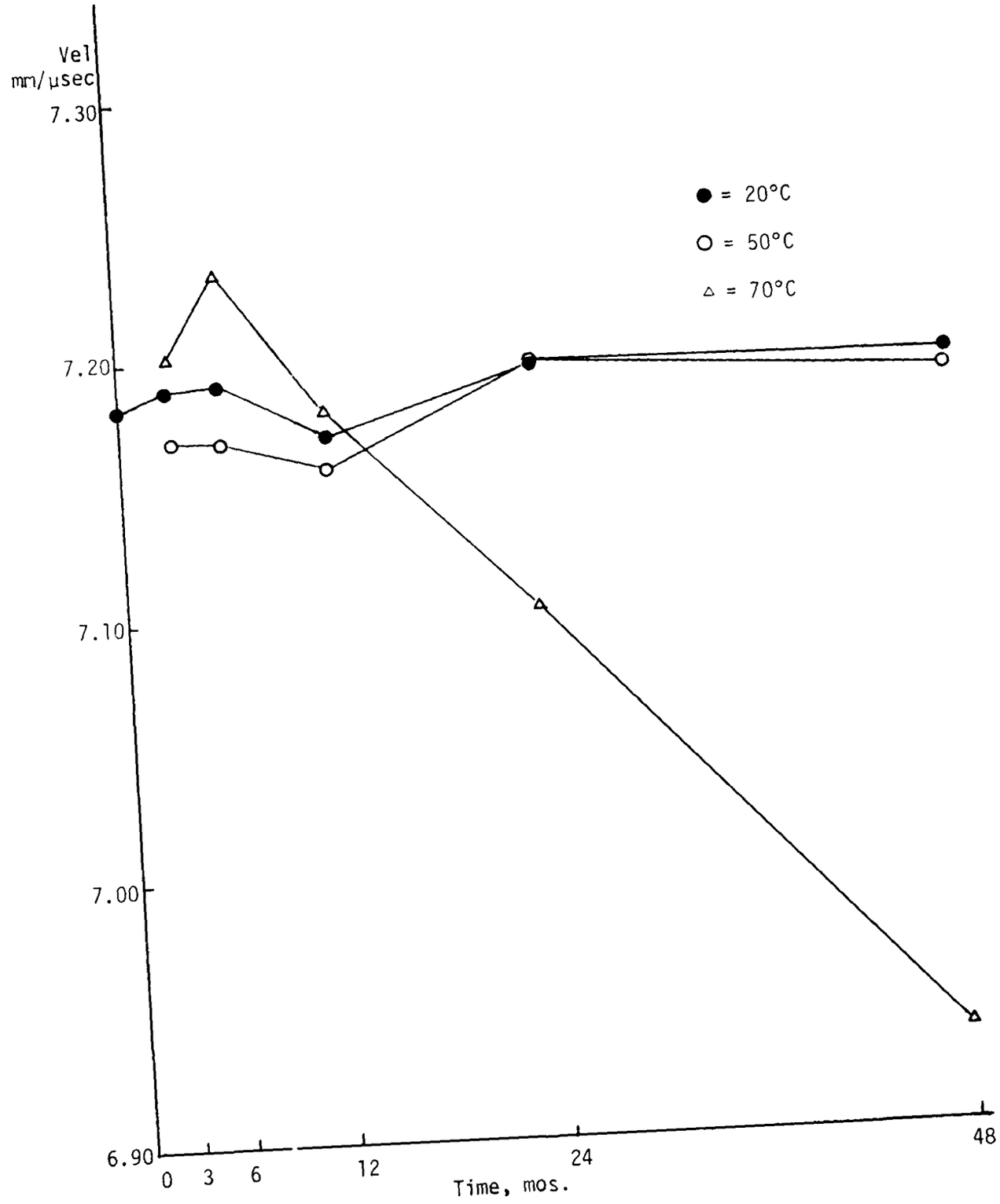

Fig. 6. Detonation velocity in .38 mm track.

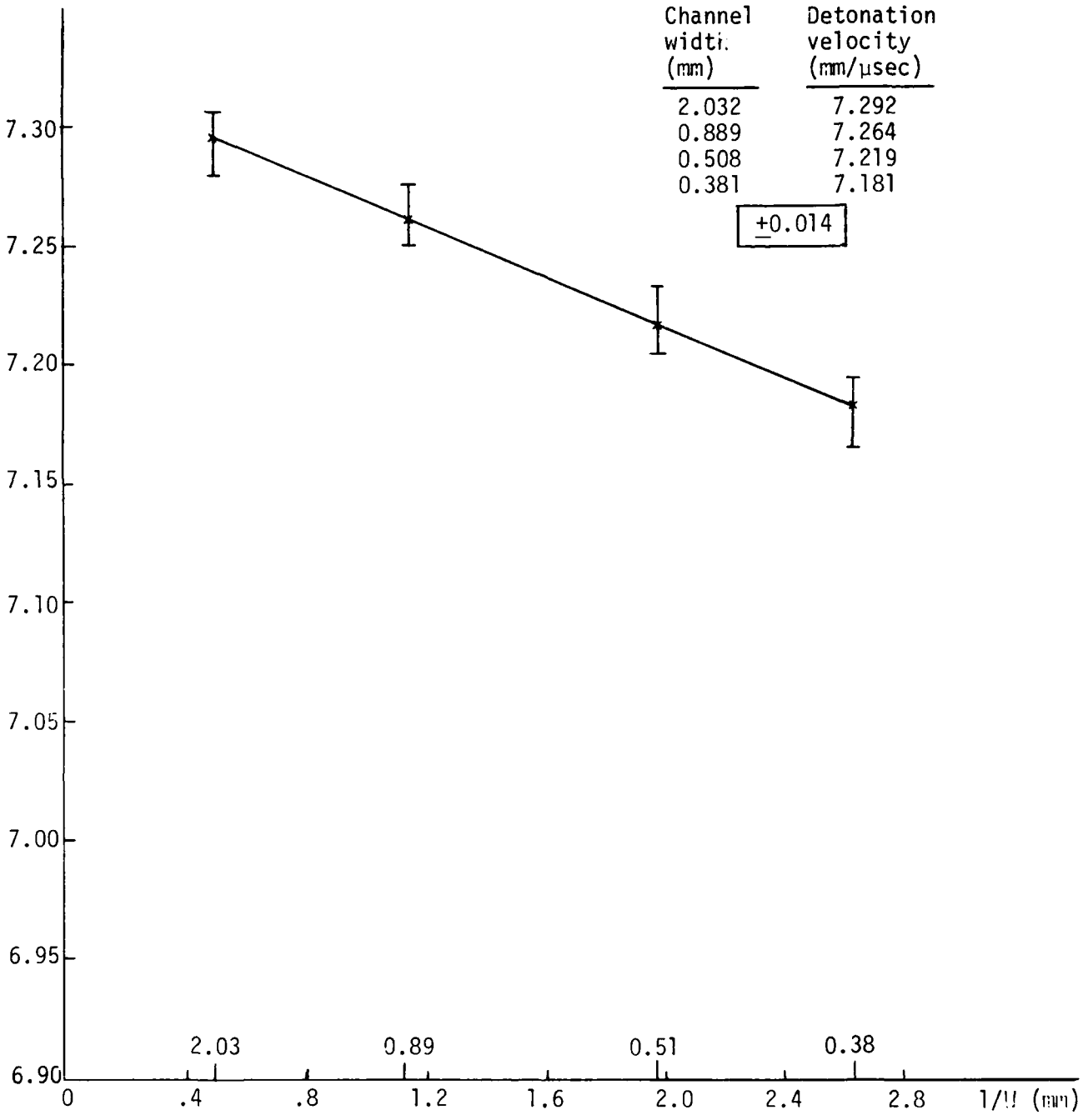

Fig. 7. Baseline data.

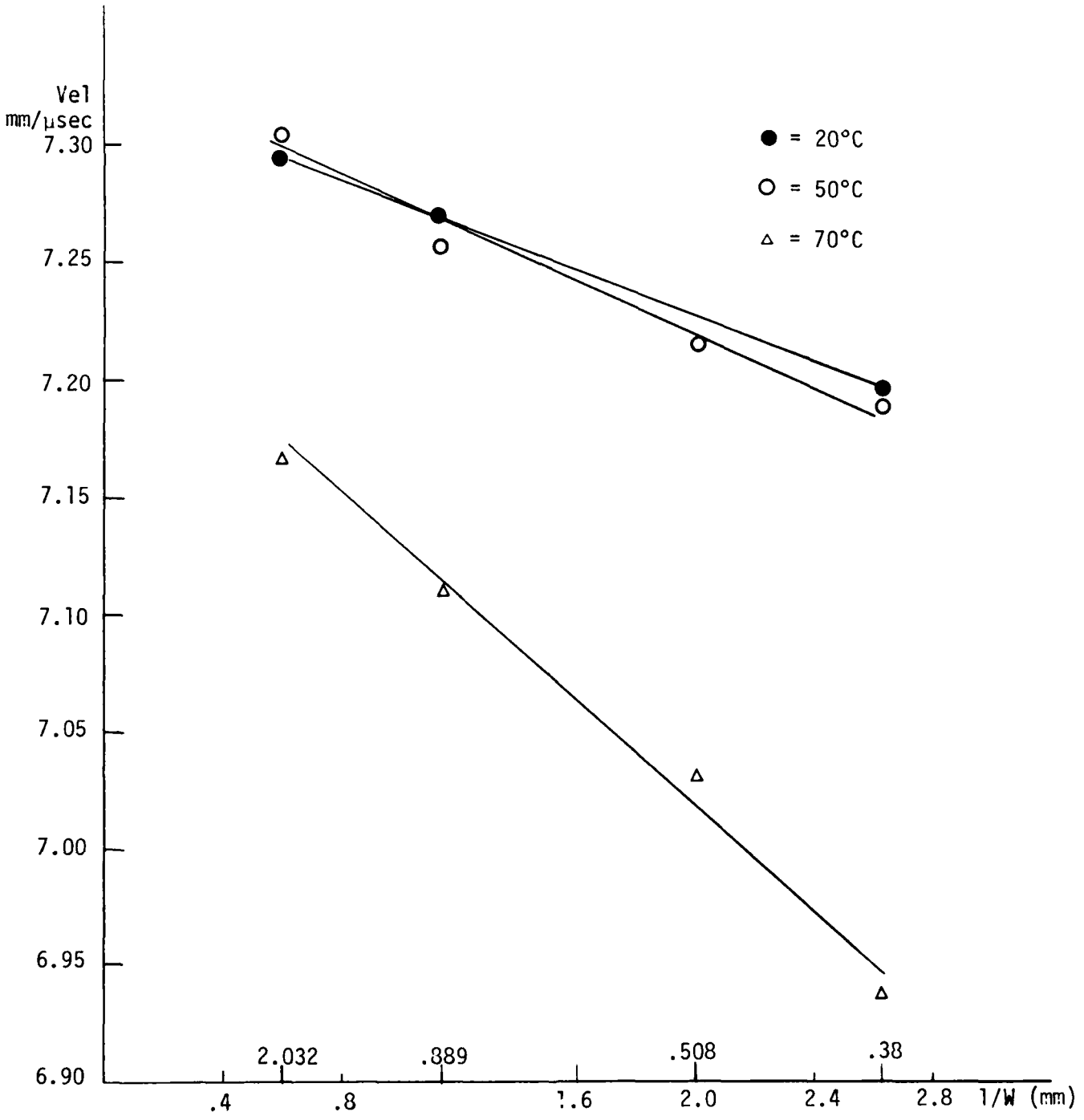

Fig. 8. 48-month data.

$$\frac{D}{D_i} = 1 - \frac{a}{W-W_c} \qquad (2)$$

where W_c is a critical width. This approach appealed to us because the Eyring model is not valid at very small values of W since in the limit of $W \to 0$ the equation diverges. However, when we applied our data to the modified model it yielded numerous negative coefficients, which made use of the equation impractical. One big advantage in using Eyring's theory is that we can reduce the numerous experimental data into simple meaningful parameters.

Our data shows that during the aging process the detonation velocity initially increases in time and then begins to decrease. An analysis of variance shows that this is real and not an artifact. At the lower temperatures (20-50°C), the velocity changes are statistically insignificant. At 70°C the effects of aging are much more dramatic and are statistically significant. We have some concern that there may be a different aging mechanism at 70°C than at temperatures below 50°C. Nevertheless, we treated the data as a continuum, including the 70°C data.

According to Eyring's absolute rate theory:[1]

$$\frac{a}{a_i} = \left(\frac{D_i}{D}\right) e^{\frac{\Delta H^{\ddagger}}{T_i R}\left[\left(\frac{D_i}{D}\right)^2 - 1\right]} \qquad (3)$$

where: a = the reaction zone length for a given track size.

a_i = the reaction zone length at the infinite track width.

D = the velocity for a given track size.

D_i = the velocity for an infinite track width.

$\Delta H^{\ddagger}$ = heat of activation for the reaction, cal mole^{-1}.

T_i = detonation temperature in the reaction zone.

R = gas constant, 1.986 cal deg^{-1} mole^{-1}.

Therefore, the reaction zone and the velocity parameters are dependent on the heat of activation. To simplify the following discussion, we define $h = \frac{\Delta H^{\ddagger}}{T_i R}$ as a calculated effects parameter. As shown in Fig. 9, h initially decreases with time up to ~2 years and then increases non-linearly in the logarithmic time domain. In this study we use temperature to accelerate the aging properties. This permits us to apply the Arrhenius law for chemical reaction rate, i.e., we assume that the following general model is valid:

$$\ell nh = f\left(\frac{1}{T}, \ell nt\right). \qquad (4)$$

This unknown function is expanded into a Taylor series:

$$\ell nh(T,t) = \beta_0 + \beta_1(\ell nt) + \beta_2\left(\frac{1}{T}\right) + \beta_3(\ell nt)^2 + \beta_4\left(\frac{1}{T}\right)^2 + \beta_5\left(\ell nt \cdot \frac{1}{T}\right) \qquad (5)$$

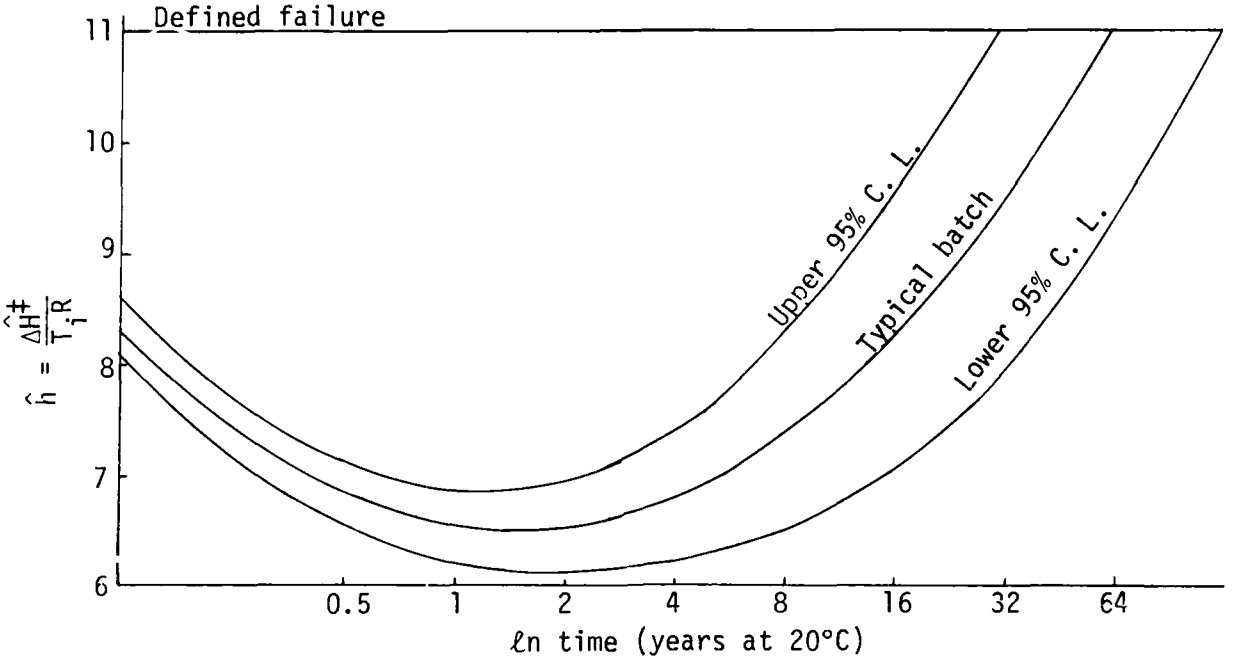

Fig. 9. Changes of h with time.

The response surface methodology[3,4] was then used to express the effect parameter h as a function of the experimental temperature and time variables. The outcome of this process is a response surface equation:

$$\ell n\hat{h} = \ell n\left(\frac{\Delta\hat{H}^{\ddagger}}{T}\right) = 9.38 + 0.58(\ell nt) - 5.22\left(\frac{10^3}{T}\right) + 0.04(\ell nt)^2 + 0.89\left(\frac{10^3}{T}\right)^2 - 0.24\left(\frac{10^3 \ell nt}{T}\right) \quad (6)$$

where ℓnt is the natural logarithm of time in months and T is the temperature in °K. This equation adequately describes the data (σ = .04). To use this equation for the prediction of service life, we must first establish a failure criterion. We define failure as the inability of a given track size to support a steady detonation velocity. Our analysis of this data indicates that we would expect failure if the Eyring parameters approach a detonation velocity of 6.1 mm/sec. in a track width of 0.318 mm. This corresponds to a value of h = 11 for the failure criterion. Using this criterion and the response surface equation, we calculated an empirical equation relating service life with surface temperature (°C):

$$\text{Service life (years)} = 147\, e^{(-.0286)(T)} \quad (20°C \leq T \leq 70°C). \quad (7)$$

This relationship is shown in Fig. 10 and indicates that these batches of XTX-8003 would function for more than 30 years when stored at 20°C.

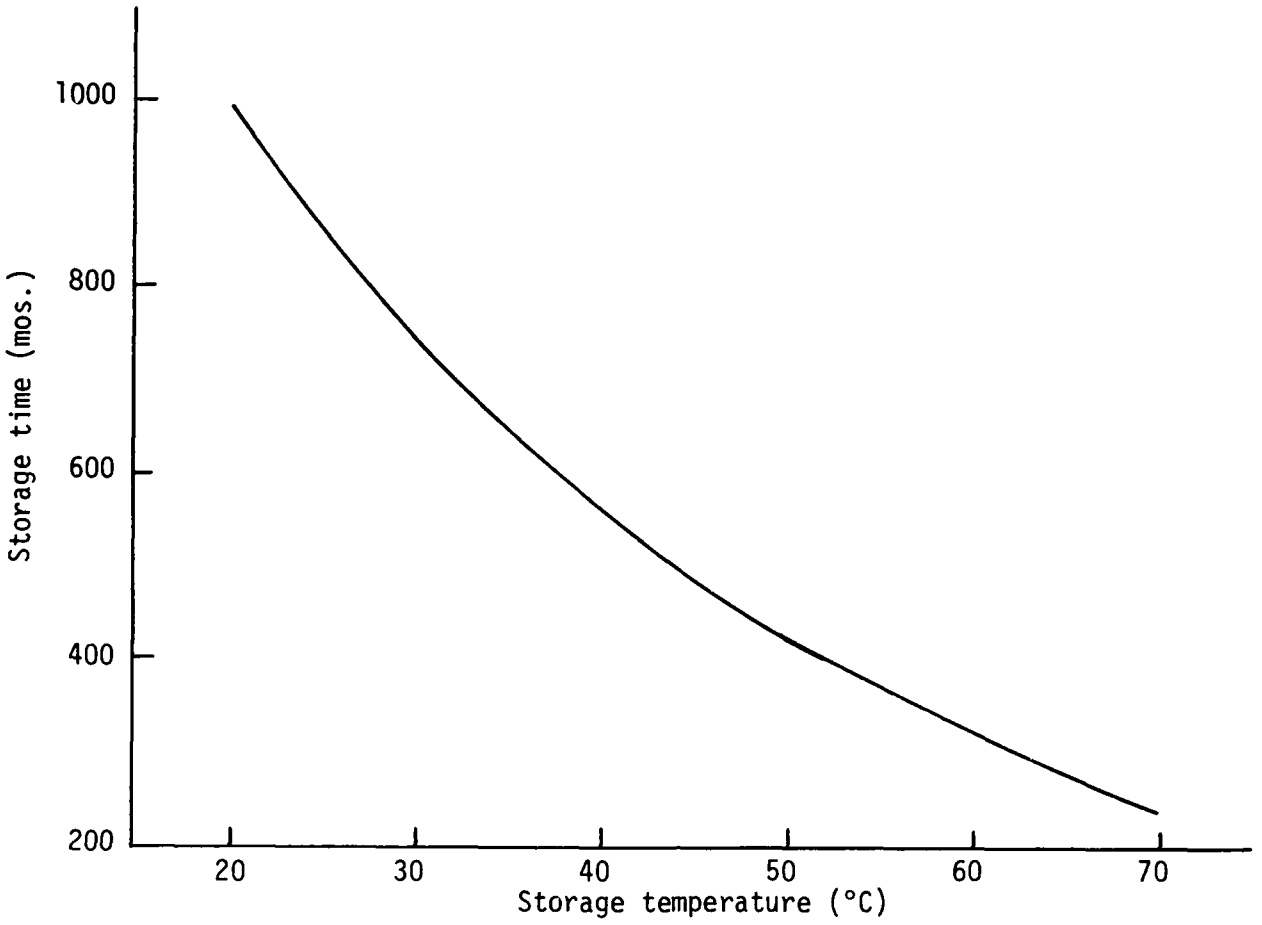

Fig. 10. Service life.

REFERENCES

1 H. Eyring, R. E. Powell, G. H. Duffey, and R. A. Parlin, Chemical Reviews, 45 (1949)69-181.
2 A. W. Campbell and R. Engelke, in Proc. 6th Int. Symp. on Detonation, Aug. 24-27, 1976.
3 W. H. Hill and W. G. Hunter, Technometrics, 8(1966)571-590.
4 C. E. Arthur, A. E. Heller, and A. W. Thakker, AFML-TR-74-185, Air Force Materials Laboratory, Wright Patterson Air Force Base, OH (1974).

Effects of Thermal Cycling on Trinitrotoluene and Tritonal Explosive Compositions

D. S. Ellison, R. A. Alcorn and E. Neal
Materials Analysis and Technology Division Weapons Quality Evaluation Center
Naval Weapons Support Center Crane, IN 47522

ABSTRACT

The effects of thermal cycling of Trinitrotoluene (TNT) and tritonal were studied using unprocessed virgin TNT, reclaimed TNT and laboratory prepared tritonal. Small quantities of explosives were temperature cycled through ranges designed to simulate aerodynamic heating. The thermal chemical kinetics at isothermal temperatures were investigated using differential scanning calorimetry methods. Physical and Chemical changes were studied using Scanning Electron Microscopy, X-ray diffraction, and Thin-Layer Chromatography (TLC) techniques.

INTRODUCTION

Aerodynamic heating has been shown to induce temperature rises on the surface of munitions flown on the exterior of aircraft. A study already completed by the Air Force at Armament Laboratory (AFSC) on cyclotrimethylenetrinitramine (RDX)[1] has established thermal profiles for surface temperatures encountered by ordnance during flight. In the AFSC experiment, samples of RDX were cycled several times from ambient temperature to 177°C and back again in order to simulate this aerodynamic heating. Changes in the explosive were determined by measuring the kinetic constants before and after cycling. Conclusion of the study was that small quantities of temperature cycled RDX gave test results indicating a lowering of the thermal decomposition temperature.

As in the case of RDX, bombs loaded with trinitrotoluene (TNT) and tritonal, a TNT aluminum explosive, are subjected to aerodynamic heating while being carried externally. Until now, no kinetic experiments have been conducted on unpurified military grade TNT. Investigators use recrystallized TNT purified because it is free of the low-melting impurities which are not

entirely removed during manufacturing[2]. This process may eliminate any effects these trace components might have on the thermal decomposition of the TNT. It has been shown that TNT which has been exposed to elevated temperatures for many hours will become less sensitive[3], but under those conditions the breakdown products formed may have masked a change in sensitivity caused during the initial increased temperature exposure. In aerodynamic heating, the munitions will only see elevated temperatures for short time periods. Therefore any decomposition reactions which were encountered in extended heating may not occur; however, the explosive may become unstable.

Rodgers[4] has evaluated the stability of explosives by using kinetic parameters such as the activation energy and the collision frequency factor to calculate the critical temperature at which any size and shape of explosive can self heat to explosion. Thus, the kinetic constants are related to explosive sensitivity in such a way that a decreased activation energy and frequency factor suggest a change in thermal stability. A lowered activation energy would be indicative of lower thermal stability.

OBJECTIVES

The purpose of this investigation was to determine if thermal cycling affects the stability and sensitivity of TNT and TNT based explosives. This was to be accomplished by measuring:

1. Kinetic parameters such as energy rate constants, pre-exponentials and activation energy by using isothermal calorimetry.
2. Impact sensitivity
3. Heat capacity

There were other factors which were to be considered but were not completely pursued. These involved physical and chemical changes which may have occurred during temperature cycling, such as crystal changes or the formation of compounds. Analytical techniques to study these changes included scanning electron microscopy, X-ray diffraction, and chromatography.

EXPERIMENTAL

Theory

Explosive materials decompose exothermally at a temperature dependent rate. If this rate is first order, that is without any complex secondary reactions, the activation energy can be calculated by using the isothermal DSC techniques developed by Rodgers[5] for determining rate constants. He established that for the fraction (a) reacted during the isothermal decomposition, the DSC defection (b) above the baseline is directly

proportional to the rate (dq/dt) of energy evolved or absorbed by the sample. This rate is also proportional to rate of reaction, da/dt. Therefore,

$$\alpha b = \beta dq/dt = da/dt = k\ (1-a) \qquad (1)$$

where α and β are proportionality constants and k is the rate constant. By mathematical manipulation and definition, the following are obtained:

$$\ln b = \ln k/\alpha + \ln (1-a) \qquad (2)$$

$$-\ln (1-a) = kt + c \qquad (3)$$

where c is a constant. By combining equations 2 and 3, the result is:

$$\ln (b) = \ln K/\alpha - (kt + c) = C - kt \qquad (4)$$

where c is the combined constants. For a first order reaction, the rate constant is obtained from the negative slope of a plot of deflection vs time.

It must be demonstrated that the decomposition is first order. To do this a more general form of equation (1) is used:

$$b = k\ (1-a)^n \qquad (5)$$

where n is the order of the reaction. Now equation (4) becomes:

$$\ln b = \ln (1-a)^n + \ln (k/\ ) = n \ln (1-a) + C.$$

The value of n for a first order reaction should be one.

The activation energy (E_a) and the collision frequency factor (Z) can then be calculated using the experimentally determined rate constants from the Arrhenius Equation:

$$K = Ze^{-E_a/RT}$$

where R is the universal gas constant and T is the temperature in degrees Kelvin.

Experimental Set Up

The experiment required that small quantities of explosive be sealed in DSC sample pans and subsequently temperature cycled. The pans would then be

perforated with a 0.15mm hole, so that isothermal decomposition could be conducted. The kinetic parameters would be determined from triplicate analyses on each explosive.

The temperature cycling was accomplished by weighing 2.00mg of TNT, and in the case of Tritonal 2.25mg, in Mettler TA2000B sample pans and cold weld

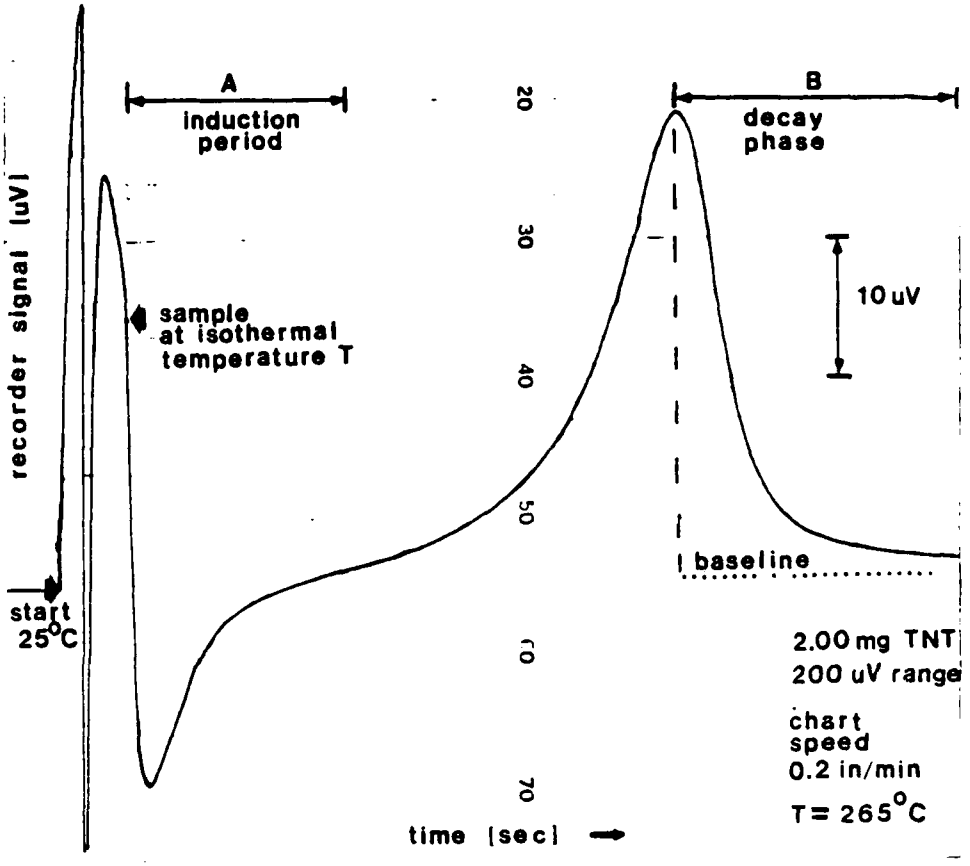

Figure 1. DSC thermogram of the isothermal decomposition of TNT

sealing. These pans were placed in the Mettler and cycled through the following temperature profiles:

a. Ambient to 150°C to ambient at 5°C/min, once

b. Ambient to 150°C to ambient at 5°C/min, twice

c. Ambient to 200°C, hold 30 minutes, return to ambient at 30°C/min

The pans were then perforated using a commercially available pivot drill bit measuring 0.15mm diameter. This type of drill bit made the hole size reproducible.

The design of the Mettler instrument does not easily permit dropping the pans on the sensors at elevated temperatures. However, the instrument can heat the samples from ambient to the isothermal temperature at a rate of 100°C/min. This was done for each kinetic analysis. A typical thermogram is shown in Figure 1. The first of the thermal parameters to be measured was

the induction period (A). This quantity was defined in this study as the difference between the time required for the sample to reach the isothermal temperature and the time the curve departed from the baseline established by the isothermal decomposition. Unlike RDX, the TNT induction period could not be measured reliably by visual means. The difficulty was in recognizing a deflection from the baseline. This was solved by using a computer to analyze the data collected by a digital to analog converter. A program was devised to pick a point where the curve begins to change significantly. The computer examined the data stored for the induction period as a series of sets of points. Each set consisted of 30 points. The value of each set was compared with the set before it, and when the value was equivalent to one and one-half divisions of the chart the computer established that value as the end of the induction period. The next thermal parameter was the decay phase (B) which began when the curve reached a maximum and ended when a baseline could be established.

The impact sensitivities were calculated by using the maximum no fire height because the 50 percent fire method would not give usable data. Approximately 2gms of explosive was cycled in a modified Dupont thermal analyzer cell. The test samples were then ground and impact sensitivity was determined. No attempt was made to do impact on chunks of explosive.

The heat capacity data was obtained using the Mettler TA2000B. Explosive samples weighing 30mg were temperature cycled. The heat capacity was determined by conducting a blank scan over the desired temperature range using an empty sample pan. The instrument recorder chart paper was then returned to the starting point and another scan was done over the same temperature range using the cycled explosive. No data was collected between 60 and 120^{o}C because of the drastic change in the thermal curve due to the melting of TNT.

Data Collection and Reduction

The data was collected using a combination system of a Canberra digitizer and dual counter/timer with a DEC PDP 11-05 minicomputer. The stored digital information was then converted back to analog form for display on a multichannel analyzer. In Figure 2a every tenth point was enhanced by the multichannel analyzer so that points could be quickly selected for calculating the rate constant. The computer stored the data from the decomposition curve indicated by the arrows in Figure 1a. A linear portion of this plot was chosen to determine the slope for the rate constant. In Figure 2c, a plot of ln b vs ln (1-x) resulted in the reaction order (n) from the slope.

The confidence limits for the kinetic constants were obtained using confidence levels for linear regression calculation as outlined by

Middlebrooks[6]. For 95 percent confidence, the Y value for any given X value is:

$$Y \pm \phi_{[.05]\,[n-2]}^{X}\, S_y$$

Tables were used for the ϕ value and two degrees of freedom were assumed. S_y represents the Y variance and is dependent on the X value.

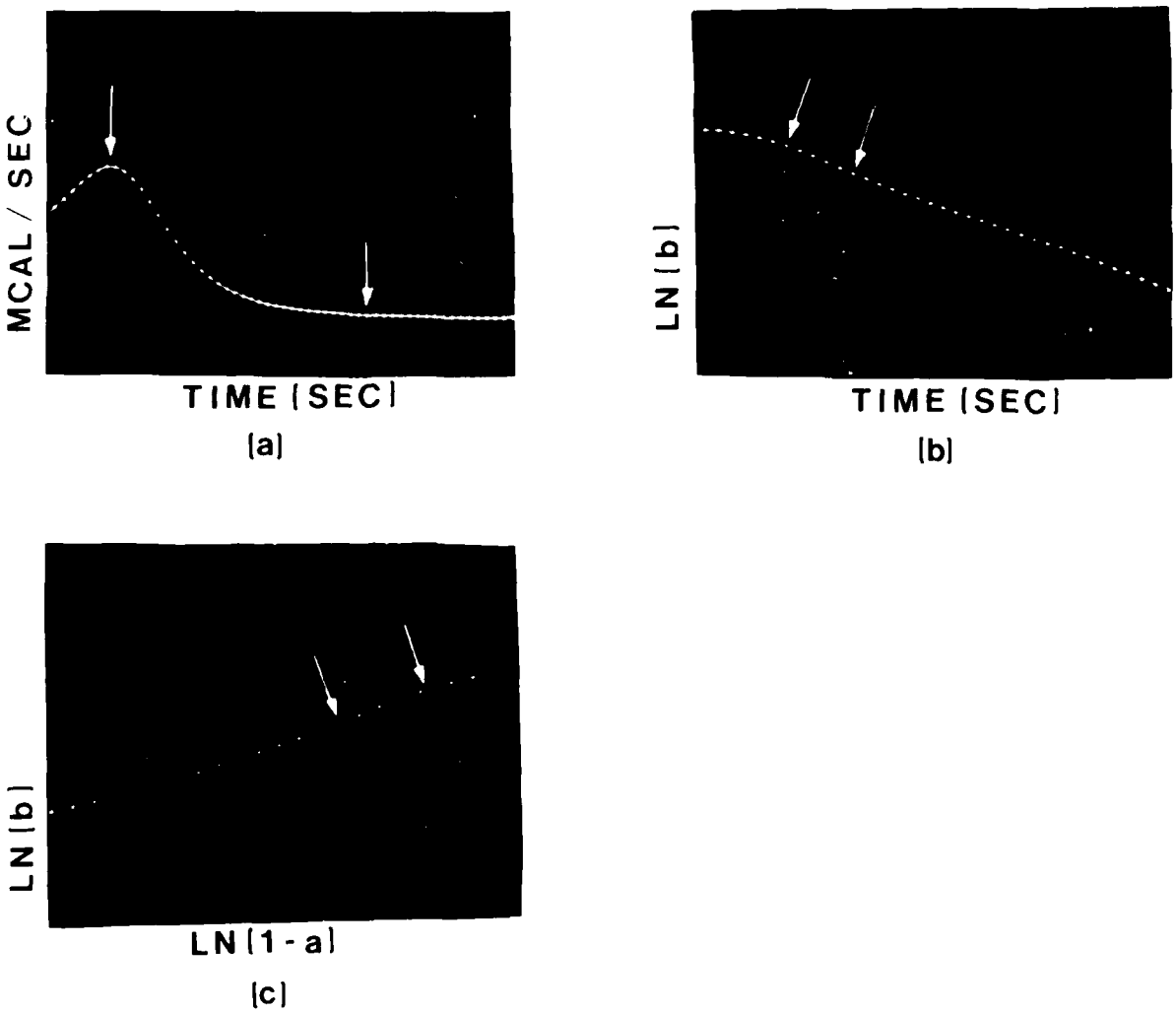

Figure 2. Multichannel Analyzer Data Display-arrows indicate sets of data used in determining:

(a) "b" deflection
(b) rate constant, K ≈ slope
(c) reaction order

DISCUSSION

Kinetics

Figures 3 and 4 were made from plots of the induction periods in Table 1 as a function of the isothermal temperature used in each kinetic analysis. The induction period (I_p) for flaked TNT decreased slightly after each successive cycle. The graph obtained for tritonal (Figure 4) would seem to indicate that (I_p) had increased after cycling. When you plot (I_p) measured for the virgin TNT used in making the tritonal and ignore the data from the uncycled tritonal, the result is a decrease in the induction period. This comparison is valid because after the first cycle the TNT tended to migrate away from the aluminum. The cycled tritonal could be treated like cycled virgin TNT. The powdered aluminum was inert material bound to the pan by a thin layer of melted TNT.

The validity of the activation energy depends upon whether the thermal decomposition is the result of a first order reaction. An examination of the reaction orders experimentally determined for the decomposition of TNT and tritonal listed in Table 2 confirm that they are first order. The nominal

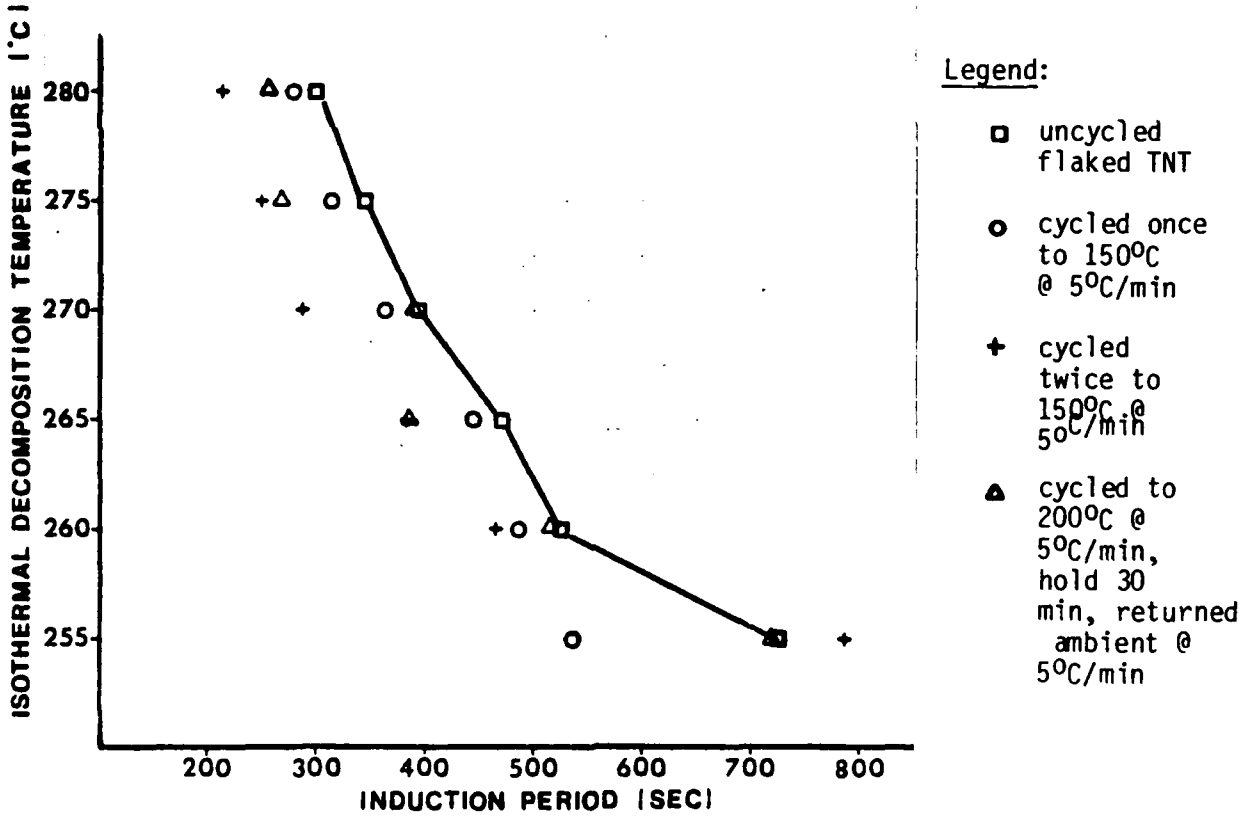

Figure 3. Induction Period of Flaked TNT vs Temperature

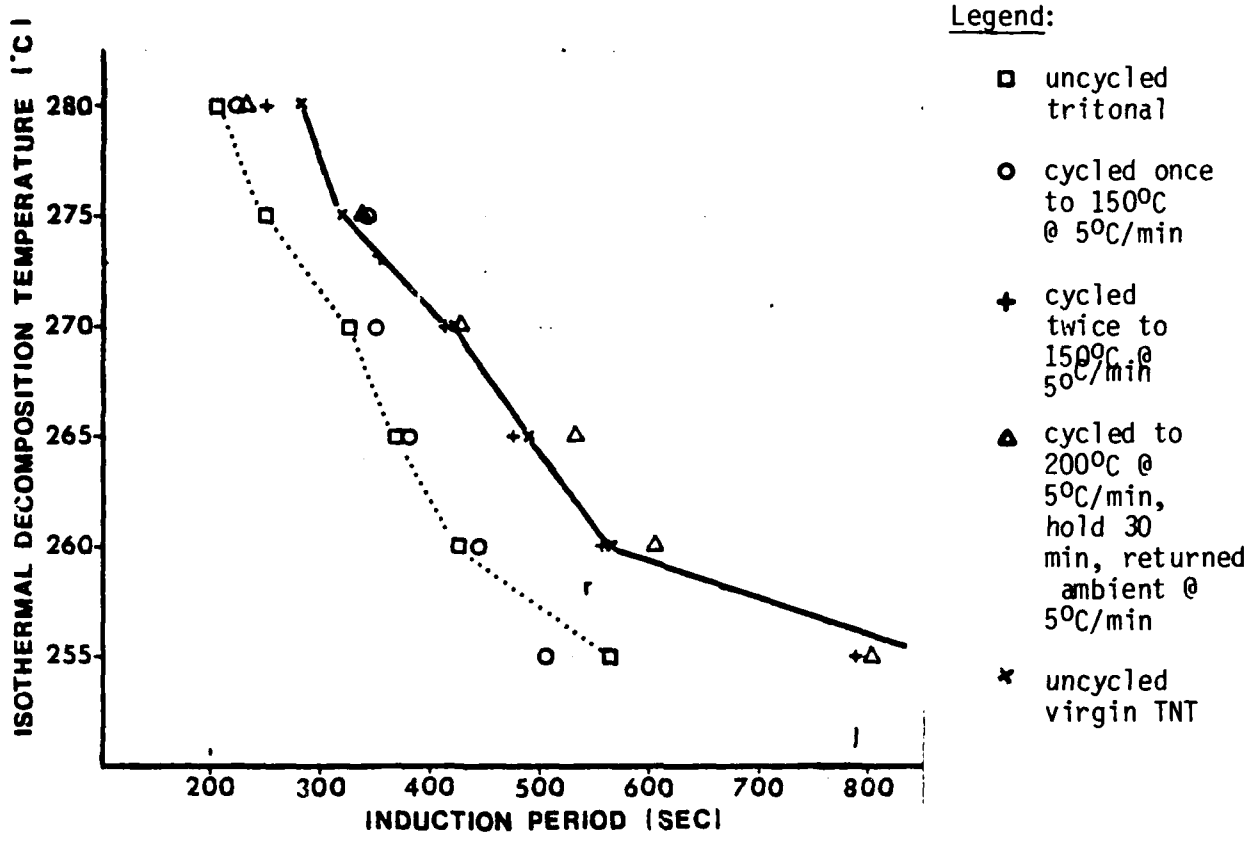

Figure 4. Induction Period of Tritonal vs Temperature

value was one. The rate constants in Table 3 were used in the Arrhenius Equation to calculate activation energy for each of the uncycled and cycled explosives. The values obtained (Table 4) are for the temperature range 255 to 280°C. The reduced E_a value after cycling TNT and tritonal connotes that they both became more sensitive to thermal degradation. It also appears that the initial cycle was the most critical one. Additional cycles resulted in no further decrease in the activation energy.

Impact Sensitivity

The impact sensitivity data in Table 5 suggest that temperature cycling has reduced the sensitivity of virgin TNT and flaked TNT, whereas the tritonal remained about the same. Since the explosives were ground for the impact testing, it is believed that the grinding may have altered the results. Kinetic analyses should have been conducted on the ground material in order to evaluate any changes which the grinding may have caused.

A possible method to improve on the impact test might be to use the DSC sample pans and perform impact directly on the pans after temperature cycling.

Heat Capacities

The heat capacity data is provided in Table 6. A slight increase in heat capacity was measured after thermal cycling. A possible explanation for this increase may be due to the presence of liquid TNT in the crystal latice of the cycled explosive. There is no evidence to confirm this theory. Scanning electron microscopy cannot detect liquid materials since sample preparations force the crystallization of the liquid. The more likely reason is during the melting a change in the pan-to-sample contact caused a better energy transfer to the Mettler TA2000B sensors.

Figure 5 curve 1 is a thermogram of TNT used to determine its heat capacity. Curve 2 (Figure 5) is the same sample of TNT which has been supercooled to 40°C and then heated up again. The significance of these two curves is the large differences between the heat capacity of the liquid and solid TNT below the melting point.

TABLE 1

TNT Thermal Decomposition Induction Periods (Sec)*

TNT Sample	Temperature (°C) 255	260	265	270	275	280
Flake, Uncycled	725	526	469	394	344	300
Flake, Cycled Once at 150°C, 5°C/min	537	488	444	412	313	281
Flake, Cycled Twice at 150°C, 5°C/min	785	463	382	288	250	213
Flake, 200°C Hold for 30 min	719	513	375	388	269	256
Virgin, Uncycled	881	563	488	420	319	281
Tritonal, Uncycled	563	425	369	325	275	206
Tritonal, Cycled Once at 150°C, 50°C/min	506	444	381	350	343	225
Tritonal, Cycled Twice at 150°C, 5°C/min	788	556	475	412	337	250
Tritonal, 200°C Hold for 30 min	800	604	531	425	337	232

*Average from three analyses per temperature

TABLE 2

TNT Thermal Decomposition Reaction Orders *

TNT Sample	Temperature (°C) 255	260	265	270	275	280
Flake, Uncycled	.91	.92	1.02	1.04	1.07	1.08
Flake, Cycled Once at 150°C, 5°C/min	.88	.98	1.06	1.06	1.14	1.15
Flake, Cycled Twice at 150°C, 5°C/min	.90	.97	1.05	1.06	1.11	1.20
Flake, 200°C Hold for 30 min	.89	.97	1.04	1.08	1.16	1.19
Virgin, Uncycled	.89	.98	1.03	1.07	1.12	1.23
Tritonal, Uncycled	.93	.97	.99	1.09	1.14	1.15
Tritonal, Cycled Once at 150°C, 50°C/min	.88	.97	1.04	1.08	1.13	1.16
Tritonal, Cycled Twice at 150°C, 5°C/min	.83	.93	1.03	1.09	1.14	1.14
Tritonal, 200°C Hold for 30 min	.85	.93	1.03	1.05	1.11	1.14

*Average from three analyses per temperature

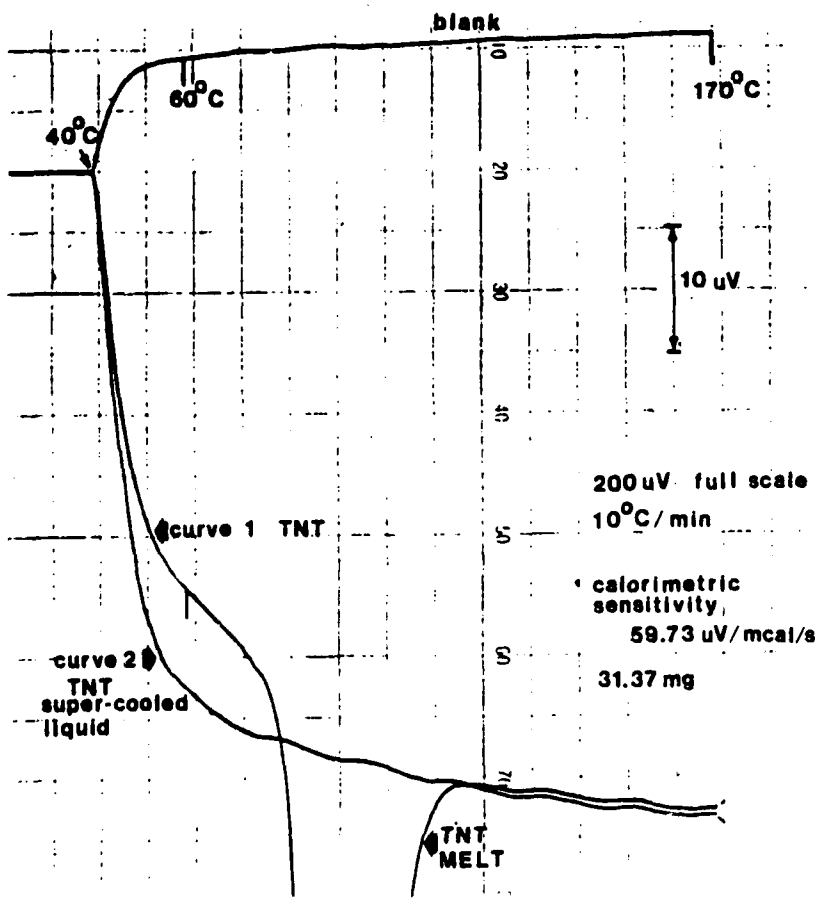

Figure 5. Heat Capacity Thermograms

TABLE 3

TNT Thermal Decomposition Rate Constants (Sec -1)*

TNT Sample	Temperature (°C) 255	260	265	270	275	280
Flake, Uncycled	.0070	.0110	.0118	.0148	.0187	.0229
Flake, Cycled Once at 150°C, 5°C/min	.0080	.0092	.0118	.0147	.0184	.0220
Flake, Cycled Twice at 150°C, 5°C/min	.0080	.0095	.0112	.0144	.0181	.0222
Flake, 200°C Hold for 30 min	.0081	.0098	.0113	.0154	.0189	.0223
Virgin, Uncycled	.0085	.0096	.0133	.0148	.0192	.0222
Tritonal, Uncycled	.0085	.0104	.0135	.0158	.0192	.0236
Tritonal, Cycled Once at 150°C, 50°C/min	.0090	.0108	.0128	.0158	.0189	.0228
Tritonal, Cycled Twice at 150°C, 5°C/min	.0097	.0115	.0138	.0161	.0197	.0250
Tritonal, 200°C Hold for 30 min	.0090	.0110	.0131	.0164	.0196	.0227

*Average from three analyses per temperature

TABLE 4

TNT Thermal Decomposition Kinetic Parameters (255-280 o) DSC Isolthermal Method

TNT Sample	Activation Energy, Ea (Kcal Mol^{1})	Log Pre-Exponential Factor, Log Z (sec^{1})
Flake, Uncycled	26.6 ± 2.0	8.9 ± .8
Flake, Cycled Once at 150°C, 5°C/min	24.5 ± 1.7	8.0 ± .7
Flake, Cycled Twice at 150°C, 5°C/min	24.0 ± 2.1	7.8 ± .9
Flake, 200°C Hold for 30 min	24.0 ± 2.1	8.0 ± .9
Virgin, Uncycled	23.3 ± 2.0	7.5 ± .8
Tritonal, Uncycled	23.6 ± 1.4	7.7 ± .6
Tritonal, Cycled Once at 150°C, 50°C/min	21.7 ± 1.0	6.9 ± .4
Tritonal, Cycled Twice at 150°C, 5°C/min	21.5 ± 1.9	6.7 ± .8
Tritonal, 200°C Hold for 30 min	21.7 ± .9	6.9 ± .4

TABLE 5

Heat Capacity For TNT and Tritonal
Units In Calories/Gram-^{o}C
Values Within + 0.015

Temperature ^{o}C	Flake TNT Uncycled	Flake TNT Cycled to 150^{o}C @ 5^{o}C/min	Virgin TNT Uncycled	Virgin TNT Cycled to 150^{o}C @ 5^{o}C/min	Tritonal Uncycled	Tritonal Cycled 150^{o}C @ 5^{o}C/min
20	.247	.255	.270	.278	.237	.247
30	.257	.266	.280	.290	.246	.255
40	.265	.274	.289	.299	.254	.262
50	.276	.286	.300	.311	.264	.271
60	.286	.296	.311	.321	.273	.278
120	.359	.372	.386	.392	.333	.338
130	.361	.374	.388	.395	.335	.340
140	.367	.381	.396	.402	.341	.346
150	.369	.384	.398	.404	.343	.349
160	.375	.387	.405	.411	.349	.354

TABLE 6

Impact Sensitivity, 2 Kg Weight
Data is Maximum
No Fire Height in CM

Sample	Uncycled	Cycled Once to 150^{o}C at 5^{o}C	Cycled Twice to 150^{o}C at 5^{o}C	Ambient to 200^{o}C at 40^{o}C/min Hold for 30 min
Virgin TNT	42	58	56	84
	42	52	64	60
Reclaimed	50	58	54	-
Flake TNT	52	64	60	
Tritonal	74	82	60	70
	64	72	74	56

Scanning Electron Microscope (SEM) Evaluation

SEM micrographs of uncycled and thermally cycled TNT material are presented in Figures 6 through 10. Four samples were analyzed: recrystallized TNT, uncycled; flake TNT, uncycled; flake TNT, cycled once to 150^{o}C; and flake TNT, cycled twice to 150^{o}C. Figure 6 includes low power 100X magnification photographs of the four samples. The recrystallized TNT appears broken into several irregular, plate-like crystals. The reclaimed flake TNT (having undergone steam processing), uncycled, reveals smaller crystals compressed together. This is indicative of the steaming process, melting smaller crystals and smoothing those larger. The cycled flake TNT appears continuous with noticeable cracks and voids, which is characteristic of material that has melted. There is more evidence of voids in the twice cycled material than once cycled.

Figures 7 and 8 contain photographs of the four samples at magnifications of 400X and 1000X, respectively. Again, the uncycled flake TNT has more compact, indiscrete crystals than the recrystallized material. Crystallization sites appear on the surface of cycled TNT, which were formed during the solidification

Recrystallized, Uncycled

Flake, Uncycled

Flaked, Cycled Once
at 150°C, 5°C/min

Flaked, Cycled Twice
at 150°C, 5°C/min

Figure 6. SEM Photographs of TNT Samples, 100X

Recrystallized, Uncycled

Flake, Uncycled

Flaked, Cycled Once
at 150°C, 5°C/min

Flaked, Cycled Twice
at 150°C, 5°C/min

Figure 7. SEM Photographs of TNT Samples, 400X

Recrystallized, Uncycled

Flake, Uncycled

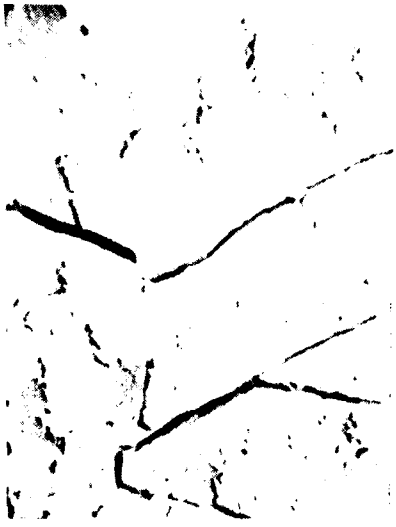

Flaked, Cycled Once
at 150°C, 5°C/min

Flaked, Cycled Twice
at 150°C, 5°C/min

Figure 8. SEM Photographs of TNT Samples, 1000X

Recrystallized, Uncycled

Flake, Uncycled

Flaked, Cycled Once
at 150°C, 5°C/min

Flaked, Cycled Twice
at 150°C, 5°C/min

Figure 9. SEM Photographs of TNT Samples, 4000X

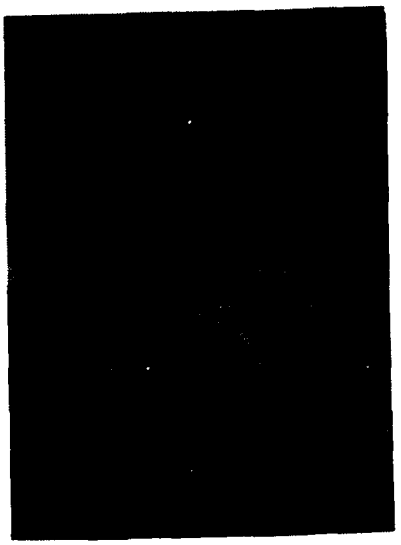

Recrystallized, Uncycled

Flake, Uncycled

Flaked, Cycled Once
at 150°C, 5°C/min

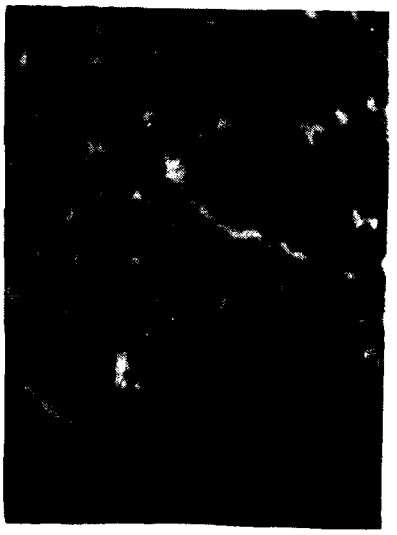

Flaked, Cycled Twice
at 150°C, 5°C/min

Figure 10. SEM Photographs of TNT Samples, 10,000X

transition. No analytical method was available to determine composition of these particular sites. The high magnification photographs of 4000X and 10,000X (Figures 9 and 10), reveal a smooth topography for recrystallized TNT. This is in contrast with the minute speckled formations on the surface of flake TNT, uncycled or cycled. These bump-like features appear to be bubbles or gas-relief pores on the surface, rather than separate crystals.

The morphological information from SEM examination can reveal differences between recrystallized TNT and TNT that has been subjected to thermal conditions above the melting point. No significant difference is noticed between material thermally cycled once or twice. Crystal nucleation during the solidifying process forms a topography with small crystallization sites covering the surface. It is believed these structures are the result of TNT crystal formations during soldification, rather than any change in chemical composition due to thermal treatment.

X-Ray Diffraction Studies

X-ray diffraction patterns were obtained for virgin TNT using 12 and 24 hour exposures because at 24 hours some of the lines which appeared broad were better resolved. Extra lines which showed in cycled TNT were very faint. They occurred near the same D spacing which might indicate a formation of something during cycling, but with only two very faint lines it is not possible to learn the nature of the material.

The laboratory prepared tritonal had several lines which could not be attributed to TNT or aluminum. These lines may be shifted from their true position, but no cause for such a shift is apparent at this time. Faint lines similar to those found in the virgin TNT lines were encountered in tritonal. These weak lines do not constitute sufficient evidence to support the conclusion that similar changes have occurred in both explosives.

The computer search of the patterns of TNT and cycled TNT samples revealed a large number of possible matches. The compound which seemed to be most probable from the search was p-dinitrobenzene.

Thin-Layer Chromatography

The results of the analysis in two solvent systems indicate that the source TNT sample itself contains as many as four relatively nonpolar contaminants detectable at the 10,000 ppm level; the reclaimed TNT contains two detectable contaminants at 10,000 ppm; and the tritonal sample at 10,000 ppm contains five contaminants. No additional products were detected in any of the samples after they were cycled once or twice at 150°C. However, all samples cycled at 200°C yielded an additional product (with an R_f value of 0.38). The product apparently is polar in nature, since it was detected only after development in the polar solvent system. This

experiment did not attempt to identify the material or estimate any increase in any of the contaminants after each cycling. Further tests are planned to confirm these products.

SUMMARY AND CONCLUSIONS

This study suggests that thermal profiles experienced on current munitions either during capture flight or storage may result in the alteration of the decomposition mechanisms and cause sensitivity changes.

The thermal cycles studied under this phase were similar to a temperature profile of an aircraft traveling mach 1.5 - 2.0 at various altitudes on a standard hot day.

Decomposition kinetics on explosives having undergone an evaluated heat profile showed a drop in the activation energy (E_a) which may mean an increase in sensitivity to thermal decomposition.

A rise in the heat capacity for TNT and tritonal over the temperature range of $20^{o}C$ - $160^{o}C$ was noted. No physical changes were observed by scanning electron microscopy under the test conditions. However, the drop hammer impact tests were suggestive of a decrease in sensitivity to impact. It should be noted this test data was very erratic and could have been affected by sample homogeneity; i.e., particle size and sample spread.

Preliminary thin-layer chromatography experiments found an unidentified material in the explosives cycled to $200^{o}C$ which was not present in the other cycled samples.

ACKNOWLEDGEMENTS

This work was in support of the U.S. Air Force Armament Laboratory, Elgin AFB, Florida, project 25600505 under project order ATL-8-281. It was initiatiated and monitored for the Air Force by Mr. Thomas G. Floyd representing Elgin AFB.

REFERENCES

1. Thomas G. Floyd, "Reaction Kinetics of Temperature Cycled Cyclotrimethylenetrinitramine (RDX)", Air Force Armament Laboratory, Eglin Air Force Base, Florida.

2. William F. McGarry, Theodore W. Stevens, "Detonation Rates of the More Important Military Explosives at Several Different Temperatures", Picatinny Arsenal Technical Report 2383, November 1956.

3. S. D. Stein, "The Problem of TNT Exudation", Picatinney Arsenal Technical Report 2493, April 1958.

4. R. N. Rodgers, Thermchimica Acta, 11 (1975), 131-139.

5. R. N. Rodgers, Analytical Chemistry, 44 (1972), 1336-1337.

6. E. Joe Middlebrooks, Statistical Calculations--How to Solve Statistical Problems; Ann Arbor Science Publications Inc., 1976.

A DRYER MODEL

E. P. BERGMANN[1]

ABSTRACT

In a recent program it was necessary to examine and evaluate several types of dryers as alternatives for drying a product. During the course of this investigation it became evident that the drying process is not particularly predictable with the current state-of-the-art. The ability to dry a particular material is often determined only through experimentation and any prediction of the drying time is usually pure conjecture. Subsequent to the dryer assessment, curiosity lead to an examination of the parameters affecting the drying process. It was felt that the technique of similitude modeling could be used to obtain an empirically developed relationship which can be used to predict the drying process with a little more accuracy than is presently available generally. To this end, then, a model was developed which can be used to predict drying trends grossly. The model has limitations in applicability - primarily because the data base available was limited to the drying of one material. However, the model does serve as a foundation for an extension of the state-of-the-art and should be amenable to generalization eventually. This paper presents the background, some of the evolution of the model development, the model as it stands currently, and trends of some of the drying parameters with respect to the drying time.

INTRODUCTION

In a recent program it was necessary to examine and evaluate several types of dryers as alternatives for drying a product. During the course of this investigation it became evident that the drying process is not particularly predictable with the current state-of-the-art. The ability to dry a particular material is often determined only through experimentation and any prediction of the drying time is usually pure conjecture. Subsequent to the dryer assessment, curiosity lead to an examination of the parameters affecting the drying process. It was felt that the technique of similitude modeling could be used to obtain an empirically developed relationship which can be used to predict the drying process with a little more accuracy than is

[1]Senior Engineer, Southwest Research Institute, 6220 Culebra Road, San Antonio, Texas

presently available generally. To this end, then, a model was developed which can be used to predict drying trends grossly. The model has limitations in applicability - primarily because the data base available was limited to the drying of one material. However, the model does serve as a foundation for an extension of the state-of-the-art and should be amenable to generalization eventually. This paper presents the background, some of the evolution of the model development, the model as it stands currently, and trends of some of the drying parameters with respect to the drying time.

There are many variables involved in the drying process. The number of parameters, the difficulty in measuring their properties and the complexity of the air and heat flow have presented a problem that is not readily amenable to a theoretical treatment. Indeed, evan an empirical evaluation is not without difficulty. Some 28 potential parameters, shown in Table 1, are in three generic groupings: Those parameters that relate to the medium used to dry the product; those elements that relate to the product; and the time to dry. In this particular model the data available related to

TABLE 1

Potential parameters

Medium parameters

Specific Heat of Air (C_{P_A})
Air Speed (X_A)
Air Density (ρ_A)
Pressure (Static) (P_S)
Dry Bulb Temperature (T_{DB})
Wet Bulb Temperature (T_{WB})
Air Directionality Factor (θ)

Material parameters

Specific Heat of Water (C_{P_W})
Specific Heat of Material (C_{P_M})
Heat of Vaporization of Water (h_{fg})
Thermal Conductivity of Water (K_W)
Thermal Conductivity of Material (K_M)
Convection Heat Transfer Coefficient of Water (L_W)
Convection Heat Transfer Coefficient of Material (L_M)
Surface Area of Water (A_{SW})
Surface Area of Material (A_{SM})
Projected Area of Material (A_M)
Weight of Water (W_W)
Weight of Material (W_M)
Material Thickness (h_M)
Material Density (ρ_M)
Material Porosity (ϕ_M)
Moisture of Material (μ)
Temperature of Water (T_W)
Temperature of Material (T_M)
Particle Size of Material (d_M)
Availability of Moisture (α)

Temporal parameter

Drying Time (t_D)

drying a ball propellant with the use of air. The medium, then, is air and the propellant is the material. Of the 28 parameters considered as affecting the drying process, seven parameters relate to the air and 20 to the propellant.

The key to believing that an empirical relationship could be established was the recognition that all of the heat and heat transfer parameters are based on empirically derived constants. In a typical drying process, the moisture is in the form of water and the drying medium is air. The parameters relating to those elements should be amenable to generalization. Material parameters are generally material peculiar and need to be defined for most drying processes - primarily through experimentation. The problem, now, becomes one of arranging the parameters in a manner that allows an analysis to be made and then to cast the groupings in terms of the experimental data available.

The model analysis used in this study is based on Buckingham's Pi theorem, which is the basis for most dimensional analyses. A physical relationship is expressed in a set of dimensionless products called "π terms". In many cases these products can be grouped in a log linear fashion to establish a predictive model. Potential π terms for the dryer model are shown in Table 2. The Pi terms relate to factors which influence or control the drying process. They include: energy, pressure, moisture, heat,

TABLE 2

Potential π terms

Energy Factor	$\frac{\rho_M \, h_M \, T_M \, g}{\rho_A \, (\theta \, \dot{X}_A)^2 \, T_{DB}}$	Pressure Factor	$\frac{P_S}{P_o}$
Moisture Factor	$\frac{\frac{T_{WB}}{T_{DB}}}{\frac{\mu_F}{\mu_o}}$	Thickness Factor	$\frac{\bar{d}_M}{h_M}$
Porosity Factor	$\frac{\bar{d}_M}{d_{max}}$	Time Factor	$\frac{t_D \, (\theta \, \dot{X}_A)}{h_M}$
Heat Factors	$\frac{C_{P_W} \, W_W}{C_{P_A} \, \rho_A \, h_M \, A_M}$		$\frac{C_{P_M} \, W_M}{C_{P_A} \, \rho_A \, h_M \, A_M}$	$\frac{h_{fg} \, W_W}{C_{P_A} \, \rho_A \, h_M \, A_M \, T_{DB}}$
Conductivity Factors	$\frac{\rho_A \, \theta \, \dot{X}_A \, A_M \, C_{P_A}}{K_W \, h_M}$		$\frac{\rho_A \, \theta \, \dot{X}_A \, A_M \, C_{P_A}}{K_M \, h_M}$
Convection Factors	$\frac{\rho_A \, \theta \, \dot{X}_A \, C_{P_A}}{L_W}$		$\frac{\rho_A \, \theta \, \dot{X}_A \, C_{P_A}}{L_M}$

heat transfer, thickness and time. The terms are then combined into a functional format which relates the primary term of interest to the other factors. For the dryer model the primary term of interest is the time factor. The initial relationship that is postulated is given in Equation (1). (The Pi terms are identified in Table 2 and the parameters are listed in Table 1.)

$$\left[\frac{t_D\ (\theta\ \dot{X}_A)}{h_M}\right]^a = K\left[\frac{\rho_M\ h_M\ T_M\ g}{\rho_A(\theta\ \dot{X}_A)^2\ T_{DB}}\right]^b \left[\frac{P_S}{P_o}\right]^c \left[\frac{\frac{T_{WB}}{T_{DB}}}{\frac{\mu_F}{\mu_o}}\right]^d \left[\frac{\bar{d}_M}{h_M}\right]^e \left[\frac{\bar{d}_M}{d_{max}}\right]^f X$$

$$\left[\frac{C_{P_W}\ W_W}{C_{P_A}\ \rho_A\ h_M\ A_M}\right]^S \left[\frac{C_{P_M}\ W_M}{C_{P_A}\ \rho_A\ h_M\ A_M}\right]^h \left[\frac{h_{fs}\ W_W}{C_{P_A}\ \rho_A\ h_M\ A_M\ T_{DB}}\right]^i X$$

$$\left[\frac{\rho_A\ \theta\ \dot{X}_A\ A_M\ C_{P_A}}{K_W\ h_M}\right]^i \left[\frac{\rho_A\ \theta\ \dot{X}_A\ A_M\ C_{P_A}}{K_M\ h_M}\right]^k \left[\frac{\rho_A\ \theta\ \dot{X}_A\ C_{P_A}}{L_W}\right]^\ell X \left[\frac{\rho_A\ \theta\ \dot{X}_A\ C_{P_A}}{L_M}\right]^M \quad (1)$$

Equation (1) is somewhat complex and it must be simplified to a form compatible with the type of empirical data normally available. A simplification is possible by grouping several of the empirically derived constants into the form:

$$\frac{C_{PW}}{C_{P_A}} \qquad \frac{C_{P_A}}{K_W} \qquad \frac{C_{P_A}}{L_M}$$

$$\frac{C_{P_M}}{C_{P_A}} \qquad \frac{C_{P_A}}{K_M}$$

$$\frac{h_{fg}}{C_{P_A}} \qquad \frac{C_{P_A}}{L_W}$$

These constants relate air, water and material coefficients. Where the air and water coefficients are combined with "K" the model remains general. Where the material coefficients are combined with "K" the model becomes material peculiar to the extent that the material factors have a significant influence. Also - W_W can be expressed as $\mu\ W_M$. Equation (1) can now be expressed as:

AD-A169 165 JOINT SYMPOSIUM ON COMPATIBILITY OF PLASTICS/MATERIALS WITH EXPLOSIVES PR..(U) AMERICAN DEFENSE PREPAREDNESS ASSOCIATION ARLINGTON VA L R BARTRON ET AL. MAY 79 3/4

UNCLASSIFIED F/G 19/1 NL

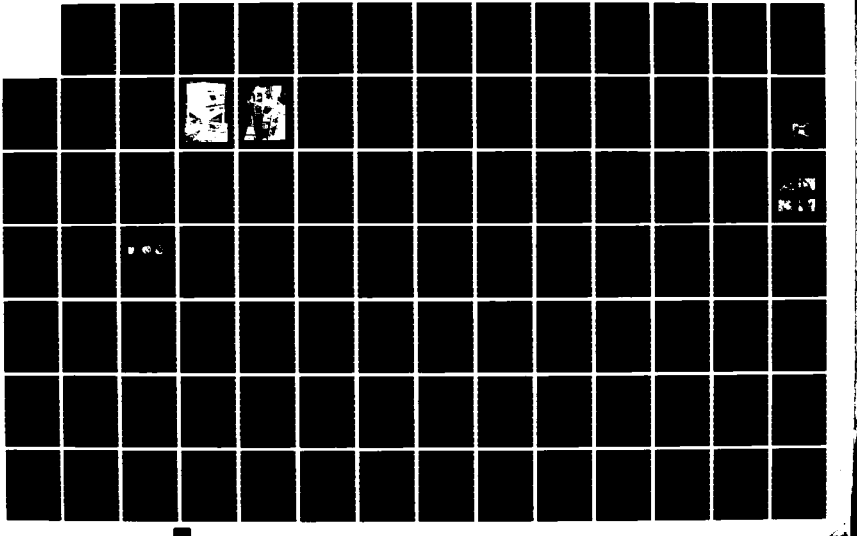

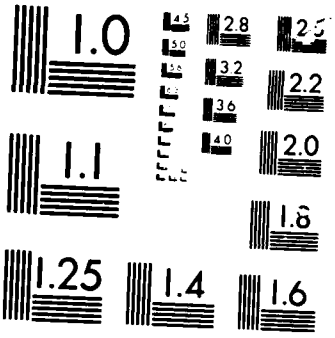
1.0
1.1
1.25
1.4
1.6
1.8
2.0
2.2
2.8
3.2
3.6
4.0

$$\left[\frac{t_D\ (\theta\ X_A)}{h_M}\right]^a = K\left[\frac{\rho_M\ h_M\ T_M\ g}{\rho_A\ (\theta\ X_A)^2\ T_{DB}}\right]^b \left[\frac{P_S}{P_o}\right]^c \left[\frac{T_{WB}\ \mu_o}{T_{DB}\ \mu_F}\right]^d \left[\frac{\bar{d}_M}{h_M}\right]^e \left[\frac{\bar{d}_M}{d_{max}}\right]^f X$$

$$\left[\frac{\mu_o}{T_{DB}}\right]^i \left[\rho_A\ \theta\ X_A\right]^p \left[\frac{A_M}{h_M}\right]^k \left[\frac{\rho_M}{\rho_A}\right]^n \qquad (2)$$

Equation (2) is still somewhat cumbersome and must be simplified further to allow an empirical fit to the data available. Simplification is possible through the following assumptions.

$\frac{\mu_o}{T_{DB}} \cong \frac{.07}{140} = .0005$ Neglect

$\frac{P_S}{P_{S_o}} = 1$ For the non-vacuum dryer data available

$\frac{\bar{d}_M}{d_{max}}$ = Constant for the data available

$\frac{\rho_M}{\rho_A}$ = Constant for the data available

$\rho_A\ \theta\ \dot{X}_A$ Effect is incorporated into the first term

$T_M = T_{DB}$

$\frac{A_M}{h_M}$ becomes $\frac{A_M}{h_M^2}$ to restore the nondimensionality.

Equation (2) then takes the form:

$$\left[\frac{t_D\ \theta\ X_A}{h_M}\right]^a = K\left[\frac{\rho_M\ h_M\ g}{\rho_A\ (\theta\ \dot{X}_A)^2}\right]^b \left[\frac{T_{WB}\ \mu_o}{T_{DB}\ \mu_F}\right]^d \left[\frac{\bar{d}_M}{h_M}\right]^e \left[\frac{A_M}{h_M^2}\right]^k \qquad (3)$$

The problem now is to determine if the simplification used in transforming Equation (1) into Equation (3) precludes a meaningful prediction of the drying process. Data was available on the use of a tray dryer and a fluidized bed dryer to dry a solid propellant. The tray dryer used relatively low velocity air blowing across the material bed to effect the drying. The fluidized bed dryer used higher

velocity air blowing up through the material bed. The drying data are given in Tables 3 and 4. For the moment, ignore the right hand column (the drying time predicted).

By using the data of Tables 3 and 4 to structure the π terms of Equation (3) and isolating as many factors as the data allows, estimates are made for the exponents and the constant (K). The dryer model then takes the general form of:

$$\left[\frac{t_D\ \theta\ \dot{X}_A}{h_M}\right]^{1.40} = K\left[\frac{\rho_A\ (\theta\ \dot{X}_A)^2}{\rho_M\ h_M\ g}\right]^{.50}\left[\frac{T_{WB}\ \mu_o}{T_{DB}\ \mu_F}\right]^{2.40}\left[\frac{\bar{d}_M}{h_M}\right]^{1.25}\left[\frac{h_M^2}{A_M}\right]^{.50} \qquad (4)$$

Since the interest is in the drying time Equation (4) can be re-arranged to the form:

$$t_D = 44{,}940\left[\frac{\rho_A}{\rho_M\ A_M}\right]^{.357}[\bar{d}_M]^{.893}\left[\frac{T_{WB}\ \mu_o}{T_{DB}\ \mu_F}\right]^{1.714}\left[\frac{h_M^{.464}}{(\theta\ \dot{X}_A)^{.286}}\right] \qquad (5)$$

where: t_D = Drying time, minutes
ρ_A = Air density, lb/ft^3
ρ_M = Material density, lb/ft^3
A_M = Bed area, ft^2
$\bar{d}_M$ = Mean material diameter, ft

TABLE 3
Drying data, tray dryer

θ	$\dot{X}_A$ (FPS)	h_M (ft)	ρ_M (lb/ft^3)	ρ_A (lb/ft^3)	T_{DB} (°F)	T_{WB} (°F)	μ_o	μ_F	$\bar{d}_M$ (ft)	A_M (ft^2)	Drying Time (min.) Meas.	Pred.
.003	0.9	.083	62.0	.076	140	84	.0734	.0481	.0025	2.0	30	15
								.0230			60	50
								.0165			90	88
								.0111			120	175
								.0104			150	195
								.0102			180	202
								.0100			210	210
							.0764	.0542			30	20
								.0422			60	30
								.0300			90	53
								.0221			120	90
								.0156			150	165
								.0126			180	238
								.0108			210	310
								.0103			240	337
								.0100			270	353

TABLE 4

Drying data, fluidized bed dryer

θ	$\dot{X}_A$ (FPS)	h_M (ft)	ρ_M (lb/ft^3)	ρ_A (lb/ft^3)	T_{DB} (°F)	T_{WB} (°F)	μ_o	μ_F	$\bar{d}_M$ (ft)	A_M (ft^2)	Drying Time (min.)	
											Meas.	Pred.
1.00	6.4	.17	62.0	.076	119	79	.059	.038	.0015	6.5	5	5
					120			.031			10	7
					121			.024			15	11
					123	80		.019			20	16
		.15			121	79		.014			25	26
		.17			152	86	.053	.030			5	5
					150			.021			10	9
					149			.016			15	15
		.15			151			.010			20	30
		.33			150		.057	.030			5	8
					152			.022			10	13
					150			.015			15	25
		.29			151			.009			20	56
	2.2	.17			150		.050	.033			5	5
					152			.023			10	10
					155	87		.016			15	17
		.15			153			.010			20	38
	6.4	.50			124	80	.049	.036			5	6
					124			.027			10	10
					123			.022			15	15
					124			.017			20	23
		.46			122			.012			25	42
		.17			150	86		.037			5	3
					155	87		.026			10	5
					153			.013			15	18
		.15			153			.011			20	23
		.50			151	86	.059	.042			5	6
					150			.039			10	6
					152			.028			15	11
					150			.020			20	20
					150			.017			25	26
		.46			151			.013			30	39

T_{WB} = Air wet bulb temperature, °F

T_{DB} = Air dry bulb temperature, °F

μ_o = Initial moisture, fraction of dry weight

μ_F = Final moisture, fraction of dry weight

h_M = Bed thickness, ft

$\dot{X}_A$ = Air speed, ft/sec

θ = Air directionality factor, dimensionless

θ = .003 for across the bed flow

θ = 1.00 for through the bed flow

The air directionality factor was arbitrarily set at 1.0 for the fluidized bed dryer whereby the flow is through the bed. This factor was then determined for the flow across the bed.

The question to be asked next is, how well does the prediction match the data? Tables 3 and 4 can be reviewed and the two righthand columns examined to see if the prediction is "reasonable". The graphical representation of the predicted time versus the measured time to dry the material is shown in Figure 1. The line of equal predicted and measured times is shown on the graph. A perfect predictive model would result in all of the points laid on this line directly. It is evident that the model provides a "reasonable" fit for drying times covering a range of almost three orders of magnitude.

If the measured time is used as a basis, the average error for either the tray or the fluidized bed model is about 29%. Clearly there is room for improvement. However, considering that the data was not based on closely controlled experiments, and the simplifying assumptions that were made leading to Equation (3), the model is not too bad.

Figures 2 through 8 illustrate the sensitivity of drying time to some of the parameters. The sensitivities are illustrated for a fluidized bed dryer, but the trends would be similar for the tray dryer.

Figure 2 shows the effect of air speed. As would be expected, the higher the air speed the shorter the drying time. The steepness of the curve, however, indicates that a relatively large increase in air speed is required to attain a small decrease in drying time. If the material to be dried tends to produce dust, the higher air speeds tend to compound the dust problem. In the drying of energetic materials, such as propellants, explosives, plastics, etc., the high dryer air speeds which produce high dust levels tend to create a hazard problem.

Figure 3 shows the effects of initial and final moisture on drying time. Unlike the air speed, a relatively small change in the initial or final moisture has a significant affect on drying time. Final moisture is usually a process requirement and, thereby, cannot be increased greatly. The final moisture, however, should be set as high as is practical. The sensitivity trend shows that it is also important to control the initial moisture to control the minimum drying time.

Bed depth-drying time trends are shown in Figure 4. The steepness of the line shows that a significant increase in bed depth results in a proportionately smaller increase in drying time. This trend was reasonable for bed depths of up to six inches. Extrapolation of the trend beyond this depth should be done with caution since a saturation function would be expected at some point.

Figure 5 shows the effect of wet and dry bulb temperature. Clearly, there is a drying time payoff in both dryer and hotter air. Figure 6 shows the effect of the bed area on drying time. Although there is a payoff in increased bed area, the steepness of the line indicates that the drying time is not strongly sensitive to the bed area. The effect of particle size (average) on drying time is shown in Figure 7. The relationship shows an increase in particle size results in a

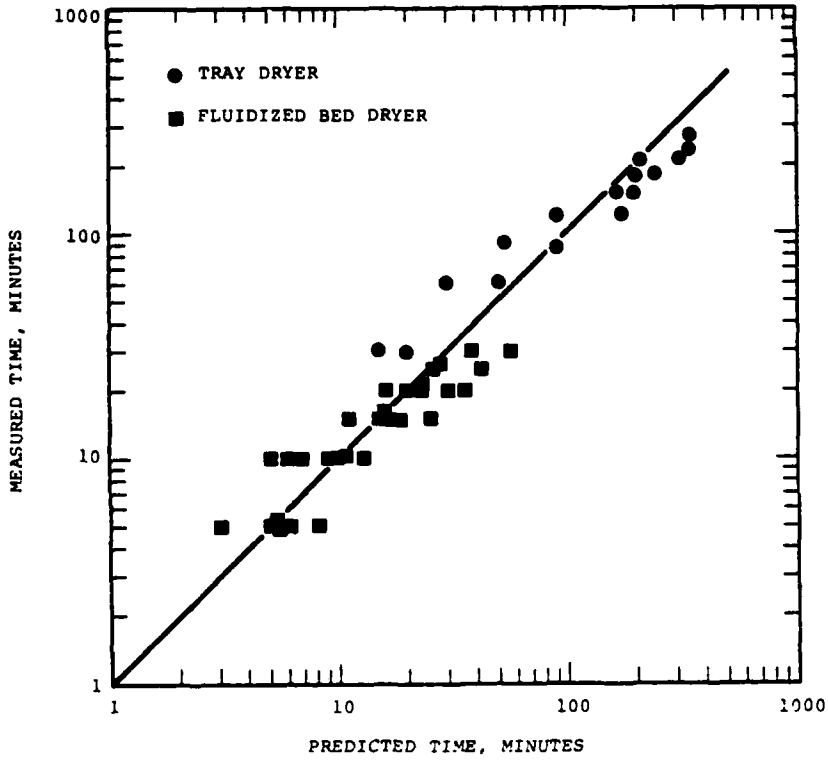

Fig. 1. Measured versus predicted drying time

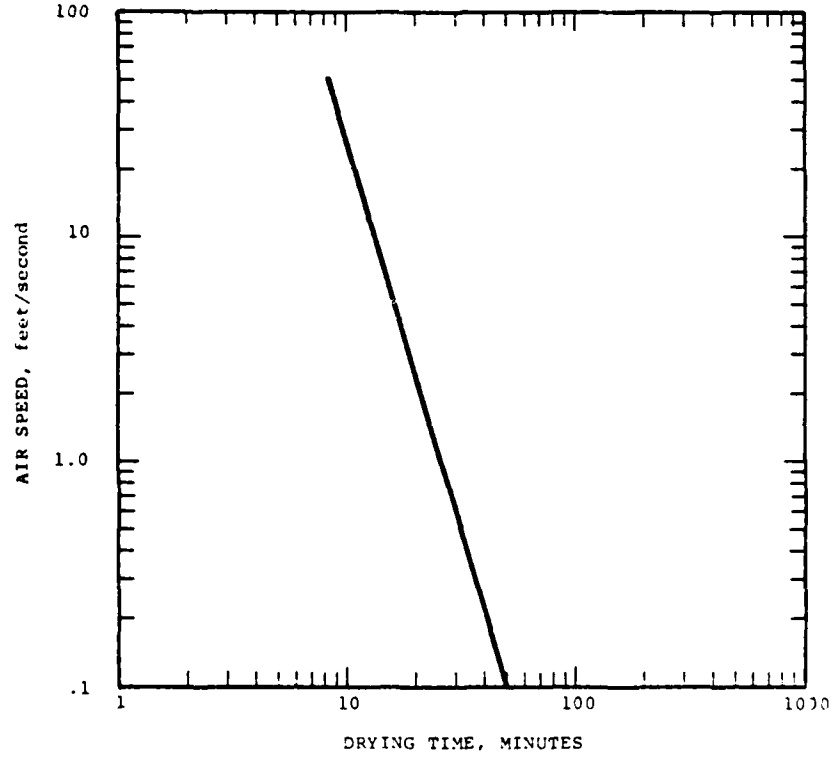

Fig. 2. Air speed-drying time trend

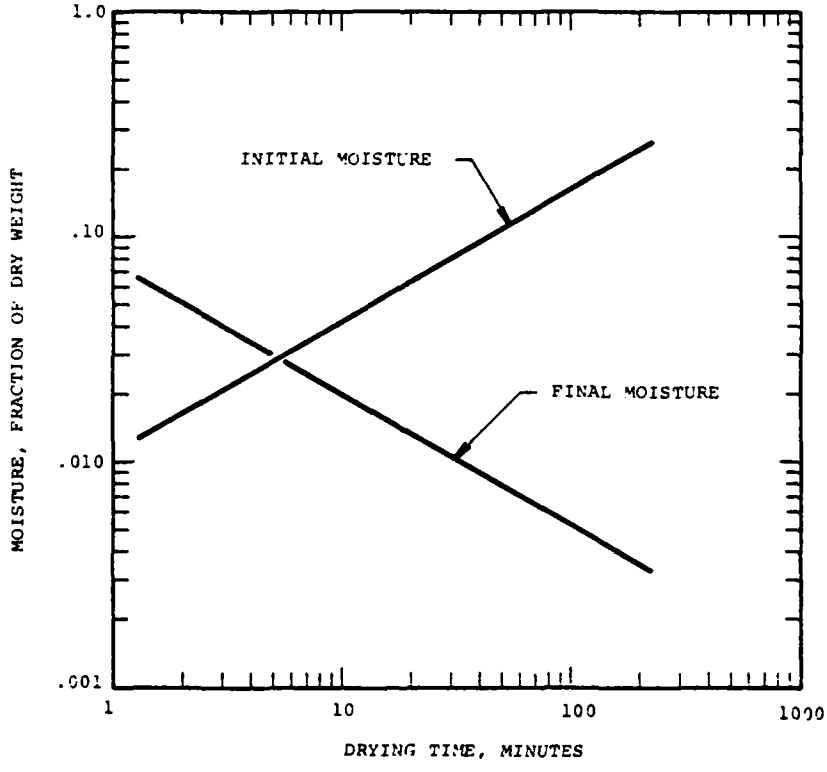

Fig. 3. Moisture-drying time trend

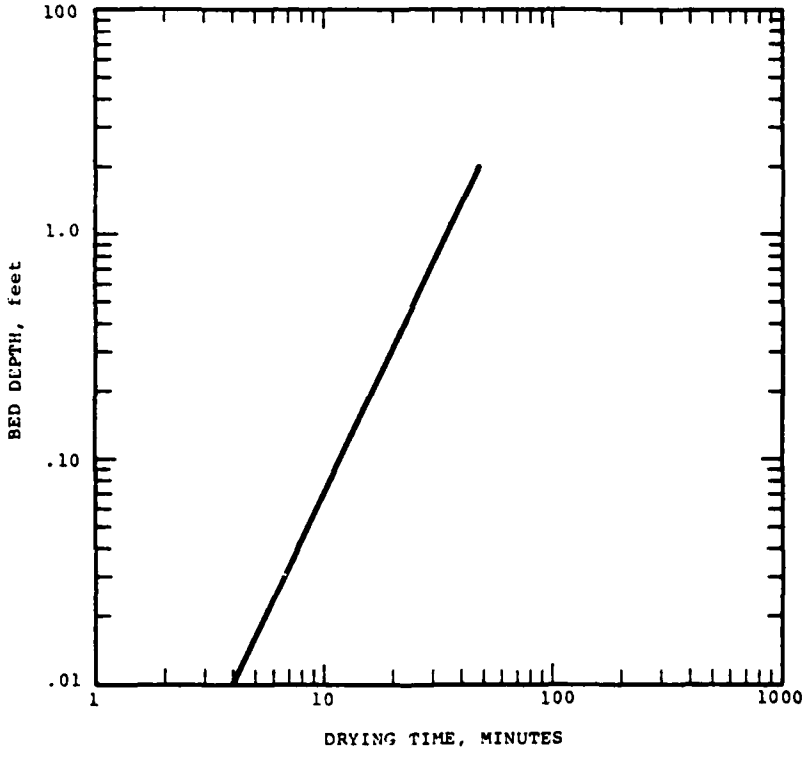

Fig. 4. Bed depth-drying time trend

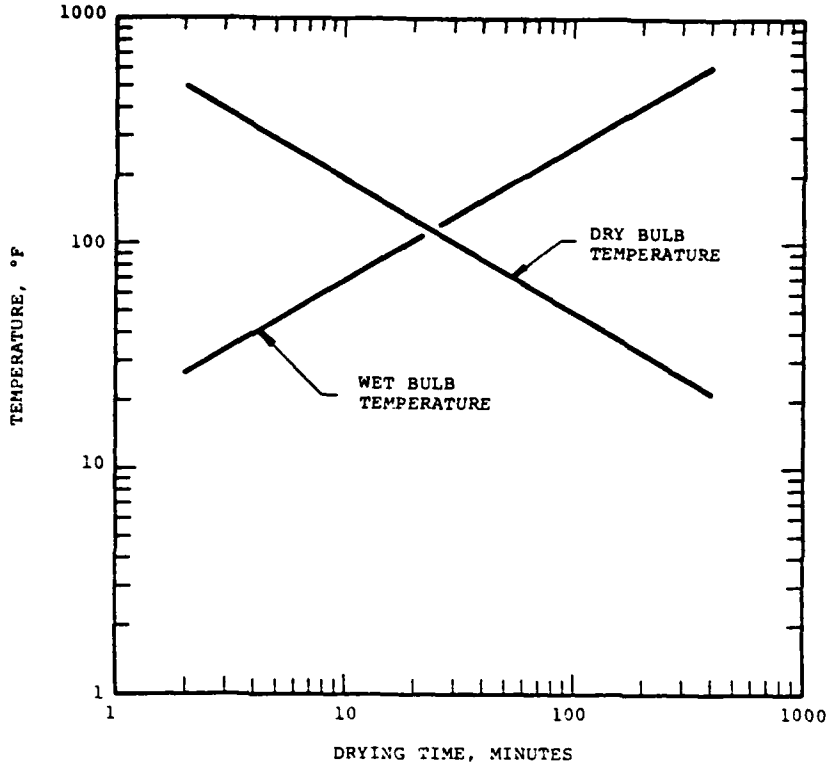

Fig. 5. Temperature-drying time trend

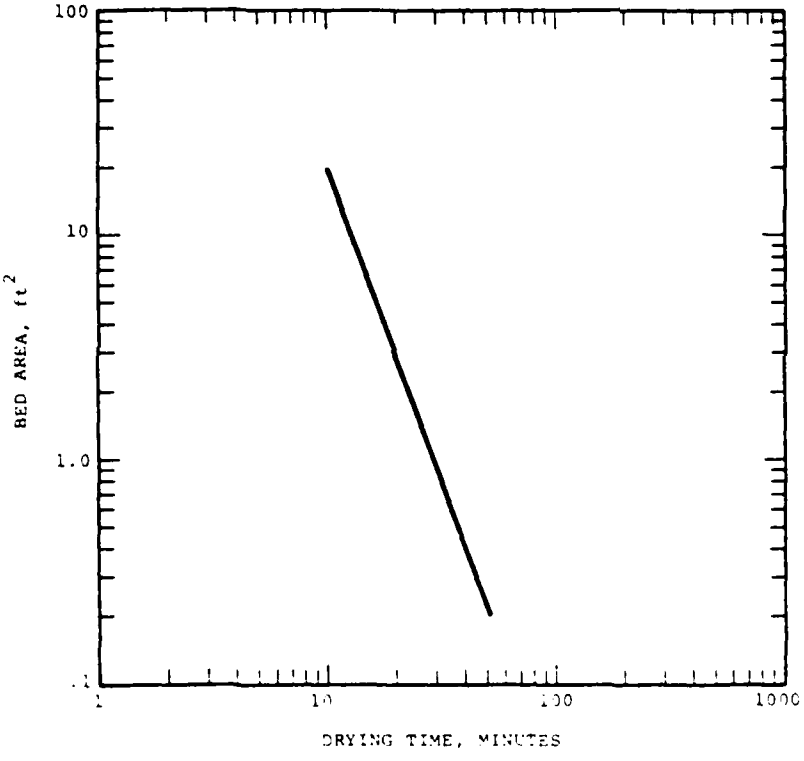

Fig. 6. Bed area-drying time effect

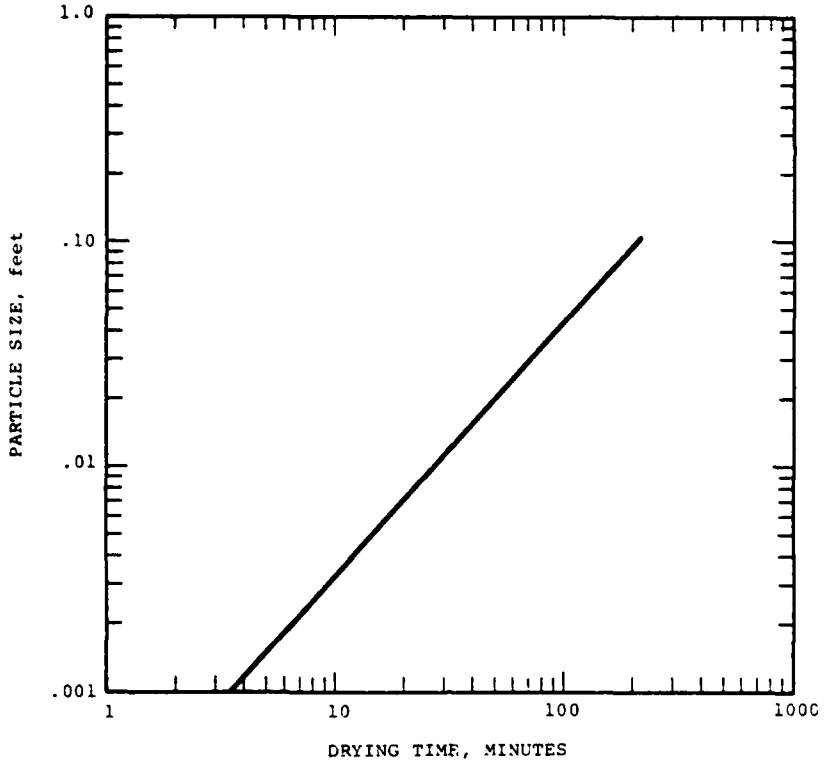

Fig. 7. Particle size-drying time effect

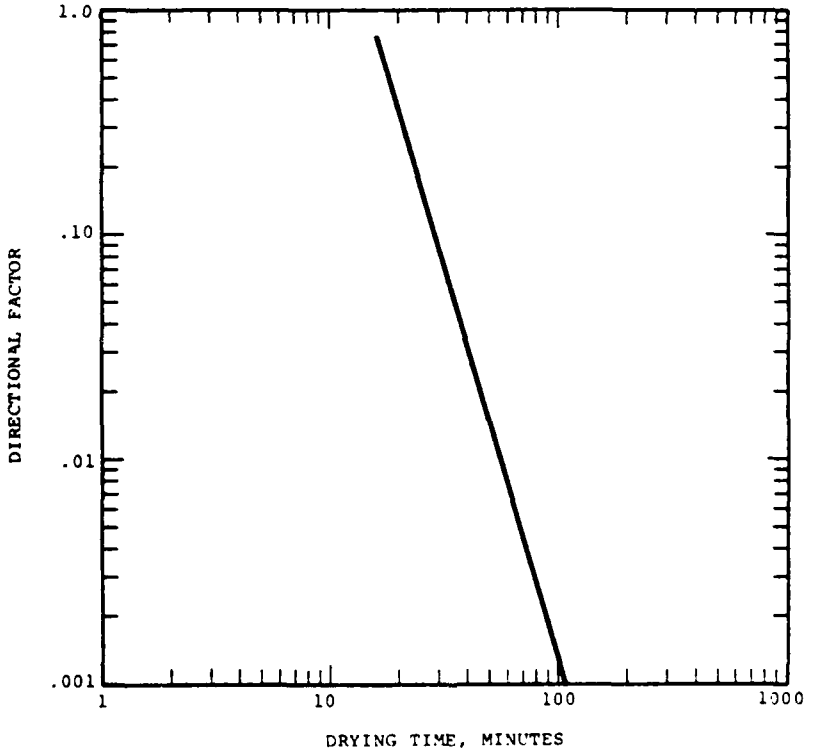

Fig. 8. Directionality factor-drying time effect

longer drying time. Since the slope of the curve is relatively shallow, the drying time can be expected to be sensitive to particle size.

Figure 8 shows the effect of the direction of the air flow on drying time. Changing the flow from across the material ($\theta = 1.0$) decreased the drying time by a factor of 5. If the generation of dust is not a problem, there is a significant payoff in drying time by blowing the air through the bed rather than across it.

The drying model presented in this paper is by no means complete. But it is interesting to note that the model does predict the drying time of two significantly different types of dryers through the use of one generic model. Also, the trends predicted by the model appear to make sense, e.g. increased temperature should decrease the drying time and the prediction agrees with this trend. In order to improve the accuracy of the drying model, some of the simplifications that were made to make the model commensurate with the level of data available should be deleted. The model should also be extended to other dryers and other materials through the use of additional drying data.

This experimental-analytical model was characterized and cast to incorporate the drying data in less than two months. A theoretical-analytical model would require significantly more effort to yield the same level of accuracy. Further, the modeling technique presented herein can be extended to provide a means of predicting trends and sizing process equipment for many additional process elements.

ESTABLISHMENT OF PROPELLANT HAZARDS CLASSIFICATION VIA VENTED VESSEL TESTING

By

J. L. Evans, F. T. Kristoff and W. T. Bolleter
Hercules Aerospace Division
Hercules Incorporated
Radford Army Ammunition Plant
Radford, Virginia 24141

INTRODUCTION

The hazards classification of small-arms and cannon propellants during manufacture, loading, or in storage is defined in the United States by procedures in Department of the Army document AMCR 385-100 and Technical Bulletin TB 700-2. Two divisions of major importance under Class 1 are burning only, Division 3, and detonation, Division 1. For the most part, these classifications are based on propellant granule web thickness, nitrocellulose content, and/or nitroglycerin content (see Table 1). This method of classification does not directly make use of two basic parameters related to rate of pressurization in a process vessel or in a storage facility; namely, degree of confinement and total propellant surface area. A hazard classification system failing to fully consider these parameters could either overclassify a propellant resulting in added construction cost or reduced production, or underclassify, resulting in an unrecognized hazard to personnel or facilities.

An alternative procedure is to perform simulated full-scale tests. For example, existing criteria dictated a Class 1, Division 1, hazard for 200 Kg of single-base propellant in a holding hopper designed for an automated production line. To avoid the high facility construction cost to protect against a Class 1.1 hazard, the holding hopper was redesigned for venting and full-scale tests were conducted. The full-scale vessel was successfully tested in the configuration shown in Figure 1. However, this method of testing has two main disadvantages; viz., cost of test vessels and quantity of propellant being tested. A second alternative is to test lesser quantities of propellant in relatively low cost subscale vessels and correlate the results to full-scale vessels.

This paper describes the results of a study to determine through subscale testing the in-process hazard classification of 680 Kg of M26 propellant when processed through the propellant dryer shown in Figure 2. Using the published criteria, the drying operation would be classified as a Class 1.1 mass-detonating hazard because the nitroglycerin content in the M26 composition is greater than 20 percent. It was estimated that approximately one million dollars could be saved in facility construction if the dryer system were a Class 1.3 burning hazard. Since full-scale prototype tests were prohibitive from a cost and exposure standpoint, subscale vented vessel models were investigated. Three different size vessels were tested at various levels of vent area to determine the effects of vent area and scale (size) on the pressurization rate for the M26 double-base propellant.

EXPERIMENTAL

Test Design

The test program to determine the hazard classification of M26 in the dryer consisted of testing up to 85 Kg of M26 propellant in subscale vessels. The test vessels were scaled to the dryer dimensions (size and wall thickness) to achieve one-fourth, one-third and one-half scale models (linear dimensions). These yielded propellant test weights equivalent to 1/64, 1/27 and 1/8 of the 680 Kg dryer propellant weight when scaled according to the cube of the linear scale factor. Vessels having a wall thickness of 6.4 mm and 12.8 mm were tested at vent ratios (propellant surface/vent area) ranging from 267 to 1500. The test program and basic vessel dimensions are shown in Figure 3.

Two M1 Atlas match squibs were used to ignite the propellant. Pressure-time data were recorded from strain patches bonded to one side and one end of the vessels having 6.4 mm wall thickness and from pressure transducers located in one side and one end of the vessels having 12.8 mm wall thickness as shown in Figure 4. Pressure-time data were reduced to maximum pressure and to rate of pressure rise from ignition to maximum pressure.

RESULTS AND DISCUSSION

The relationship between rate of pressure rise and vent ratio for the three subscale vessels tested is summarized in Table 2 and plotted as scaled rate of pressure rise versus scaled vent area in Figure 5. Three conclusions can be drawn from the data; namely, (1) maximum pressure is observed to increase with vent ratio, (2) rate of pressure rise increases with vent ratio, and (3) for a given vent ratio, all parameters, particularly rate of pressure rise, decrease as scale (vessel size) increases. The first two effects are as expected. The third would not be expected without modeling of the propellant/vessel system.

In Figure 6, the rate of pressure rise versus volume (scale) curves for the different vent ratios exhibit different slopes indicating an interaction between vent ratio and scale. The magnitude of this interaction could not be determined from the limited tests performed. However, the data indicate this interaction to be in a fail safe direction.

The predicted performance of the full-scale dryer is shown by the dashed lines in Figures 5 and 6. The rate of pressure rise for the dryer indicates a burning only Class 1.3 hazard.

MATH MODELING

The curve shown in Figure 5 is best described by the equation $\dot{P} = a\bar{A}^{-b}$. Since $\bar{A}$ is directly related to the vent ratio R, the equation can be rewritten as $P = aR^b$. Thus the rate of pressure rise is a function of both propellant surface area, S, and vessel vent area, A_v, since by definition $R = S/A_v$.

The curves in Figure 6 show a decrease in rate of pressure rise as vessel scale increases at a constant vent ratio. This effect can be shown to be caused by the scale factor λ as follows. The subscale vessel produces the same maximum pressure at a given vent ratio as the full-scale vessel, i.e., $P = aR^m$, and the pressure rate of rise in a full-scale vessel is $\dot{P} = P/t$. However, since a subscale vessel contains less propellant than the full-scale vessel, the burning distance is reduced by λ. The burning time in the subscale vessel is also reduced by λ, and the rate of pressure rise becomes

$$\dot{P}_{subscale} = \frac{P}{\lambda t}$$

Thus the pressure rate of rise is seen to increase with a decrease in vessel size.

The relationship in the pressure rate of rise between full and subscale vessels of constant vent ratio is therefore

$$\dot{P}_{full\text{-}scale} = \lambda \dot{P}_{subscale}$$

Where vent ratio is not constant, the relationship becomes

$$\dot{P} = \dot{P}_o f(R, \lambda, R\lambda).$$

For propellants of different formulations, differences in values for c and n from the propellant burning rate equation $r = cP^n$ must be considered. To construct a model for all propellants requires the addition of these terms to obtain the form

$$\dot{P} = \dot{P}_o f(R, \lambda, R\lambda, c, n)$$

Thus the rate of pressure rise in any process vessel can be calculated from subscale test results. By knowing the strength of the process vessel as a function of rate of pressurization, it will be possible to determine whether the vessel will vent, rupture from overpressurization, i.e., explode or transit to a detonation. To preclude a calculated detonation, the vent area of the vessel should be increased. To prevent damage from a calculated overpressurization, more venting could be provided and/or use lower strength materials of construction for all or part of the vessel to allow the vessel to rupture at relatively low pressures.

Table 1

HAZARDS CLASSIFICATION CRITERIA

PARAMETER	FORMULATION	GRANULATION	CLASS 1.1 CRITERIA
NC CONTENT	SB	ALL	> 98
NG CONTENT	DB or TB	ALL	> 20
WEB	SB	SINGLE PERF	> 19 mil
TWO TIMES BURNING DISTANCE	SB	MULTI PERF	< 19 mil
	DB	SINGLE PERF	N/A
	DB	MULTI PERF	> 19 mil
	DB	ALL	< 0.0075

Table 2

RANGE OF RESULTS FOR SUBSCALE TESTS

SCALE	PROP. WT., Kg.	VENT RATIO RANGE	MAX. PRESSURE, RANGE Kpa	RATE OF PRESSURE RISE RANGE, MPa/s
1/4	10.6	800-1500	758-2041	43.6-53.6
1/3	25.2	500-1100	146-1717	4.1-47.3
1/2	85.0	267-1100	74-1151	2.9-21.2

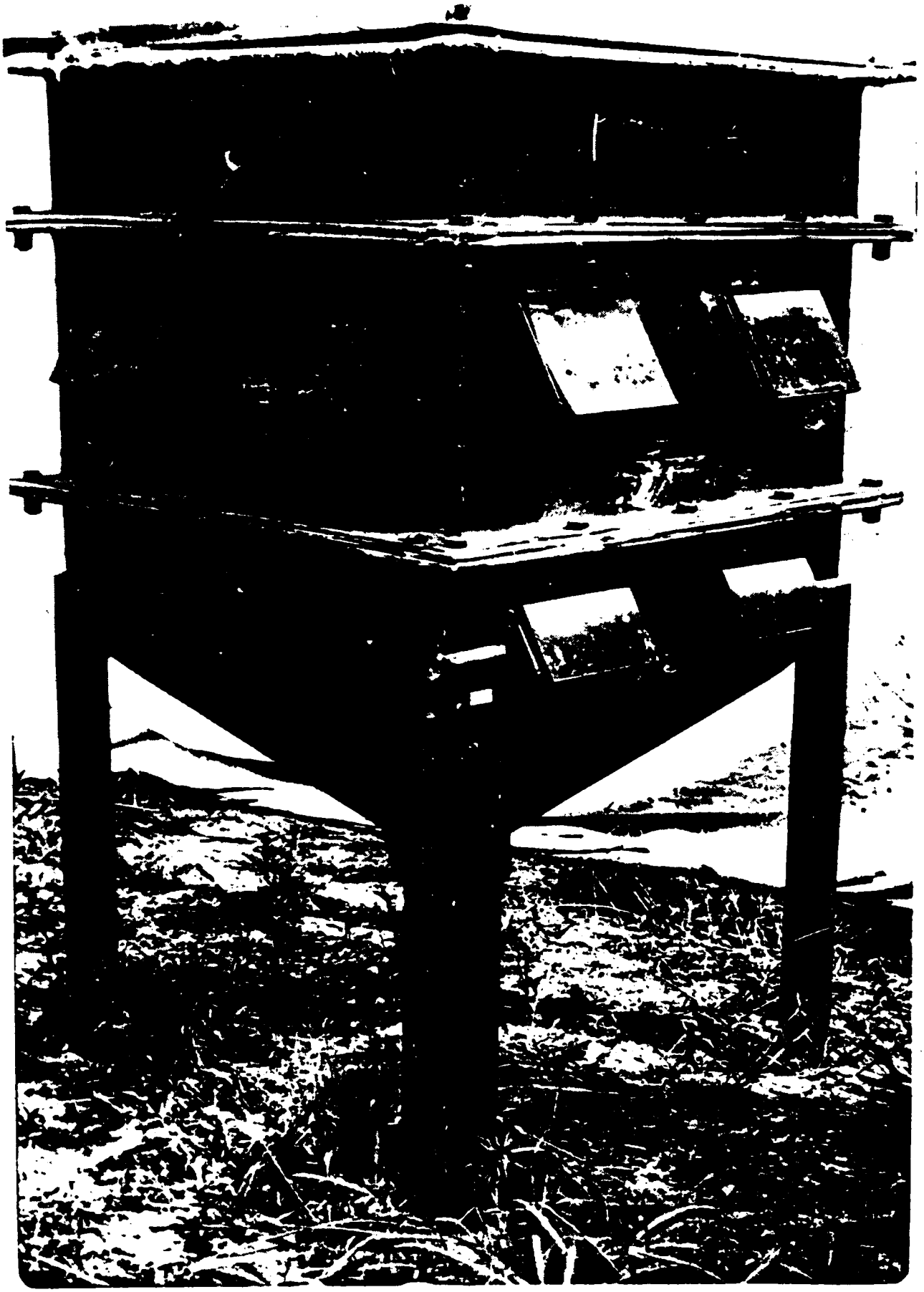

Figure 1. Full-Scale Model for Hazards Classification Tests

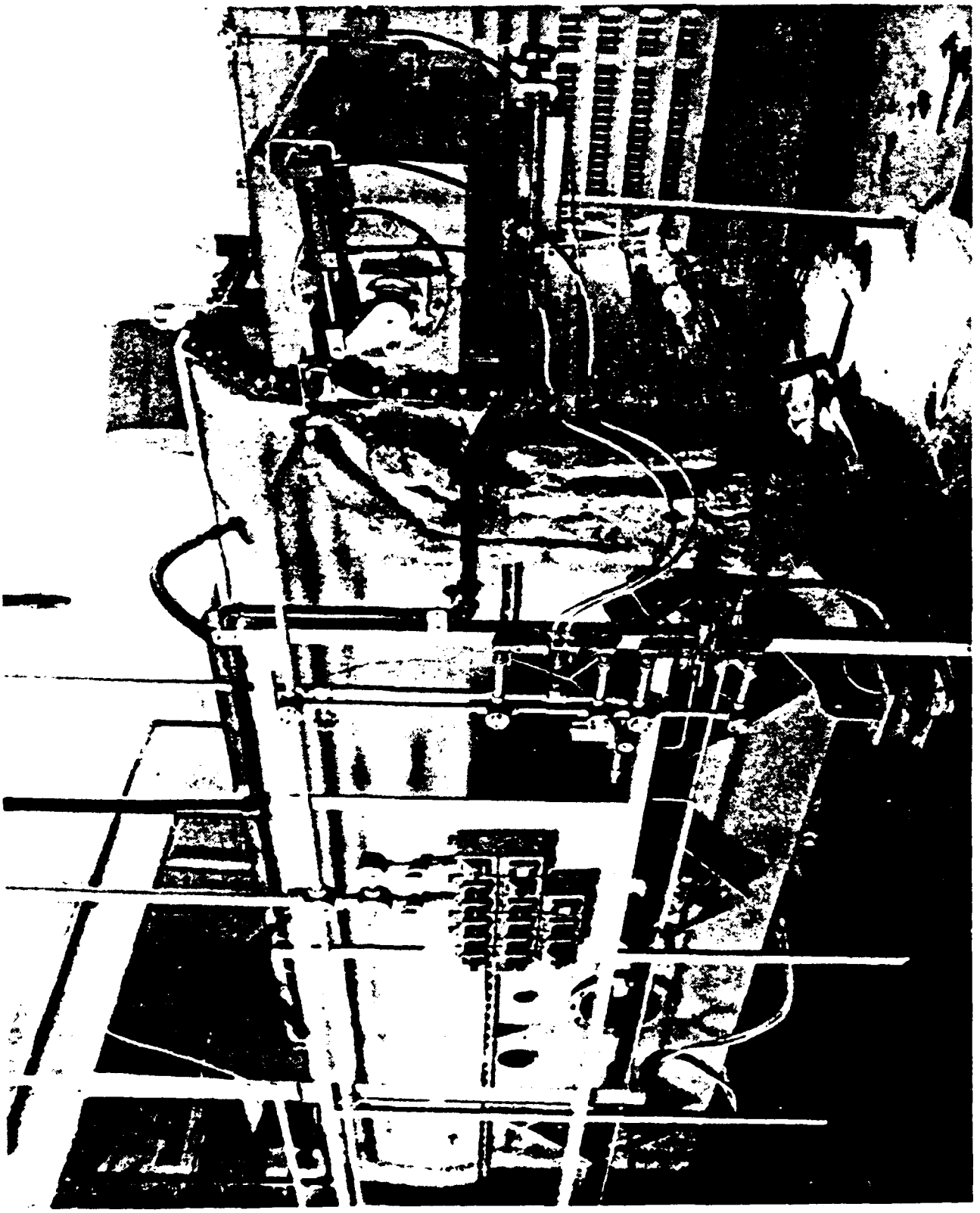

Figure 2. Full-Scale Propellant Dryer

VESSEL AND PROPELLANT VARIABLES FOR SUBSCALE TESTS

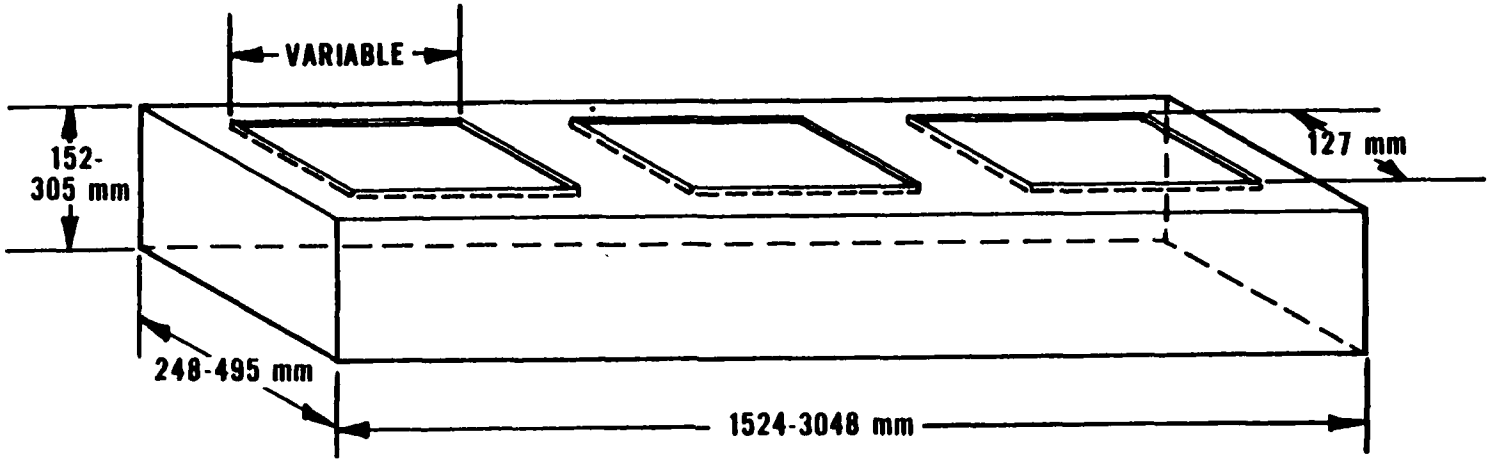

VESSEL SCALE	PROPELLANT MASS, kg	VESSEL VOL. m^3	PROPELLANT AREA, m^2	VENT RATIO	VENT AREA, m^2
1/4	10.6	0.0574	9.89	800-1500	0.007-0.013
1/3	25.2	0.1360	23.4	500-1100	0.021-0.047
1/2	85.0	0.4602	79.1	267-1100	0.072-0.296

Figure 3. Subscale Test Vessel and Nominal Dimensions

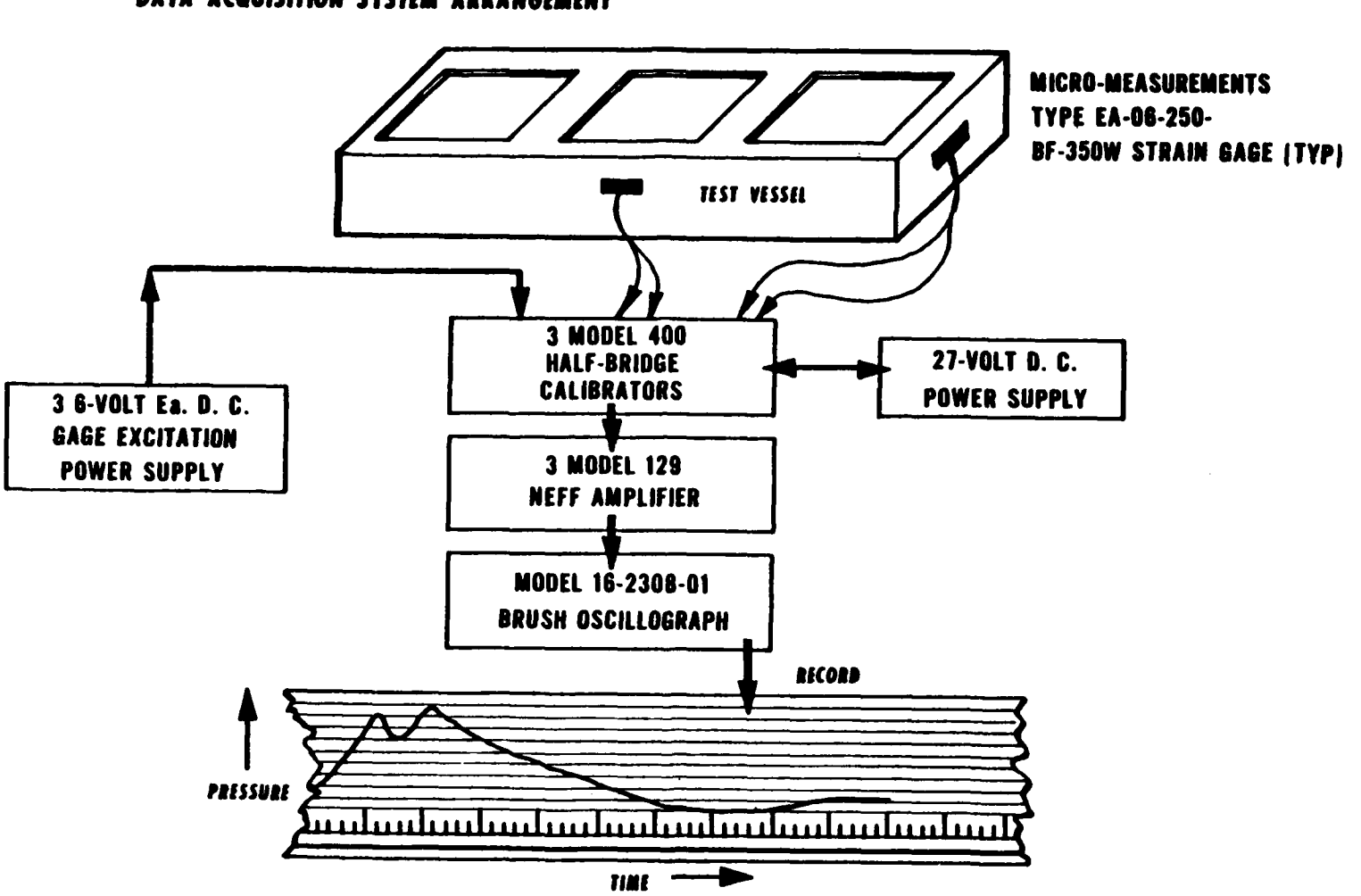

Figure 4. Typical Data Acquisition System

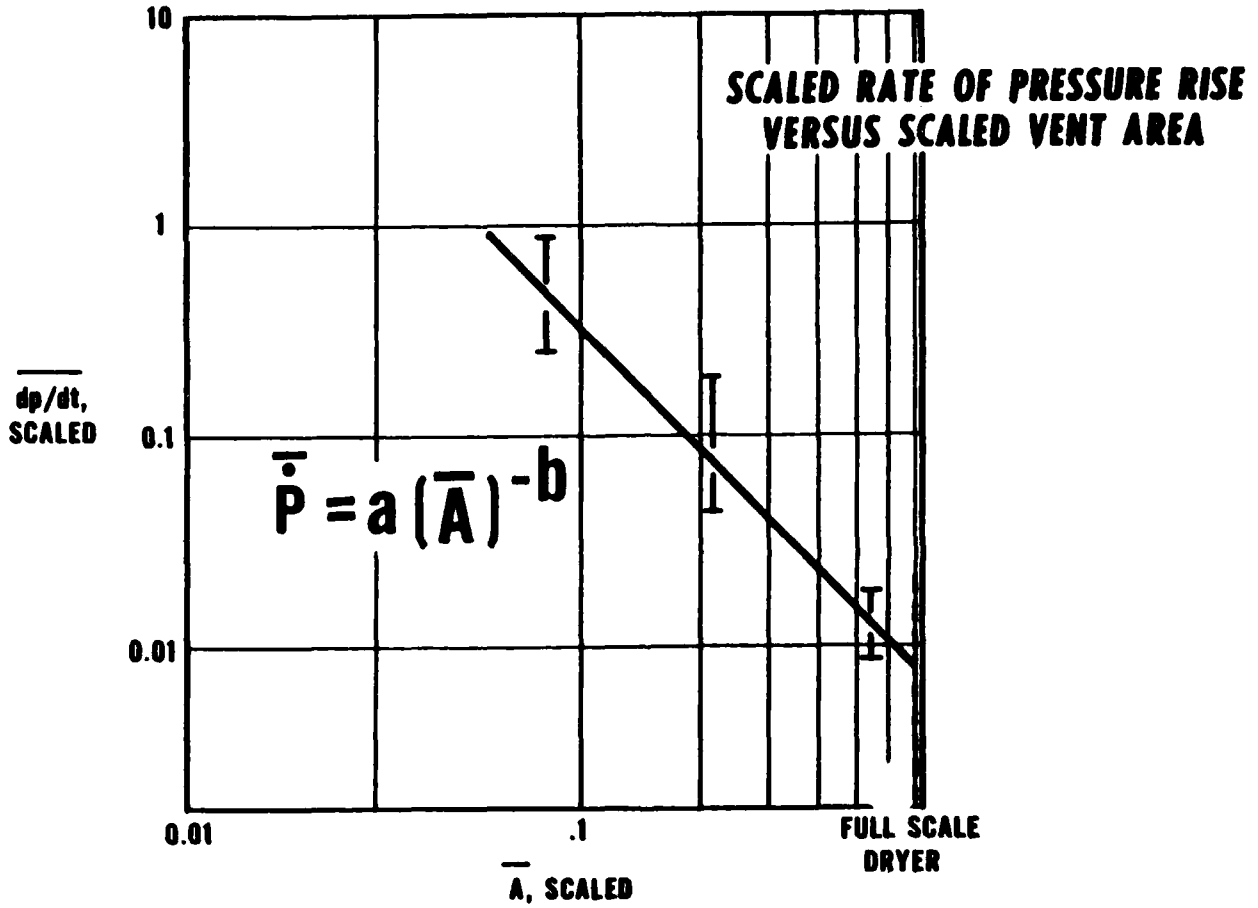

Figure 5. Scaled Rate of Pressure Rise Versus Scaled Vent Area

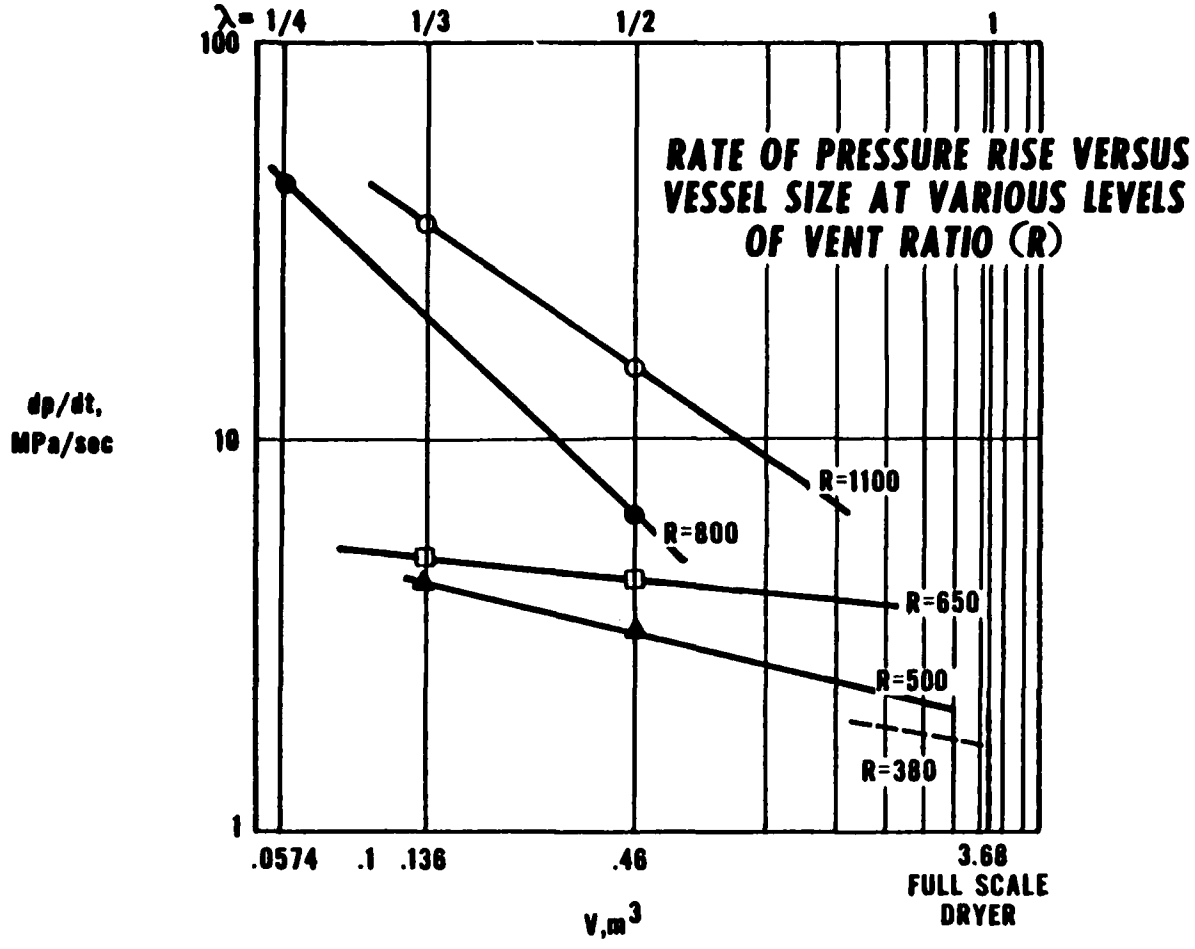

Figure 6. Rate of Pressure Rise Versus Scale at Constant Vent Ratio

THE CHEMICAL REACTIVITY TEST - A COMPATIBILITY SCREENING TEST FOR EXPLOSIVES

L. C. MYERS
Quality Division, Mason & Hanger - Silas Mason Co., Inc., Pantex Plant,
Amarillo, Texas 79177

ABSTRACT

The chemical reactivity test is used to evaluate the compatibility of explosives with other materials. This test has been in use at Pantex for more than 15 years, and during this time several improvements have been made in the test apparatus.

The basic test apparatus consists of a gas chromatograph with subambient temperature programming. A special inlet and a calibration system were designed and added to the chromatograph. Samples are conditioned in specially designed sample holders.

A description of the test apparatus is given and data from a variety of different types of materials with explosives are discussed. Examples of various types of information which can be obtained from the test are also discussed.

DISCUSSION

The chemical reactivity test[+] is an explosive compatibility test used to evaluate the stability of an explosive when in contact with another material. This test uses gas chromatography to identify, as well as measure, the amounts of decomposition gases evolved from heated samples.

To evaluate the compatibility of a material with an explosive, samples of the explosive, the material, and a 50/50 mixture of the explosive and material are tested. Each sample is conditioned in a stainless steel container with a 103 to 138 kPa (15 to 20 psi) helium atmosphere at a constant temperature for a predetermined time (normally 120 C for 22 hours). At the end of the conditioning period, the gaseous products are analyzed by gas chromatography. Normally the gases measured are nitrogen, oxygen, carbon monoxide, nitric oxide, carbon dioxide, and nitrous oxide.

At Pantex this test has replaced the vacuum stability test. The vacuum stability test is similar, but it only compares the total volume of gases

[+]A New Explosive Compatibility Test, UCRL No. 6244, 1960.

from the explosive, the material, and a 50/50 mixture of the explosive and material. The test cannot distinguish such things as solvent and water vapors from decomposition products. Therefore, the chemical reactivity test gives a much more detailed analysis of complex decomposition reactions than the vacuum stability test.

The first CRT system used a 0.9 metre polypropylene glycol column to separate the more volatile reaction products from the water and solvents. Column number two was a 1.7 metre silica gel used to determine the nitrous oxide and carbon dioxide. A 0.9 metre Linda 5-A (molecular sieve) was used for a third column to determine the oxygen, nitrogen, nitric oxide, and carbon monoxide.

To simplify the operation of the three-column gas chromatography system the third column (Linda 5-A) was omitted and the 1.7 metre silica gel column was replaced with a 4 to 5 metre silica gel column. This two-column system would not resolve nitrogen from oxygen or carbon monoxide from nitric oxide, but it was successful with explosives systems containing HMX, RDX, TNT, and PETN.

To further simplify the operation and to increase the information from this test, a Porapak Q[+] column was used with subambient temperature programming. Using only a single Porapak Q column, it is possible to separate N_2, O_2, CO, NO, CO_2, N_2O, water, and a number of solvents. By using a standard two-column gas chromatograph, it is possible to simplify its operation and to obtain much more information about the chemical reactivity of the samples.

The chemical reactivity apparatus currently being used by the Development Division at Pantex is a Varian Model 1820-3 dual-column gas chromatograph equipped with a thermal conductivity detector and an automatic linear temperature programmer with the subambient temperature option.

It was necessary to add a special sample inlet system to the Varian gas chromatograph for the chemical reactivity sample holders. The sample inlet system was made from a Varian gas sampling valve. Fig. 1 is an illustration of the sample inlet system. This system is enclosed in a small oven and the line into the gas chromatograph is heated to keep less volatile products from condensing.

To simplify the calibration of the gas chromatograph, a manifold and another Varian gas sampling valve were added to the instrument as shown in Fig. 2. The volume of this valve was determined prior to calibration.

To calibrate the Varian gas sampling valve, a glass loop illustrated in Fig. 3 attaches to the chemical reactivity sample injection system. The volume of the glass loop was determined from the weight of the mercury required to fill the loop. Once the volume of the glass loop was known, it was filled with a gas

---

[+]Trademark of Waters Associates, Inc.

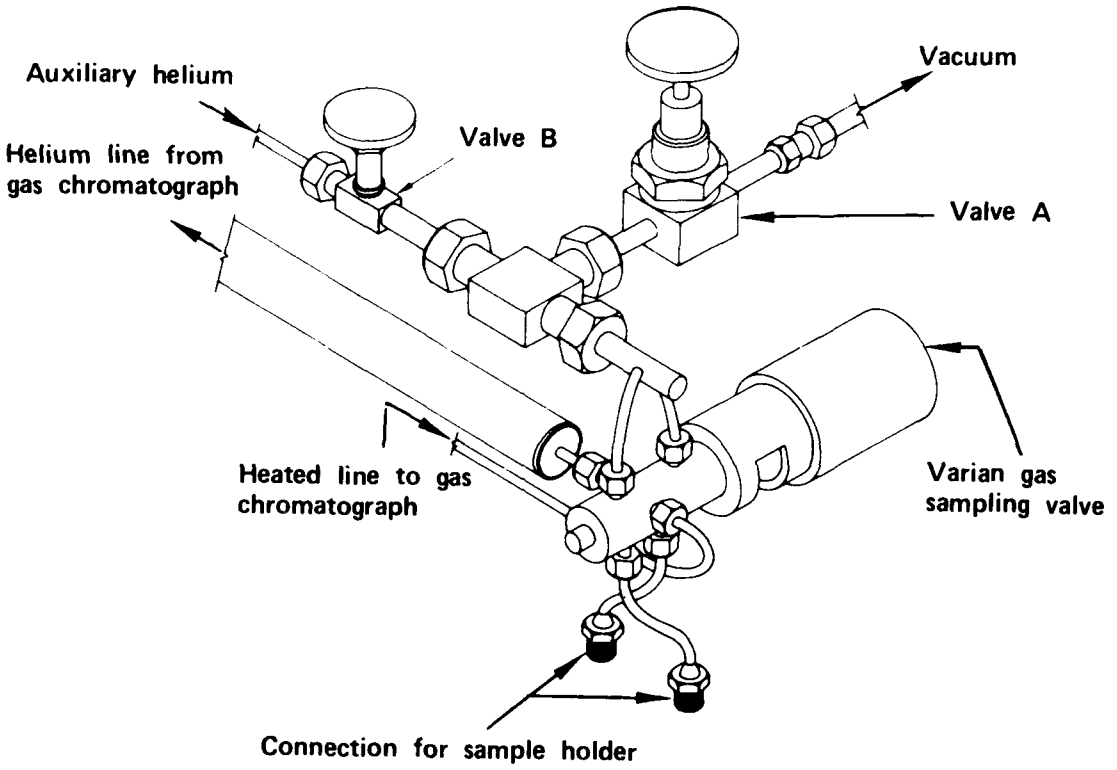

Fig. 1. Sample Injection Assembly

A - Helium Supply
B - Flow Controllers
C - Varian Gas Sampling Valve
D - Sample Injection System
E - Liquid Injection Ports
F - Columns
G - Thermal Conductivity Dectors
H - MKS Baratron Transducer

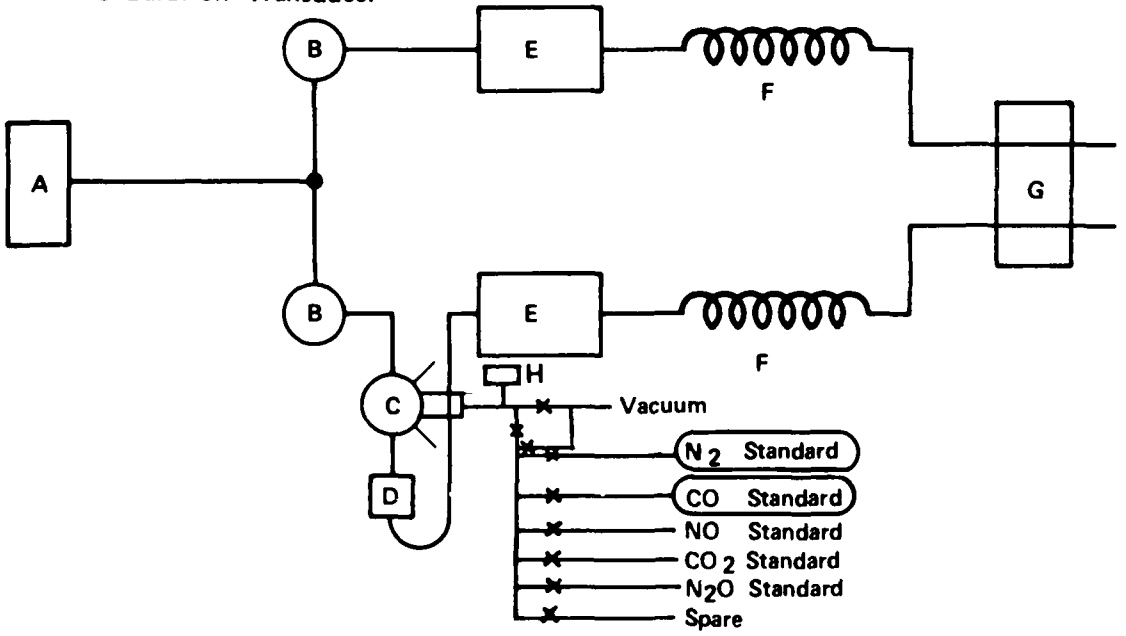

Fig. 2. Helium Flow Diagram for the Gas Chromatograph

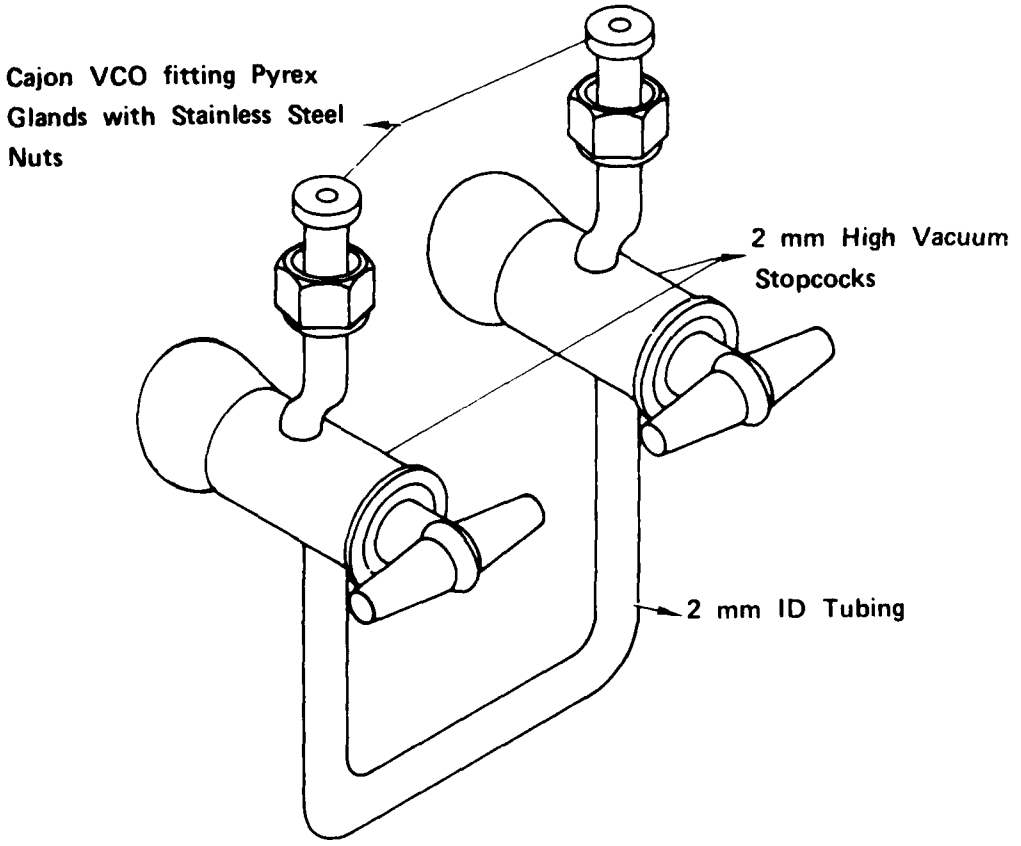

Fig. 3. Glass Calibration Loop

at a known pressure and temperature and injected into the gas chromatograph and a calibration constant calculated. The Varian valve was then used to introduce a sample of known pressure and temperature. By using the calibration constant determined with the glass loop, the volume of the Varian gas sampling valve was calculated.

The chemical reactivity sample containers were designed (Fig. 4) to obtain the best sample injection. These holders were made from stainless steel with all butt welds to eliminate any internal volumes which would slowly bleed the sample into the chromatograph. Stainless steel spacers are used in the sample containers to reduce internal volume.

Fig. 5 is a photograph of the chemical reactivity test apparatus used by the Pantex Plant Development Division Laboratories.

The following sequence is used to inject a sample into the chromatograph:

1. The sample holder is attached to the injection assembly (Fig. 1) which is in the sample position.
2. Then valve A is opened and the lines between the injection assembly and the sample container valves are evacuated to the desired pressure with valve B closed.

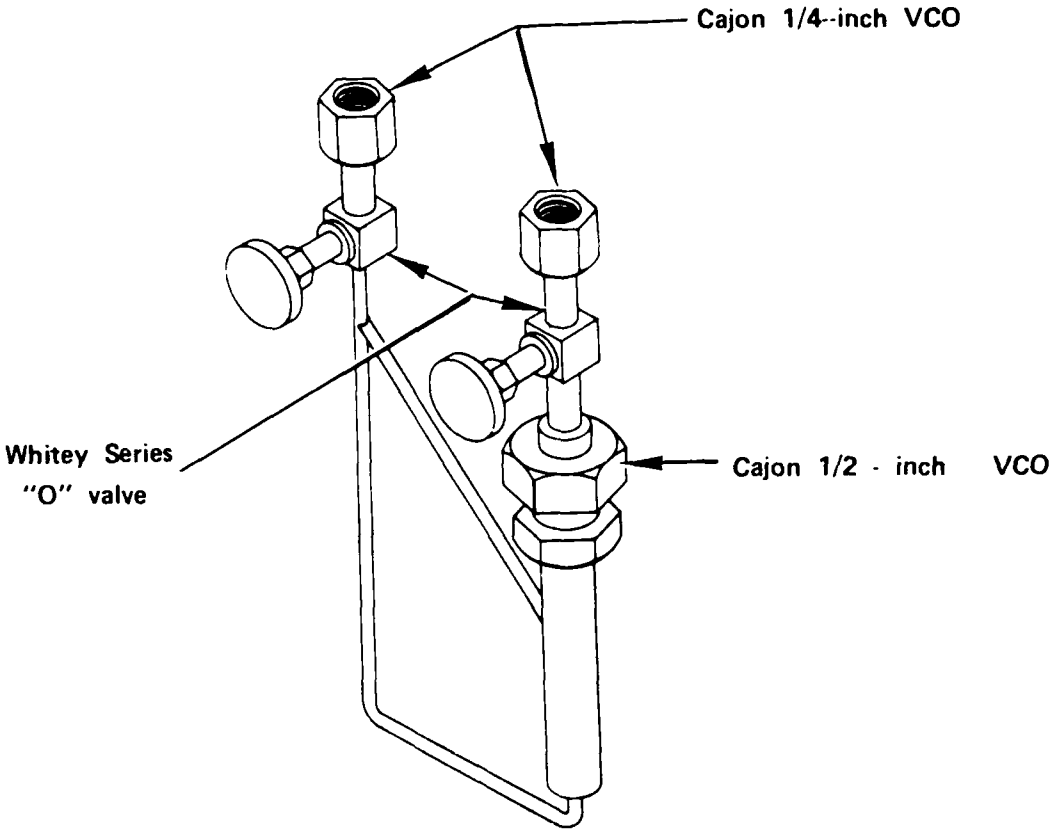

Fig. 4. Chemical Reactivity Test Sample Holders

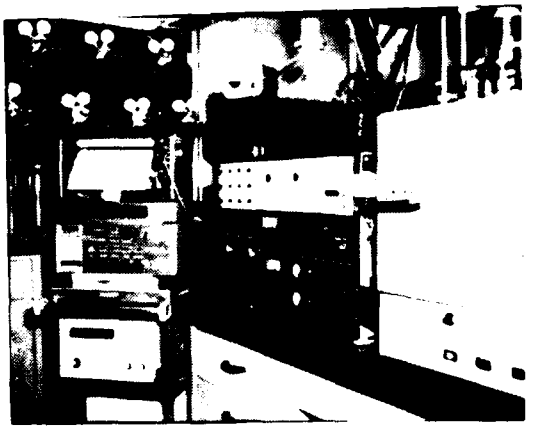

Fig. 5. Chemical Reactivity Test Apparatus

3. Valve A is closed and then valve B is opened and the evacuated volume is pressurized with helium to equal the pressure in the chromatograph. This eliminates a baseline shift due to any change in pressure in the instrument. Valve B is closed.

4. The gas sampling valve is then switched to the "inject" position and the sample container valves are opened.

The operation conditions for the chromatograph are:

Helium flow rate	30 cc/min
Column Porapak Q	4.5 m
Initial Temperature	-100 C
Final Temperature	200 C
Heat Rate	10 C/min
Holding Time at Maximum Temperature	30 min

The examples that follow illustrate typical data obtained with the chemical reactivity test apparatus, as well as data from a special investigation which show some of the additional information which can be obtained from the instrument.

The CRT chromatogram of LX-13 (Fig. 6) is given to illustrate the separation of the decomposition products. Since nitrogen and oxygen are separated, the oxygen can be used to determine if the sample holder leaked. Peak No. 8 is MF Freon which was used in processing LX-13. Peak No. 9 is acetone which is trapped in the PETN crystals during recrystallization.

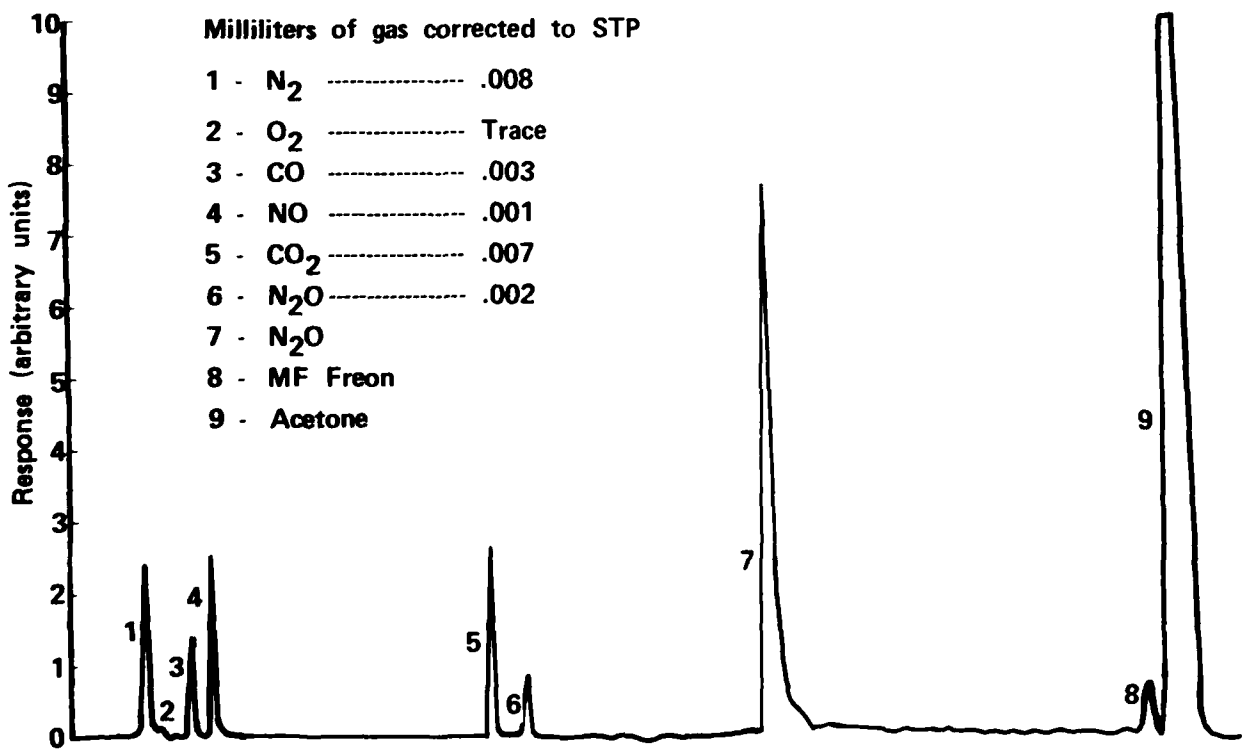

Fig. 6. Chemical Reactivity Chromatogram of LX-13

The chromatogram (Fig. 7) of the double based propellant AHH illustrates how this system can separate other compounds.

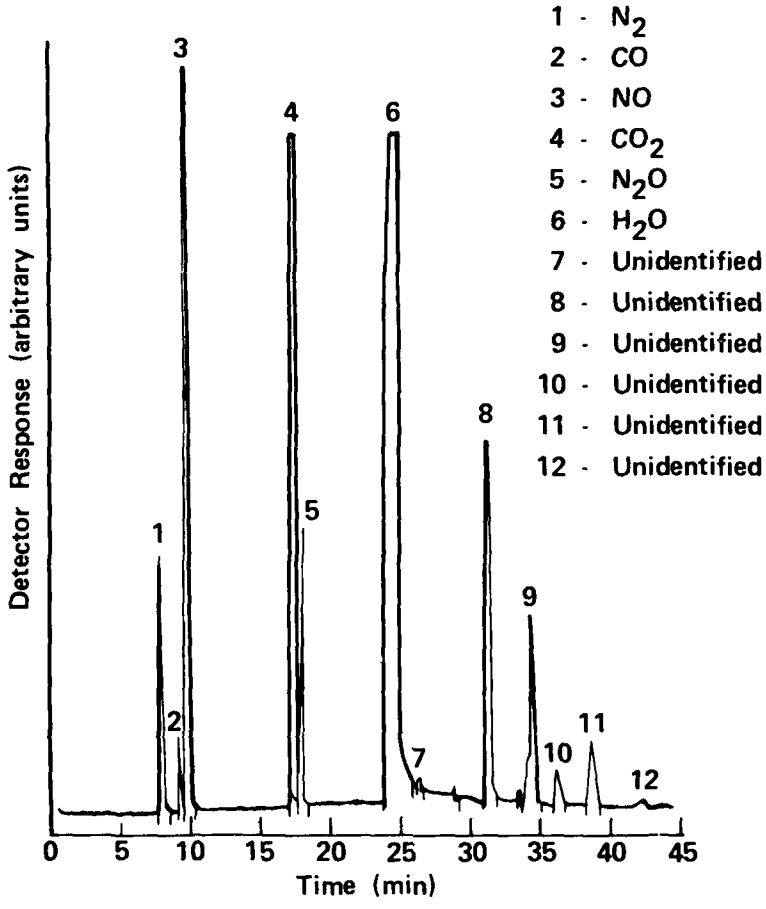

Fig. 7. Chemical Reactivity Test Chromatogram for a Typical Run on the Propellant AHH (Sample Conditioned at 100 C for 22 Hours)

The degree of reactivity of an explosive with another material is determined by the ratio of the volume of gas evolved by the mixture to the sum of the volumes of gas evolved by each component. The greater this ratio, the greater the reactivity. The acceptable degree of reactivity will depend on the application. If the materials are to be in contact for long periods of time then the ratio must be smaller, but larger ratios can be accepted if the contact time is shorter. If the ratio is very large then it may be unsafe for the material to be in contact with the explosive for short periods of time.

Table 1 gives data obtained for LX-13 and two mold releases. These data show the Price Discroll to be reactive and the zinc stearate to be nonreactive. From these data, it was recommended that the zinc stearate be used rather than the Price Discroll.

TABLE 1

Chemical Reactivity Test Results for LX-13 with Two Mold Releases (mℓ of Gas Corrected to STP)

	N_2	CO	NO	CO_2	N_2O	Total
LX-13	0.012	-	-	0.002	-	0.014
Price Discroll	0.015	-	-	0.003	-	0.018
LX-13 + Price Discroll	0.042	-	0.016	0.040	0.088	0.186
Zinc Stearate	0.009	-	-	0.006	-	0.015
LX-13 + Zinc Stearate	0.015	-	-	0.005	0.001	0.021

PBX 9404 was tested with Epon 828 cured with different curing components and data are given in Table 2. These data show that the component used to cure the Epon 828 affects the reactivity with PBX 9404 and that Ajicure C003 is less reactive than the other curing agents. However, in both cases there was an increase in nitrous oxide and nitrogen and a decrease in nitric oxide and carbon monoxide in the mixtures.

TABLE 2

CRT for PBX 9404 with Epoxies (mℓ of Gas Corrected to STP)

	N_2	CO	NO	CO_2	N_2O	Total
PBX 9404	0.025	0.043	0.197	0.122	0.021	0.408
	0.023	0.038	0.205	0.116	0.020	0.402
Epon 828/	0.010	-	-	0.025	-	0.034
Ajicure LX-1	0.005	-	-	0.025	-	0.027
PBX 9404 + Epon 828/	0.268	0.004	0.034	0.120	0.962	1.390
Ajicure LX-1	0.276	0.004	0.052	0.136	1.074	1.540
Epon 828/	0.011	-	-	0.014	-	0.025
Ajicure C003	0.012	-	-	0.010	-	0.022
PBX 9404 + Epon 828/	0.110	0.004	0.010	0.072	0.268	0.470
Ajicure C002	0.102	0.004	0.008	0.070	0.276	0.462
CPR 1009-7B	0.084	-	-	0.053	-	0.137
PBX 9404 + CPR	0.118	0.004	-	0.102	0.018	0.242
1009-7B	0.142	0.006	-	0.118	0.018	0.282

The data obtained with PBX 9404 and CPR 1009-7B gave some unexpected results. The total volume of gas for the mixture was less than the sum of the components and there was no nitric oxide in the mixture. This indicated that CPR-1009 acts as a stabilizer for the nitrocellulose in the PBX 9404. This was also supported by the blue color of the PBX 9404 after the test. Normally, the PBX 9404 turns a light brown due to the nitration of its stabilizer diphenylamine.

Table 3 gives CRT results of extremely reactive materials. RX-08 is an experimental explosive developed by LLL and alone it is thermally stable, but with Epon 828 it is very reactive.

TABLE 3

Chemical reactivity Test Data for RX-08 with Epon 828 (mℓ of Gas Corrected to STP)

	N_2	CO	NO	CO_2	N_2O	Total
RX-08	0.030	0.001	0.001	0.015	0.002	0.067
Epon 828	0.007	0.008	-	0.001	-	0.015
RX-08/Epon 828	1.016	0.398	0.525	2.263	1.814	6.015

The CRT apparatus has been used to investigate the thermal decomposition of PETN and the propellant AHH.

An investigation was planned to study the low temperature decomposition of PETN using the CRT system, but some preliminary runs on various lots of PETN gave completely different results. These differences were investigated and it was determined that the thermal decomposition rate of PETN is particle size-dependent as can be seen in Fig. 8.

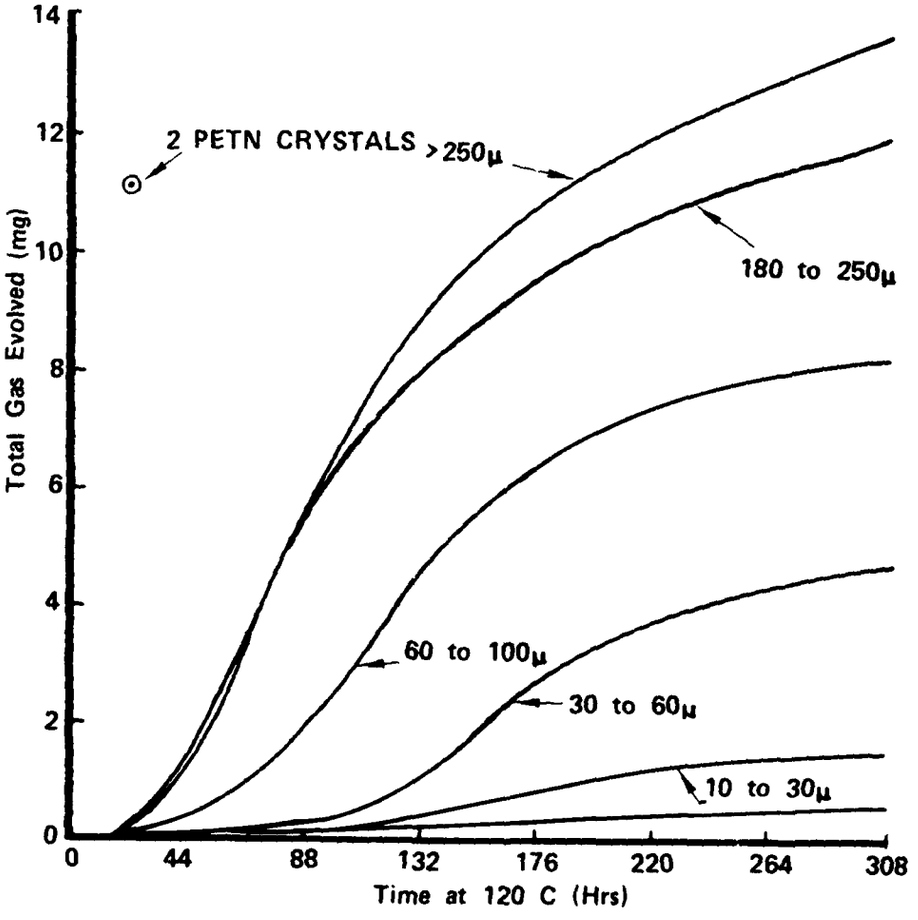

Fig. 8. Total Gas Evolved from PETN Samples of Different Particle Sizes

To identify some of the additional peaks, the CRT system was interfaced to a Bendix Model 14-107 time-to-flight mass spectrometer. From CRT/MS runs on different lots of PETN four different compounds were detected and identified. These are given in Table 4.

TABLE 4

Compound Identified in CRT From PETN

Cyanogen	Decomposition Product
Hydrogen Cyanide	Decomposition Product
Carboyl Sulfide	From a Sulfur Impurity Introduced During
Carbon Disulfide	Synthesis

The thermal decomposition rates were determined for the double base propellant AHH[+] using the CRT system. Fig. 9 is a plot of the gas evolved per gram of sample as a function of time at different temperatures. The log of the total volume of gas and the log of CO_2 evolved were plotted as a function of the reciprocal of the absolute temperature as shown in Fig. 10.

For CO_2 the 110 C to 60 C data are linear, but there is a change in the kinetics at 50 C.

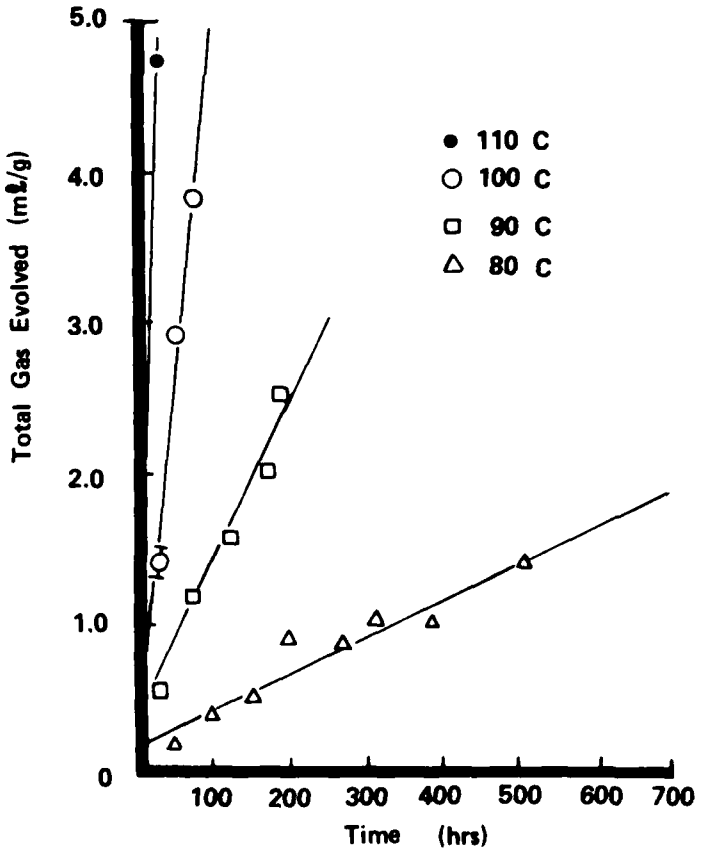

Fig. 9. Total Gas Evolved per gram of AHH Propellant as a Function of Time at Different Temperatures

[+]L. C. Myers, Thermal Decomposition of a Double-Based Propellant AHH - Part II, MHSMP-77-59, October 1977.

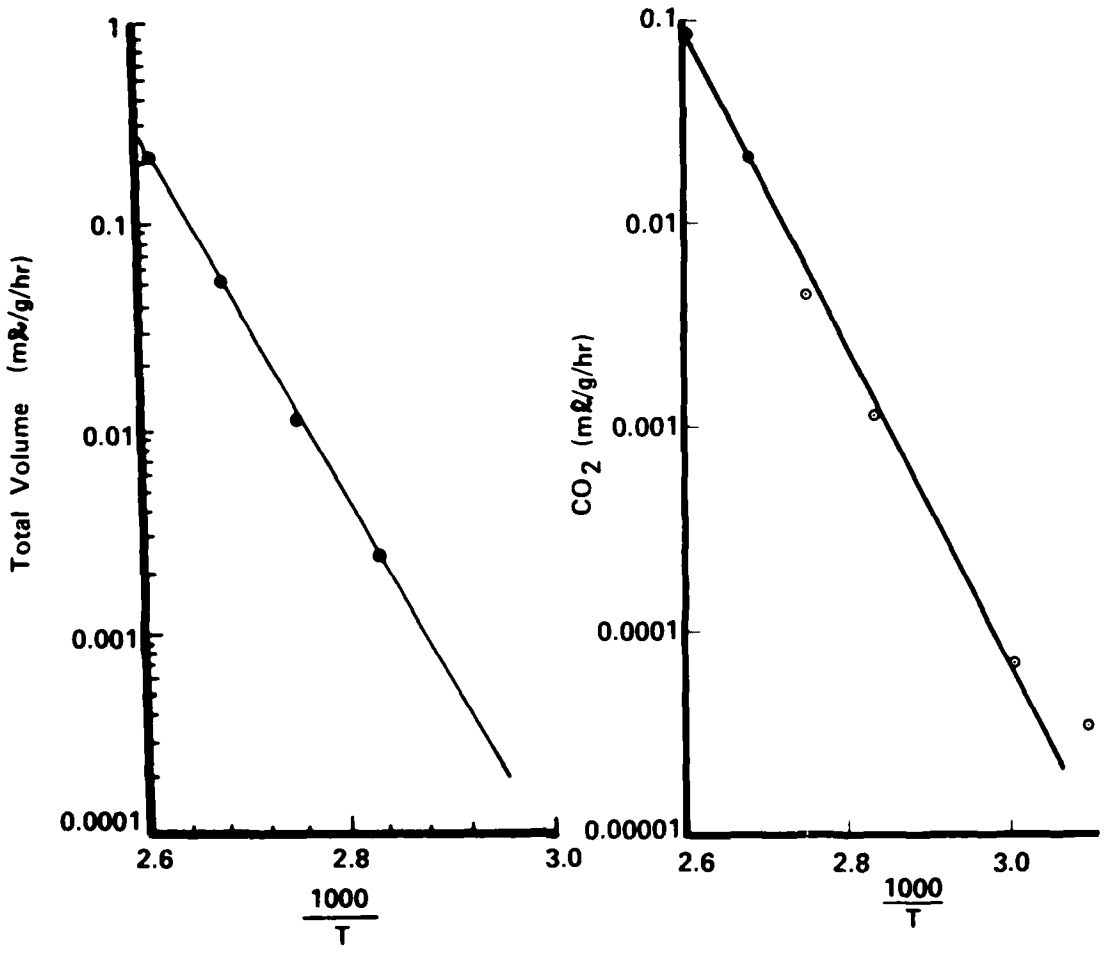

Fig. 10. Arrhenius Plots of Total Gas Volume and CO_2 Evolved from AHH Propellant

PROCESS ASPECTS OF RDX/HMX COMPOSITIONS

T. V. SACHAR
Office of the Project Manager for Munitions Production Base Modernization and Expansion, Dover, New Jersey

ABSTRACT

Historically, the manufacture of RDX and HMX specialty products has had several "bottlenecks" which have contributed to lengthy batch processing cycles, higher costs and non-uniform particle size distributions. The filtration and recrystallization steps are two unit operations where significant process improvements are underway.

A prototype reciprocating pan filter is being installed at Holston AAP which has been custom designed to safely process fine hot acidic HMX and RDX slurries. The rate of filtration will be increased several fold for HMX. In addition, a pilot plant which can continuously recrystallize all classes of RDX and HMX using DMSO solvent is also being installed at Holston AAP. Throughput is expected to be substantially increased for most RDX/HMX granulations, plus tighter control realized on particle size.

INTRODUCTION

This paper describes two of several constraints in the manufacture of RDX/HMX compositions and the process improvements underway to increase production capacity, reduce costs, minimize safety hazards, and obtain more consistent and uniform RDX/HMX granulations.

Current HMX/spent acid slurry is filtered in screen-bottom wash tanks equipped with filter cloths. The slurry is kept above 140°F to prevent any RDX impurity from coming out of solution. Vacuum is applied and spent acid is withdrawn through the filter cloth. HMX cake is washed to reduce the acidity to specified levels. The filter and wash cycle is extremely slow requiring from 8 to 24 hours to process an 850 lb batch HMX. Fine RDX (Aqueous) is filtered via nutsche filter probes.

A prototype continuous reciprocating pan filter is being installed at Holston AAP which in particular can filter fine HMX in a hot acid environment. This filter can be used for acid or water RDX slurries.

Crude RDX and HMX are recrystallized to obtain crystal purification, specific granulation, and crystal structure for HMX. Current cyclohexanone and acetone

solvents used are readily ignitible, are inefficient considering capacity and energy consumption, and present difficulties in achieving tight granulation requirements.

Dimethyl sulfoxide (DMSO) has been found to be a safer and significantly superior solvent for most RDX and HMX granulations based on laboratory investigations. A pilot plant will shortly be operated to determine DMSO's production potential in RDX/HMX manufacture.

BENEFITS (Continuous Filtration)

1. Individual Building Production Capacity Increased

A typical filter/wash building at Holston AAP can process 540 lbs/hr HMX using the screen bottom wash tanks. The prototype reciprocating pan filter is designed to filter 1000 lbs/hr HMX.

Typical dewatering cycle for nutsche filtration of class 5 RDX is 920 lbs/hr vs. 4000 lbs/hr on the continuous reciprocating pan filter.

2. Improved Safety

Continuous filtration by virtue of its faster throughput causes less accumulation of mass detonable explosives in a process building.

3. Lower Costs

At high rates of production (390,000 - 700,000 lbs/mo HMX) Holston AAP would only need to operate one filter/wash building in lieu of two buildings. Lower construction costs would obviously result at a new site for the same reason.

4. Versatility

Since the reciprocating pan filter does not possess a supportive elastomer belt which can readily be attacked by hot acetic acid present in HMX/spent acid slurries, it can be used to filter and wash crude HMX or RDX. One such filter is planned on the multi-product line at the new RDX/HMX complex. A comparison of the slurries to be processed is illustrated below:

TABLE 1

	RDX	HMX
Input Rate (lbs/hr)	52,000	18,700
Slurry Temp ^{O}F	104	147
Percent solids	16.7	5.3
Percent Acetic Acid	50.0	75.8
Percent Ammonium Nitrate	2.6	4.5
Percent Nitric Acid	2.1	1.2
Percent Water	26.5	10.3

Percent Others	2.1	2.9
Solid Size (Microns)	20-40	10-15
Output Rate (Wet Cake, lbs/hr)	9240	1490
Output Rate (Dry Basis, lbs/hr)	8400	745

Holston prior to selecting the reciprocating pan filter had conducted bench scale studies on numerous solid-liquid separating processes such as centrifugal separation, flocculation, settling basins, continuous decanters, membrane permeation and dense media separation. The prototype reciprocating pan filter is manufactured by Bird Machine Company which has acquired the license rights from Pannevis Holland. It was discovered at the 1975 Chem Show in New York City. Subsequent investigation revealed that Pannevis filters are used extensively in Europe and in fact for the filtration of RDX at Poudreries Reunis DeBelgique, (Balen, Belgium). Operational testing of the prototype filter is expected to be completed by November 1979.

BENEFITS (DMSO Recrystallization)

1. Individual Building Production Capacity Increased

Laboratory work at Holston AAP demonstrated the superiority of DMSO as a recrystallization solvent over the conventional cyclohexanone and acetone solvents.

TABLE 2 - Solubility Comparison

	RDX Solubility g/100 ml	HMX Solubility g/100 ml	Rel. Solubilities RDX	HMX
Cyclohexanone	20.0	8.7	1.0	2.74
Acetone	12.0	3.2	0.6	1.00
DMSO	60.0	56.5	3.0	17.80

TABLE 3 - Crystal Yield (90 Percent Conc.)

	Yield g/100 ml
Cyclohexanone	23.0
Acetone	10.3
DMSO	67.9

Consequently much higher throughputs of products at the recrystallization step is expected with DMSO (rates four to five times higher for certain RDX/HMX granulations now requiring cyclohexanone and fifteen times higher for HMX granulations now requiring acetone).

2. Improved Safety

Fire hazards are significantly reduced with DMSO as evidenced by the comparison below:

TABLE 4

	Flash Point, °F	Fire Hazard Group
Acetone	0	4
Cyclohexanone	111	2
DMSO	203	1

NOTE: Most Hazardous = 4

Toxicity studies conducted by Edgewood Arsenal in 1970 demonstrated that DMSO introduces no new health hazards. Infrared analyses revealed no α - HMX polymorph in any RDX samples and only a normal amount in HMX samples. Massive α - HMX presence increases the sensitivity of RDX/HMX compositions during processing.

3. Lower Costs

Based on significantly increased throughput DMSO offers substantially reduced labor and energy costs. Based on laboratory test data potential operational cost savings are depicted below:

TABLE 5

Composition	Class Explosive	Potential Per pound Savings
A-5	3 - RDX	4.61¢
C-4	5 - RDX	15.64¢
	coarse 1 - RDX	1.09¢
Cyclotol 70/30	4 - RDX	4.51¢
	7 - RDX	1.09¢
HMX	II/80S - HMX	40.54¢
Octol 75/25	1 - HMX	17.43¢
	4 - HMX	29.36¢
	5 - HMX	55.14¢

The DMSO recrystallization process will require significantly smaller equipment than the current process. It is estimated that the installed equipment costs to recrystallize coarse HMX using DMSO would be half of that for the current process.

4. Versatility

A 20 lb per hour pilot plant being installed at Holston AAP will be utilizing a controlled nucleation classified product removal (CNCPR) crystallizer with auxilliary screening and quenching apparatus for the production of a wide spectrum of RDX/HMX granulations. The DMSO solvent which is miscible in water will be recovered via a multi-stage rectification column.

5. Performance

Based on laboratory batches made crystal clarity and shape were improved with DMSO for both RDX and HMX. Acceptable batches of composition B, Octol 70/30, and cyclotol were produced. Successful end item testing was concluded using DMSO-recrystallized octol fill in M72A2 rocket (LAW) rounds.

Additional product qualification and end item performance tests are planned on material to be produced in the pilot plant. Physical and chemical product testing is scheduled to be completed by September 79 with end item testing completion by August 80.

Acknowledgements

The writer wishes to extend his appreciation to the US Army Research and Development Command (ARRADCOM), Holston Defense Corporation and the Ralph M. Parsons Company for much of the material used in this presentation.

References:

1. Project status report, Project 5744249, "Separation of Fine Explosives From Acid or Water Slurries," HDC-PE-29, May 31, 1976, Holston Army Ammunition Plant.

2. Final Report, "MM&TE Projects," RDX/HMX Production Facility, August 27, 1976, The Ralph M. Parsons Company in association with Hercules Incorporated, A. T. Kearney, Inc.

3. Technical Report No. HDC-PE-15, "Recrystallization and Growth of HMX-RDX, A Study of Methods and Equipment, Phase I," May 1972, by D. M. Mahaffey.

4. Technical Report No. HDC-19-74, "Recrystallization and Growth of HMX-RDX; A Study of Methods and Equipment, Phase II," April 1974, by M. D. Rothrock.

5. Edgewood Arsenal Report, "The Toxicology of RDX and HMX solutions in Dimethylsulfoxide, Cyclohexanone and Acetone," Septemper 1970.

THE EFFECT OF STATE OF GELATINIZATION AND BIOLOGICAL ORIGIN OF NITROCELLULOSE ON PROPELLANT MECHANICAL PROPERTIES

J.M. Hammond, B.H. James and R.C. Warren
Department of Defence, Weapons Systems Research Laboratory, Defence Research Centre
Salisbury, South Australia

ABSTRACT

For a highly plasticised cast double base rocket propellant, the uniaxial failure properties were found to be governed primarily by the state of gelatinization and not the biological origin of the nitrocellulose. The state of gelatinization has its greatest effect on failure strain.

Below ambient temperature, well gelatinized propellants have considerably lower failure strains than their poorly gelatinized counterparts, while above ambient temperature the reverse situation applies.

The findings may have significance for improvements in other NC-based propellants.

INTRODUCTION

The mechanical properties of gun and rocket propellants are important because of the requirement for physical integrity during manufacture, storage and firing. Any imperfection, such as a crack or deformation, can lead to a catastrophic ballistic malfunction. A common belief is that propellants made from nitrocellulose (NC) derived from cotton linter cellulose have mechanical properties superior to those of propellants made from NC derived from wood pulp cellulose (refs. 1-2). Cotton NC propellants are believed to have higher values of stress and strain and consequently, are tougher and stronger than their wood NC counterparts.

In Australia, NC derived from wood pulp cellulose is used to make all NC based gun and rocket propellants. However, the range and sophistication of locally made propellants is steadily increasing and difficulties have been experienced in recent years in matching the mechanical properties of some propellants which had originated overseas and were made from cotton NC in the country of origin (ref. 3). NC is manufactured in Australia by mechanical nitration of wood cellulose supplied as rolls of alpha cellulose board. The traditional grade of wood board cellulose has been Rayonier P, and more recently Rayonier Q, imported from Northern America. Recently, however, a small shipment of nitration grade

Buckeye cotton linters in board form (INR75) was imported from the US for evaluation in Australian gun and rocket propellants.

As part of a development programme for a cast double base (CDB) rocket propellant, for which particular difficulty had been experienced in obtaining adequate mechanical properties, a few uniaxial mechanical properties tests were conducted on a series of identical formulation wood NC based propellants which had been processed with solvents of different strengths to produce dissimilar states of NC gelatinization. The results did not indicate a strong influence of gelatinization state on modulus or tensile strength but a consistent pattern was apparent in failure strain. Poorly gelatinized propellants had greater failure strains than their better gelatinized counterparts below ambient temperature but smaller failure strains above ambient temperature.

There appeared therefore, to be two factors concerning NC which could affect propellant mechanical properties, the state of gelatinization and the biological origin. This paper summarizes a preliminary investigation into the effects of the relative importance of these two factors on the mechanical properties of a highly plasticised CDB rocket propellant. Four propellants of identical formulation were manufactured, two from wood NC and two from cotton NC. One wood NC and one cotton NC propellant were processed to approximately the same poor state of gelatinization and the other pair to approximately the same good state of gelatinization. The propellants were tested in uniaxial tension over a series of temperatures and in addition, the form of the failure surface was noted.

EXPERIMENTAL

The nominal compositions of the four casting powders and propellants are given in Table 1.

TABLE 1

Nominal composition of casting powders and propellants

	Powder (%)	Propellant (%)
Nitrocellulose (12.6%N)	60.0	42.0
Nitroglycerine	33.3	46.1
Triacetin	-	6.9
Ballistic modifiers	4.8	3.4
Stabiliser	1.9	1.6

A common mixing procedure was used to manufacture 800 g batches of the four powders. The state of NC gelatinization was controlled by adjusting the ethanol/acetone solvent ratio. For the poorly gelatinized wood NC powder the ratio used was 3:1, for the poorly gelatinized cotton NC powder 3.5:1, for the well gelatinized wood NC powder 0.5:1 and for the well gelatinized cotton NC powder 0.8:1. The total solvent proportion was 45 percent of the NC content of the batch.

Each powder was pressure cast in 50 mm corsetry and the resultant propellants cured for 3 days at 60°C. The propellants were designated PGW (poorly gelatinized wood NC), PGC (poorly gelatinized cotton NC), WGW (well gelatinized wood NC) and WGC (well gelatinized cotton NC). Light uniaxial test pieces were machined from each casting and tested on an Instron tensile testing machine at a strain rate of 0.11 min^{-1} at temperatures of -40, -20, 0 and 40°C. The state of gelatinization was checked by optical microscopy. Thin slices (15μ) of propellant were cut on a microtome and mounted in oil between glass slides. Photographs of 20 x magnification were taken using polarized white light, with the polarizer set at 0° and the analyser at 10°.

RESULTS AND DISCUSSION

Micrographs of sections of the four propellants are reproduced in Figure 1.

(a) Cotton NC
(Poorly gelatinized)

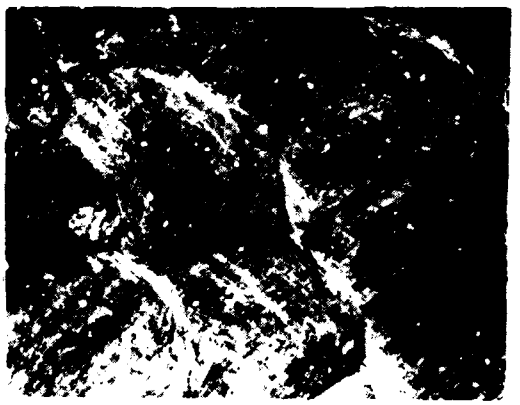

(b) Cotton NC
(Well gelatinized)

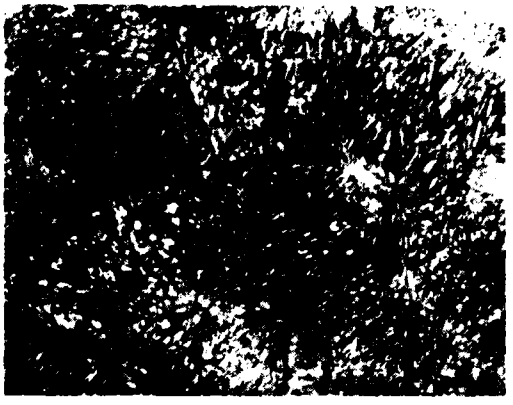

(c) Wood NC
(Poorly gelatinized)

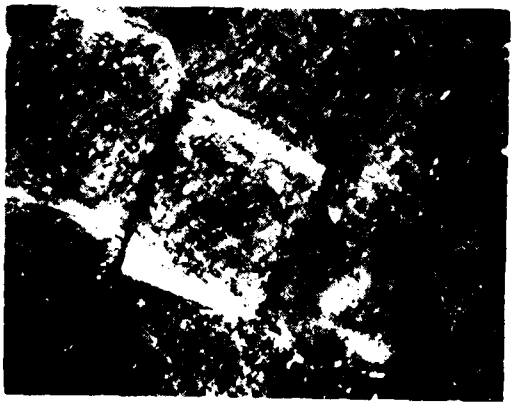

(d) Wood NC
(Well gelatinized)

Fig. 1. Micrographs of propellants

For propellants WGW and WGC only a few ungelled NC (white) particles can be seen which indicates that these propellants are well gelatinized. The two micrographs are almost identical and consequently the state of gelatinization of the two propellants is considered to be approximately the same. For propellants PGW and PGC there are large amounts of ungelled NC apparent which indicates that the propellants are poorly gelatinized. The similarity between the micrographs again suggests that the state of gelatinization of the two propellants is approximately the same.

The uniaxial mechanical property data is summarized in Table 2 and the failure strain data is also shown in graphical form in Figure 2.

TABLE 2

Uniaxial mechanical data

	Temperature (°C)	Propellant			
		WGW	PGW	WGC	PGC
Modulus (MPa)	-40	511.0	485.0	643.0	443.0
	-20	200.0	150.0	205.0	152.0
	0	52.0	40.5	70.0	42.6
	40	3.4	4.0	4.1	4.7
Maximum stress (MPa)	-40	11.5	13.5	12.2	19.5
	-20	8.5	10.3	10.2	11.0
	0	3.9	4.2	5.4	5.5
	40	0.8	0.5	0.9	0.5
Strain at maximum stress (%)	-40	4.2	3.4	3.0	5.6
	-20	11.1	28.5	15.9	31.4
	0	30.6	52.0	34.1	54.5
	40	65.6	35.4	72.5	39.7

The data indicates that NC gelatinization state is more important than biological origin in determining mechanical properties. However, neither factor has much effect on propellant strength or modulus over most of the temperature range. The strengths of the processing solvents used in this study were such as to produce propellants at the extreme gelatinization states found in normal production propellants. There appears therefore to be little scope for significant improvements in propellant strength or modulus to be gained from varying the cellulose precursor or nitrocellulose gelatinization state. Failure strain, on the other hand, shows a marked dependence on gelatinization state (see Fig. 2). Below ambient temperature the poorly gelatinized propellants have a marked superiority with the situation reversing itself above ambient temperature. It is interesting to note that all four propellants have similar failure strains at ambient temperature so that the use of ambient temperature testing for mechanical property quality control purposes may be unfortunate. The failure strains of all four propellants are very similar at -40°C, which is close to the glass transition temperature for these propellants.

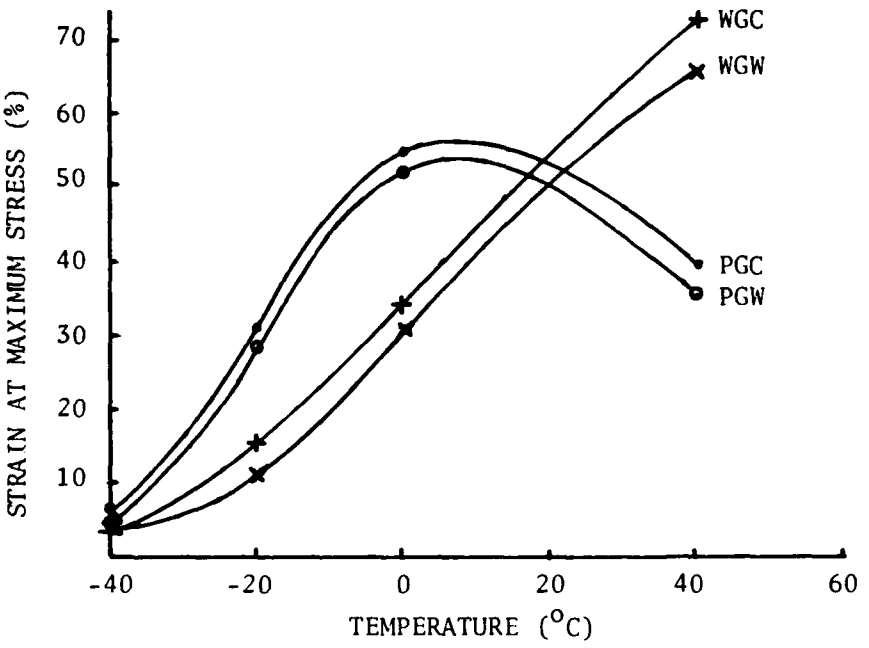

Fig. 2. Failure strain vs temperature

The observed fracture surfaces of the propellants are summarized in Table 3. Typical photographs of the surfaces at 3 X magnification are reproduced in Figure 3.

TABLE 3

Fracture surfaces*

Temperature (°C)	Propellant			
	WGW	WGC	PGW	PGC
-40	B	B	B	B
-20	B	B	$\frac{1}{2}$B/$\frac{1}{2}$AG	$\frac{1}{2}$B/$\frac{1}{2}$AG
0	AG	AG	$\frac{1}{4}$AG/$\frac{3}{4}$TG	$\frac{1}{4}$AG/$\frac{3}{4}$TG
40	$\frac{1}{2}$AG/$\frac{1}{2}$TG	$\frac{1}{2}$AG/$\frac{1}{2}$TG	TG	TG

* B-Brittle Failure; AG-Around Grains Failure; TG-Ductile Through Grain Failure

The fracture surface also depends upon the state of gelatinization of the NC rather than its biological origin. At low temperatures brittle failure propagating through the grains occurs, while at higher temperatures the failure surface propagates around the grains leaving whole grains exposed. The latter failure surface was only observed to be fully developed in the well gelatinized propellants. At higher temperatures still, failure is ductile with the failure surface again propagating through the grains. The temperatures at which the transitions from one failure mode to another occur is a function only of gelatinization state.

This preliminary study of NC gelatinization state and biological origin on propellant mechanical properties answers one or two questions but raises several others. For example, gelatinization state appears more important than biological

origin in governing uniaxial failure properties. Does this still hold true for failure under multiaxial stress states? Then again, only one composition has been tested, a highly plasticised CDB propellant. Are the findings for this propellant general? Finally, what significance, if any, have the results for gun propellants? Further work to find answers to these questions should be undertaken. If this additional work were to disprove the traditional view that cotton NC is inherently superior to wood NC, a wider use of wood NC in multibase propellants would afford considerable cost benefits.

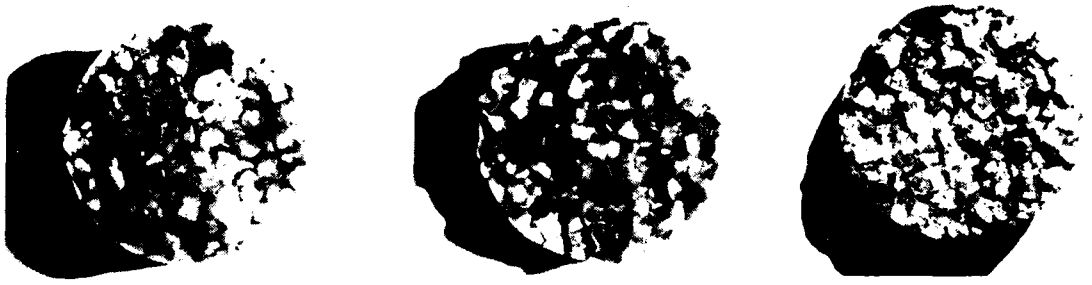

$-40^{o}C$ $0^{o}C$ $40^{o}C$

Fig. 5. Fracture surfaces

CONCLUSIONS

For a highly plasticised CDB rocket propellant neither state of gelatinization nor biological origin of the NC appear to be important factors governing modulus or tensile strength. The state of gelatinization has however, a significant effect on uniaxial failure strain. Below ambient temperature poorly gelatinized propellants have significantly higher failure strains than their well gelatinized counterparts whereas above ambient temperature the situation is reversed.

The form of the failure surface at a given temperature is also governed by the state of gelatinization. At low temperatures brittle failure occurs, while at high temperatures failure is ductile. In both cases the failure surface propagates through the propellant grains. At intermediate temperatures the failure surface propagates around the grains leaving whole grains on the surface exposed.

REFERENCES

1 B. Eraude, the Chemistry of Propellants, Pergamon Press, New York, 1960, p.505.
2 V.I. Camp, DS Survey on Nitrocellulose for Military Propellants, RAS Summary Report for The Technical Cooperation Programme, Panel W-1 (Propulsion Technology), June 1977.
3 J.E. Stutchbury, The Influence of the Source of Cellulose on Properties of Nitrocellulose Propellants, Paper Presented to Second Meeting of The Technical Cooperation Programme, Panel W-1 (Propulsion Technology), London, UK, November 1974.

THE LEACHING OF CANNON PROPELLANTS: ANALYSIS OF DEVELOPMENTAL DATA AND ESTIMATION OF PRODUCTION CAPACITY

by

Joel M. Goldman and Koon-Wing Ng
US Army Armament Research and Development Command

ABSTRACT

A review of process development efforts in conjuction with the selection of methylene chloride as the replacement for benzene-ethyl acetate in the nitrocellulose recovery phase of ball propellant manufacture was conducted. A discrepancy between the solid-liquid equilibrium curves, based upon the laboratory and pilot plant studies, was found which made the prediction of a reliable production capacity difficult. An analysis of the available data showed that the failure to properly account for the methylene chloride in the propellant used in the laboratory experiments caused the discrepancy in the two data sets. Using the pilot plant data, production rates are estimated on the basis of making no changes in the existing extraction equipment at Badger Army Ammunition Plant. An analysis of the agitation requirements with the new solvent showed that the optimum production process is a three-stage countercurrent leaching process followed by separate stripping of residual methylene chloride from the propellant of each extraction batch. It is, also, shown that production capacity will be approximately the same when methylene chloride is substituted for benzene-ethyl acetate in the extraction operation.

A DIGITAL ELECTRONIC THERMAL INTEGRATOR FOR MONITORING CHARGE AGEING

D. Kilpin and M.J. Mildren*
Department of Defence, Weapons Systems Research Laboratory, Defence Research Centre
Salisbury, South Australia (* Advanced Engineering Laboratory, DRCS)

ABSTRACT

An instrument for monitoring rocket motor ageing is described. The unit measures temperatures in a magazine and produces an electrical output proportional to the rate of deterioration of the charge. This signal is integrated and the accumulated data stored in a memory which can be interrogated by an external readout unit to yield an "effective age" of the charge. The low cost long life instrument is accurate and versatile and offers substantial labour savings over present methods.

INTRODUCTION

During the storage of a rocket propellant charge for long periods of time chemical reactions and physical changes occur which result in the deterioration of the charge until ultimately safety or performance requirements are no longer met. Deterioration occurs more rapidly at higher than at lower temperatures so a temperature penalty system is often applied to a store which is subjected to a varying thermal environment. The penalty factor employed is derived from service life assessment studies and in effect expresses the activation energy of the most crucial degradation process. The factor is used in conjunction with a temperature history of the store to calculate equivalent life at 20°C which is compared with the nominated expiry life at 20°C to determine the status of the store. Since continuous records of actual propellant temperatures are rarely available for this purpose, approximate calculations are performed, usually based on daily maxima. A more accurate record would be obtained by using a small, self contained "thermal integrator". The thermal integrator should have a maintenance free lifetime comparable to that of the store, and a temperature accuracy of about 0.2°C to yield age accuracies of better than 2%.

DESIGN AND OPERATION OF THE UNIT

This thermal integrator would need to monitor the temperature continuously to assess the rate of deterioration to accumulate the rate-time integral and,

thereby, to indicate the accrued extent of deterioration. Such a device could utilize chemical reactions but electronic and/or optical instrumentation would be required to measure accurately the extent of reaction or "effective age". Purely electronic systems were investigated as a preferred alternative since they also offered flexibility in selecting and altering the activation energies of the deterioration processes. For design purposes it has been assumed that the rate controlling step in the deterioration is a first order process with an activation energy of 16 kilocalories per mole and the application is a store with a nominated expiry life of 5 years at 20°C. Other activation energies and/or reaction rates could be used, but higher order, concentration dependent reactions are not considered in this paper.

Essentially the unit consists of four sections which are the temperature sensor, function generator, age integrator, and a power-control and timing centre. Power is conserved by switching on the first two sections at each measurement for only the minimum time necessary for accurate readings. Battery drain, although continuous for the crystal oscillator, programmable timer and volatile accumulator, is only about 50 μA so that battery lifetimes of 5 years should be achieved with modest sized batteries. A block diagram of the system is shown in Figure 1, which also shows an external readout unit for displaying the accumulator contents and the battery voltages. A reading of the "effective age" stored in the accumulator of each thermal integrator unit can be taken with a single readout/display unit at convenient intervals, e.g. weekly or monthly. The total age of a store can be determined by using a thermal integrator attached to it, or more economically by totalling the thermal integrator "ages" relevant to the calendar periods spent in each magazine.

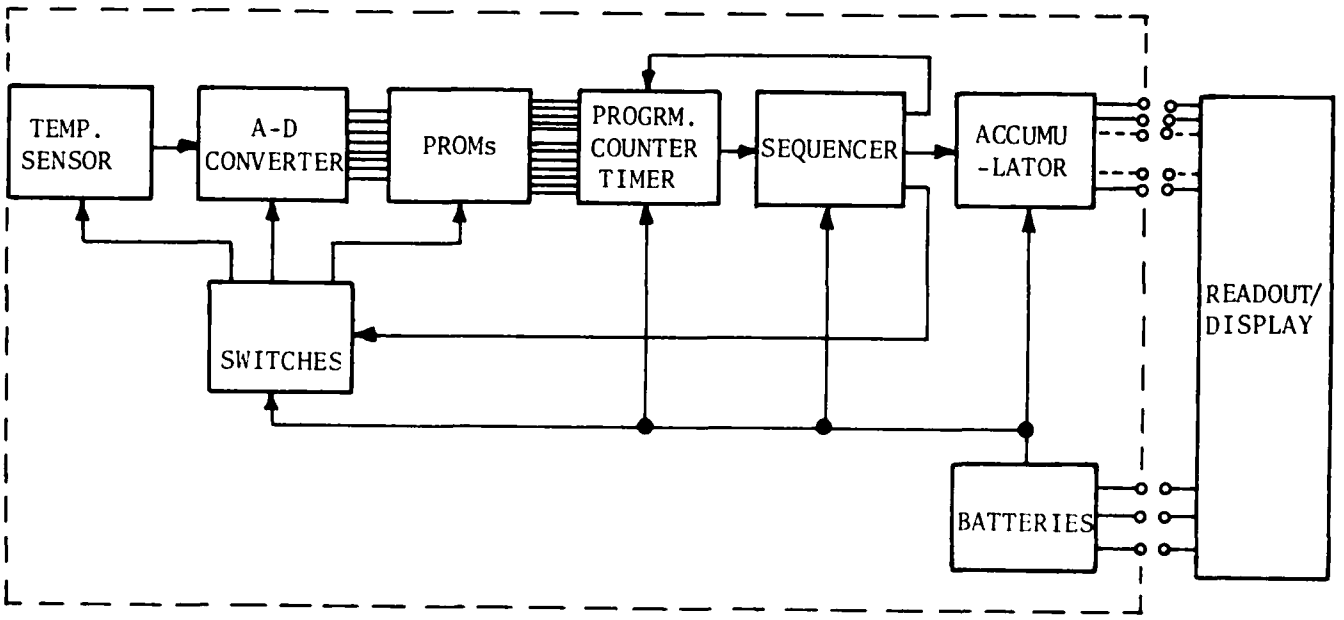

Fig. 1. Block diagram, thermal integrator

Isothermal temperature testing of a prototype unit is now being carried out. Temperature cycling and vibration tests will soon be undertaken and will then be followed by distribution of several prototypes for long life testing under magazine conditions.

Future development will concentrate on the "age" accumulator and improvement of component lifetimes, especially of batteries, although current drain reductions would also be desirable to decrease the number of batteries required and thereby the total bulk of the unit. The first prototype unit uses a volatile 16 stage accumulator from which all stored data is lost when power is unavailable. Subsequent models will probably incorporate non-volatile memories and perhaps only 10 or 8 binary bits of resolution.

SERVICE USE

As a unit for service use the thermal integrator will measure about 15 x 15 x 10 cm and weigh about 4 kg including batteries and case. The compact size and low thermal mass of the unit will permit it to be secured at an appropriate position in a magazine to measure temperatures typical of those experienced by the stores. The lightweight unit may be removed easily from the magazine to an electronic readout or printout device for the calendar time/effective age log of that magazine.

The cost of this instrument is expected to be about the same as the recording thermograph which it will replace. It offers savings in chart costs and maintenance and a considerable reduction in time expended on determining service life. With a thermograph, the chart must be removed (usually at weekly intervals) and the daily maximum and minimum temperatures transcribed from it to log books for later calculation of temperature penalties. Laborious manual processing of these records, and the errors arising therefrom, will be replaced by a direct accurate reading from a thermal integrator. All that is required with a thermal integrator is interrogation with a readout unit to display the accumulated life of stores accompanying the unit. Such interrogation would occur at regular intervals and whenever stores are transferred.

Although one activation energy for the deterioration process has been considered here, different stores may have appreciably different factors of temperature dependence. These factors are readily incorporated in an instrument by programming a different temperature function in the PROMs for stores of one kind. However, when stores of several types (of activation energies of ageing) are held in one magazine, only two thermal integrators of different activation energies will be required. "Effective ages" for other activation energies can be readily determined by interpolation or extrapolation from that pair of results.

CONCLUSION

The thermal integrator described here will provide a convenient method of

measuring the "effective age" of a store. It is readily suited to a wide variety of stores where the temperature dependences of the ageing processes are known. New knowledge of deterioration rates of the stores will require a change of the temperature-rate function stored in the memory. It may also be necessary to introduce a second variable, such as the concentration of a diffusing or deteriorating reactant which varies with time, temperature or extent of reaction. Such sophistication can be readily incorporated when the parameters controlling the ageing process are better understood. The present device, under typical temperature conditions of storage, should enable the "age" of a particular store to be determined to an accuracy of about 2% and thus provide the maximum utilization of expensive stores.

APPENDIX

DETAILS OF THE THERMAL INTEGRATOR

The electronic system uses components that were chosen to work from power rails as low as 5 V, so that sufficient voltage is provided by only four mercury cells (5.4 V). In the variable time system of integration used a constant number (a "1", equivalent to about 40 minutes ageing at $20^{o}C$) is added to a store at different time intervals determined by the measured temperature and stored temperature function.

The temperature sensor is the LX 5600 (National Semiconductor) integrated circuit with a current drain of approximately 1 mA. Its output is linear at 10 $mV/^{o}K$ but it contains an operational amplifier which can provide gain and offset for scaling purposes. While A-D converters usually require $\pm$ 12 V power rails, the AD 7570 is a CMOS integrated circuit capable of using + 5 V only, and requiring a comparator amplifier (LM 311) which uses $\pm$ 5 V, with the combination drawing about 5 mA current.

Output from the 8 bit A-D converter addresses the Programmable Read Only Memory (PROM) in which the temperature-rate function is stored. These 8 bits give 256 addresses, so 250 function values at $1/5^{o}C$ intervals are stored for the 0 to $50^{o}C$ range. PROM outputs are used to preset a counter which counts down to zero to produce the variable time interval which is derived from the ageing rate in the following way :

Time interval i.e. counter preset P = constant/k

where k = ageing rate = $6.4542 \times 10^{12} e^{-16000/1.987(T + 273)}$ T in ^{o}C

By setting the constant at 3995 gives $P = 6.1975 \times 10^{-10} e^{8052/(T + 273)}$

Then at $0^{o}C$ P = 3995 (Binary 1111, 1001, 1011)

and at $50^{o}C$ P = 42 (Binary 0000, 0010, 1010)

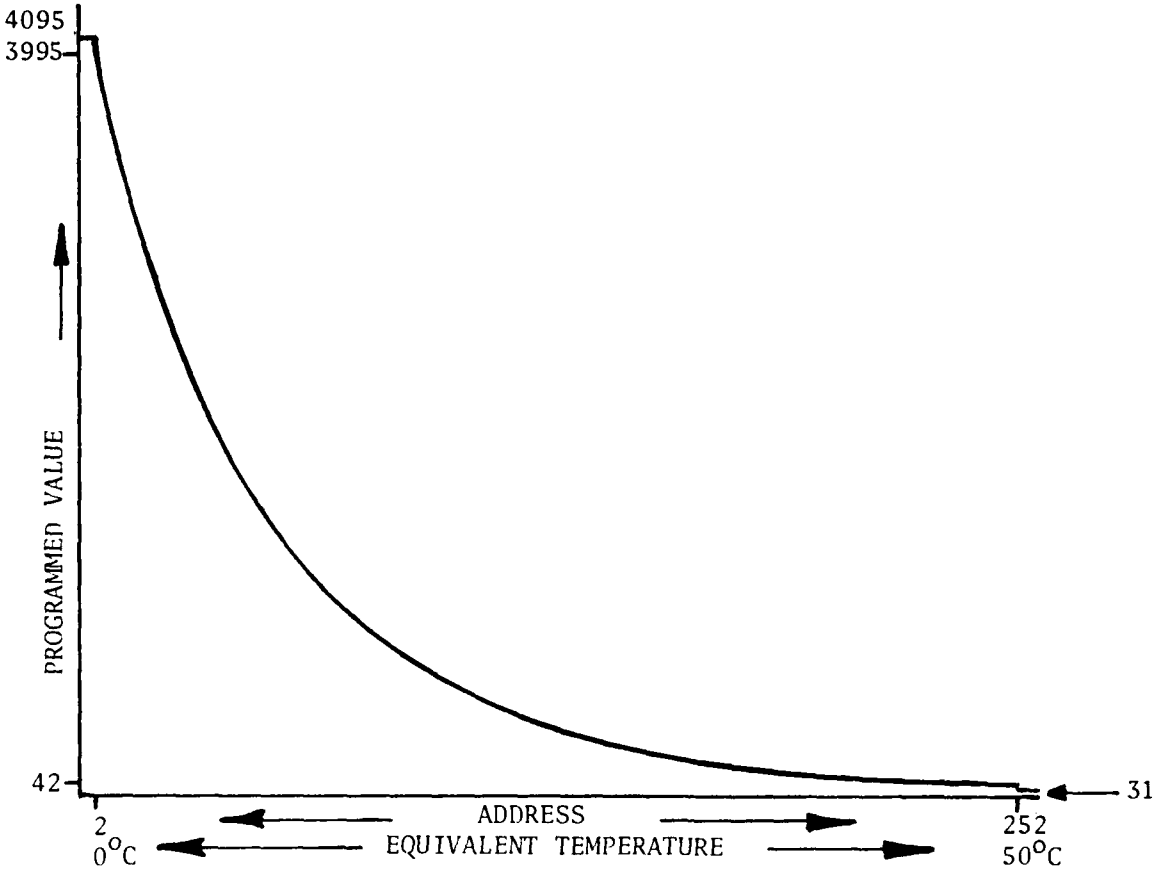

Fig. 2. Temperature function stored in PROMs

Values outside the working range are set arbitrarily as shown in Figure 2 at 4095 below $0^{o}C$ and at 31 above $50^{o}C$. Note that at $50^{o}C$ the programmed value is 42 while at $49.4^{o}C$ it is 44 showing the 12 bit output gives resolution of $0.3^{o}C$ at the high temperature end. PROMs used are Intel 3621 which are 256 x 4 bit (3 required) and can operate on 5 V drawing 150 mA each.

The programmable counter uses a crystal oscillator as the main clock with a divider producing 0.22 Hz, so that at $50^{o}C$ an interval of 3.18 minutes results (0.22 Hz ÷ 42) while at $0^{o}C$ the interval is 5 hours (0.22 Hz ÷ 3995).

The sequencer is a CMOS circuit which detects the zero count of the counter and produces pulses to (1) switch on the temperature sensor and A-D converter, (2) after the temperature sensor has settled, start the converter, (3) after conversion is complete, switch on PROMs, (4) load the counter and switch off PROMs, and (5) switch off temperature sensor and A-D converter, and then add 1 to accumulator. The accumulator is a simple 16 stage counter which at $50^{o}C$ would total 2^{16} intervals of 3.18 minutes (totalling 0.389 years) or at $0^{o}C$, 2^{16} intervals of 5 hours (totalling 37.4 years).

Battery drain is continuous for the programmable counter and the accumulator which draw approximately 50 μA. PROMs which draw most of the current, only do so during measurement (which can be less than one millisecond). The temperature

sensor has the longest settling time of the components after switch on, but even that is only 250 μsec. For normal conditions the total current drain is about 0.5 A for 0.5 msec every 20 minutes to give an average current of 0.25 μA which is negligible compared with the counter, accumulator and leakage currents. A generous safety margin of current capacity would therefore be provided by two parallel sets of RM42R batteries.

PREPARATION OF 2- [5-CYANOTETRAZOLATO]PENTAAMMINECOBALT (III) - PERCHLORATE, CP, A NEW MATERIAL FOR DETONATOR APPLICATIONS

WAYNE FLEMING and JOHN W. FRONABARGER
Unidynamics/Phoenix, Inc.
JIMMIE Q. SEARCY
Sandia Laboratories, Albuquerque

ABSTRACT

CP is a relatively new explosive developed for low-voltage hot-wire initiated detonators. This paper gives the preparation procedure for CP and outlines the tests that are used for quality assurance of the final product.

CP is a Co^{+3} coordination compound that is prepared by a four-step synthesis procedure. Briefly, these steps involve 1) the preparation of $[Co(NH_3)_5CO_3]NO_3$ by a well established procedure, 2) the conversion of $[Co(NH_3)_5CO_3]NO_3$ to $[Co(NH_3)_5H_2O](ClO_4)_3$ by reaction with perchloric acid, 3) the synthesis of 5-cyanotetrazole by the reaction of cyanogen with buffered hydrazoic acid, and 4) the reaction of $[Co(NH_3)_5H_2O](ClO_4)_3$ and cyanotetrazole in aqueous media. Crude CP product is purified and the particle size adjusted by two recrystallizations.

Quality assurance tests include several different chemical analyses, as well as the determination of particle size, surface area, and impact sensitivity. The product that meets acceptance criteria in these tests is being used in one DOE production component and is scheduled for use in at least one additional item.

INTRODUCTION

A long term study of high energy coordination compounds by various staff members at Sandia Laboratories and at Unidynamics/Phoenix, Inc. has culminated in the development of the explosive 2- [5-cyanotetrazolato]pentaamminecobalt (III) perchlorate (designated as CP). CP is an unusual explosive with characteristics of either a primary or secondary explosive depending on density and degree of confinement. The unconfined powder behaves like a secondary explosive in that it is relatively insensitive to impact and does not sustain combustion from open flame or spark. When pressed into detonators or suitably confined, the material can be initiated by hot wire, flame, or spark and builds rapidly to detonation. CP thus

offers a significant safety improvement over more conventional primary explosives. It can also be used for the output charge and thus offers simpler detonator designs. Table 1 summarizes some typical properties of CP.

TABLE 1

Typical properties of CP

Property	Value
Impact sensitivity of loose powder, 2 Kilogram, Bureau of Mines (10% level)	Depends on particle size and crystal form; lowest values, 40-50cm, highest values, >100cm.
Electrostatic sensitivity, ergs, total stored energy (600 pico-farads, 500 ohms series, variable voltage)	Increases in sensitivity with increased density and decreased particle size. Typical: $>10^7$ for loose powder 1.2×10^6 for $\rho = 1.3$ g/cm^3 10^5 for $\rho = 1.5$ g/cm^3
Thermal response characteristics - differential scanning calorimetry, 20°C/minute, open cup.	
Onset of Exotherm, °C	286
Peak of Exotherm, °C	315
Autoignition temperature (hot plate)	
No-fire, 5 minutes, °C	308
Instantaneous fire, 1 second, °C	340
Weight loss	0.013%/hour for 1st 200 hours at 171°C (340°F) (atmospheric conditions)
Crystal Density, g/cm^3	2.01
Physical form	Free-flowing yellow-orange crystals
Explosive yield at 1.0 gram/cm^3 (percent of TNT at 1.00 gram/cm^3) by Steel Witness Plate Method	100
Detonation Velocity, meters/second	5,900, $\rho \simeq 1.57$ g/cm^3 (78% crystal density), measured in 5.6 grains/ft aluminum mild detonating fuse

Several years ago it was decided to use CP in a Sandia Laboratory designed detonator, and the need arose for a procedure to produce production lots of uniform particle size and purity. After consideration of the amounts required for production of the planned detonator, possible future production items, development needs, and safety considerations, the decision was made to set up a pilot plant for the production of 1-2 kg batches of CP.

An outlying building at Unidynamics/Phoenix, Inc. was selected and modified for use in CP production. The same building also houses equipment for production of other experimental explosives and pyrotechnics as well as a laboratory area for preparation of small batches of experimental materials.

PREPARATION PROCEDURE FOR CP

Chemical synthesis

The chemical synthesis of CP is outlined by the following four reactions:

Carbonatopentaamminecobalt (III) nitrate (CPCN).

$$2Co(NO_3)_2 + 8NH_3(aq) + 2(NH_4)_2CO_3 + 1/2O_2 \xrightarrow{H_2O}$$

$$2\ [Co(NH_3)_5CO_3]NO_3 + 2NH_4NO_3 + H_2O \qquad (1)$$

Aquopentaamminecobalt (III) perchlorate (APCP).

$$[Co(NH_3)_5CO_3]NO_3 + HClO_4 \xrightarrow{H_2O} [Co(NH_3)_5HCO_3](ClO_4)(NO_3)$$

$$(Co(NH_3)_5HCO_3](ClO_4)(NO_3) + 2HClO_4 \xrightarrow{H_2O} [Co(NH_3)_5H_2O](ClO_4)_3 +$$

$$CO_2 + HNO_3 \qquad (2)$$

5-cyanotetrazole (CT).

$$HCl + NaN_3 + NC\text{-}CN \xrightarrow[\text{cold}]{H_2O} \text{(5-cyanotetrazole)} + NaCl \qquad (3)$$

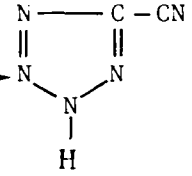

5-cyanotetrazolatopentaamminecobalt (III) perchlorate (CP).

$$[Co(NH_3)_5H_2O](ClO_4)_3 + \text{(5-cyanotetrazole)} \xrightarrow[90°C]{H_2O}$$

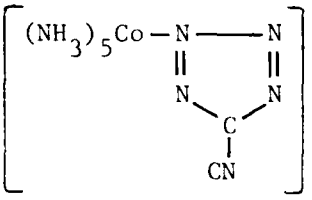

$$(ClO_4)_2 + HClO_4 \qquad (4)$$

The preparation procedure for CP consists of four major processes that correspond to each of the above synthesis steps, and a final recrystallization that adjusts the particle size. These processes are outlined in the following sections.

Preparation process for carbonatopentaamminecobalt (III) nitrate (CPCN). A schematic for the preparation process for CPCN is presented in Figure 1. The procedure involves stirring a slurry of ammonium carbonate and cobalt nitrate in an ammonia solution. Air is bubbled through the mixture to oxidize Co^{+2} to Co^{+3}. CPCN is not flammable or explosive and no special precautions are observed during handling.

Ammonium carbonate for this process is purchased in the form of very hard chunks and must be powdered prior to use. An 18 inch Simpson mix-muller is used

to reduce a 12 kg batch to a fine powder. The reactor is charged with 30 liters of ammonium hydroxide and the stirrer started. The powdered ammonium carbonate is added and a flow of 500 ml/min. of filtered air through the solution is established. A solution of 5985 g of cobalt nitrate hexahydrate in 6 liters of water is added and the suspension is allowed to aerate for 96 hours. The progress of the reaction is indicated by the slow appearance of the deep red color of CPCN. After 96 hours, aeration is stopped and the suspension is heated to 70-75°C to dissolve CPCN. The solution is filtered to remove small amounts of dark solid, probably oxides of cobalt, then cooled to 0-5°C. CPCN crystallizes out and is collected in ~500 g batches on a coarse glass frit. Each batch is washed with 600 ml of cold water followed by 600 ml of 6:4 isopropanol/water and 1 liter of isopropanol. The product is transferred to pyrex trays and left to dry under ambient conditions. The yield is 3.6 - 4.0 kg and the material is of sufficient purity for use in the preparation of APCP.

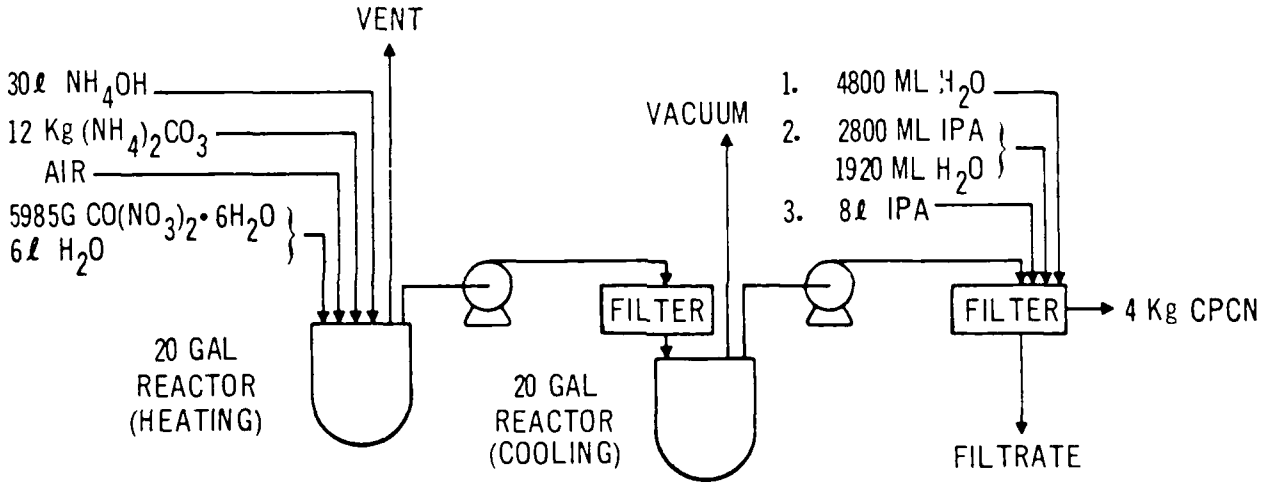

Fig. 1. Preparation of CPCN.

Preparation process for aquopentaamminecobalt (III) perchlorate (APCP). A schematic for the synthesis of APCP is presented in Figure 2. CPCN is treated with a large excess of perchloric acid. The conversion proceeds in two distinct steps. The first chemical equivalent weight of perchloric acid converts the coordinated carbonate to bicarbonate without observable evolution of carbon dioxide. The reaction is strongly exothermic and requires a very slow addition of acid. Addition of the second mole-equivalent of acid results in conversion of the bicarbonate to carbon dioxide and APCP. This second step appears to be mildly endothermic and the rate of addition of acid is limited only by the amount of foaming that can be tolerated. A large excess of perchloric acid is used to convert from the nitrate anion to perchlorate anion. The solubility difference

between nitrate and perchlorate is small and the transformation depends on the mass action effect.

The crude APCP still contains appreciable nitrate, as well as some other unidentified impurities. The crude APCP is purified by dissolving in warm water and precipitation with a large excess of perchloric acid. The product still contains some nitrate but is suitable for use in subsequent reactions.

APCP is an oxygen rich explosive with rather low output. It is not particularly sensitive to spark or impact, but will deflagrate rapidly when ignited and must be considered a hazardous material. An aluminized suit and leather gloves are worn whenever dry APCP is handled.

The mechanical aspects of this process are relatively simple. A 20 gallon reactor is charged with 5 kg of CPCN and 10 liters of water. The slurry is cooled to <10°C and stirred rapidly while cold 35% perchloric acid is added slowly.

The rate of addition is controlled to hold the temperature below 10°C. After the addition is complete, the suspension is cooled to <5°C and the solid collected on a glass frit in small batches of about 200 g each. Each batch is washed with 200 ml of isopropanol, placed in a separate Velostat* tray, and left to air dry. The crude yield is about 6 kg.

Purification is accomplished by dissolving the crude APCP in 50 liters of warm water and adding 10 liters of 70% perchloric acid. After cooling to <10°C, the APCP is again collected and washed in small batches. Yield at this point is again 6 kg and, in fact, the final product often weighs more than the crude. The weight gain is thought to result from displacement of residual nitrate by the heavier perchlorate.

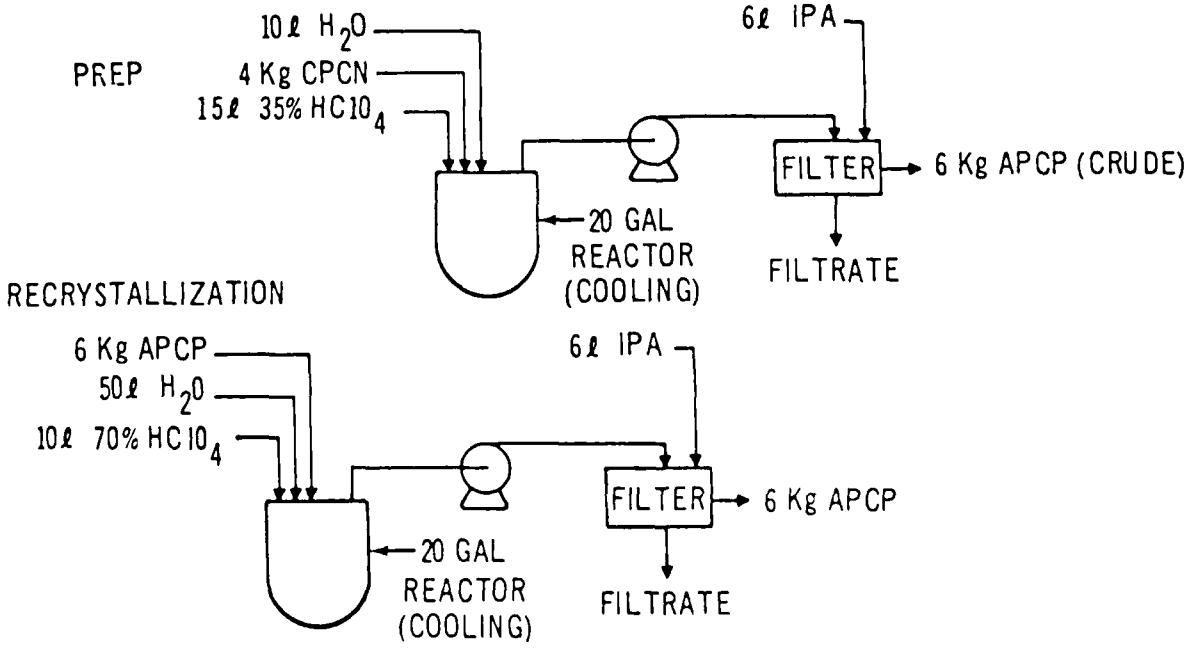

Fig. 2. Preparation and purification of APCP.

*Trademark of 3M Company

Preparation process for 5-cyanotetrazole (CT). CT synthesis is considerably more involved and presents more difficulties and potential hazards than any other step in the production of CP. The reaction involves simply the addition of azide ion to a molecule of cyanogen. The reaction proceeds rapidly at 0°C in good yield as long as the solution is kept cold. If the temperature is allowed to rise above 10°C, two other reactions may occur. A second mole of azide can react with the product to produce a bitetrazole, and the nitrile group of the desired product can be hydrolyzed to give 5-carboxamidotetrazole. The hydrolysis product is observed in solid CT which has been stored at ambient temperatures, but none is detected in freshly prepared CT if the reaction temperature is kept at less than 8°C.

Two major difficulties arise during the preparation of CT. The first problem involves personnel safety. Cyanogen is a highly toxic gas that is comparable to hydrogen cyanide in its physiological effects. Cyanogen is also highly energetic and flammable. Some undetermined amount of hydrazoic acid is formed in the reaction and this gas is also highly toxic and potentially explosive. The physiological effects of CT are not known, but the solid has a high vapor pressure and is acidic. Contact with CT will cause extensive skin problems, with the skin peeling off in sheets after heavy or repeated exposure. The preparation of CT is carried out in a closed system contained in a large fume hood. Personnel wear a fresh air breathing system at all times when exposure to cyanogen is possible. Protective gloves are worn at all times when exposure to CT is possible.

The second problem is the extraction and subsequent drying of product from the aqueous reaction mixture. CT is extremely soluble in water, but it can be removed from the water by numerous extractions with ether. The resulting ether solution is saturated with water and must be dried. Calcium chloride has been found to be a more effective drying agent for the ether solution than calcium sulfate or magnesium sulfate, but no drying agent tried has removed all water from the ether solution. CT has great affinity for both ether and water and a long stripping operation is necessary to remove the solvents. CT in contact with water and ether is not stable at temperatures above 70°C, so the maximum temperature used in stripping is 40°C. Residual water is a problem for two reasons. It is often present in sufficient quantities to form an ice layer that partially blocks the cold trap protecting the high vacuum pump. Also, if the final product is not dry, it will hydrolyze during storage.

The current process for CT production is shown in Figure 3. The reactor is filled with 7500 ml of water and 925 g of sodium azide. An ice bath around the flask provides for cooling. The stirred solution is cooled to 5°C and 75 ml of concentrate hydrochloric acid added. Cyanogen is bubbled through the solution at a rate that does not cause the temperature to rise above 8°C. The reaction

is complete when cyanogen is no longer absorbed. Cyanogen flow is stopped and stirring continued for one hour. The system is purged with air for 15 minutes, then 1425 ml of concentrated hydrochloric acid is added at a rate that keeps the temperature below 5°C. Finally, 1 kg of NaCl is dissolved in the reaction mixture to aid in the subsequent extraction step. The solution is then pulled into a rotary evaporator and stripped at 25°C until evolution of gas ceases. At this point, it is assumed that cyanogen is no longer a hazard and gas masks are not required. All subsequent operations are carried out in a fume hood. The solution is transferred manually to a 20 liter separatory funnel and extracted with 2 liters of ether three times, then once with 1 liter of ether. The funnel is equipped with an air-driven stirrer so manual shaking is not required. The ether extract is dried over calcium chloride for one hour, then decanted onto fresh calcium chloride and dried overnight. The ether solution is filtered and most of the ether stripped off using a rotary evaporator under low vacuum with a bath temperature of 40°C. The rotary evaporator is then connected to a high vacuum system (<0.2 mm Hg) protected by a dry ice-acetone trap and stripping continued for 3-4 hours. The residue from the stripping operation is collected and stored at -20°C. The yield is about 1200 g of white solid which is suitable for use in CP synthesis. Properly dried material melts at 98-102°C while samples containing solvent melt at 90-100°C.

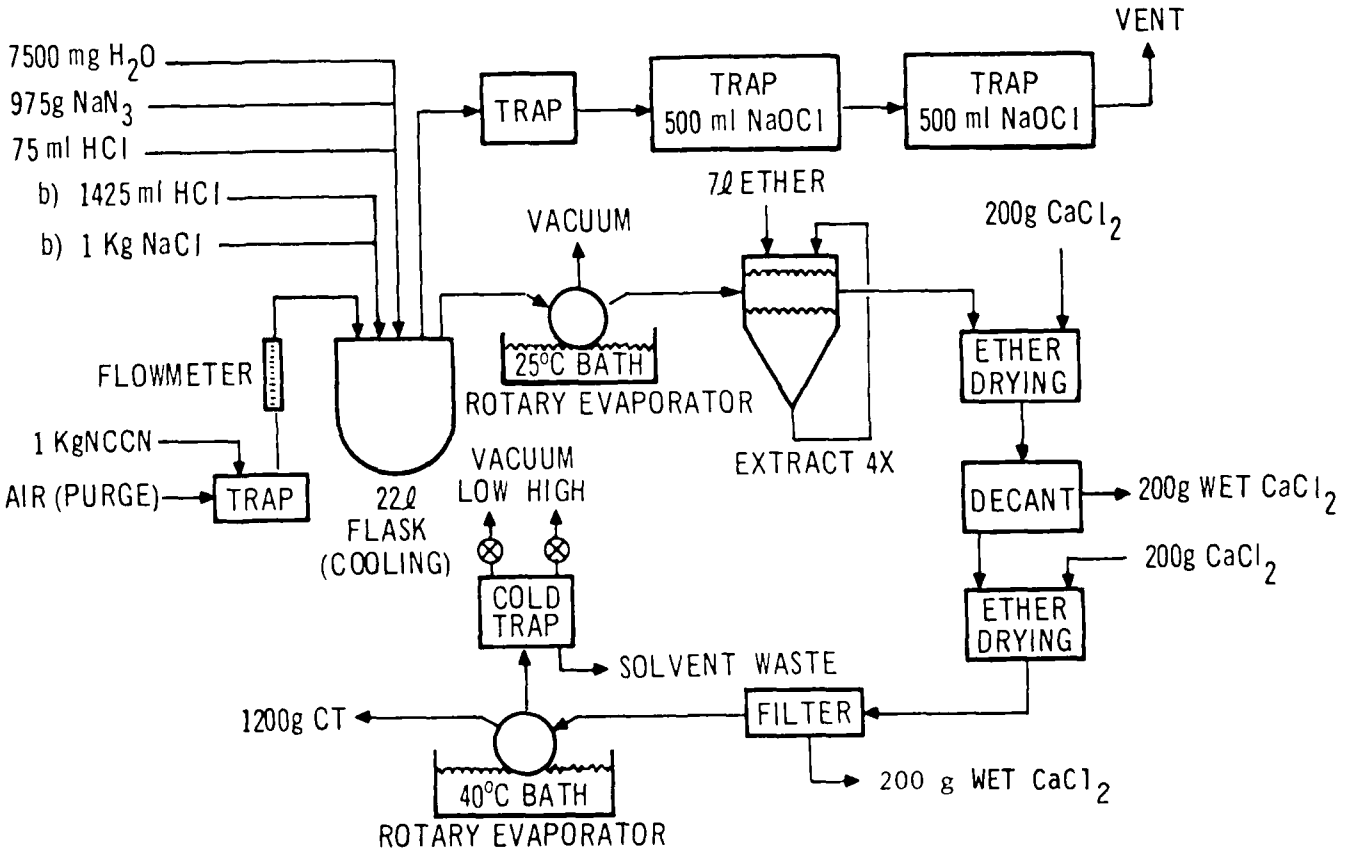

Fig. 3. Synthesis of CT.

Preparation process for CP. CP is prepared by heating a solution of APCP and CT in water at 85-90°C for 3 hours. Some CP precipitates during the reaction, but most of the product precipitates when the mixture is cooled. Several impurities are formed during the reaction and some unreacted starting materials remain. It has been found that a superior product is obtained if the reaction mixture is cooled only to ambient (25°C) before the product is collected. Cooling to 0-5°C gives a substantially higher yield, but also gives a much less pure product. The major impurity in CP is formed by the hydrolysis of the nitrile group on the CT molecule during the final reaction. This impurity is 5-carboxamidotetrazolatopentaamminecobalt (III) perchlorate, and it is referred to here as "amide complex". Amide complex is present in concentrations of about 10% in crude CP collected at 25°C. A second fraction that is collected by cooling the filtrate to 0°C will contain about 15% amide complex as well as considerable APCP and an "unknown complex". (ref. 1)

Purification of CP is accomplished by recrystallization from a solution containing added ammonium perchlorate. For some unknown reason, excess perchlorate acts to reduce the amount of "amide complex" in the product. Excess perchlorate also helps to ensure that other anions such as residual nitrate or the 5-cyanotetrazolate are minimized. CP after the purification step contains 3-4% amide complex as the only impurity detectable by thin layer chromatography. The yield is 1.6 kg of large yellow crystals which are impact sensitive and far too large for use in detonator applications. The particle size is reduced by adding a hot aqueous solution of purified CP to cold isopropanol. By controlling the temperature of the isopropanol during the addition, a product of the desired particle size is produced.

The mechanical aspects of the CP preparation process are shown in Figures 4, 5 and 6. A 50 liter glass flask is charged with 3600 g of APCP, 1000 g of CT, and 18 liters of water. The solution is stirred and heated at 85-90°C for 3 hours, then transferred using vacuum to a second flask where it is cooled to 25°C. Vacuum is used to pull part of the CP slurry out into a collection vessel. The crude CP is then collected on a Buchner funnel in batches of 50-100 g and washed with 200 ml of isopropyl alcohol. Each batch is placed in a Velostat tray and left to air dry.

Crude CP is returned to the 50 liter flask and 24 liters of water is added. A trace amount of perchloric acid is added to keep the pH slightly acidic and the suspension is heated until the CP dissolves. A solution of 1 kg of ammonium perchlorate in 6 liters of water is added and the solution transferred using vacuum to a second flask where it is cooled to 25°C. The product is collected on a Buchner funnel as described above. The yield is about 1.6 kg of purified CP.

In the particle size adjustment step, purified CP (~1.6 kg) is returned to the 50 liter flask and 19.2 liters of water is added. A trace of perchloric acid

is added and the suspension heated to 75-80°C to cause dissolution. The CP solution is then transferred using vacuum to a second flask which contains 6400 ml of isopropanol at $\leq$ 5°C. An in-line filter is used to remove any solid impurities that may have been introduced during previous steps. The rate of transfer is varied so that the temperature of the receiving flask remains at 30-35°C. Control of this temperature is quite critical, since at higher temperatures, large particle sizes result, and at lower temperatures, a very fine powder with poor handling properties is produced. After transfer is complete, the mixture is cooled to 25°C and the product collected and dried at 25°C in a vacuum oven. The product is remotely screened in small batches, through a USS-ASTM standard size 140 stainless steel sieve. After screening, the CP is vacuum dried at 60 ± 5°C and at a vacuum greater than 25 inches of Hg for 2 hours. It is packaged in 50 g batches in 4 oz. Nalgene* bottles and stored under desiccation.

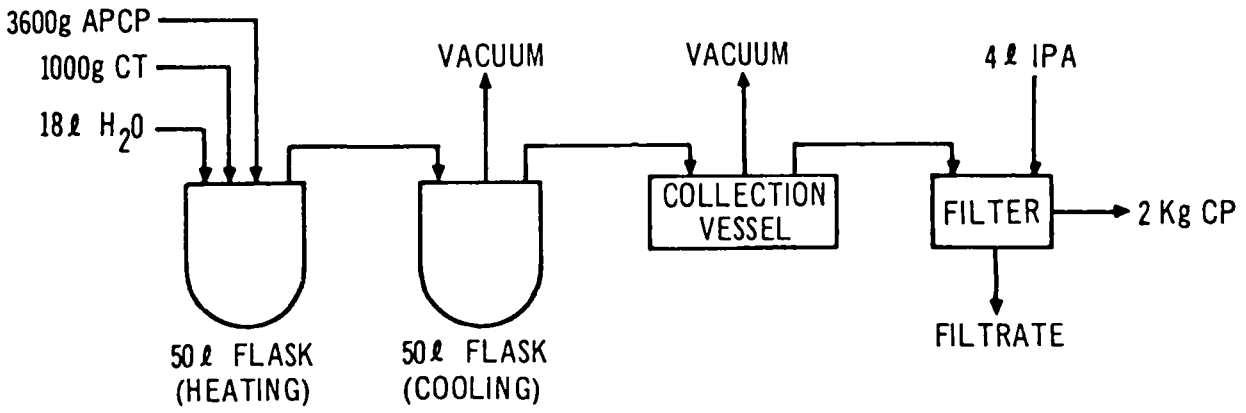

Fig. 4. Synthesis of CP.

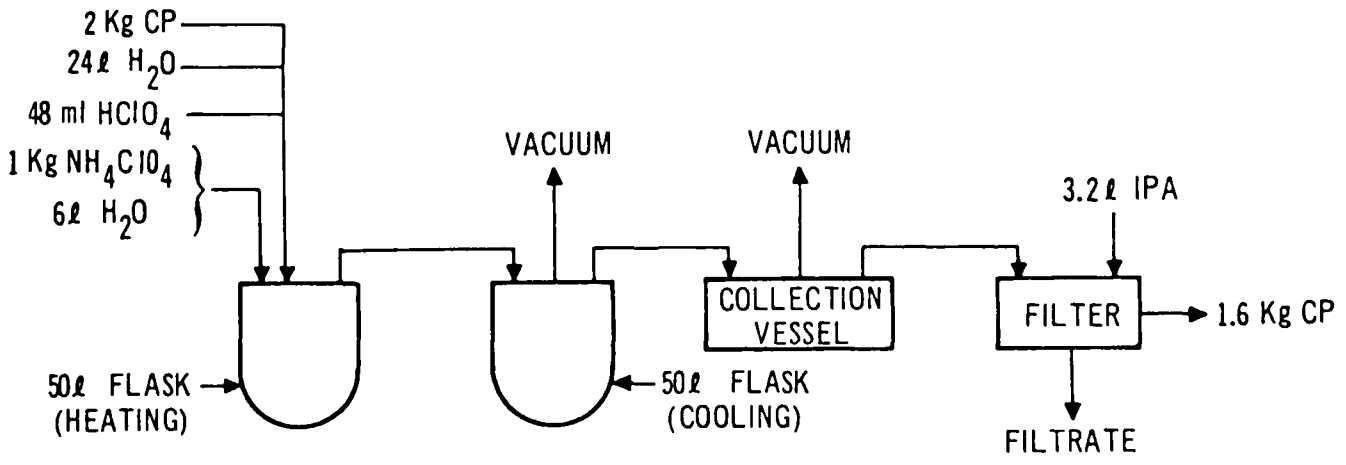

Fig. 5. Purification of CP.

*Trademark

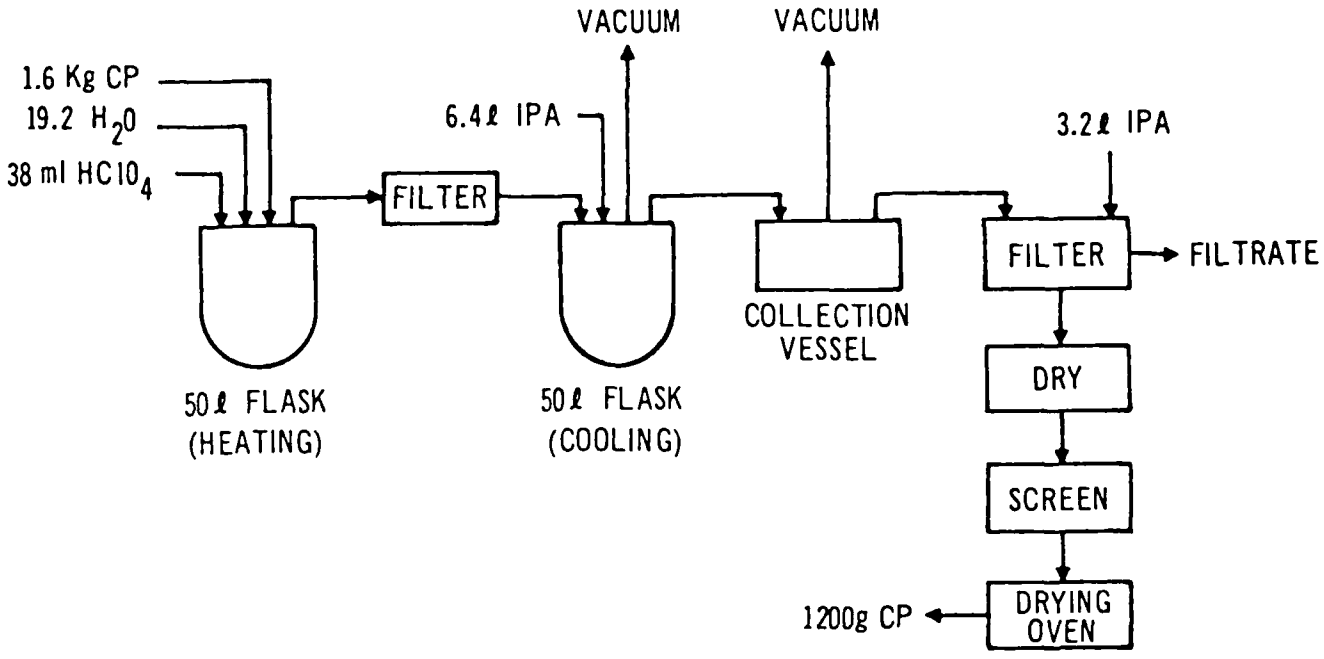

Fig. 6. Final processing of CP.

QUALIFICATION OF CP

The following tests are required for qualification of each lot of CP:

a. Moisture content
b. Water uptake at 98% humidity
c. pH of a 1% standard CP solution
d. Chloride ion content
e. Perchlorate content
f. Cobalt content
g. 5-carboxamidotetrazolatopentaamminecobalt (III) perchlorate content
h. Ammonium ion content
i. Functionality tests in detonator hardware
j. Surface area analysis by low temperature Krypton absorption (BET technique)
k. Nitrate ion content
l. Free cyanide ion content
m. Trace metal content
n. Infrared and UV-Visible spectrum
o. Impact sensitifity

The last five tests in the above list are information only, and no specified limits are currently required for these tests.

Requirements and a typical analysis are presented in Table 2.

Most of the analytical procedures are relatively straightforward. Moisture content (Test a) is actually weight loss on drying, and water uptake at 98% humidity (Test b) is determined by weight gain of the same sample dried in Test a. The chloride ion (Test d) and ammonium ion (Test h) concentration are determined using specific ion electrodes (ref. 2). Perchlorate (Test e) is determined gravimetrically as tetrapentylammonium perchlorate (ref. 3). Cobalt (Test f)

is determined by the classical method of electrolytic deposition of metal (ref. 4) after digestion of the sample in sulfuric acid.

TABLE 2

Analysis of CP, lot EL-47345

Test	Requirements	Results
Perchlorate	45.54 ± 0.3%	45.58, 45.67, 45.79
Impact sensitivity	--	>100 cm
Amide complex	<5.0%	3.7, 3.4
Cobalt	13.44 ± 0.3%	13.62, 13.60
pH	>4.5	5.6
Chloride	<100ppm	not detected (<30ppm)
Ammonium	<100ppm	not detected (<30ppm)
Nitrate	--	100ppm
Cyanide	--	not detected
Trace metals	--	obtained (no metal greater than
Ultraviolet-visible and Infrared spectra	--	obtained 0.02%)
Moisture, content	<0.1%	0.020, 0.013
uptake	<0.2%	0.120, 0.123
Surface area	0.4 - 0.6 m^2/g	run 1: 0.406, 0.441
		run 2: 0.422, 0.426

Methods for the determination of "amide complex" (Test g) have not been entirely satisfactory. A reasonable estimate can be made using thin layer chromatography, but the method cannot give precise results. R. Jungst of Sandia has developed an IR method which can give accurate and reproducible results (ref. 5), but apparently requires considerable care. Attempts to replicate the method developed by Jungst at Unidynamics/Phoenix have not been entirely successful. Efforts are continuing at Mound Facility of the Monsanto Research Corporation and at Sandia Laboratories to develop a more rapid and direct method for determination of amide complex concentration.

Functionality (Test i) is the critical evaluation. The all-fire and no-fire levels in actual detonator hardware are determined. The surface area (Test j) is determined by low temperature krypton absorption (BET technique), and a specified requirement exists. However, the surface area requirement can be waived if the functionality test is satisfactory. Nitrate ion (Test k) is determined by a colorimetric method using diphenylbenzidine (ref. 6). Cyanide (Test l) is determined by a titrametric method based on the following reaction (ref. 2):

$$HCN + I_2 \longrightarrow HI + ICN$$

Starch indicator is used to detect the disappearance of iodine. Trace metals (Test m) are determined spectrographically after the sample has been digested in a mixture of nitric and sulfuric acid.

CP of acceptable purity and particle size for use in detonators can be produced in 1 kg size lots. The process has been developed and documented to the extent that good reproducibility can be expected for subsequent lots. Total elapsed time for the preparation and qualification of a lot of CP is 6-8 weeks exclusive of functionality tests.

REFERENCES

1 On the basis of ^{1}H and ^{13}C NMR, Infrared and elemental analysis the "unknown complex" has been tentatively identified as an amidine chelate isomeric with CP. L. Gerchman and L. Carey, SRI International, A private communication, 1977.

2 R. M. Merrill, "Chemical Analysis Technique for the Determination of Chloride, Ammonium & Cyanide in the Explosive, 5-Cyanotetrazolatopentaamminecobalt (III) Perchlorate (CP), Sandia Document SAND77-1899, March 1978.

3 R. G. Dosch, Anal. Chem. 40, (4) 829 (1968).

4 A. I. Vogel, "Quantitive Inorganic Analysis", Longmans, Green and Co., New York, 1951, Page 524.

5 R. G. Jungst and P. K. Peterson, "Analysis of Amide Complex Impurity in CP Explosive by Infrared Spectroscopy", Sandia Document SAND78-1395, August 1978.

6 Fritz Feigl, "Spot Tests in Inorganic Analysis". Elsevier Publishing Co., New York (1958), Page 328.

THERMAL ANALYSIS OF LIQUID AND SOLID PROPELLANTS

A. S. TOMPA

Research and Technology Department, Naval Surface Weapons Center, White Oak
Silver Spring, Maryland 20910

ABSTRACT

Kinetic constants from differential scanning calorimetry data using heat evolution and variable heating rate methods were obtained for the thermal decomposition of a liquid monopropellant; good agreement was found between the observed and predicted half-life for the first order decomposition reaction. The rate of volatilization of nitroglycerin in a crosslinked double base propellant was investigated by isothermal and dynamic thermogravimetry and was found to be first order. The effect of sample size, atmospheric environment, aging and crosslink density of the propellant on the volatilization rate was determined. It was observed that the rate increased as (1) the sample was changed from a cylindrical plug to a powdered form, (2) the atmosphere around the sample was changed from nitrogen to helium to vacuum, (3) as the thermal stability of the sample decreased, and (4) the relative crosslink density was changed from a higher to a lower value. A kinetic compensation effect was found for cylindrical plugs but not for powdered samples.

INTRODUCTION

Differential Scanning Calorimetry (DSC) and Thermogravimetry (TG) techniques have been applied towards the characterization of propellants and explosives (ref. 1). In the present study the kinetics of decomposition of a liquid monopropellant was followed by DSC. The data were analyzed by four methods and three of them were in good agreement. The thermal stability of original and aged crosslinked double base propellant (CDB) was determined by an isothermal TG study of the volatilization of the plasticizer (nitroglycerin, NG). The effects of sample size, atmospheric environment, and relative crosslink density on the volatilization of NG in a CDB propellant were investigated.

EXPERIMENTAL

Instrumentation

A DuPont 990 Thermal Analyzer with 990 DSC and TG modules was used.

Liquid Monopropellant

The sample mass was 1 to 3 mg. The heating rate was $5^{o}C$/min with a time base of 2 min/in. Unsealed gold pans were used i.e. sample pans with covers. The DSC runs were carried out in a nitrogen atmosphere using a flow rate of 100 ml/min. The DSC module was isothermally heated to about $135^{o}C$, the sample pan was placed in its position and the run started. In addition a variable heating rate study was carried out at 1 to $20^{o}C$/min.

Crosslinked Double Base Propellants

Five samples were investigated. They were labelled CDB-1, aged CDB-1 (aged 6 months at $120^{o}F$ and 81.2% relative humidity), CDB-2, aged CDB-2 (aged 18 months at $120^{o}F$ and 20% relative humidity) and CDB-3. The CDB-1 samples were ground into powder form using a Wiley Mill. The mass of the powdered samples used in the TG runs was 15 $\pm$ 2 mg. The CDB-2 and CDB-3 samples were cylindrical plugs and were about 0.12 in. by 0.12 in. and weighed 60 $\pm$ 5 mg. The CDB-1 and CDB-2 samples were similar in composition and had approximately nine times more nitrocellulose content than CDB-3 and therefore had a higher relative crosslink density because of the higher concentration of hydroxyl groups available for crosslinking. Scale expansion was used to follow the volatilization of NG. The TG data was expressed as fraction volatilized (α) and varied from 0 to 1 for NG. The NG volatilizes in a temperature range where the rest of the propellant is thermally stable. The atmospheric environment was varied from nitrogen to helium using a flow rate of 100 ml/min. When vacuum was used, it was 29 inches. The TG furnance was equilibrated at the desired temperature before the sample and quartz furnace tube were inserted into the furnace. Time base runs were varied from 10 to 1 min/in. Dynamic TG runs were carried out at heating rates of 0.5, 1 and $2^{o}C$/min.

DISCUSSION

Kinetic Methods

The kinetic data generated by DSC were analyzed by four methods. They were as follows, (1) Urichek (ref. 2) method where:

$$\Delta \log \left(\frac{\Delta H/\Delta t}{A-a}\right) / \Delta \left(\frac{1}{T}\right)$$

is plotted to obtain E/2.3R. In this equation $\Delta H/\Delta t$ is the rate of heat flow, (A-a) is the area of the unreacted portion of the curve, and E is the activation energy; (2) Rogers and Morris (ref. 3) method where Δ (log D) versus $\Delta(1/T)$ is plotted to obtain E/2.3R. In this case (D) is the vertical displacement from the baseline to the DSC curve; (3) the third method (ref. 4) is where the reaction rate doubles in the temperature interval (ΔT); the differential form of the Arrhenius equation becomes $E = 1.38\ T^2/\Delta T$; thus by measuring the temperature interval of ΔT during which the curve displacement from the baseline doubles, an estimate of the activation energy may be made; and (4) the variable heating rate method developed by Flynn and Wall (ref. 5) and Ozawa (ref. 6). The basic equation is $\Delta \log \beta/\Delta (1/T) \simeq 0.457\ E/R$ where β is the programmed heating rate (^oC/sec) and T is the temperature at a constant degree of conversion which in the DSC run is the reaction peak maximum. Thus as the heating rate is increased the reaction peak shifts to higher temperature and therefore an estimate of the activation energy may be made. The pre-exponential factor (A) is conveniently obtained in the first order form by Rogers and Smith (ref. 7) using the equation $A = (\beta E/RT^2_{max}) \exp (E/RT)$. All the parameters are known so no additional measurements need to made. Methods 1 to 3 assume a first or zero order reaction while method 4 is independent of the order of the reaction.

The kinetic data generated by isothermal TG were analyzed by three methods. They are as follows, (1) Manche-Carroll (ref. 8) method where $\log (\Delta\alpha/\Delta t)/\Delta(1/T)$ is plotted to obtain E/2.3R, α is the fraction reacted and $\Delta\alpha/\Delta t$ is the rate at fixed values of α. The Arrhenius frequency factor is obtained from the equation $\log A = E/2.3RT - \log (\Delta\alpha/\Delta t)$; (2) a first order plot of $\log (1-\alpha)$ versus time to obtain the rate constant (k/2.3) followed by a plot of $\Delta \log k/\Delta(1/T)$ to obtain E/2.3 R; and (3) Kishore (ref. 9) method where $\Delta \log t_{0.5}/\Delta(1/T)$ is plotted to obtain E/2.3R, $t_{0.5}$ is the time when the fraction reacted, $\alpha = 0.5$. In addition the Avrami-Erofeev equation $(-\ln(1-\alpha))^{0.5}$ and the contracting area equation $1-(1-\alpha)^{0.5}$ were tried but found not to be applicable. Values of α in the range of 0.3 to 0.7 were used in the calculation of kinetic constants.

Dynamic TG runs were carried out at heating rates of 0.5, 1 and 2^oC/min. Doyle (ref. 10) developed a relationship between isothermal and dynamic TG runs. By plotting $\Delta(\log t)_{ISO}$ versus $\Delta(1/T)_{DYN}$ for fixed values of α, a slope of 0.457 E/R was obtained. Flynn and Wall (ref. 5) and Ozawa (ref. 6) methods originally developed for dynamic TG were used also. As before $\Delta(\log \beta)/\Delta(1/T) \simeq$ 0.457 E/R is plotted for fixed values of α.

Liquid Monopropellant

The liquid monopropellant studied was a liquid nitrate ester which contained a few percent of a desensitizing agent and a stabilizer. Figure 1 shows the DSC curve for the sample. Kinetic data were obtained along points 1 to 8 for the

for the Urichek and Rogers and Morris methods. It should be noted that two baselines were drawn. A slanted line which followed the DSC curve and a dashed horizonthal baseline whereby the decay and acceleratory portions of the DSC curve were fitted to the same baseline level. Straight line kinetic plots are shown in Figures 2 and 3. There is good agreement in the values obtained for the activation energy (Table I) by the different methods except for Uricheck's. In the latter case if the band shape is made more symmetric by extending it to the dashed baseline then good agreement is obtained with this method also. This observation points out the value in using more than one method for calculating the activation energy. Still an independent check on the activation energy would be desirable. Duswalt (ref. 4) proposed an isothermal test for predicting the half-life for the reaction at some convenient temperature using the kinetic values in question. This suggestion was followed. Kinetic values obtained from the variable heating rate method of Flynn and Wall (ref. 5) and Ozawa (ref. 6) were used. The half-life for a first order reaction is 0.693/k. At 180°C the half-life was calculated to be 15.6 minutes. The sample was then heated for this time in the DSC cell, the sample and cell cooled to room temperature and then programmed through the reaction peak at 5°C/min. The heat of reaction for decomposition was measured and found to be 65 cal/gram. The original value found at a heating rate of 5°C/min was 135 cal/gram. The percent change was 66/135 = 49% which is in excellent agreement with the theoretical value of 50%. This also proved that the decomposition of this liquid monopropellant was first order

Crosslinked Double Base Propellants

Effect of atmosphere on volatilization of NG. A typical isothermal TG curve for the volatilization of NG in a CDB propellant is shown in figure 4. The curves are redrawn with emphasis on the time required to reach an α value of 0.8; the actual figures are curved below and above α values of 0.2 and 0.8 respectively and linear as shown in between. The effect of the atmosphere on the volatilization rate of NG in a CDB propellant is shown in figure 5; the rate decreases in the order vacuum > helium > nitrogen. The observation in helium and nitrogen indicate that the rate of volatilization of NG is proportional to the thermal conductivity of the atmosphere. Helium has a thermal conductivity approximately six times greater than that of nitrogen. In addition helium has a smaller molecular volume than nitrogen and may therefore more readily diffuse through and displace the layer of volatilization gases than lie above the surface of the sample and thereby increase the volatilization rate. It may because of its smaller size penetrate deeper into the surface of the sample and facilitate the displacement of volatile plasticizer. Caldwell (ref. 11) et al. observed the same type of atmospheric effect on the thermal decomposition of calcium carbonate.

Effect of sample geometry on volatilization of NG. The effect of sample size of the CDB propellant i.e. powder (15 mg) or cylindrical plug (60 mg) on the volatilization rate of NG is shown in figure 6. The volatilization rate of NG is faster in a CDB powder than in a cylindrical plug because of the greater surface area in the powder and consequently the volatilization of NG is facilitated.

Effect of aging on volatilization of NG. The effect of aging on the volatilization rate is seen in figure 6. Aged CDB-1 is more thermally degraded than the original because it was aged in a high relative humidity environment and consequently it has a higher volatilization rate of NG. Conversely aged CDB-2 has a lower volatilization rate of NG than the original and this may be due to the fact that CDB-2 was aged in a low relative humidity environment and consequently may have undergone postcure and thus is more thermally stable.

Effect of crosslink density on volatilization of NG. CDB-3 has a higher volatilization rate of NG than CDB-2. Both are cylindrical plug samples. The latter has a higher relative crosslink density than the former because its nitrocellulose content is nine times greater and thus has extra hydroxyl groups available for crosslinking, consequently it has a lower volatilization rate of NG.

SUMMARY OF EFFECTS ON VOLATILIZATION OF NG

It appears that the rate of volatilization of the plasticizer NG in CDB propellants depends upon the physical state of the propellant. That is, if the sample has more crosslinks either through post cure or by having extra hydroxyl groups available for crosslinking then there is a greater physical entrapment of the plasticizer and hence it is more difficult for the plasticizer to migrate and reach the surface of the propellant and volatilize upon being heated. Conversely if crosslink bonds are broken by hydrolysis as happens in aging a sample at a high relative humidity then it is easier for the plasticizer to migrate to the surface and volatilize. Finally, the larger the surface area of the sample then the more plasticizer there is on the surface and consequently it will volatilize at a faster rate since the slow step in the volatilization process would be the diffusion of the plasticizer from the interior to the surface of the propellant.

Dynamic Thermogravimetry

Dynamic TG curves for the volatilization of NG in CDB propellants are shown in figures 7 and 8. In the former the effect of the heating rate is shown i.e. an increase in the heating rate causes the TG curves to shift to higher temperature and in the latter figure the effect of the atmospheric environment is shown i.e. the fraction volatilized of NG comes at a lower temperature in the series vacuum < helium < nitrogen. It is apparent in figure 8 that the three curves are converging near 160°C. This indicates that the NG has volatilized by this temperature and that the atmospheric environment does not appear to have an effect on the initial stage of the decomposition of the propellant but only has an effect on the volatilization

of the plasticizer. By inspection the dynamic TG curves do not appear to be as useful as the isothermal TG curves in following the volatilization rate of NG in CDB propellants.

Reduced Time

A reduced time plot i.e. $t_R = t/t_{0.5}$ where $t_{0.5}$ is the time when $\alpha = 0.5$ is shown in Figure 9. The utility of this plot is that if the curves at different isothermal temperatures superimpose under an α versus t_R plot then the order of the reaction at different temperatures is constant i.e. the kinetic behavior remains the same. It is seen in figure 9 that the points fall on the same line whether a powder or cylindrical sample is used and regardless of the atmospheric environment. Garn (ref. 12) suggested plotting $d\alpha/dt$ vs t_R and showed theoretical plots for different model processes. This type of plot is shown also in figure 9 and it resembles Garn's plot for a phase boundary control process. The plot in nitrogen is not shown but it is also a straight line with a slope only one-fifth that in vacuum or helium.

Kinetics of Volatilization of NG

Typical straight-line kinetic plots for the volatilization of NG in CDB propellants are shown in figures 10 to 12 using Manche-Carroll, Kishore and Arrhenius plots. The kinetic reaction appears to be first order. An isothermal versus dynamic TG plot (Doyle) is shown in figure 13. Figure 14 shows curved lines for an Avrami-Erofeev or contracting area plots and thus these expressions are not applicable in the α value range of 0.3 to 0.7.

Activation energies for the volatilization of NG from cylindrical plugs of CDB propellant are given in Table II. Good agreement was obtained for the activation energies using the isothermal TG methods of Manche-Carroll, Kishore, and the first order Arrhenius equation. Higher values were found using the dynamic TG methods of Doyle or Ozawa. Zsako (ref. 13) observed a similar disagreement in activation energies obtained by isothermal and dynamic TG and ascribed it to the influence of the heating rate. The activation energy values are in the order vacuum < helium < nitrogen and CDB-3 < CDB-2 < aged CDB-2. The rate constants and half-life for the volatilization reaction were calculated for 40°C and are given in Table II. The half-life ratio for helium to nitrogen parallels the thermal conductivity ratio (5.9 at 0°C) for helium to nitrogen. For cylindrical plug samples it appears that the activation energy and the rate of volatilization for NG were influenced by the atmospheric environment and the relative crosslink density of the sample. As the crosslink density increased due to postcure or extra hydroxyl groups available for crosslinking, the rate of volatilization decreased and the activation energy increased.

Activation energies for the volatilization of NG from powdered CDB propellants are given in Table III. The values are the same in the different atmospheric

environments and whether the sample is aged or original did not make any difference. However the rate constants for the volatilization of NG were different. Thus it appears that the surface area of the sample influenced the determination of the activation energy for the volatilization of NG in powdered samples while the rate constants were influenced by the atmospheric environment and relative crosslink density of the sample. A powdered CDB propellant aged in a high humidity environment undergoes hydrolytic degradation owing to the cleavage of crosslink bonds by hydrolysis, consequently the diffusion of the NG plasticizer to the surface is facilitated. The ratio of the half-life in helium to nitrogen for the volatilization of NG in powdered CDB propellants parallels the ratio of their thermal conductivities. This was observed also with cylindrical plug samples. Thus this is convincing evidence that the mechanism for the volatilization of NG in these samples is thermal transport.

The overall order for the rate of volatilization of NG from powdered and cylindrical plugs of CDB propellant based on first order rate constants at 40°C is: aged CDB-1 > CDB-1 > CDB-3 > CDB-2 > aged CDB-2. This is the same order as powdered > cylindrical plugs and lower crosslink density > higher crosslink density.

Compensation Effect

A kinetic compensation effect was observed for the volatilization of NG from cylindrical plugs (figure 15) but not for powdered CDB samples. This is probably due to the difference in geometry of the two types of samples and the four-fold difference in sample mass i.e. 60 mgs (plugs) vs 15 mgs (powdered). A kinetic compensation effect is so called because it was observed with some reactions that a change in the activation energy was not accompanied by a corresponding change in the rate constant because of a compensating change in the pre-exponential factor. A linear relationship between the activation energy and pre-exponential factor implies a linear relationship or compensation between the enthalpy (ΔH) and entropy ($T\Delta S$) for the reaction (ref. 14). The compensation effect is given by the equation: $\log A = aE + b$ which resembles the Arrhenius equation $\log A = E/2.3RT + \log k$ where $a = 1/2.3RT$ and $b = \log k$. The parameters were found to be $a = 0.5$ and $b = -1.5$. Thus although the kinetic parameters varied for the different cylindrical plug samples of CDB propellants, the compensation parameters a and b remained the same. This is in agreement with Zsako's (ref. 15) observation that even though the kinetic parameters for individual runs may vary, the compensation parameters a and b will not vary for the whole series.

REFERENCES

1. L. W. Collins and L. D. Haws, Thermochim. Acta, 21 (1977) 1.
2. M. Urichek, Perkin-Elmer Instrum. News, 17 (1966) No. 2.
3. R. N. Rogers and E. D. Morris, Jr., Anal. Chem., 38 (1966) 412.
4. A. A. Duswalt, Thermochim. Acta. 8 (1974) 51.
5. J. H. Flynn and L. A. Wall, J. Res. N.B.S., Phy. Chem., 70A (1968) 478.
6. T. Ozawa, J. Therm. Anal., 2 (1970) 301.
7. R. N. Rogers and L. C. Smith, Anal. Chem., 39 (1967) 1024.
8. E. P. Manche and B. Carroll, Thermochim. Acta, 25 (1978) 77.
9. K. Kishore, Thermochim. Acta, 19 (1977) 226.
10. C. D. Doyle, J. App. Polym. Sci., 6 (1962) 639.
11. K. M. Caldwell, P. K. Gallagher and D. W. Johnson, Jr., Thermochim. Acta, 18 (1977) 15.
12. M. Selvaratnam and P. D. Garn, J. Am. Ceram. Soc., 59 (1976) 376.
13. J. Zsako, J. Therm. Anal., 7 (1975) 33.
14. K. J. Laidler, Trans. Far. Soc., 55 (1959) 1725.
15. J. Zsako, J. Therm. Anal., 9 (1976) 101.

TABLE I

KINETIC DATA FOR LIQUID MONOPROPELLANT

1. ACTIVATION ENERGY BY DIFFERENT METHODS

URICHEK	ROGERS AND MORRIS	DOUBLE REACTION RATE	VARIABLE HEATING RATE
		E, KCAL/MOLE	
48.1 (40.4)*	37.4 (35.9)*	39.1 (37.7)*	39.8

*VALUES FOUND USING DASHED BASELINE

2. VARIABLE HEATING DATA

β, ^{o}C/MIN	1	2	5	10	15	20
T_{MAX}, ^{o}C	187.5	197.5	204.5	212.5	216	222

3. HEAT EVOLUTION DATA

CURVE FRACTION	HEIGHT BLOCKS	AREA*, IN^2	TEMP., ^{o}C
1	3.6	0.24	176.5
2	5.6	0.42	181
3	9.3	0.74	186.5
4	14.5	1.31	191.5
5	18.5	1.83	194.5
6	22.2	2.26	196.5
7	31.4	3.63	201.5
8	39.5	5.41	206.5

*TOTAL AREA OF CURVE IS 13.63 IN^2

TABLE II

KINETIC CONSTANTS FOR THE VOLATILIZATION OF NITROGLYCERIN IN A CROSSLINKED DOUBLE BASE PROPELLANT (CYLINDRICAL)

SAMPLE	CONDITION	E(1) KCAL/MOLE	LOG A MIN^{-1}	K(2)	$T_{0.5}$(3) DAYS
CDB-2	VACUUM	8.5	2.97	1.09×10^{-3}	0.4
	HELIUM	13.0	5.16	1.22×10^{-4}	3.9
	NITROGEN	16.7	6.97	2.05×10^{-5}	23.5
AGED CDB-2	VACUUM	9.8	3.22	2.40×10^{-4}	2.0
	HELIUM	15.4	6.43	4.78×10^{-5}	10.1
	NITROGEN	19.2	8.34	8.66×10^{-6}	55.6
CDB-3	VACUUM	6.9	2.23	2.58×10^{-3}	0.2
	HELIUM	12.2	4.86	2.20×10^{-4}	2.2
	NITROGEN	13.8	5.39	5.72×10^{-5}	8.4
CDB-3	HELIUM	12(4)			
	HELIUM	12(5)			
	HELIUM	18(6)			
	HELIUM	18(7)			

(1)ACTIVATION ENERGY OBTAINED FROM LOG ($\Delta\alpha/\Delta t$) DATA (MANCHE-CARROLL METHOD)

(2)RATE CONSTANT IN MIN^{-1} AT 40°C

(3)HALF-LIFE IN DAYS AT 40°C FOR FIRST ORDER REACTION

(4)VALUE FROM FIRST ORDER PLOT

(5)VALUE FROM KISHORE PLOT

(6)VALUE FROM OZAWA PLOT

(7)VALUE FROM DOYLE PLOT

TABLE III

KINETIC CONSTANTS FOR THE VOLATILIZATION OF NITROGLYCERIN IN A CROSSLINKED DOUBLE BASE PROPELLANT (POWDER)

SAMPLE	CONDITION	$E^{(1)}$ KCAL/MOLE	LOG A MIN^{-1}	$K^{(2)}$	$T_{0.5}{}^{(3)}$ DAYS
CDB-1	VACUUM	18	10.26	4.95×10^{-3}	0.1
	HELIUM	18	3.78	1.64×10^{-4}	2.9
	NITROGEN	18	8.21	4.40×10^{-5}	10.9
AGED CDB-1	VACUUM	18	10.37	6.38×10^{-3}	0.07
	HELIUM	18	8.83	2.06×10^{-4}	2.3
	NITROGEN	18	8.35	6.02×10^{-5}	8.0
CDB-1	HELIUM	18(4)			
	HELIUM	18(5)			

(1) ACTIVATION ENERGY OBTAINED FROM LOG ($\Delta\alpha/\Delta\tau$) DATA (MANCHE-CARROLL PLOT)

(2) RATE CONSTANT IN MIN^{-1} AT 40°C

(3) HALF-LIFE IN DAYS AT 40°C FOR FIRST ORDER REACTION

(4) VALUE FROM FIRST ORDER PLOT

(5) VALUE FROM KISHORE PLOT

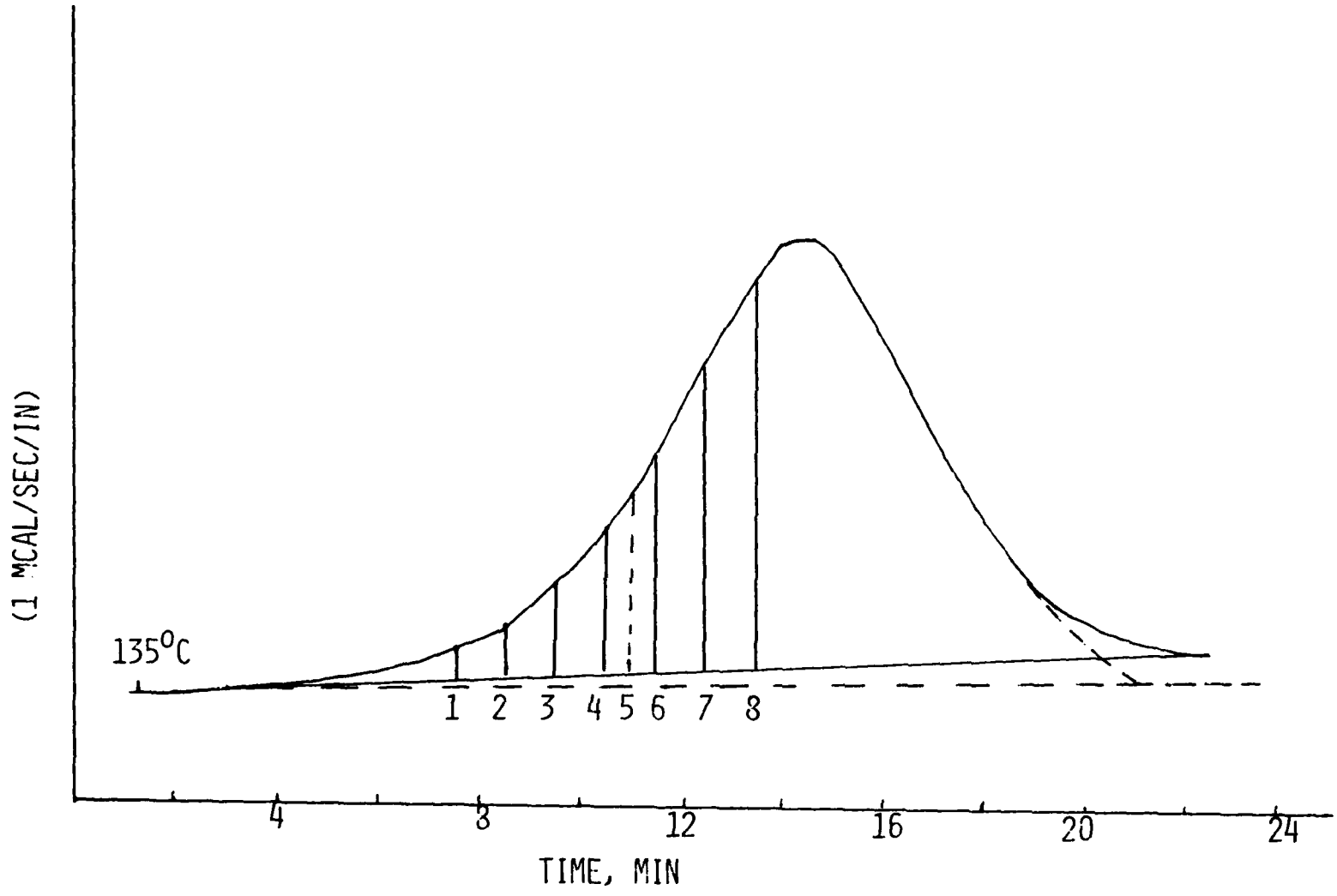

FIGURE 1: DSC CURVE FOR LIQUID MONOPROPELLANT

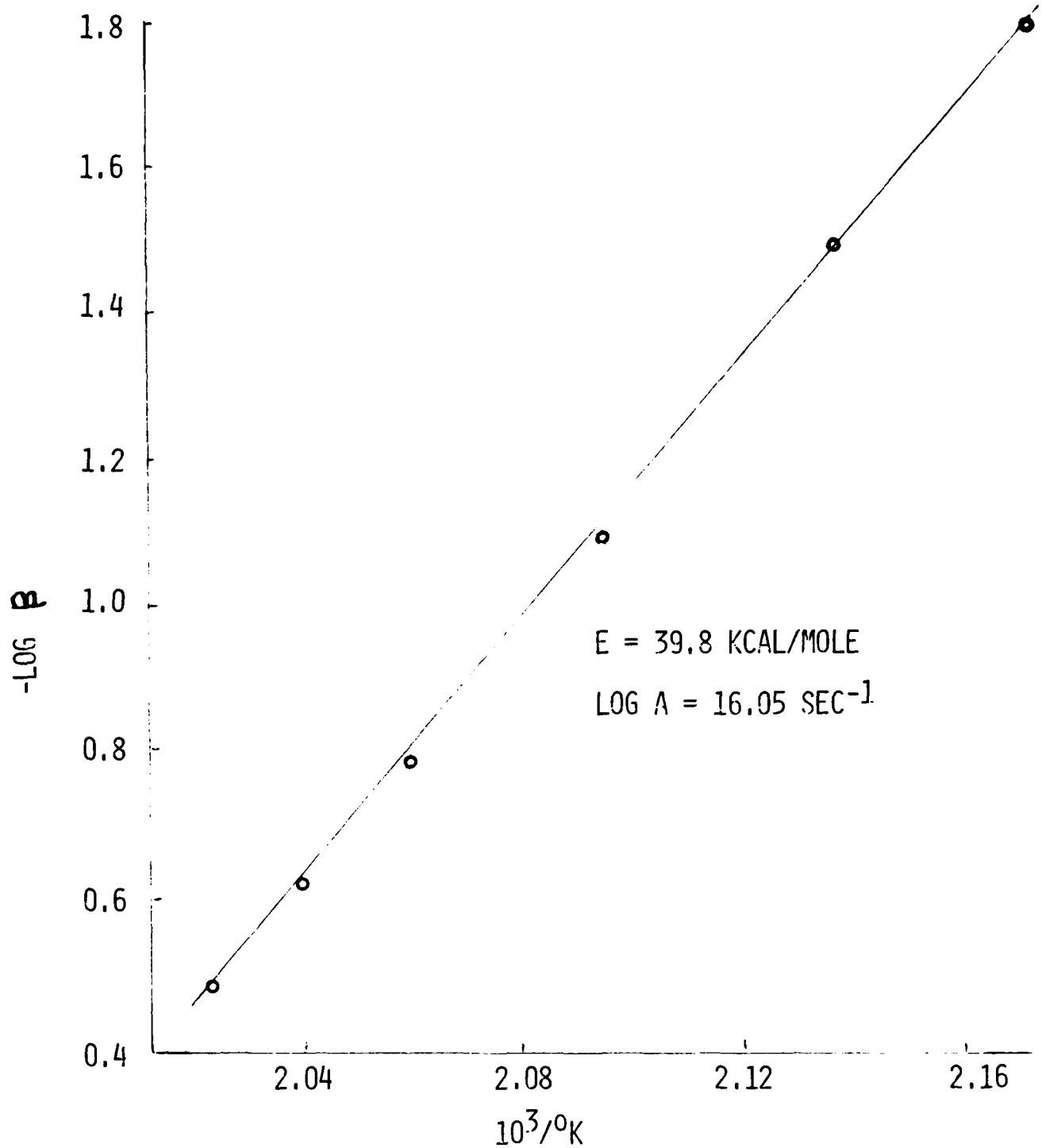

FIGURE 2: VARIABLE HEATING RATE VERSUS RECIPROCAL OF THE ABSOLUTE TEMPERATURE (OZAWA PLOT) FOR A LIQUID MONOPROPELLANT

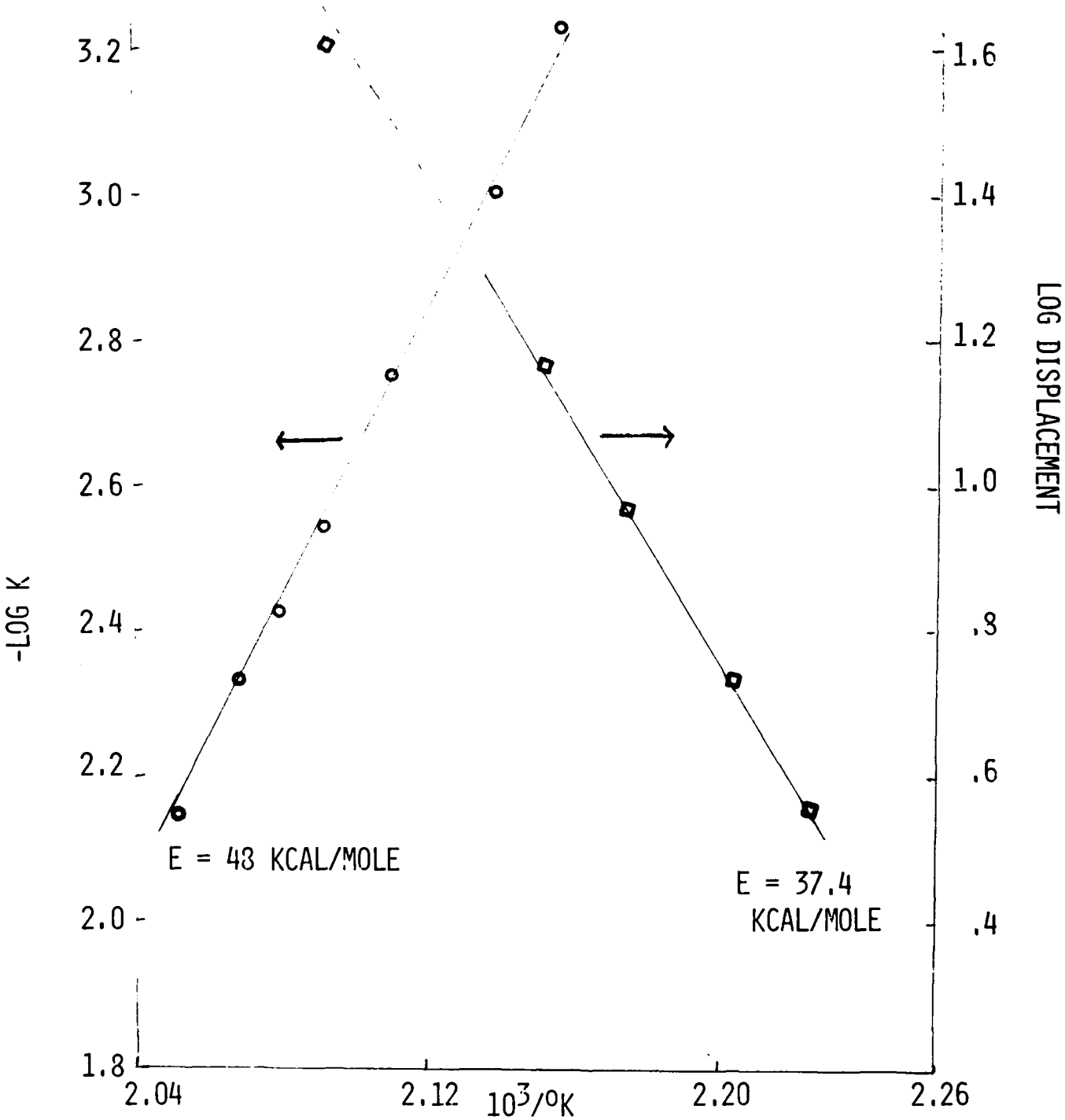

FIGURE 3: PLOT OF LOG K (URICHEK) AND LOG DISPLACEMENT (ROGERS AND MORRIS) VERSUS RECIPROCAL OF THE ABSOLUTE TEMPERATURE FOR A LIQUID MONOPROPELLANT

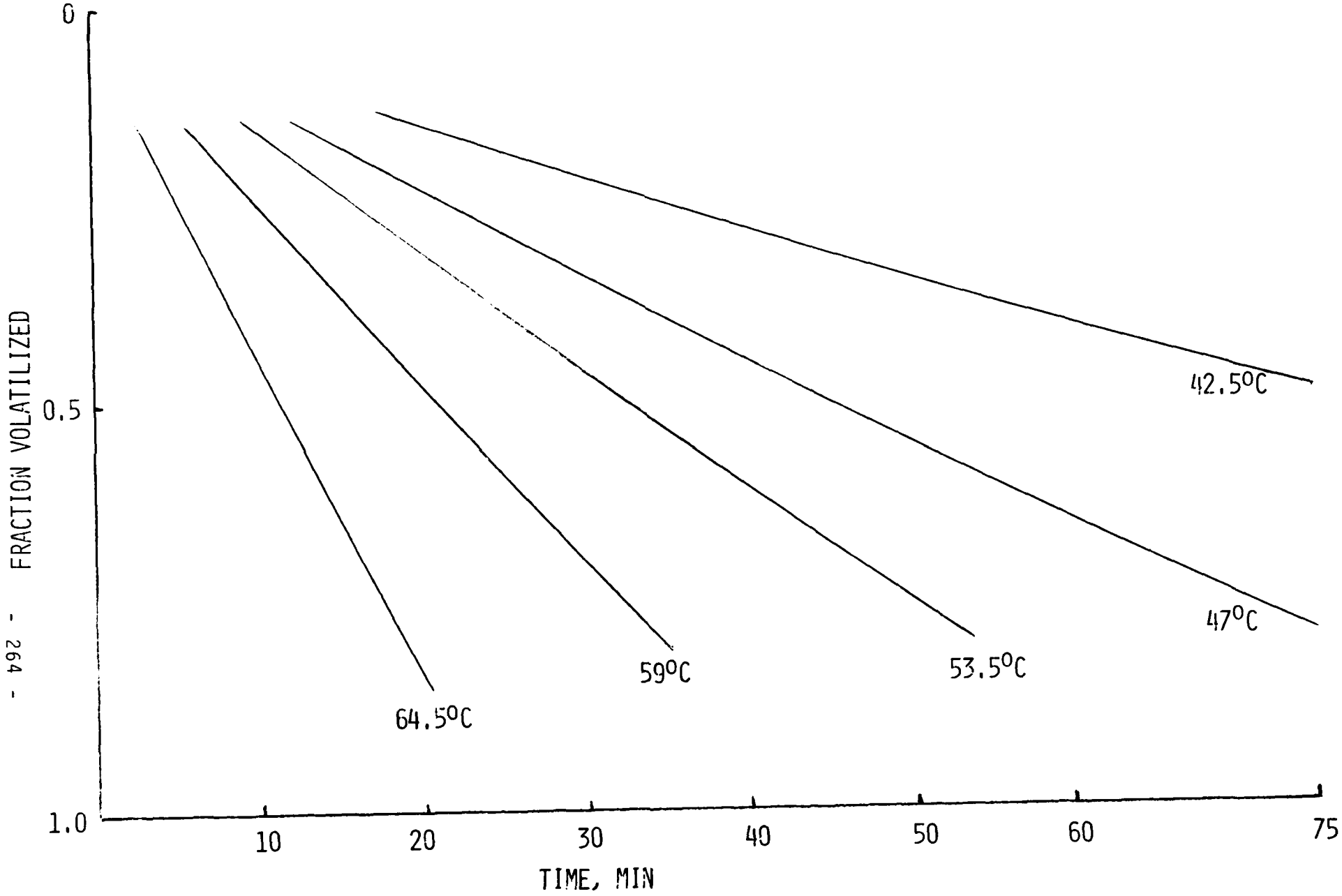

FIGURE 4: ISOTHERMAL TG CURVES IN VACUUM FOR NITROGLYCERIN IN CROSSLINKED DOUBLE BASE PROPELLANTS (CDB-1, POWDER FORM)

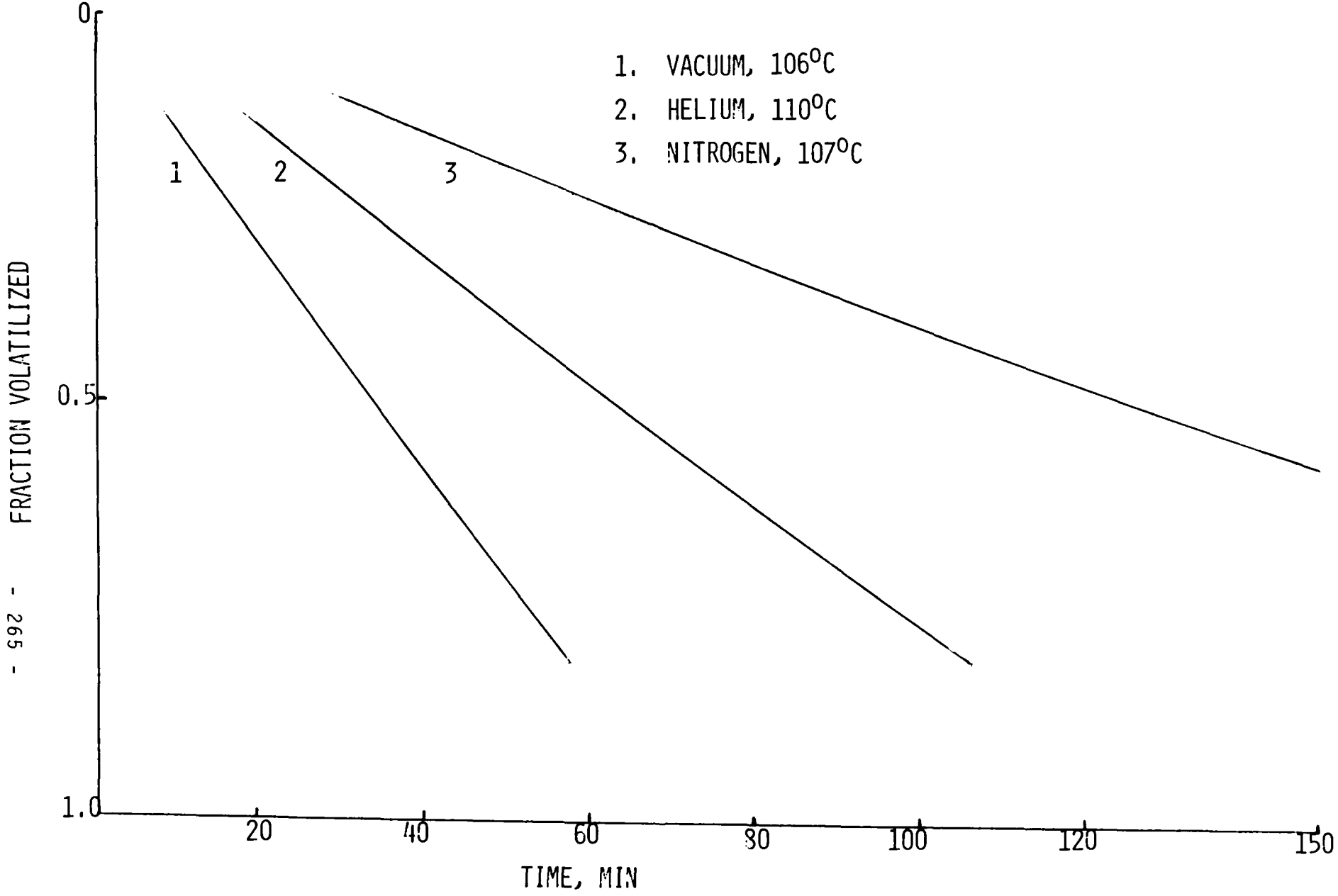

FIGURE 5: ISOTHERMAL TG CURVES FOR NITROGLYCERIN IN CROSSLINKED DOUBLE BASE PROPELLANTS (CDB-3) IN VACUUM, HELIUM, AND NITROGEN

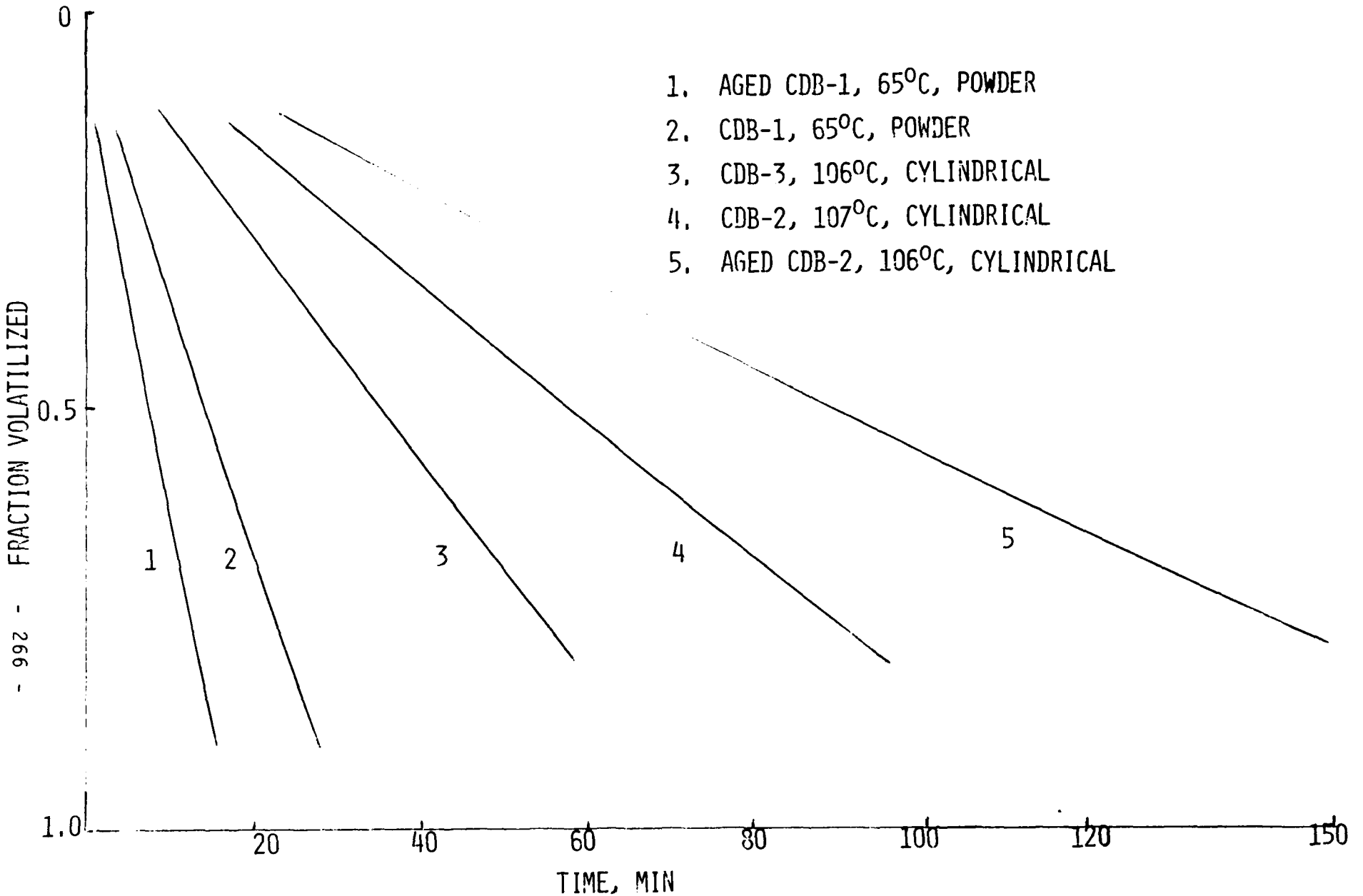

FIGURE 6: ISOTHERMAL TG CURVES IN VACUUM FOR NITROGLYCERIN IN CROSSLINKED DOUBLE BASE PROPELLANTS IN THE FORM OF POWDERS AND CYLINDRICAL PIECES

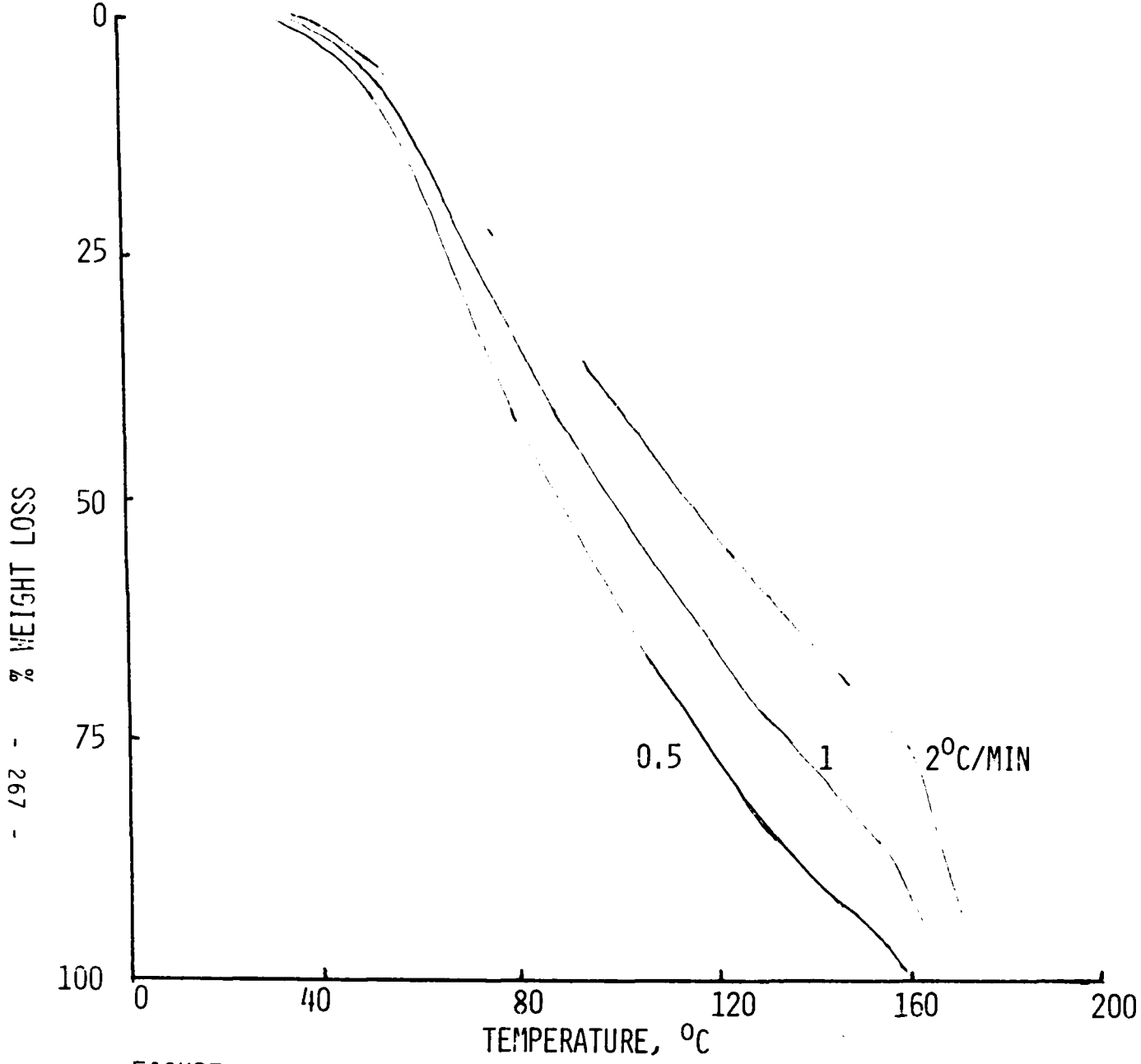

FIGURE 7: DYNAMIC TG CURVES FOR NITROGLYCERIN IN CROSSLINKED DOUBLE BASE PROPELLANT (CDB-2) IN VACUUM AT DIFFERENT HEATING RATES

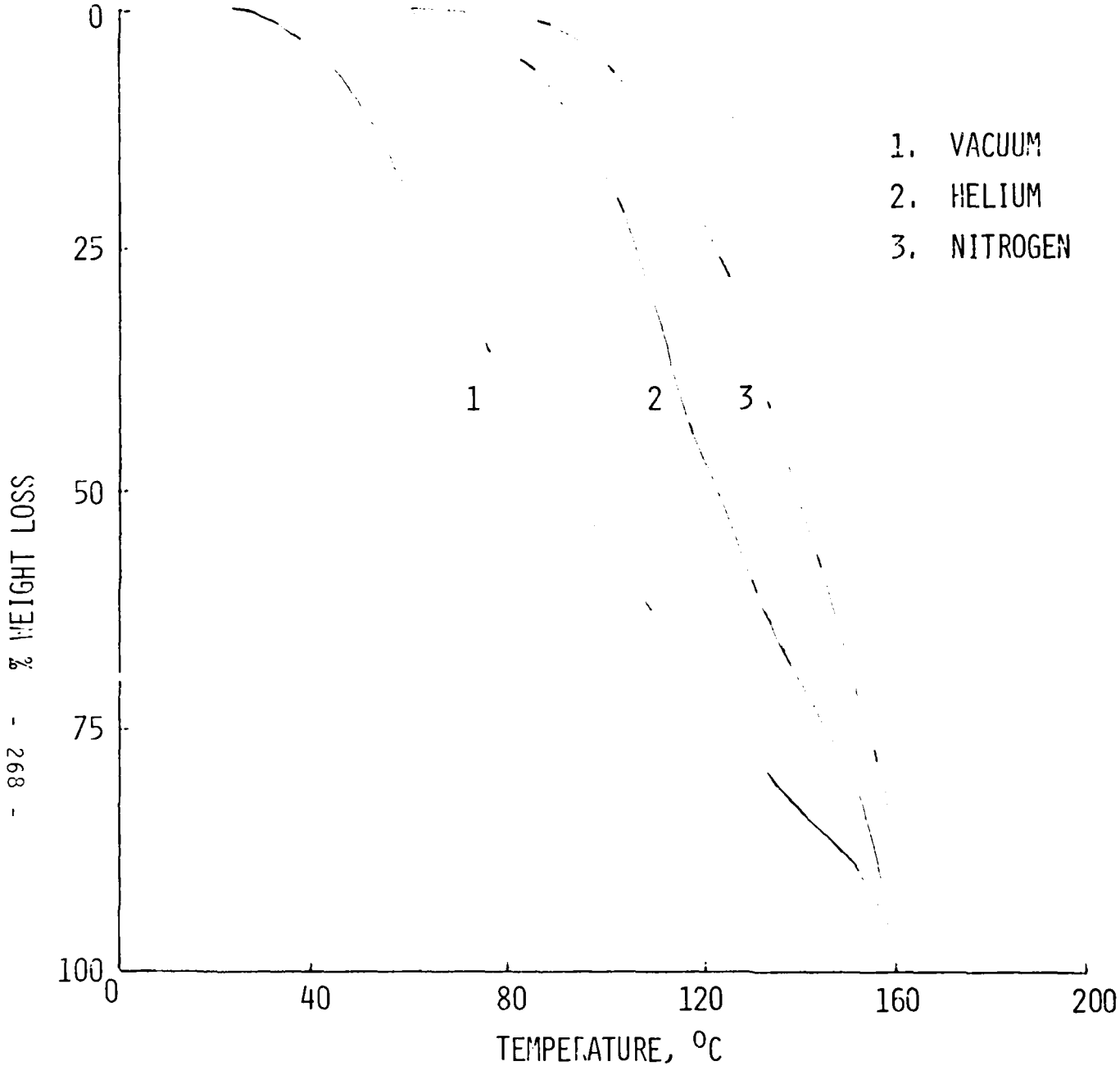

FIGURE 8: DYNAMIC TG CURVES FOR NITROGLYCERIN IN CROSSLINKED DOUBLE BASE PROPELLANTS (AGED CDB-2) IN VACUUM, HELIUM, AND NITROGEN AT 0.5°C/MIN

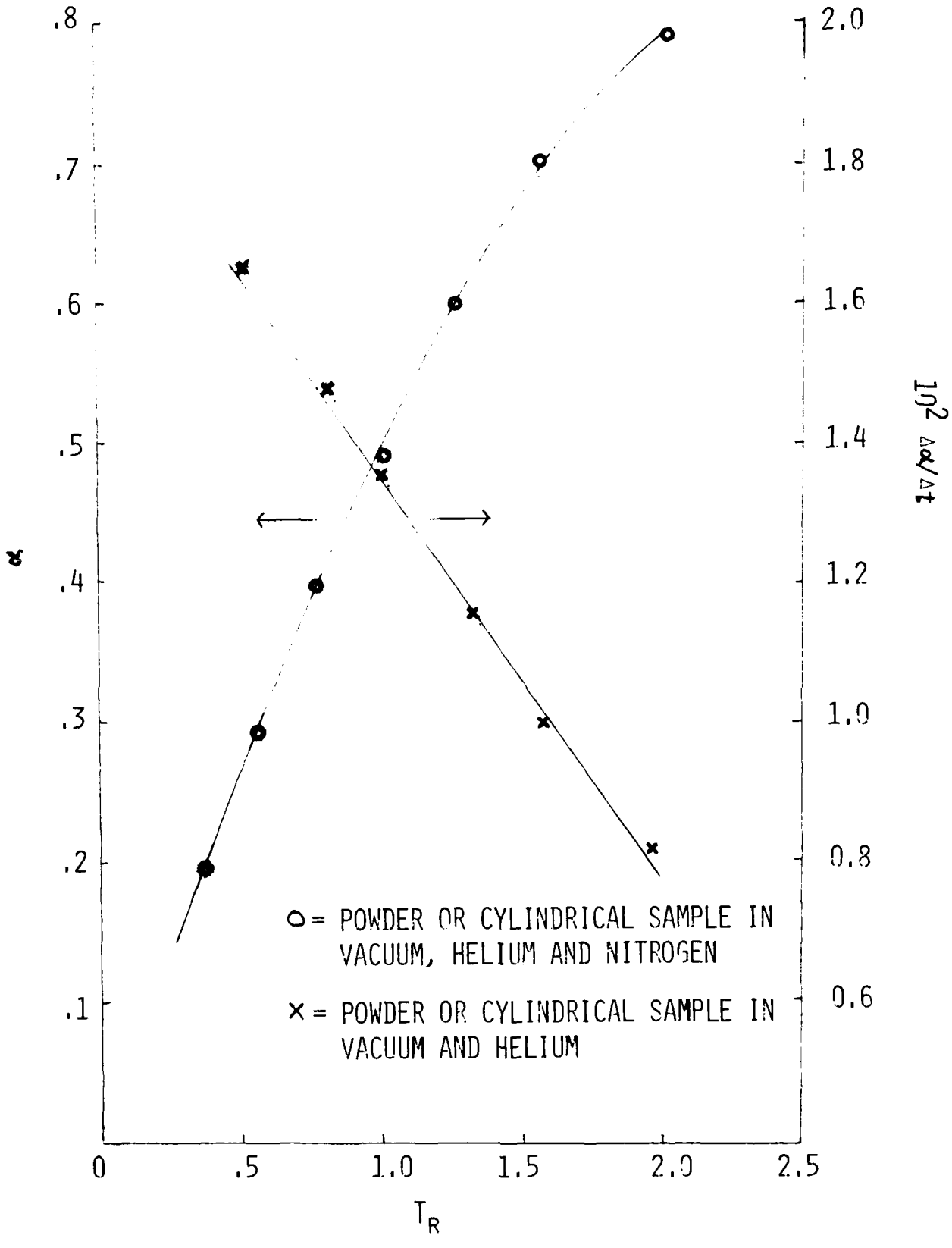

FIGURE 9: REDUCED TIME PLOT FOR VOLATILIZATION OF NITROGLYCERIN IN A CROSSLINKED DOUBLE BASE PROPELLANT (CDB-1 POWDER, CDB-3 CYLINDRICAL)

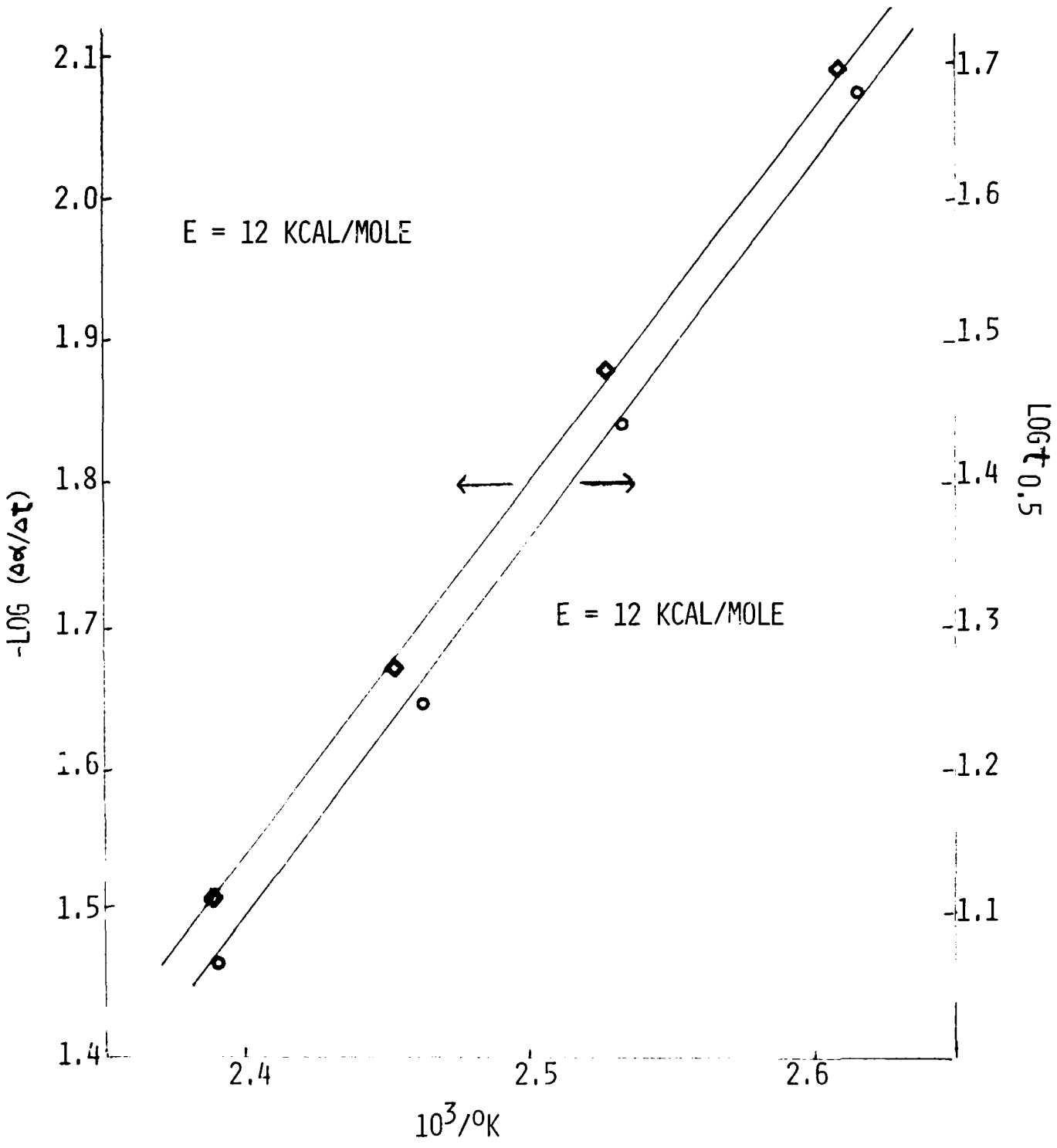

FIGURE 10: PLOT OF LOG (Δα/Δt) (MANCHE-CARROLL) AND LOG $t_{0.5}$ (KISHORE) VERSUS RECIPROCAL OF THE ABSOLUTE TEMPERATURE FOR VOLATILIZATION IN HELIUM OF NITROGLYCERIN IN A CROSSLINKED DOUBLE BASE PROPELLANT (CDB-3, CYLINDRICAL)

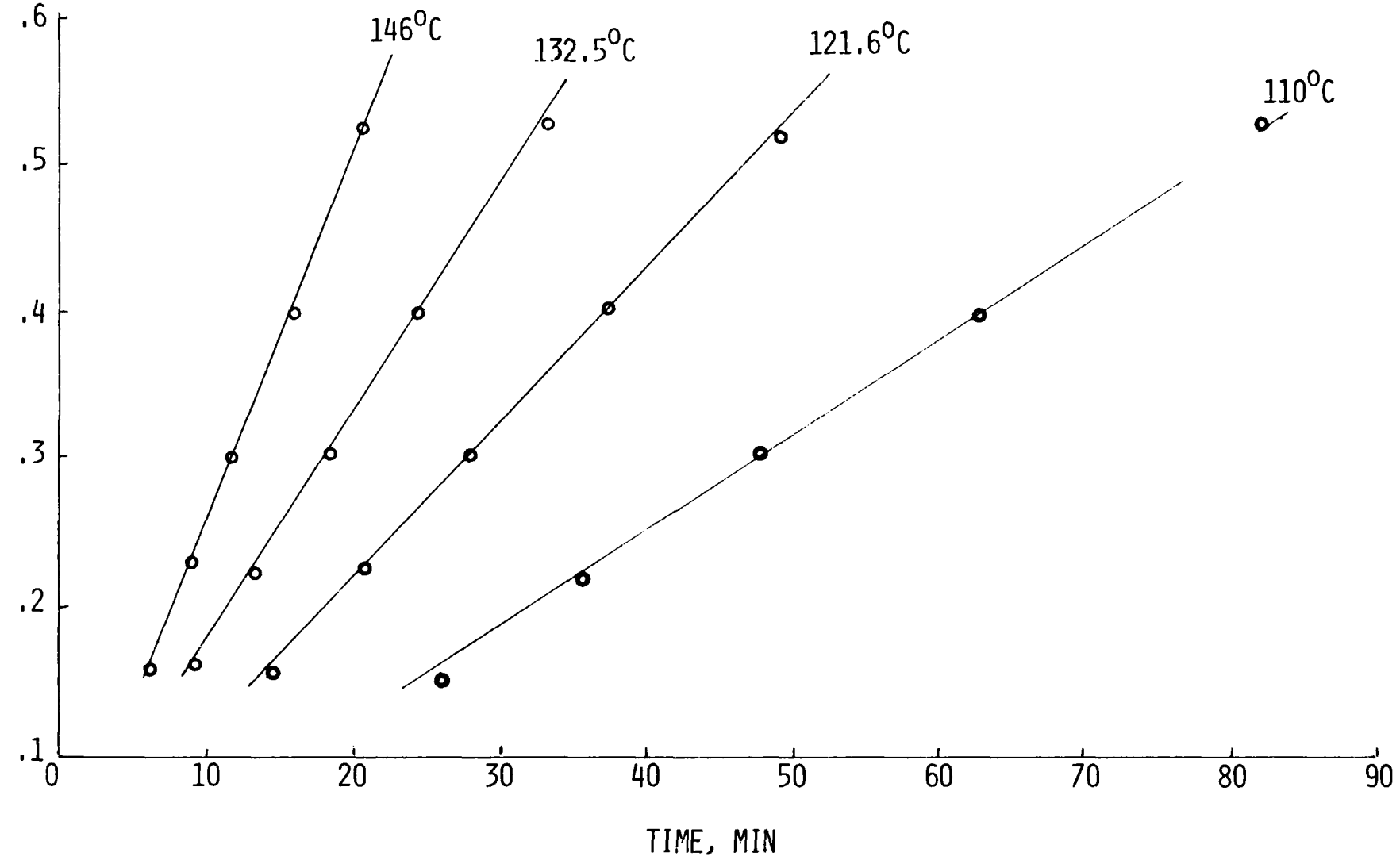

FIGURE 11: PLOT OF LOG (1-∝) (FIRST ORDER) VERSUS TIME FOR VOLATILIZATION IN HELIUM OF NITROGLYCERIN IN A CROSSLINKED DOUBLE BASE PROPELLANT (CDB-3, CYLINDRICAL)

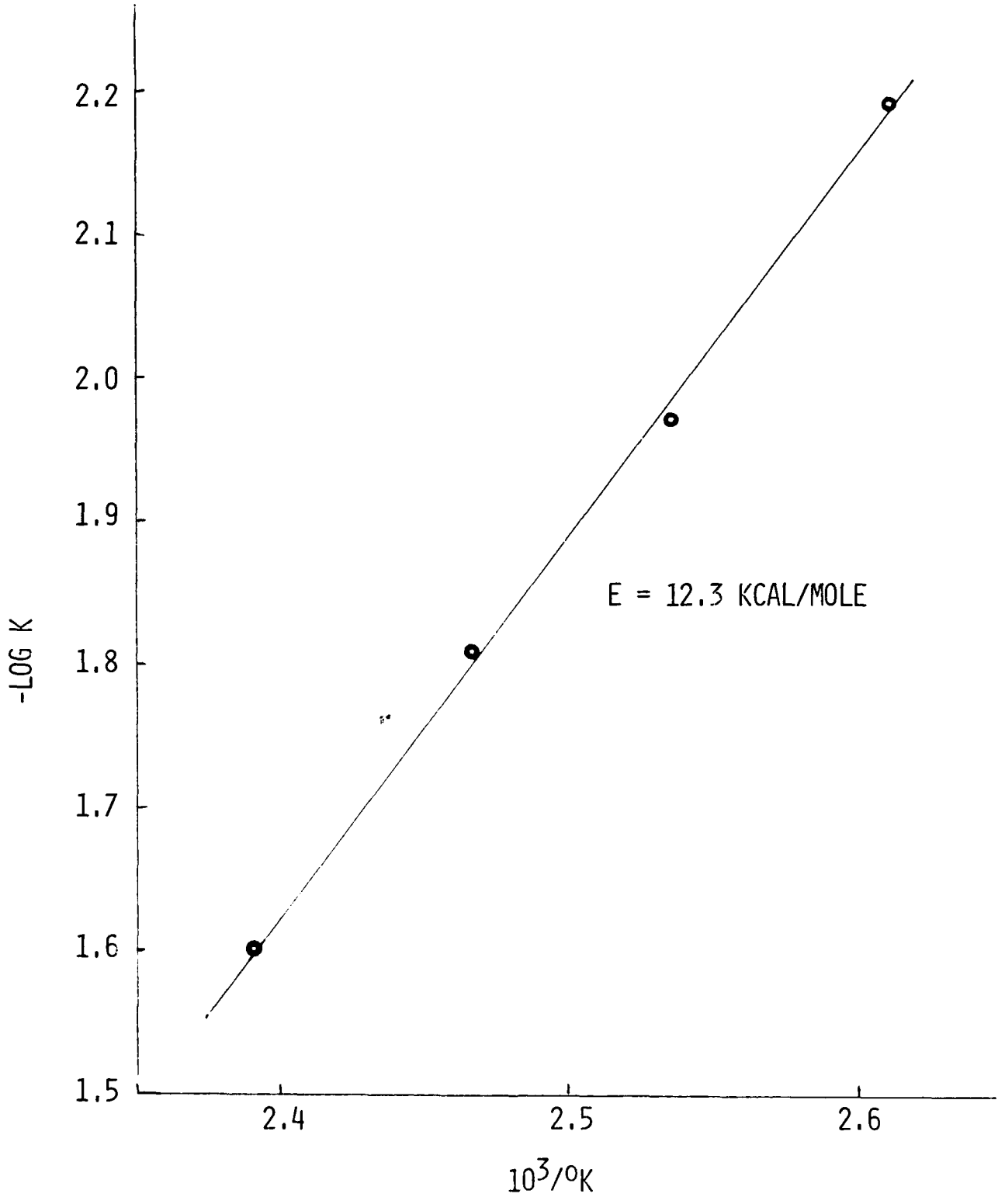

FIGURE 12: ARRHENIUS PLOT FOR VOLATILIZATION IN HELIUM OF NITROGLYCERIN IN A CROSSLINKED DOUBLE BASE PROPELLANT (CDB-3, CYLINDRICAL)

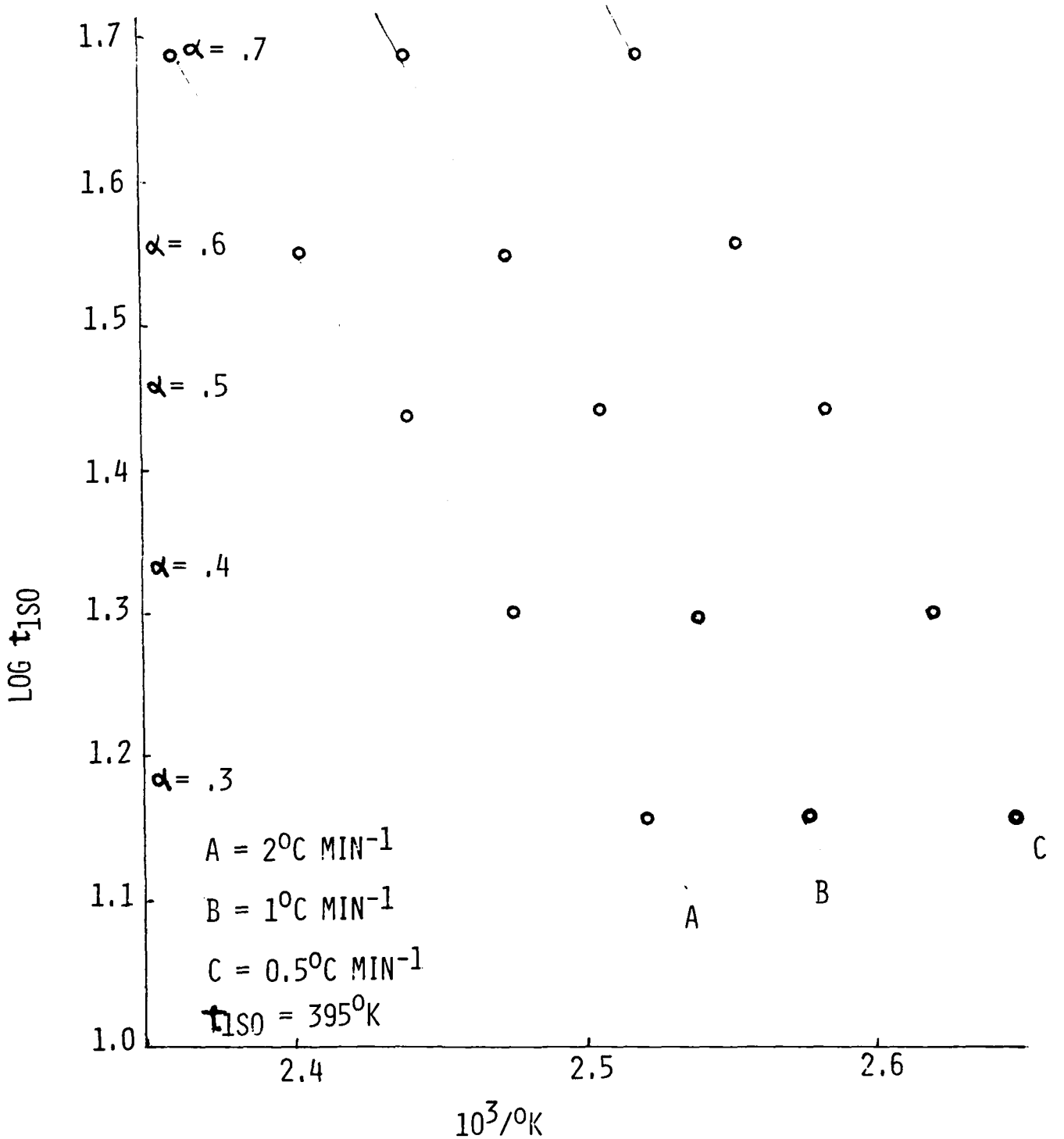

FIGURE 13: CORRELATION BETWEEN ISOTHERMAL AND DYNAMIC HEATING AT THE SAME VOLATILIZATION FRACTION (DOYLE'S METHOD) IN HELIUM OF NITROGLYCERIN IN A CROSSLINKED DOUBLE BASE PROPELLANT (CDB-3, CYLINDRICAL)

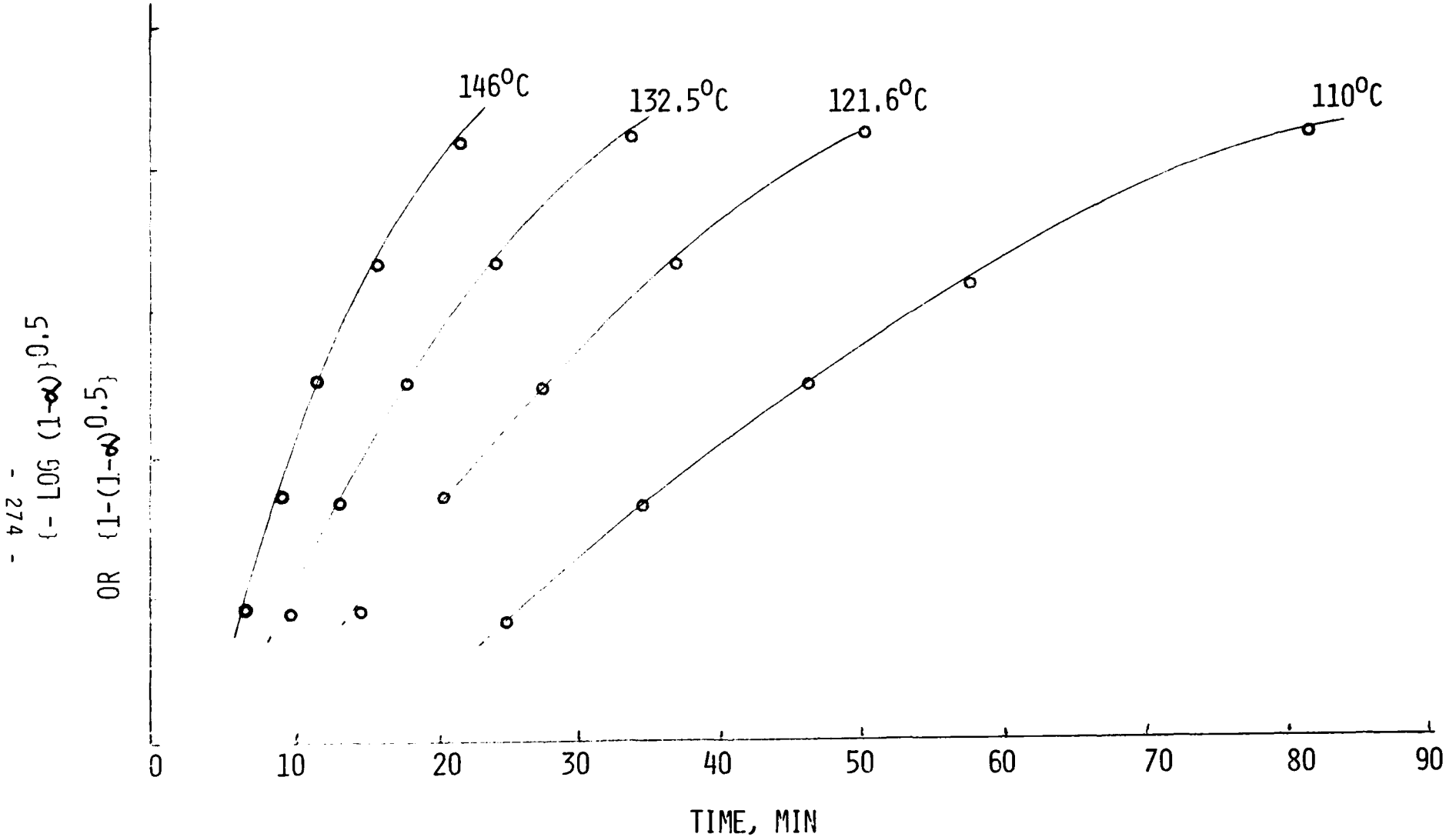

FIGURE 14: PLOT OF $\{-\text{LOG}\ (1-\alpha)\}^{0.5}$ (AVRAMI-EROFEEV) OR $\{1-(1-\alpha)^{0.5}\}$ (CONTRACTING AREA) VERSUS TIME FOR VOLATILIZATION IN HELIUM OF NITROGLYCERIN IN A CROSSLINKED DOUBLE BASE PROPELLANT (CDB-3, CYLINDRICAL)

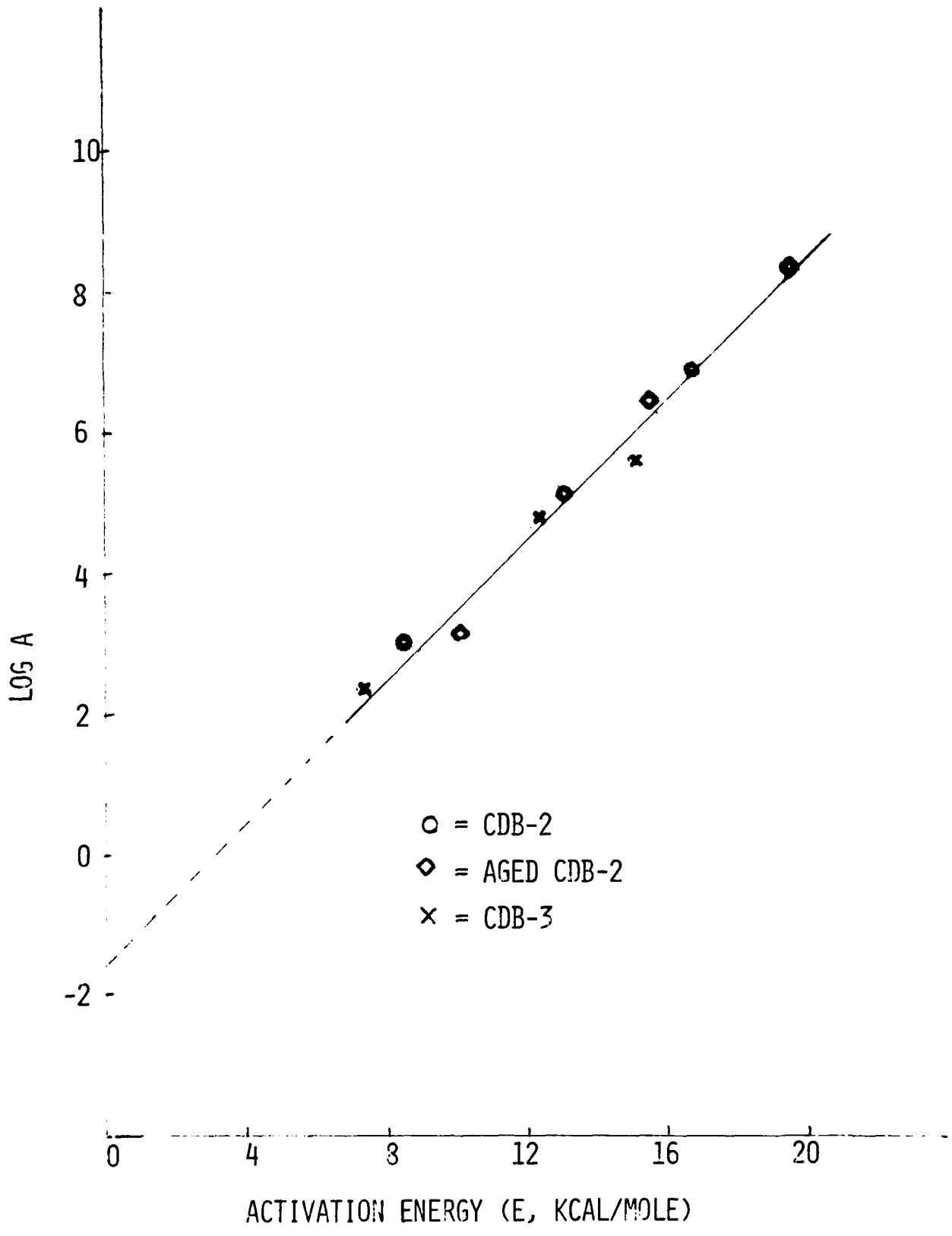

FIGURE 15: KINETIC COMPENSATION PLOT FOR ISOTHERMAL TG DATA IN VACUUM, HELIUM AND NITROGEN FOR VOLATILIZATION OF NITROGLYCERIN IN CROSSLINKED DOUBLE BASE PROPELLANTS (CDB-2 AND CDB-3, CYLINDRICAL)

REAL-TIME LOW TEMPERATURE NC AND PBX 9404 DECOMPOSITION STUDIES

by

Dr. Hermann N. Volltrauer and Dr. Arthur Fontijn
AeroChem Research Laboratories, Inc.

ABSTRACT

The use of chemiluminescence techniques has made it possible to make continuous real-time measurements of trace quantities of gases. This development, originally aimed at atmospheric (pollution) studies, has in the present work been extended to obtain information on the NO_2/NO production kinetics from nitrocellulose (NC), PBX 9404, and (eventually) other explosives. Measurements are made in the 20-140°C range at pressures from 0.02-1 atm. Data are obtained by passing inert gas over samples contained in temperature controlled cells and measuring the NO_2/NO content in the effluent. The chemiluminescence technique is sufficiently sensitive to detect 0.01 part per billion of NO_2/NO in the effluent.

Measurements at 1 atm on 12% nitrogen content NC powder in the 20-80°C temperature range yield a rate coefficient for NO_x (= NO_2 + NO) evolution of $3.4 \times 10^7 \exp(-13000/T)$ sec^{-1}. A different decomposition mechanism dominates at temperatures above 100°C where a rate coefficient of $1.2 \times 10^{16} \exp(-19500/T)$ sec^{-1} is measured. These rate coefficients are in terms of moles of NO_x released per submole ($\approx$ 280 g) NC. After NC samples are exposed to temperatures above 80°C, their lower temperature NO_x evolution rate is increased by an amount dependent on the temperature and, to a lesser extent, time of such exposure. This effect can be attributed to NO_2 absorption by the NC when evolved at high rates at elevated temperature; the activation energy of the subsequent desorption process is 16 kcal $mole^{-1}$. Experiments in which the inert gas pressure is varied indicate that NO_2 is the primary NC decomposition product and NO is produced by the NO_2 reduction near the molecular release site in the solid. Adding large quantities of NO_2 to the carrier gas flow has little effect on the NC decomposition rate below 80°C as measured by NO evolution; neither does the addition of the secondary gaseous NC decomposition products N_2O, CO_2, and O_2. However, addition of CO leads to definite increases in NO_x evolution. These and additional observations will be discussed in terms of decomposition mechanisms.

The NO_x evolution rate of PBX 9404 below 80°C is $4.5 \times 10^8 \exp(-13000/T)$ sec^{-1}, calculated based on its 3% NC content, i.e., a factor 45/3.4 = 13 higher than calculated from the corresponding NC decomposition rate coefficient. Since NC is thought to be by far the least stable component of PBX 9404, this is a surprising result but it is in agreement with independent observation at the Lawrence Livermore Laboratory. Several possible causes for these observations will be discussed. Tests on PBX 9404 and further constituent components (HMX, diphenylamine) are under way to help establish the correct explanation.

METHODOLOGY OF COMPATIBILITY, STABILITY AND SAFETY EVALUATION DURING RESEARCH AND DEVELOPMENT OF ENERGETIC MATERIALS FOR GUN AMMUNITION PROPELLING CHARGES

M. STEPHAN and B. ZELLER

Société Nationale des Poudres et Explosifs, Centre de Recherches du BOUCHET
91710 VERT LE PETIT (FRANCE)

ABSTRACT

At each stage of research and development of energetic materials for gun ammunition propelling charges, compatibility, stability and safety tests are needed. Results of these tests may modify development or even stop it.

In the field of compatibility, main methods are vacuum test and differential scanning calorimetry. In the case of solvent-extruded propellants, specific methods are needed to test the compatibility of ingredients with solvents.

Stability tests performed may use new methods such as chemiluminescence or heat flow calorimetry. A stabiliser consumption test at 50°C is now widely used.

Safety tests include sensitivity tests, a specific extrusion test, determination of critical height of explosion and predetonation length. In some cases vulnerability to shaped charge jets is determined.

INTRODUCTION

The need for higher performances in the field of artillery and small caliber weapons involves development of new propellants having improved properties and also of new concepts such as consolidated charges, caseless ammunitions and combustible cartridges.

A part of these developments includes the use of new energetic materials generally obtained by mixing energetic and inert components. Another part lies in the improvement of existing products, which involves some modifications either of the ingredients or of the manufacturing process.

In order to achieve development of these new products, it is necessary to perform compatibility, stability and safety tests at various steps of the investigations.

Figure 1 represents schematically the various stages and corresponding tests from initial ingredients to finished products.

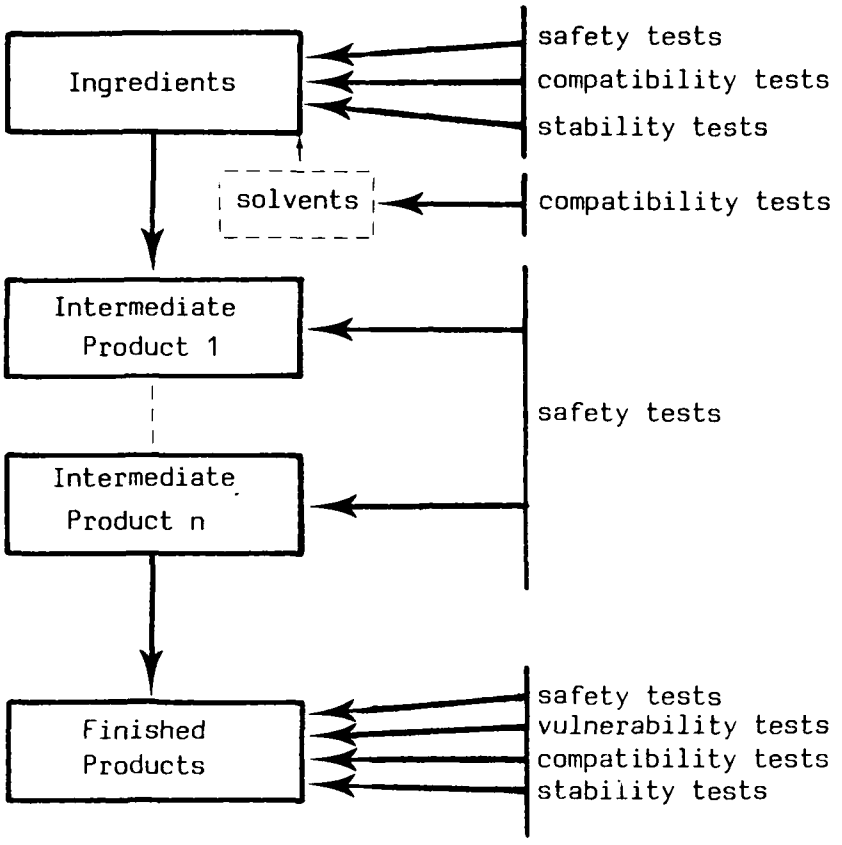

Fig. 1. Diagram of methodology of compatibility, stability and safety evaluation during research and development of energetic materials.

- compatibility tests are required between ingredients, between ingredients and solvents (for solvent-processed propellants) and between final products and other materials (such as plastics) depending on their employment.

- stability tests are also required both on ingredients and on finished products.

- safety tests are needed on the ingredients, on intermediate products (such as solvent wet mixtures or "green" grains) and on finished products.

COMPATIBILITY

Compatibility tests are performed on ingredients of a given mixture mainly in order to avoid the possibility of rapid decomposition reaction. In the case of solvent-processed propellants, the problem of compatibility of ingredients with solvents appears. On finished products, compatibility tests are also performed in order to determine the conditions in which they can be used.

Compatibility between ingredients

Research of new propellants is mainly based on the results of preliminary thermodynamical computations which help defining compositions having interesting properties : high force, high density, moderate flame temperature, low flammability combustion products.

It is necessary to check compatibility of ingredients one with another and all together.

Compatibility is tested in two steps : the first step uses differential scanning calorimetry, the second step uses vacuum test.

Differential scanning calorimetry

It is mainly used

- to detect the ingredients having a poor thermal stability and which cannot be incorporated in a formulation.

- to show strong incompatibilities which would induce violent and hazardous reactions.

- to detect incompatibilities which do not induce gas evolution and could not be detected by vacuum test.

Two ingredients are not compatible when decomposition temperature (observed by D.S.C.) is lower than lowest of the two decomposition temperatures of ingredients alone.

Usually only strong incompatibilities are revealed by this test.

Vacuum test

The second step of compatibility evaluation is based on vacuum test. The method and the requirements are not absolutely rigid and are adapted to the specific problem.

Currently the test is performed on one gram of a mixture of ingredients. Accumulation time is 200 hours at 100°C. Volume of generated gas is measured and compared with volume of gas evolved by ingredients alone.

If gas evolution is low ($\leqslant 5$ cm^3) under these time and temperature conditions, ingredients are compatible and no more test is performed at this stage.

If vacuum testing gives some amount of gases ($\geqslant 5$ cm^3), test temperature is lowered (for instance down to 80°C or 60°C) depending on temperatures encountered during manufacturing and employment of the finished product.

In order to get more information about possible reason of incompatibility, gas generated during the test is collected and analysed by mass spectrometry : it can determine whether gas is generated by actual decomposition reactions of the energetic material or only by side reactions (such as reaction of isocyanate on water which produces carbon dioxide).

The curve of gas evolved versus time is also recorded, because it gives information on reaction process.

General procedure is represented on figure 2.

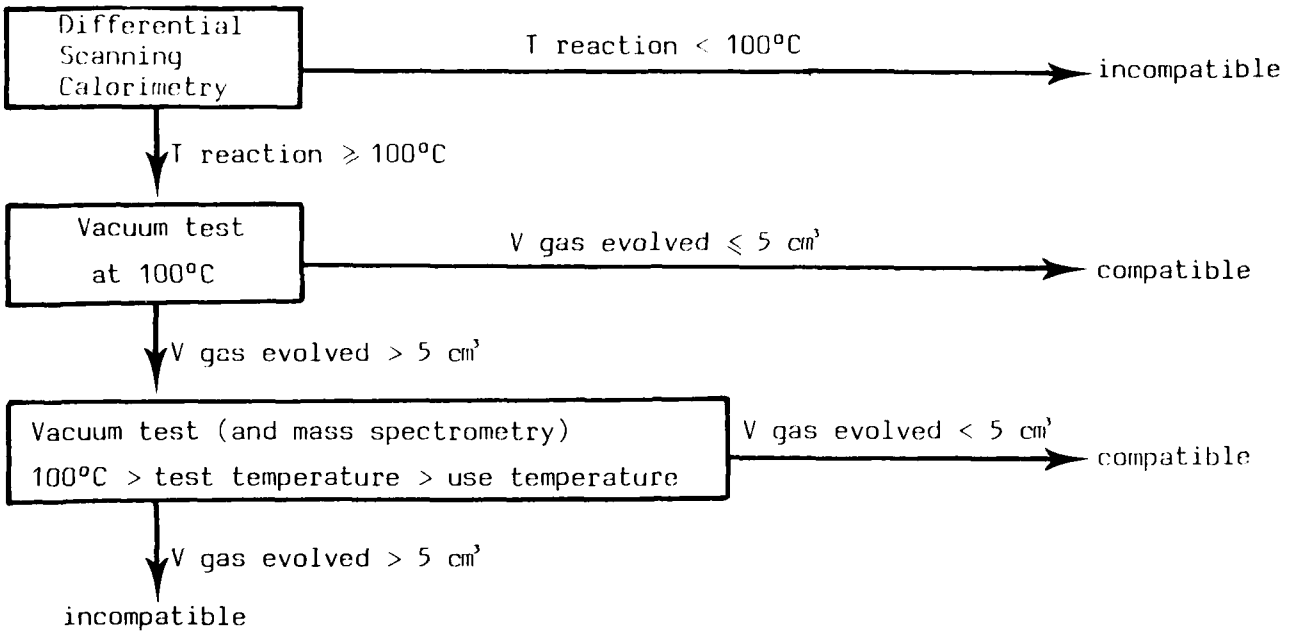

Fig. 2. General procedure for testing compatibility of ingredients

This procedure requires to know what temperatures will be encountered during processing and employment of the product.

It was applied to mixtures of nitrocellulose (NC) and hexamethylenediisocyanate (HMDI). Requirement was that temperature had to be lower than 80°C.

D.S.C. did not show any strong incompatibility. Vacuum test at 100°C, 80°C and 60°C revealed a poor compatibility which was checked by mass spectrometry : gas evolved is not only CO_2 but also N_2 and NO (see table 1). Incompatibility is actual above 80°C, but this mixture may be processed and used below 80°C.

TABLE 1

Compatibility of HMDI and NC at various temperatures using vacuum test and mass spectrometry

Differential Scanning Calorimetry	Vacuum Test			Mass spectrometry Analysis
Reaction temperature	Time (hours)	Temperature (°C)	Volume of gas (cm^3)	Gas evolved
N.C. alone 189°C	200	100	23.2	CO_2, N_2
N.C. + HMDI 162°C	200	80	5.76	CO_2, N_2
Rate of temperature increase : 8°C/mn	200	60	2.38	NO

Compatibility of ingredients with solvents

Nitrocellulose gun propellants are generally processed through gelatinization of nitrocellulose by means of low boiling point solvents (which are removed later) and extrusion through dies. The solvents are typically mixtures of ethyl ether and ethyl alcohol or acetone and ethyl alcohol.

The methods of studying compatibility which have been described above are no more adequate mainly because of the temperatures at which the tests are performed. Moreover, because of the limited time of contact of great quantities of solvent with the ingredients, compatibility requirements are not identical.

The method used to test compatibility of ingredients with solvents consists :

- first, to mix small quantities of ingredients and solvents at ambient temperature in order to check whether they react quickly (it can be seen by gas evolution, heat generation, changes of appearance or colour).

- second, if the results of the first test is negative, to mix larger quantities of ingredients and solvents (about 500 g of mixture) in a small remote-controlled (for safety purpose) sigma-blade mixer until gelatinization occurs (or not). After mixing the dough is examined,routine safety tests are also performed on it. This method reveals slow chemical reactions, yet fast enough to prohibit the use of a specific ingredient or solvent.

An example is the slow reaction between acetone and triaminoguanidine nitrate. Binary compositions containing nitrocellulose (NC) and triaminoguanidine nitrate (TAGN) have promising thermodynamical properties : high force with moderate temperature of explosion. It seems quite normal to use a mixture of acetone and ethyl alcohol to gelatinize them. The method described above has been applied :

- no visible reaction occurs when mixing small quantities of acetone and TAGN.

- the mixture of acetone-alcohol-TAGN-NC in the sigma-blade mixer does not lead to the gelatinization, some water appears : it is not possible to extrude the dough.

Complementary investigations showed that acetone have reacted slowly with TAGN.

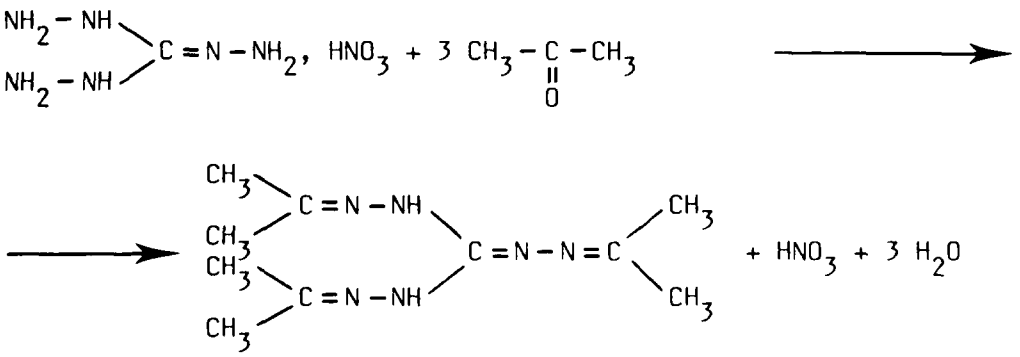

Reaction scheme is similar to that of hydrazines on acetone. Acetone cannot be used with TAGN. A mixture of ethyl acetate and ethyl alcohol is convenient (it was checked that ethyl acetate does not react with TAGN).

Compatibility of finished products

Specific tests are performed on finished products, depending on their use.

Routine compatibility tests are performed on mixtures of gun propellant and plastics used in some propelling charges.

Specific methods are used to test the compatibility of combustible cartridges or caseless ammunitions with hydraulic fluid.

Also the problem of migration of nitroglycerin from either the propellant or ignition tube into the combustible cartridge (a mixture of kraft fibers, nitrocellulose fibers and synthetic resin) has to be studied by moderately accelerated agings.

Tests depend on the product and its employment conditions.

STABILITY

Chemical stability tests are performed on energetic ingredients and on finished products.

Routine methods are sometimes inadequate and new methods have been or are developed. They allow to refine the judgment on the stability of a product. Three of these new methods are described below.

Chemiluminescence

Numerous tests depend on detection or measurement of gas evolution to estimate nitrocellulose stability. All of them either need a long time before they give any significant result or are performed at so high temperatures that it becomes difficult to interpret their results.

One of the advantages of chemiluminescence technique is the possibility of studying thermal decomposition of nitro compounds (for instance nitrocellulose) by a continuous real-time measurement of NO/NO_2 emission.

This technique, which has already been applied to test compatibility of propellants with plastics [1], depends on the quantitative emission of light when nitric oxide reacts with ozone (nitrogen dioxide is reduced into nitric oxide by a catalytic converter before analysis).

Nitrocellulose sample is held in a special cell which is designed in order that carrier gas (helium) passes through test sample before flowing into NO/NO_2 chemiluminescence analyser. The cell is in an adjustable temperature oven. At each temperature NO and NO_2 signals are recorded (figure 3).

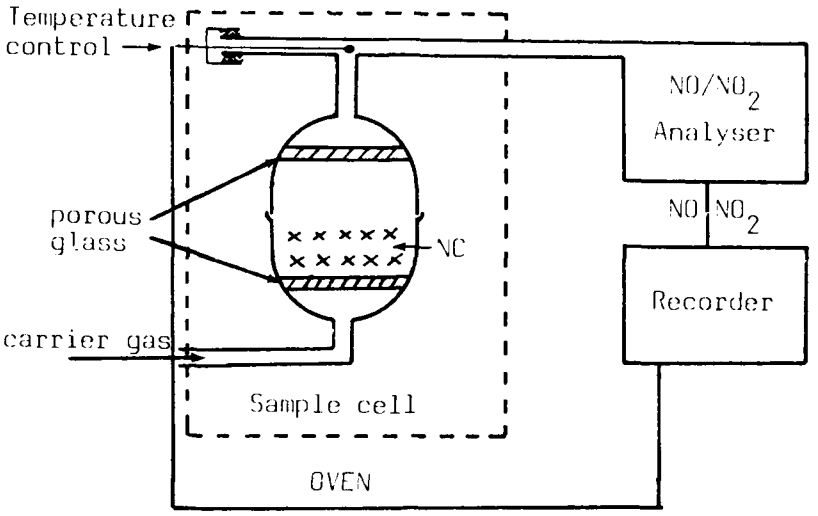

Fig. 3. Chemiluminescence : Schematic drawing of the apparatus

Measurements are performed at temperatures ranging from + 35°C up to + 110°C. Activation energies of decomposition reaction are computed by plotting Log NO_x versus 1/T. Figure 4 shows that there are two different decomposition mechanisms for a 13.4 % nitrogen content nitrocellulose :

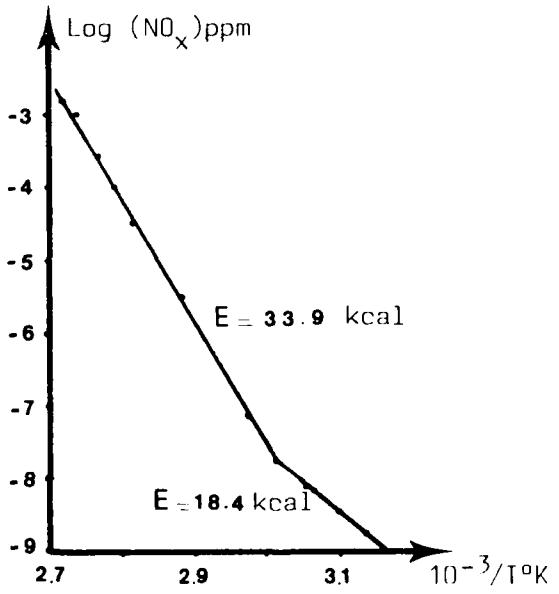

Fig. 4. Nitrocellulose (13.4 % N_2) NO + NO_2 emission between 45°C and 95°C

One, below 59°C, with an activation energy of 18.4 kcal/mole, the other above 59°C with an activation energy of 33.9 kcal/mole.

Chemiluminescence is not yet used as a routine test, but it is already useful, for instance to compare nitrocelluloses obtained by different processes.

AD-A169 165 JOINT SYMPOSIUM ON COMPATIBILITY OF PLASTICS/MATERIALS WITH EXPLOSIVES PR..(U) AMERICAN DEFENSE PREPAREDNESS ASSOCIATION ARLINGTON VA L R BARTRON ET AL. MAY 79 4/4

UNCLASSIFIED F/G 19/1 NL

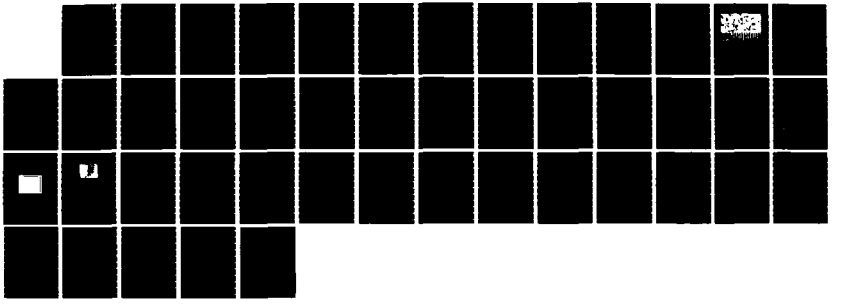

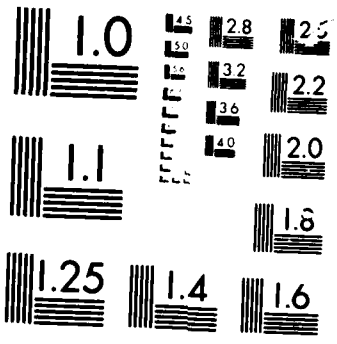
1.0
1.1
1.25
1.4
1.6
1.8
2.0
2.2
2.8
3.2
3.6
4.0

Main advantages of the methods are :

- possibility of studying nitrocellulose or nitrocellulose propellant decomposition at low temperatures (down to 20°C).
- rapidity (half a day is enough to obtain the results plotted on figure 4).
- continuous real-time measurements which allow to observe primary decomposition products (before any secondary reaction occurs).

Heat flow calorimetry

This method of continuous measurement of heat generated by a sample of energetic material at constant temperature may be applied to the assessment of self-ignition hazards of products developing heat (2) and also to the evaluation of compatibility of two materials (3).

Method and apparatus

The method of determining rate of heat generated at a given temperature by a sample of energetic material located in a cell consists in measuring the heat flowing out of the cell into the calorimetric block by means of a great number of thermocouples generating a proportionnal electric tension.

The apparatus used is a CALVET* microcalorimeter. Its sensitiveness is 60 µV per mW. It can detect generation rates as low as 1 µW and allows to study a test sample with a maximum volume of 90 cm³, between ambient temperature and 200°C. The rate of heat generation is continuously recorded.

Results for nitrocellulose propellants

The method is applied to nitrocellulose propellants according following conditions :

- 92 cm³ cell, gas-tight (up to 0.5 MPa).
- 40 g propellant sample (not ground).
- calorimeter temperature 80°C (tests at 60°C are performed but accuracy becomes poor).

The effect of various experimental factors on heat generation rate has been investigated (4) (effect of sample weight, of sample water content, of surrounding atmosphere).

A specific shape of the curve of heat generation rate versus time is obtained for each kind of propellant. Because the explanation of all the features of these curves is not yet complete, heat flow calorimetry is mainly used in order to test propellants comparatively. It is a good tool when either some stage of manufacturing process or some ingredients have been modified.

On figure 5 are reproduced the curves of heat generated by a single base propellant manufactured either with standard guncotton or with guncotton having a higher viscosity. Heat generation rates are not very different.

* S.E.T.A.R.A.M. Lyon (FRANCE)

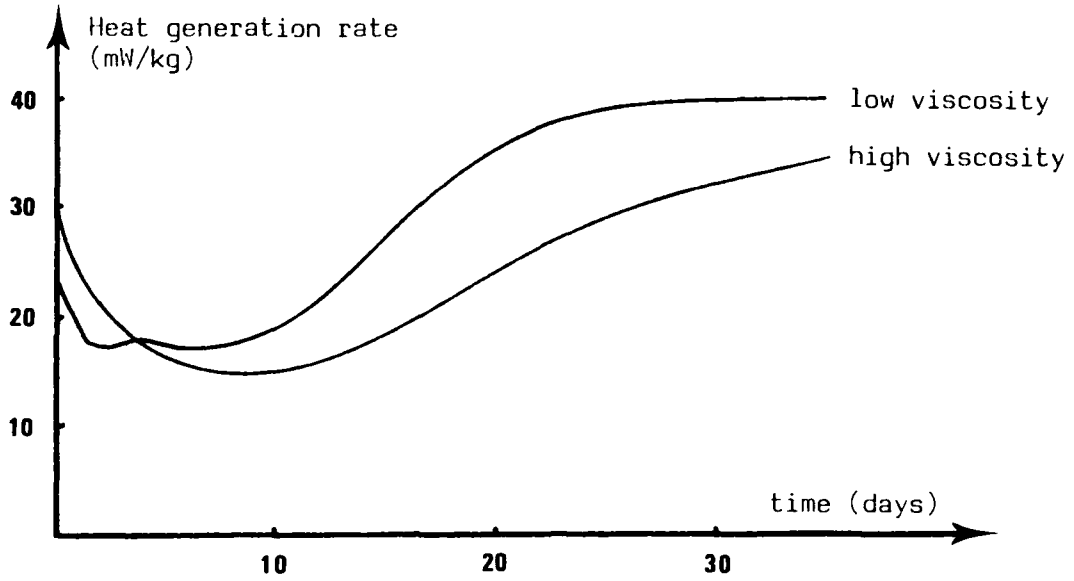

Fig. 5. Effect of guncotton viscosity on heat generated at 80°C by 40 g of single base propellant

On figure 6 are represented the records obtained from propellants containing, no stabiliser, DPA as a stabiliser, 2 NDPA as a stabiliser. When no stabiliser is used, rate of heat generation increases strongly and very quickly. Using 2 NDPA instead of DPA seems to give better results, may be because 2 NDPA is less basic than DPA.

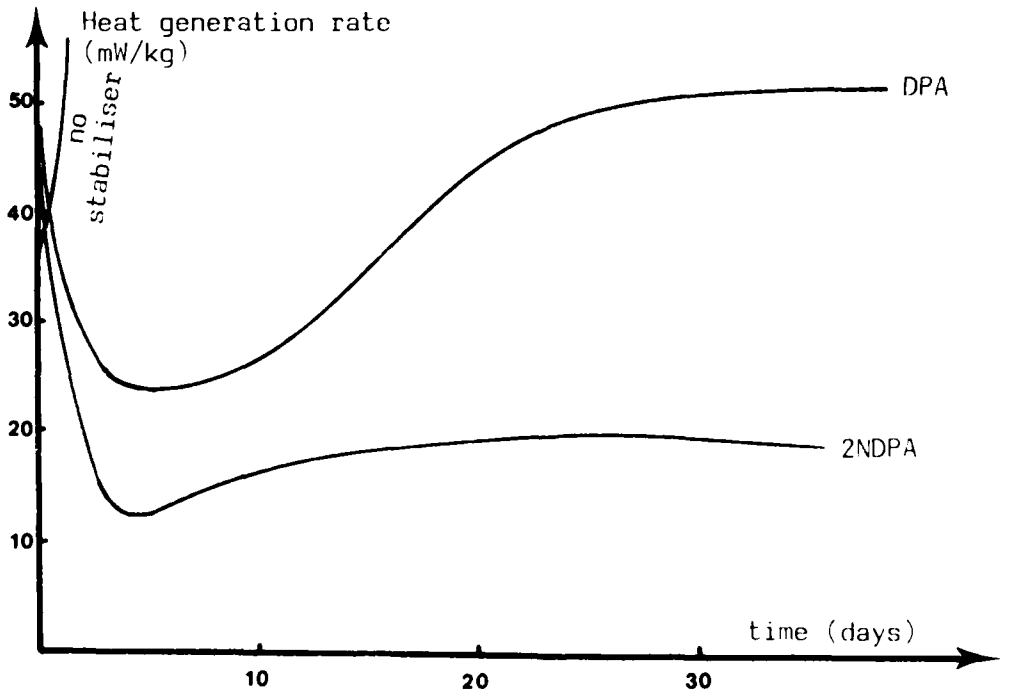

Fig. 6. Heat generation at 80°C of single base propellants without stabiliser, stabilized with DPA or 2 NDPA

Heat flow calorimetry alone is not sufficient to conclude whether and how long propellants tested are chemically stable. A stabiliser consumption test is also performed

Stabiliser consumption at 50°C

It is a test derivated from STANAG 4117 (5). Temperature is lower, 50°C instead of 65,5°C, and stabiliser content is determined by gas chromatography or high performance liquid chromatography instead of U.V. spectrophotometry (6).

25 g of propellant are introduced in a half-tight tube after conservation at 20°C and 65 % relative humidity. They are kept during forty two days at 50°C. Stabiliser content before and after accelerated aging are determined by gas or high performance liquid chromatography (7).

The test is mainly used in order to compare rates of stabiliser depletion in propellants containing the same stabiliser. On table 2 are reproduced results of stabiliser consumption for propellants differing only by viscosity of guncotton or by solvent removal process.

TABLE 2

DPA consumption (in %) after 42 days at 50°C for propellant
Initial stabiliser content is about 1 %

	Standard guncotton	High viscosity guncotton
Standard solvent removal process ..	0.40	0.25
Improved removal process	0.15	0.12

Results of both heat flow calorimetry and stabiliser consumption furnish a first opinion on chemical stability of propellants tested and allow to check whether serious problems may arise in this field.

SAFETY

Safety problems are encountered at each stage of research and development of new energetic materials : safety of ingredients, safety of intermediate products (during manufacturing process) and safety of finished products.

Safety of ingredients

Each new ingredient which has to be incorporated in a propelling composition is characterized on the point of view of its safety in order to class it in comparison with known products. In the case of energetic fillers, usual impact and friction sensitivity tests and card gap test are performed. Sensitivity to electric spark is determined both on bulk product and on particles of product dispersed in the air (small particle size fillers are often used in gun propellant for combustion and homogeneity purpose).

The initial micro-scale manufacturing process is fixed taking account of safety tests results. For instance, if sensitivity of ingredient dust to electric spark is too high, the ingredient is kept in a solvent all along the manufacturing process (it is the case for T.A.G.N.).

Safety tests during process

If safety properties of the ingredients are similar or better than those of usual ingredients used in industrial process, formulation stage is performed at laboratory in routine study facilities (remote controlled and protected).

If new ingredients are more sensitive, micro-scale formulation experiments are performed in order to check the behaviour of the dough during mixing and extrusion. A small scale sigma-blade mixer is used (see above). After mixing, drop and friction sensitivity tests are executed on the gelatinized dough at once and when some amount of solvent has escaped. Afterwards extrusion experiments are done in a special safety press. It can work with cylindrical dies of various diameters and lengths. Maximum pressure on the dough is more than 200 MPa, maximum speed of dough in the die during extrusion is more than 100 m/s.

The mixing and extrusion process for laboratory scale work are fixed according to the results of these experiments.

Safety of finished products

In the case of granular propellants some safety tests are performed systematically in order to know whether the propellant displays a "normal" behaviour or not.

These tests are :

- drop hammer test (using a 30 kg hammer).
- determination of predetonation length.
- determination of critical height of explosion and detonation.

The first test requires 100 g of product with a 30 kg hammer dropping from a height comprised between 0.25 m and 4 m. Generally no positive results is observed with non porous nitrocellulose propellants.

The second test determines the minimum distance where transition to detonation occurs when a confined bed of granular propellant is ignited with a hot wire at one end of an horizontal steel tube of 1200 mm length and 40 mm diameter. Predetonation length is lower than 1200 mm only for very quick propellants.

The third test determines the minimum height of a propellant bed for which explosion or detonation occurs in a vertical steel tube of 82.5 mm diameter and 1000 mm length. Propellant is ignited at the bottom of the tube by a hot wire. The tube is open at the top end. A lot of results is available for industrial propellants.

Results of the tests allow to define a first small scale manufacturing process. In some cases, it may happen that development is stopped (for example if critical height of explosion is lower than 10 cm).

Depending on the use of the propellant, some specific tests are performed.

Propellants for aircraft ammunitions must withstand cook-off tests.

Propellants for tank gun ammunitions undergo tests of vulnerability to shaped charge jets.

Figure 7 shows a schematic drawing of the test assembly.

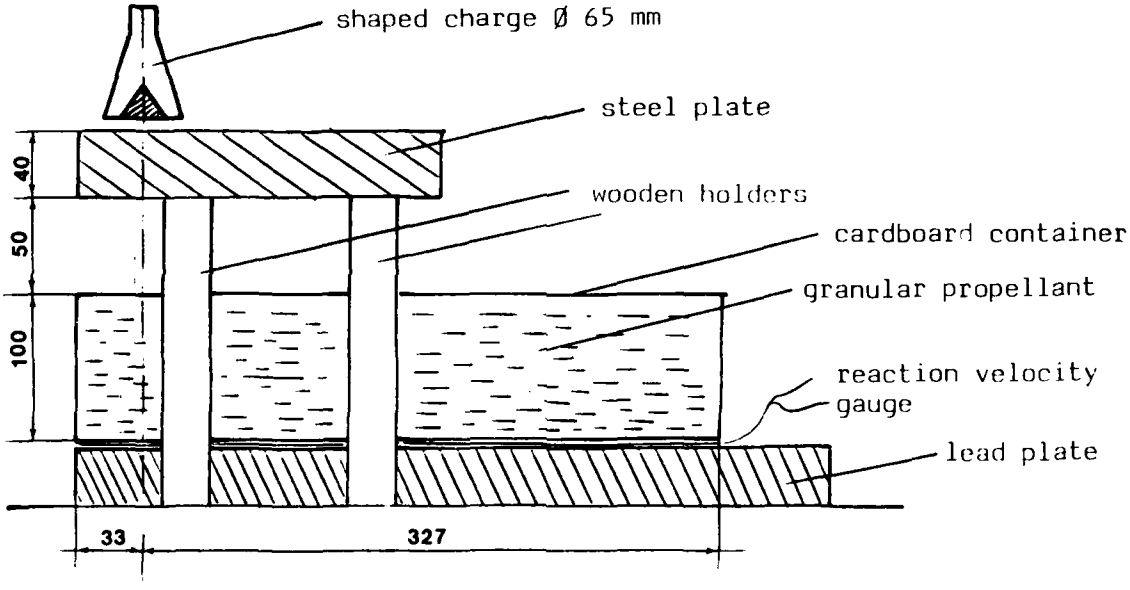

Fig. 7. Schematic drawing of the assembly for testing vulnerability of propellants beds to shaped charge jets

This kind of test will develop because of increasing interest in low vulnerability propelling charge.

CONCLUSION

The tests described in this paper are only a part of all those required for the development of new energetic materials. They do not include all safety tests demanded by storage and transportation regulations.

However, compatibility, stability and safety tests during the stage of research of new energetic materials for gun ammunition propelling charges are performed with the purpose of detecting as soon as possible -and solving- problems arising in these fields.

It allows, either to stop a research program at its beginning when not too much money has been spent, or to extend the research and to build at each stage reliability and safety of finished products and also safety of manufacturing process.

The need for significant and sensible tests is great. Every improvement in this domain would permit to save time during the development of new energetic materials.

ACKNOWLEDGEMENTS

This work was partly supported by Service Technique des Poudres et Explosifs.

We thank Mauricette RAT, Jean Paul LUCOTTE (SNPE/CRB) for helpful discussions.

REFERENCES

(1) R.P. KELLER, M.T. TARI, D.E. AYER
Chemiluminescence as a compatibility testing technique
Symposium on the compatibility of plastics and other materials with explosives, propellants and pyrotechnics, A.D.P.A., 27-29 Apr 1976

(2) J.L.C. VAN GEEL
Self ignition hazards of nitrate ester propellants, Ph D Thesis, Technological Lab., RVO-TNO, RISWIJK, NETHERLANDS (1962)

(3) N.J. BLAY, D.G. DAVIES, E.R.D.E. Waltham Abbey, ENGLAND
Researches into methods of stability and compatibility testing
C.T.I. Einführungssymposium von 13 bis 15 Juni 1973, p 328-351

(4) M. RAT, SNPE/CRB
Application de la microcalorimétrie isotherme à l'étude de la stabilité des poudres pour armes
Proceedings of the 5th symposium on chemical problems connected with the stability of explosives, May 1979 (to be published)

(5) STANAG 4117
Stability tests procedures and requirements for propellants stabilized with diphenylamine, ethylcentralite or mixtures of both, Edition n° 2, 1970

(6) M. RAT, J. MAYET, B. ZELLER, SNPE/CRB
An improved stability test for nitrocellulose gun propellants
Proceedings of the conference on the standardization of safety and performances tests for energetic materials
Special publication ARLCD-SP-77004, U.S. ARRADCOM, Sept 1977

(7) M. LEBERT, M. STEPHAN, B. ZELLER, SNPE/CRB
Dosage de la diphénylamine, de la centralite et de leurs dérivés dans les poudres et propergols par chromatographie liquide haute pression
Proceedings of the 4th symposium on chemical problems connected with the stability of explosives, May 1976

PREPARATION AND PROPERTIES OF A NEW, STABLE AMINE NITRATE

W. S. ANDERSON and H. J. HYER
Chemical Systems Division
United Technologies Corporation
P.O. Box 358
Sunnyvale, CA 94086

ABSTRACT

When the solid crystalline sulfate of 2,2-bis(aminomethyl)-1,3-diaminopropane is treated with excess dilute nitric acid, the sulfate ion is completely displaced by nitrate ion. The resulting crystalline nitrate, $C(CH_2NH_2)_4 \cdot 4HNO_3$, is only slightly soluble in water and therefore can be easily isolated in high purity. Its identity is established by acid-base titration, proton magnetic resonance, infrared and elemental analysis. It may be stored at 150°C for many hours with negligible decomposition but decomposes in a few minutes at 200°C. Attempts to cause it to detonate have been unsuccessful. When ignited the nitrate burns slowly, leaving a carbonaceous residue; combustion is faster when copper ion is present. The low solubility, high melting point, high density, and thermal stability of this nitrate are a sharp contrast to the properties of ammonium nitrate and methyl ammonium nitrate.

INTRODUCTION

Molecules containing the rigid symmetrical five-carbon framework of neopentane have long been known to crystallize into high-melting, dense structures of low solubility. Pentaerythritol is perhaps the best known example of this principle; its melting point (260°C) is far above that of the less symmetrical polyols. The amine analog of pentaerythritol -- 2,2-bis(aminomethyl)-1,3-diaminopropane -- is a little-known material which merits further attention as an intermediate for the preparation of high-melting, stable, hydrolysis-resistant organic structures. The preparation, properties, and uses of the dithiocarbamate derived from this tetramine are described in an earlier paper (ref. 1); an easy preparation of the tetranitrate of the tetramine is described in the present communication.

PREPARATION

The tetramine may be prepared (ref. 2) and handled as its sulfate, $C(CH_2NH_2)_4 \cdot$

$2H_2SO_4$. At room temperature this salt is only sparingly soluble in water or in organic solvents and that fact allows it to be freed of more soluble materials simply by thorough washing. Although only slightly soluble (0.2%) in water, the sulfate does undergo ion exchange when treated with dilute solutions of strong acids or the salt of a strong acid, such as ammonium nitrate. In that respect it is much like an ion exchange resin, except that the concentration of functional groups in the salt is orders of magnitude higher than in a typical resin. About one hour of contact time is sufficient for ion exchange to reach equilibrium. The nitrate, like the starting material, is itself of low solubility in water and it may be freed of sulfuric acid and excess nitric acid by washing it with cold water. The conversion of tetramine sulfate to tetramine nitrate is therefore an extraordinarily simple operation, well-suited to large scale preparations with simple equipment. Details of a preparation are reported in the Experimental section.

STRUCTURE PROOF

The product of treating the tetramine sulfate with nitric acid has characteristics which immediately identify it as an alkylammonium salt rather than as a covalent substance. First, it is a high-melting, non-volatile, colorless solid which crystallizes easily from water solution. Furthermore, its water solution is electrically conductive and corrodes steel or copper. Lastly, it is freely soluble in aqueous base and may be titrated with aqueous sodium hydroxide by standard methods (ref. 3).

Its infrared spectrum (figure 1) shows absorption bands generally found (ref. 4) in nitrate salts (1,390 cm^{-1} and 835 cm^{-1}). The sulfate absorbs strongly at 1,120 cm^{-1}; this band is missing from the spectrum of figure 1.

The proton magnetic resonance pattern (in heavy water solution) consists of two signals only, at δ = 3.5 ppm and δ = 4.7 ppm. These are assignable to CH_2 protons and to the exchangeable $\overset{\oplus}{N}H_3$ protons, respectively, and are the analogs of two signals exhibited by the amine sulfate precursor.

The elemental analysis of unrecrystallized product is in good agreement with the theoretical. (Found: carbon 15.78%, hydrogen 5.37%, nitrogen 28.97%, oxygen by difference 50.2%. Calculated for $C_5H_{20}N_8O_{12}$: carbon 15.6%, hydrogen 5.2%, nitrogen 29.2%, oxygen 50.0%.)

Taken together, these data demonstrate that the product does have the expected structure, figure 2.

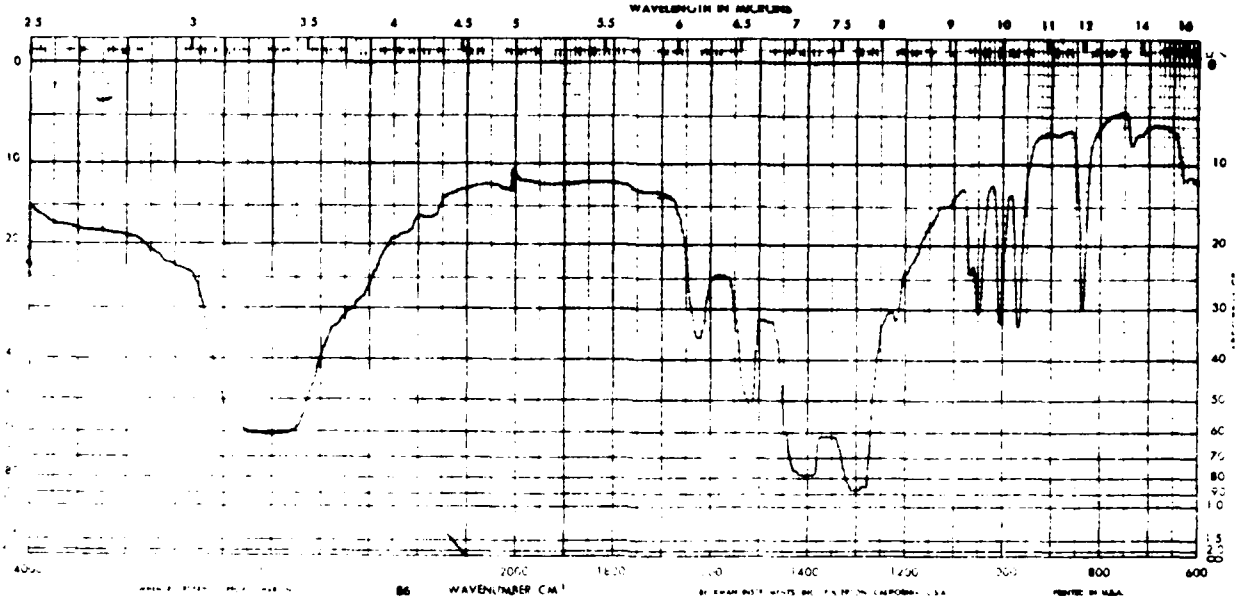

Fig. 1. Infrared spectrum of tetranitrate of 2,2-bis(aminomethyl)-1,3-diaminopropane in KBr pellet (absorbance versus wavenumber, cm^{-1}).

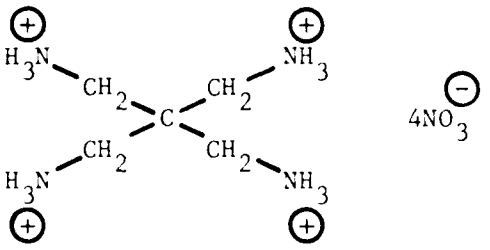

Fig. 2. Tetranitrate of 2,2-bis(aminomethyl)-1,3-diaminopropane

PROPERTIES

In several respects the tetranitrate differs sharply from the more familiar ammonium nitrate and amine nitrates used as explosives, in pyrotechnic devices, as gas generators, and as solid propellant ingredients.

First, it has exceptional thermal stability. It may be heated in a differential thermal analysis apparatus with no evidence of physical or chemical change until it reaches nearly 200°C, where an exothermic effervescence occurs. It may be stored in air at 150°C for many hours with no change in its infrared spectrum.

Secondly, its solubility in water (1.6% at 25°) is much lower than that of the typical amine nitrate, such as the nitrate of methyl amine, ethylene diamine, guanidine, hydrazine, or hexamethylene tetramine. Hygroscopicity is negligible;

the powder remains free flowing through wide changes in humidity. In many organic solvents (ethylene glycol, polyethylene glycol, dimethyl formamide) it is also sparingly soluble at room temperature. Sulfuric acid (96%) will slowly dissolve it at ice temperature; adding the sulfuric acid solution to excess water does not cause the starting material to precipitate.

Thirdly, unlike some amine nitrates, it burns at atmospheric pressure with difficulty, forming soot as a major product. If the thermal decomposition is conducted in the inlet of a mass spectrometer, large peaks are produced in the mass spectrum at m/e 30, 46, 44, and 18. These are assigned to CH_2NH_2, NO_2, CO_2 (or N_2O), and H_2O, respectively, and demonstrate the incompleteness of oxidation-reduction when conducted in a vacuum. Oxygen, although it makes up 50% by weight of the crystal, is not present in an amount sufficient to convert all of the alkylammonium structure to CO, H_2O, and N_2. As a generator of large volume of very hot gas, therefore, the compound suffers by comparison to ammonium nitrate or hydrazine nitrate. If, however, copper ion is first introduced into the structure (by treating copper hydroxide with an aqueous solution of the tetramine tetranitrate, then evaporating the water), the combustion is accelerated and proceeds with a bright blue flash. Copper ion is known to coordinate well with the tetramine (ref. 5).

Like most amine nitrates, this nitrate is relatively insensitive to impact. It may be struck with a hammer, dropped from a ten foot height, ground in a mortar, subjected to a high voltage discharge, squeezed in a hydraulic press, or dropped into a gas flame without detonation. Whether it will detonate when subjected to a blasting cap or booster impact is not known, however. It seems likely that the critical diameter for detonation has a relatively large value and conditions required for detonation will therefore not be established until large quantities of the material are assembled in one place.

When allowed to evaporate at room temperature, a saturated aqueous solution of the tetranitrate deposits large, colorless, refractive crystals with well-formed faces (figure 3). Density of the crystals is 1.7 g/ml which is well above the density of ethylene diamine dinitrate (1.58), of methylamine nitrate (1.42), of hexamethylene tetramine dinitrate (1.57) and about the same as ammonium nitrate (1.72). The crystals are sufficiently plastic, however, to press (at 5,000 psi) into clear, transparent moldings with faithful reproduction of the fine details of the die used. Under polarized light a fraction of the crystals display colorful parallel patterns which may indicate multiple twinning, glide planes or other flaws which enhance the plasticity.

Toxicity of the tetramine or its salts is not known. Certain other aliphatic polyamines are known (ref. 6) to be potential crosslinking agents for DNA and similar behavior must therefore be assumed for this tetramine.

Fig. 3. Crystals of tetranitrate of 2,2-bis(aminomethyl)-1,3-diaminopropane (smallest scale division = 1 mm).

APPLICATIONS

Use of this dense, stable substance as a generator of hot gas may be considered for environments in which sensitivity to high temperature, moisture, high vacuum, organic solvents or impact rule out the use of conventional materials. The nitrate can be made from the corresponding tetramine sulfate in high yield by a nearly hazard-free process having a minimum of corrosion and pollution problems. It should also be considered as an intermediate for the preparation of more nitrogen- and oxygen-rich (and therefore more powerful) generators of hot gas.

Good precipitants for aqueous nitrate ion are rare -- ones with low [illegible] weight are even rarer. It remains to be seen whether the nitrate ion [illegible] power described here is useful for the prevention of water [illegible] acid handling processes. The fact that the tetramine [illegible] and nitrate ion may be of some use to those nitration [illegible] volumes of both sulfuric and nitric acids.

EXPERIMENTAL

The disulfate of 2,2-bis(aminomethyl)-1,3-propane diamine was prepared by high pressure ammonolysis as described in a recent patent (ref. 2). The product was thoroughly washed with water and with benzene and was dried in a vacuum oven at 100°C. Its identity was established by acid-base titration in the presence of formaldehyde (ref. 3), from its infrared and NMR spectrum, and by elemental analysis.

The disulfate was converted to the tetranitrate as follows:

Finely ground disulfate, $C(CH_2NH_2)_4 \cdot 2H_2SO_4$, (5.7 grams, 0.017 mole) was placed in a 30 ml fritted glass filter funnel closed at the bottom with a rubber bulb. Twenty-five grams of 35% nitric acid solution was added with stirring and allowed to contact the amine sulfate at room temperature for one hour. The bulb was then removed and the acid was drawn through the funnel, discarded and replaced with a fresh 25-gram charge of 35% nitric acid. After an additional hour, this acid was drained and the solid was washed with two, five-gram portions of ice water. The solid was then dried overnight at room temperature at reduced pressure. Yield was 6.7 grams (99 to 100% of the theoretical yield).

Material prepared by this procedure has the infrared spectrum of figure 1 and has equivalent weight 95 (theoretical 96) but gives a positive test for sulfate ion when barium nitrate solution is added. Further washing and recrystallization lowers the sulfate concentration.

REFERENCES

1 H.J. Hyer, J.E. Sundberg, and W.S. Anderson, Coatings and Plastics Preprints, 173rd Meeting of the American Chemical Society, 37(1977)453, No. 1.
2 W.S. Anderson, U.S. Patent 4,117,013 (September 26, 1978).
3 T.M. Kolthoff and V.A. Stenger, Volumetric Analysis, Vol. II, Interscience, New York, 1947, p.158.
4 D.E. Chasan and G. Norwitz, Application of Infrared Spectroscopy to the Analysis of Inorganic Nitrates, Department of the Army, Frankford Arsenal, March 1969.
5 R.W. Oehmke and J.C. Bailar, Jr., J. Inorg. Nucl. Chem, 27(1965)2199.
6 S.S. Cohen, Introduction to the Polyamines, Prentice-Hall, New York, 1971.

CHARACTERIZATION AND PROCESSING of TRIPICRYLMELAMINE (TPM)

by

Dr. Michael D. Coburn and 1st Lt Douglas L. Loverro
Los Alamos Scientific Laboratory

ABSTRACT Tripicrylmelamine (TPM) is an inexpensive, thermally stable explosive that was first prepared and patented at the Los Alamos Scientific Laboratory. Hercules, Inc later obtained a license to manufacture TPM under the Los Alamos patent and they carried its development through the pilot plant stage. At the completion of their study in 1976 Hercules estimated that they could produce TPM for around $1.00/pound on a large scale.

The Air Force's interest in thermally stable explosives as a possible solution to aerodynamic heating of externally carried munitions led to the present study. The impact sensitivity of TPM could not be measured with standard type 12 tools. A 5 kg weight had to be used instead of the standard 2.5 kg weight in order to obtain a 50% point. The observed insensitivity of TPM to impact suggests that TPM may be an inexpensive alternative to TATB for IHE applications.

Pure TPM would not press; however, we found that a 95/5 TPM/Kel-F composition could be pressed to 96-98% TMD. Detonation velocity and plate dent measurements indicate that this formulation has performance exceeding that of TNT. The results of gap sensitivity and cylinder tests planned for the near future will be reported.

In addition to a pressable composition, a castable TPM composition that utilizes a highly crosslinked polyurethane binder system is being developed. Performance and sensitivity data that has been determined for this PBX will be presented.

PREDICTION OF SOLVENT AND POLYMER CHARACTERISTICS THROUGH THE USE OF EASY TO MEASURE PROPERTIES (II)

VINCENT D. McGINNISS
Battelle's Columbus Laboratories, Columbus, Ohio, USA 43201

INTRODUCTION

The ability to accurately estimate physical properties of solvents and polymers with regard to chemical structure, manufacturing and application is of practical importance throughout many diverse industries and technologies. The ability to predict which polymer structure one should attempt to synthesize in order to achieve a desired physical property without empirically trying all possible combinations is also of practical significance. Previous relationships such as solubility parameters and functional group analysis have shown a limited or somewhat specific range of predictability.[1] Listings of solubility parameters for polymers or liquids are not all inclusive and information on new materials can be difficult to determine experimentally.

It is the purpose of this work to develop simple predictive relationships for solvents and polymers but with regard to ease of experimentation in determination of required variables. The required, easily measured or calculated, variables for this study are refractive index and a knowledge of the solvent or polymer molecular structure and composition. These requirements have led to a unique set of linear equations for use in the prediction of physical properties of liquids (solvents) and polymeric materials.

RESULTS AND DISCUSSION

Liquids

Historically, simple physical property associations involving predictive capability were first developed for liquids.

The interaction of light energy with molecular structure and its relationship to density was first proposed by Lorenz and Lorentz late in the 19th Century.[2,3] This relationship

$$\text{Density} = C_{Ld}\ [n^2-1/n^2+2]\ \pm I_1 \qquad (1)$$

where C_{Ld} is the Lorenz-Lorentz density regression coefficient, n is refractive index and I_1 is the intercept value, holds extremely well for nonpolar and unassoci-
-ated liquids.

A correlation between surface tension (γ), refractive index and density has been previously devised for nonpolar liquids as well as a limited series of polar materials.[4,5] This prior relationship also takes the form of Equation 1 in that

$$\text{Surface tension } (\gamma) = C_L \left[\varepsilon-1/\varepsilon+2\right] \pm I_2 \qquad (2)$$

where C_L is the Lorenz-Lorentz surface tension regression coefficient, ε is the dielectric constant ($\varepsilon = n^2$, Maxwell's relation), and I_2 is the intercept value.

These earlier relationships fail in predictability when applied to polar liquids such as alcohols, acids, aldehydes and ketones.

Examples of predictability for Equations 1 and 2 are given in Tables I and II for a series of polar and nonpolar liquids. Both density and surface tension for aldehydes, ketones, and hydrocarbons show a high degree of correlation (0.89 to 0.96) with refractive index. Density and surface tension properties of acids, esters, and alcohols are not correlatable with a simple function of refractive index. Low correlation coefficients (0.1 to 0.7) and high standard errors of estimate show a lack of predictability for Equations 1 and 2 when applied to polar materials.

TABLE I

Correlation between density (D) and Equation 1

Class of Compounds (Total number of Liquids studied in the correlation)	Correlation Coefficient	Standard Error of Estimate
Acetals, Ethers, Ketals (96)	0.723	0.065
Acids (29)	0.111	0.080
Alcohols (152)	0.750	0.059
Aldehydes, Ketones (121)	0.886	0.044
Hydrocarbons (185)	0.959	0.029

TABLE II

Correlation between surface tension (γ) and and Equation 2

Class of Compounds (Total number of Liquids studied in the correlation)	Correlation Coefficient	Standard Error of Estimate
Acids (8)	-0.129	4.68
Alcohols (23)		
(with H_2O, H_2O_2 and N_2H_4 included)	0.268	20.25
(without H_2O, H_2O_2. and N_2H_4 (included)	0.651	9.02
Aldehydes and Ketones (11)	0.967	2.17
Hydrocarbons (25)	0.958	1.44

It is the purpose of this work to extend refractive index, density and surface tension relationships into useful correlations that include polar and nonpolar liquids or polymeric materials. This can be accomplished through utilization of a novel semiempirical predictive equation having a linear combination of variables

$$\text{Response} = C_1 n \pm C_2 \chi \pm C_3 Z' \pm I_3 \qquad (3)$$

In Equation 3, n is refractive index, χ is the weight fraction of heteroatom in the molecule or ratio of nonbonded to bonded electrons for the heteroatom, Z' is the fraction for total number of π electrons in the molecule or ratio of π electrons to the total number of electron bonds, C_1-C_3 are regression coefficients for each of their respective variables and I_3 is the intercept value. Response for this equation can be density (D), surface tension (γ), solubility parameters and their components (δ_T, δ_{dis}, δ_p, δ_H), ionization potential (IP), viscosity (η), solvent polarity, magnetic parameters and amine base strengths (σ^*, PKa).[6]

In Tables III and IV are the correlations for density and surface tension corresponding to Equation 3. The same classes of compounds and the identical members in each class are treated as those examined in Tables I and II (Equations 1 and 2). This three parameter equation (Equation 3) is an excellent predictor of density for both polar and nonpolar liquids (0.9 multiple correlation coefficients) in Table III. Similar results are observed for surface tension (Table IV).

TABLE III

Correlation between density (D) and Equation 3

Class of Compounds (Total number of Liquids studied in the correlation)	Multiple Correlation	Standard Error of Estimate
Acetals, Ethers, Ketals (96)	0.929	0.035
Acids (29)	0.967	0.021
Alcohols (152)	0.957	0.026
Aldehydes, Ketones (121)	0.925	0.037
Hydrocarbons (185)	0.968	0.026

TABLE IV

Correlation between surface tensions (γ) and Equation 3

Class of Compounds (Total number of liquids studied in the correlation)	Multiple Correlation	Standard Error of Estimate
Acids (8)	0.996	0.499
Alcohols (23) (includes H_2O, H_2O_2, and N_2H_4)	0.980	4.44
Aldehydes and Ketones (11)	0.995	0.896
Hydrocarbons (25)	0.985	0.90

Sample Calculations

$$\text{Response} = C_1 n \pm C_2 X + C_3 Z' \pm I$$

n = Refractive Index

X = Weight Fraction of Heteroatom in the Molecule

Z′ = π Electron Fraction in the Molecule

	γ dyn/cm	n	X	Z′
H_2O	72.8	1.33	16/18 = 0.88	--
Ø-CH_2OH	39	1.5396	16/108.14 = 0.015	6/108.14 = 0.005
$CH_3(CH_2)_6CH_2OH$	27.53	1.4267	16/130.23 = 0.012	--

$\gamma = 208.15\ n + 76.65\ X - 149.57\ Z' - 284.34$

23 alcohols; multiple correlation 0.98; Standard error of estimate = 4.44

Any abnormalities (hydrogen bonding, association, high surface tension, low refractive index, etc.) that occur in predicting physical properties of certain liquids can be attributed to perturbations caused by heteroatoms contained in the molecule. Also, double, multiple, or resonance carbon to carbon bonding (with or without conjugation) resulting in higher refractive index values can be attributed to π - electron cloud density. By utilizing a three parameter equation (Equation 3) it is possible to balance or separate adverse electronic- conjugative effects of the heteroatom and π-bonding systems with variables

$$\chi = \frac{\text{(number of like heteroatoms) (atomic weight of the heteroatom)}}{\text{(molecular weight of the compound)}} \qquad (4)$$

and

$$Z' = \frac{\text{(number of carbon-carbon vinyl or aromatic } \pi \text{ electrons)}}{\text{(molecular weight of the compound)}} \qquad (5)$$

The variable χ weights only the heteroatom contribution to the molecule and no distinction is made between multiple bonding or valency of the functional group (atomic weight of heteroatom = 16 for alcohols, ethers, aldehydes, ketones, 32 for acids, esters). (Sample calculations are shown in Table IV.) Physical properties of over 2,000 liquids have been correlated through utilization of this unique concept of a three parameter equation.[6]

Polymers

In polymeric materials, previous predictive relationships involved knowledge of individual group contributions of the polymer structure before any generalizations could be established. This also means extrapolation from one response surface to another is difficult and may have limited physical reality. Isolated structural group contributions such as molar refraction of a carbonyl unit (Parachor) in a

monomer repeat unit may not accurately predict solubility parameters, critical surface tension or even density of the polymer system.[1,7]

Extension of Equation (3) can be applied to polymer systems wherein a wide range of physical properties are correlatable with chemical structure as demonstrated in the following sections:

Critical Surface Tension (γ_c)

Studies of polymer adhesion to a substrate usually involve wetting and surface characterization. One way of characterizing a surface is to measure the contact angle Θ_c made by a drop of liquid, having a known surface tension, on the substrate at the point where the two phases (liquid-solid) meet. Ideal wetting occurs when $\cos \Theta_c = 1$. When $\cos \Theta_c$ is plotted for a series of liquids on a single surface, the intercept at $\cos \Theta_c = 1$ is defined as γ_c, the critical surface tension for that substrate or material.[8,9]

Table V contains a partial list of polymers having experimentally determined values of γ_c, refractive index and calculated χ values for each acrylate methacrylate monomer unit. (χ for methyl-methacrylate = two oxygen atoms 32 g/mole $\div$ 100 = Mwt of monomer unit.)

Critical surface tension of wetting for these polymeric materials can be estimated by the following expression:

$$(\gamma_c) \text{ estimated values} = 80.41\ n + 20.00\ \chi - 89.74 \qquad (6)$$

multiple correlation = 0.90

standard error of estimate = 2.9

Acrylate-methacrylate polymers have a high degree of polarity and a relatively low refractive index. It is for this reason a χ value is assigned to these polymers to balance out the correlation.

Solubility Parameters

Solubility parameters of polymer systems are important to coatings viscosity applications and swelling of crosslinked networks as a prediction of tensile strength.[10,11]

In Table V are some experimental solubility parameters of polymers (δ_T), refractive indices and critical surface tension values. These interrelationships are combined to give Equation 7 which can be used to estimate or predict values of δ_T.

$$\delta_T = -4.533\ n + 0.228\ \gamma_c + 8.347 \qquad (7)$$

multiple correlation = 0.93

standard error of estimate = 0.52

TABLE V

Physical properties of polymers

Polymers	Refractive Index	Solubility Parameter $cal^{1/2}/cm^{1/2}$	Critical Surface Tensions dynes/cm	χ
Poly(tetrafluoroethylene)	1.35	6.2	18	--
Poly(2-methylpropene)	1.51	8.0	27	--
Poly(propylene)	1.49	8.7	29	--
Poly(2-methyl-1,3-butadiene)	1.52	9.0	31	--
Poly(ethylene) High Density	1.52	8.0	31	--
Poly(1,3-butadiene)	1.516	8.4	32	--
Poly(ethylmethacrylate)	1.485	9.0	33	0.278
Poly(ethylacrylate)	1.4685	9.3	35	0.320
Poly(vinyl chloride)	1.539	10.1	39	--
Poly(vinylidene chloride)	1.60	11.0	40	--
Poly(methylmethacrylate)	1.49	11.0	38	0.320

Environmental Stress Cracking

Many plastics degrade under the combined actions of long-term stresses and contact with liquids or vapors. The resulting destruction of polymer mechanical properties is called environmental stress cracking.

Polymethylmethacrylate has been shown to have a drastic change in module/modulus of cohesion/coupling (K) depending on the medium it is exposed to (Table VI). With an increase in the polarity of the medium (methanol-ethanol), K has a relatively low value. The same is true of benzene and toluene solvents ($Z' = 6\ \pi$ electrons ÷ benzene or toluene molecular weight). Low polarity alcohols (octyl alcohol) show a less effective lowering of the cohesion coupling constant.[12] These experimental observations can be correlated with the following expression:

$$K_{(calculated)} = 835.9\ n + 178.2\ \chi - 753.3\ Z' \qquad (8)$$

multiple correlation = 0.91

standard error of estimate = 4.6

TABLE VI

Change in modulus of cohesion coupling (K) for polymethylmethacrylate as a function of Solvent Medium

Solvent	K = Kg Force/$cm^{3/2}$ Observed	Refractive Index	χ	Z'
Benzene	2.9	1.501	--	0.077
Toluene	2.9	1.497	--	0.065
Methanol	3.3	1.329	0.499	--
Ethanol	4.9	1.361	0.347	--
Butanol	7.3	1.398	0.216	--
Hexanol	14.1	1.418	0.157	--
Octanol	24.2	1.428	0.123	--

Vapor Barrier Permeability of Polymers

The barrier properties of plastic materials against various vapors and liquids are of great importance for many applications. It is of interest to correlate certain polymer structures with a measurable physical property such as permeability constant.

In Table VII is a list of nonhalogen containing polymers and their experimentally determined water vapor permeability constants (P).[13]

TABLE VII

Water vapor permeability of polymers

Polymers	Water Vapor Permeability ($P \times 10^{10}$)	Refractive Index	χ = Weight Fraction of Heteroatom in the Monomer Unit
Ethylcellulose	12,300	1.479	0.414
Poly(vinylacetate)	10,000	1.47-1.49	0.372
Cellulose Acetate	6,800	1.46-1.50	1.492
Polycarbonate	1,400	1.585	0.189
Polyethyleneterephthalate	175	1.64	0.333
Poly(ethylene) Low Density	100	1.49	0.000
Nylon 6.6	70	1.532	0.133
Polypropylene	68	1.49	0.000
Poly(ethylene) High Density	15	1.52-1.58	0.000

These polymer structures and their vapor permeabilities can be correlated with Equation 9.

$$\log P = -5.482\, n + 4.775\, \chi + 9.982 \qquad (9)$$

multiple correlation = 0.93

standard error of estimate = 0.48

This relationship (Equation 9) is derived from a simple linear function of refractive index (n) and weight fraction of oxygen heteroatom contained in the monomer repeat unit (χ).

Summary and Conclusions

A novel empirical relationship involving refractive index (n), weight fraction of like heteroatoms in a molecule (χ) and Z′ the π electron fraction or contribution to the molecule is introduced and applied to a number of physical properties for many different classes of polar and nonpolar organic liquids or polymeric materials. The only restriction to this relationship is that molecules should contain the same or multiples of the same heteroatoms to obtain the best correlation. All of thee generalizations regarding individual contributions of n, χ, and Z′ to the multiple correlation depends on the individual members chosen in each series or class of compounds studied and can vary with different selection of materials.

The fundamental reasoning behind this simple linear combination on a n, χ, and Z' is that light energy refraction can be an accurate predictive probe for many diverse types of physical property relationships. Light interaction with a molecule is a function of the total individual atomic, electronic, ionic-covalent bonding contributions to the compounds structure. All physical properties of liquids and solids must be somewhat related to these individual atomic contributions hence the first order dependency on refractive index alone as a predictive probe for density (D) and surface tension (γ) of nonpolar liquids. Any abnormality or nonpredictability of refractive index (n) for a physical property can be corrected with variables χ and Z'. Strongly attractive electronic forces are weighed by the heteroatom fraction of the molecule (χ) and increases in refractive index due to π electron density are correlated with the Z' parameter. These relationships are presently being extended into more generalized equations involving mixed heteroatom functionality.

Work is continuing in examination of predictability for oxygen permeability of polymers, viscosity relationships of polymers in solution, crosslinked polymer network analysis and electrical or other physical properties of polymers and solvents.

References

1. D. W. Van Krevelen, "Properties of Polymers", Elsevier, N.Y., 1972.
2. H. A. Lorentz, "The Theory of Electrons", Dover, N.Y., 1952.
3. Y. K. Syrkin, "Structure of Molecules", Dover N.Y., 1964.
4. C.B.F. Young, "Surface Active Agents", CPC, N.Y., 1945.
5. O. Exner, Nature, 196, 890 (1962).
6. V. D. McGinniss, Part I, this journal.
7. D. M. Koenhen, J. Appl. Polym. Sci., 19, 1163 (1975).
8. V. D. McGinniss and A. Kah, Polym. Engr. and Sci., 17 (7), 478 (1977).
9. F. M. Fowkes, Advances in Chemistry, 43, ACS (1964).
10. A.F.M. Barton, Chem. Rev., 75, 731 (1975).
11. P. E. Froehling, et al., Polymer, 17, 835 (1976).
12. Procnnost' l Razrusheniye Polimerov PRI vozdeystvii Zhidkikh Spred, IZO-VO "Naukuva Dumka", KiEV, 1975, pp 1-206.
13. Encyclopedia of Polymer Science and Tech., Vol. 2, pp 316-327 (1965).

EFFECT OF AMMONIUM PERCHLORATE PARTICLE SIZE ON ITS DETONATION CHARACTERISTICS WHEN SENSITIZED WITH SMALL AMOUNTS OF NITROGUANIDINE

ALLEN J. TULIS
IIT Research Institute, Chicago, Illinois, USA

ABSTRACT

Sympathetic detonation has already been achieved in ammonium perchlorate by adding small amounts of nitroguanidine. Although it appeared that the ammonium perchlorate was detonating at the ideal detonation velocity of the nitroguanidine additive, the effects of confinement, charge diameter, and ammonium perchlorate particle size were not assessed. The effects of confinement and charge diameter were subsequently investigated. In all these studies, however, the particle size of the ammonium perchlorate remained unchanged--nominally 200 micron Class C mil spec ammonium perchlorate. The present effort investigated the effect of variable ammonium perchlorate particle size upon the detonation characteristics of a typical ammonium perchlorate composite system: one sensitized with 5 percent nitroguanidine. Three particle size ranges--designated coarse (149 to 500 micron), medium (44 to 149 micron), and fine (0 to 44 micron)--were investigated. Screen-sieve separation was used. Although the results did confirm a general increase of detonation velocity with a decrease in ammonium perchlorate particle size, some anomalous behavior was also identified. A more comprehensive study will be needed to elucidate the effects of particle size or, more generally, the particle size distribution.

INTRODUCTION

The detonation velocity of explosives is a function of the chemical energy released, the rate at which this energy is released, the initial density of the explosive, the explosive charge diameter, and the degree of confinement. When the charge diameter is adequate, however, the detonation velocity is solely a function of initial explosive density and is completely determined by the thermohydrodynamics of the explosive. Such detonations, termed ideal detonation velocities, are constant and unique for each explosive at constant density. Figure 1 illustrates the empirical linear relationships of ideal detonation velocity as a function of density for both nitroguanidine and ammonium perchlorate (Ref. 1,2). By definition, and as can be experimentally demonstrated, the ideal detonation velocity is independent

of particle size. The relationships between ideal detonation velocity, D_i, and density, ρ, illustrated in Figure 1 are derived from:

Nitroguanidine: $D_i = 1.440 + 4.015\ \rho$ (1)

Ammonium perchlorate: $D_i = 1.012 + 2.688\ \rho$ (2)

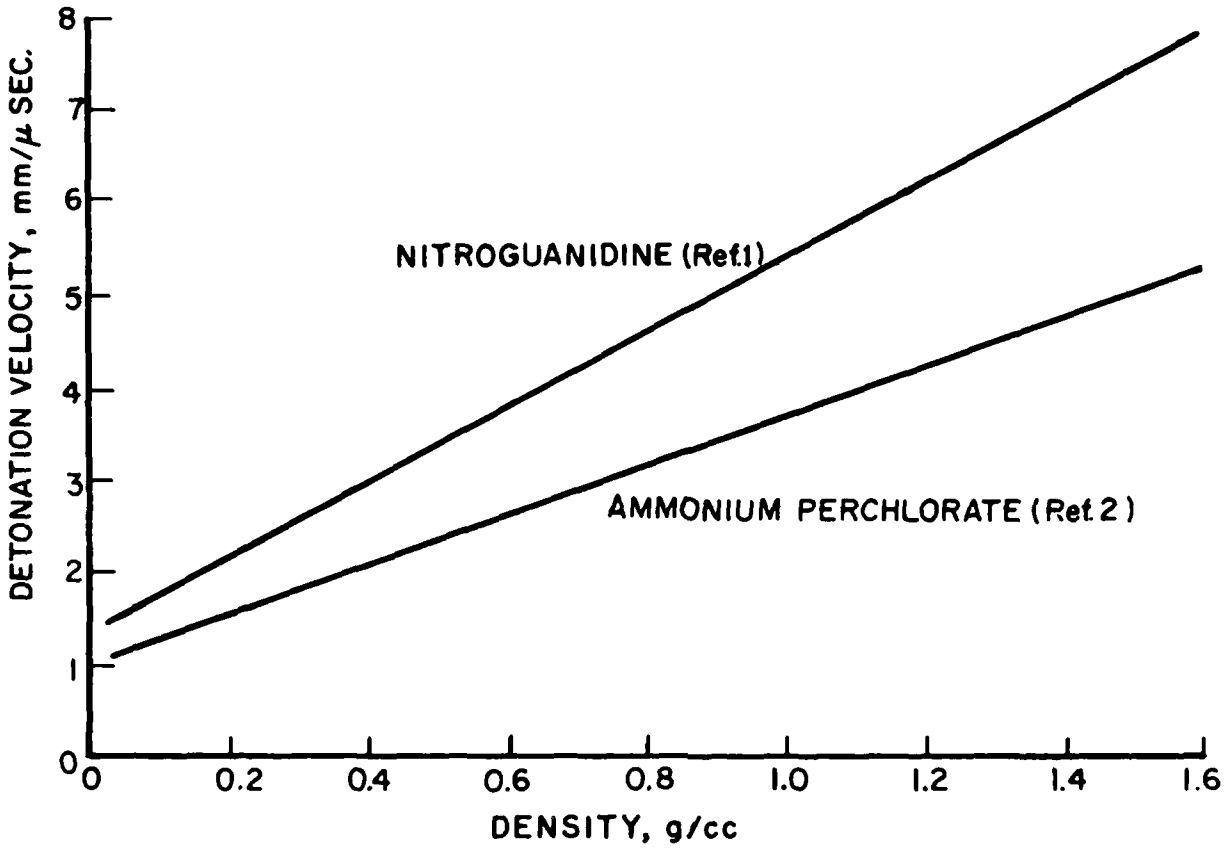

Fig. 1. Empirical linear relationship of ideal detonation velocity as a function of density for nitroguanidine and ammonium perchlorate (Ref. 1,2).

Ammonium perchlorate, although detonable, is generally not considered an explosive. In previous work (Ref. 3) we investigated the stable sympathetic detonation of ammonium perchlorate by sensitizing it with a small amount of nitroguanidine. Under the conditions investigated, the ammonium perchlorate by itself could not detonate. It was our conclusion (Ref. 3) that the small amount of nitroguanidine was detonating at or near its ideal detonation velocity and that the ammonium perchlorate was induced to detonate sympathetically at the same detonation velocity.

Explosives, and particularly explosive composites, can detonate at velocities other than the ideal detonation velocity. This generally occurs when factors such as critical diameter, confinement, and sometimes particle size, are critical. Such detonations are termed nonideal. The range of nonideal detonations can be extensive, especially for fuel-oxidizer composite explosives. There is evidence to suggest

that for certain fuel-oxidizer composites propagation rates can vary as a continuum from detonation velocities of km/sec to deflagration velocities of cm/sec. Hence the possibility that many typical pyrotechnics such as boron/potassium nitrate or aluminum/ammonium perchlorate can detonate. This has, in fact, been demonstrated (Ref. 4,5).

The present paper, however, investigates only the effects of ammonium perchlorate particle size when ammonium perchlorate is sensitized with a small amount of nitroguanidine. The resultant detonation velocity is presumed to be the ideal detonation velocity of the nitroguanidine based on its effective density, except when exceeded by the nonideal detonation velocity of the ammonium perchlorate under the restrictive conditions of charge diameter, confinement, density, and particle size.

EXPERIMENTAL

The experimental device employed in this and in previous work (Ref. 3,6) is illustrated in Figure 2. Steel confinement was used in this study and two charge diameters were investigated - 6 and 12 mm--for comparative purposes. An ammonium perchlorate system sensitized with 5 percent nitroguanidine was used as a standard. Because of the significant effect of ammonium perchlorate particle size on overall bulk density, this latter factor must be taken into consideration in the interpretation of the results of these experiments.

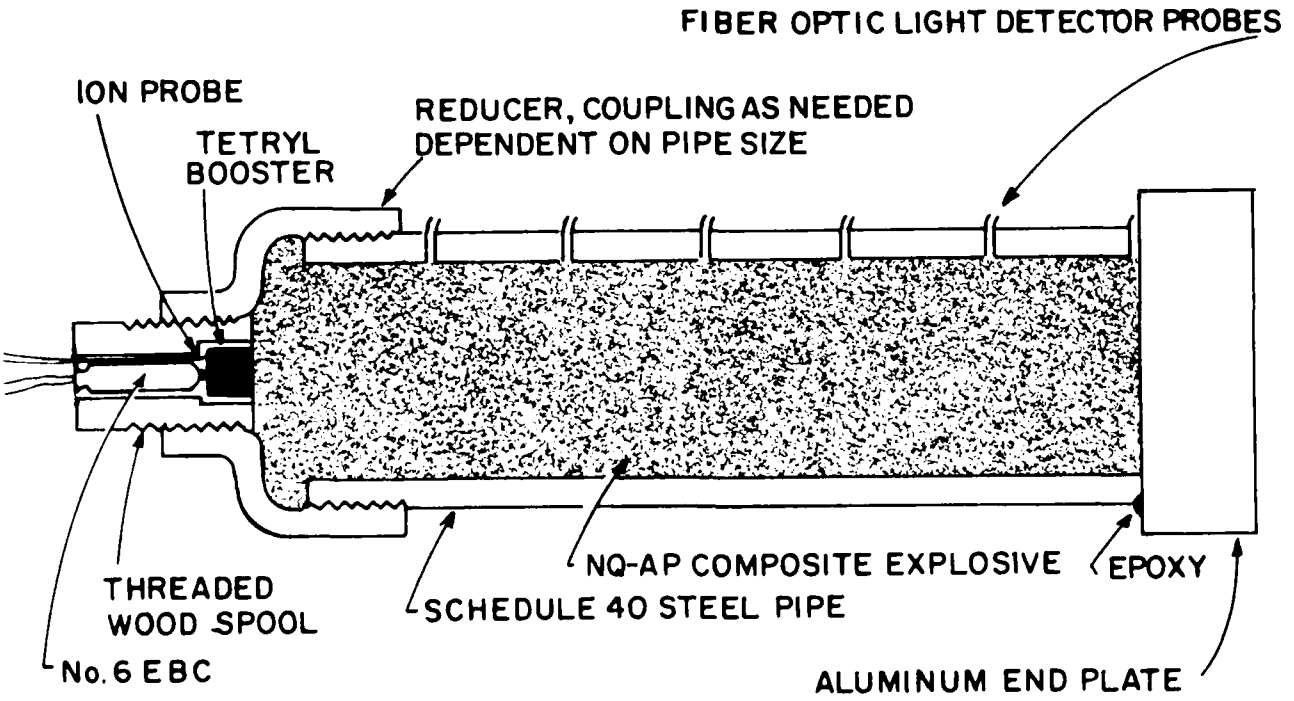

Fig. 2. Experimental test device utilized to monitor detonation velocities of explosive compositions.

As Figure 2 illustrates, the nitroguanidine-sensitized ammonium perchlorate samples were simply loaded into the pipe device. A No. 6 EBC was used in conjunction with a tetryl booster pellet to initiate detonation. The detonation velocity was monitored by light output from the detonation front as it passed the fiber optic stations of the pipe. Figure 3 shows a typical oscillograph output. Use of multiple stations substantiated whether a stable propagation velocity was or was not achieved.

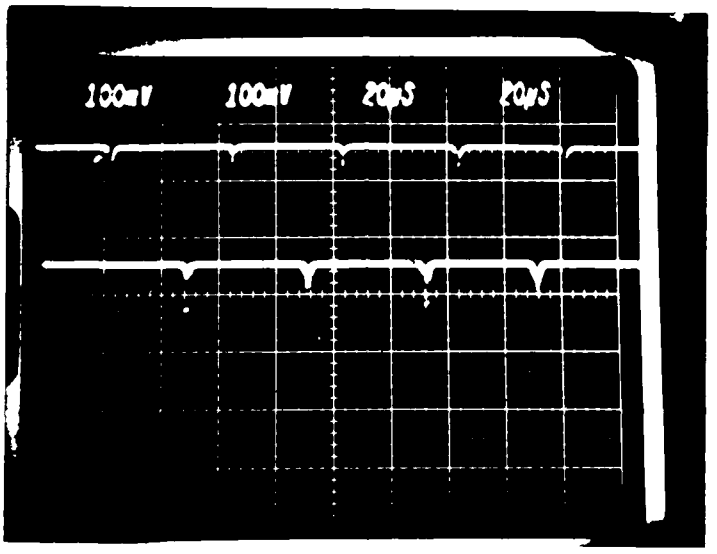

Fig. 3. Typical detonation velocity fiber optic light detector oscillograph record. Probe separation 76.2 mm - detonation velocity 1900 m/sec.

The three particle size ranges of ammonium perchlorate--designated as coarse (149 to 500 micron), medium (44 to 149 micron), and fine (0 to 44 micron)--were obtained by screen-sieve separation. Figures 4 through 6 illustrate photomicrographs of these particle size ranges. Nitroguanidine, the needle-type crystals in the figures, remained unchanged in all three systems. Note that the number of nitroguanidine crystals, which were generally 100 to 200 microns long, far exceeded the number of ammonium perchlorate crystals--even in the fine ammonium perchlorate case--although the nitroguanidine constituted only 5 percent of total mass.

Fig. 4. Photomicrograph of coarse ammonium perchlorate mixed with 5 percent nitroguanidine.

Fig. 5. Photomicrograph of medium ammonium perchlorate mixed with 5 percent nitroguanidine.

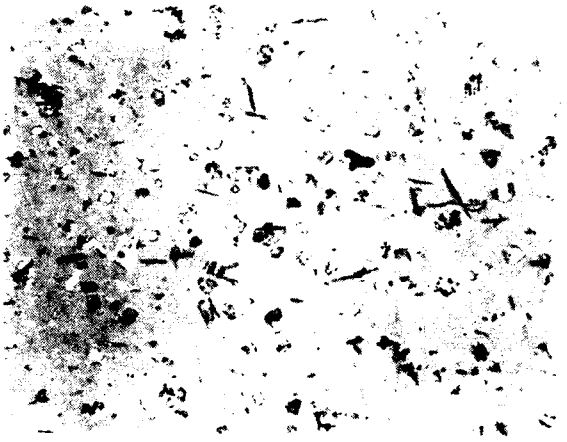

Fig. 6. Photomicrograph of fine ammonium perchlorate mixed with 5 percent nitroguanidine.

RESULTS

The results of these experiments are summarized in Table 1. As expected, the detonation velocity increases significantly with decreased ammonium perchlorate particle size between the medium and fine systems. The overall bulk density variation here should cause a decrease in detonation velocity with an overall decrease in bulk density. The effect of particle size evidently far exceeds the opposing effect of the overall bulk density. On the other hand, the case is not quite so clear between the coarse and medium systems. In this case there is a very moderate decrease in overall bulk density with decreasing ammonium perchlorate particle size. This could account for a decreased detonation velocity, evidently a stronger effect here than ammonium perchlorate particle size.

While Figures 4 through 6 certainly attest to the significant variation in the particle size of ammonium perchlorate, the particle size of these systems was nonetheless analyzed. Table 2 gives the results of this analysis. Note that the coarse system has a greater proportion of very fine particles than both the medium and fine systems. Table 3 illustrates this further by comparing the mass fraction and particle fraction ranges of the three particle size systems. The coarse system, with 94.2 percent by mass of the larger particles, has a larger percentage of fine particles than either the medium system, which has 98.2 percent by mass of medium range particles, or the fine system, which has 96.5 percent by mass of fine range

particles. The question arises: which is of greater importance: the amount or the mass of particle sizes in a specific mechanism? A recent study of the effect of particle size on the shock initiation of molecular powdered explosives (Ref. 7) concluded that larger particle sizes are more sensitive than smaller particle sizes. Once initiated, however, the smaller particles attain stable propagation more readily.

TABLE 1

Ammonium perchlorate sensitized with five percent nitroguanidine

Particle Size Range μm	Diameter mm	Density g/cc	Detonation Velocity* m/sec
149 to 500	12	1.24	2160
44 to 149	12	1.21	2030
0 to 44	12	1.06	2820
149 to 500	6	1.20	1900
44 to 149	6	1.04	1550
0 to 44	6	0.88	2350

*Detonation velocity of nitroguanidine at above density: 1660 m/sec
Detonation velocity of ammonium perchlorate at above density: 4000 m/sec

TABLE 2

Ammonium perchlorate particle size analysis

Type	Percent of μm size						
	<8.1	8.1-16	16-41	41-81	81-168	168-315	315-525
Coarse	31.4	33.9	27.0	3.9	1.1	2.3	0.37
Medium	5.9	2.7	15.3	19.8	43.2	13.1	0
Fine	22.3	28.4	32.0	16.6	0.54	0.01	0

TABLE 3

Ammonium perchlorate particle versus mass distribution

Type	Sieve Size	Mass		Particles	
		%	Range	%	Range
Coarse	149-500	94.2	168-525	92.3	0- 41
Medium	44-149	98.2	81-315	63.0	41-168
Fine	0- 44	96.5	16-168	82.7	0- 41

SUMMARY

The objective of this work was to investigate the effect of ammonium perchlorate particle size upon the detonation characteristics of an ammonium perchlorate system sensitized with a small amount--5 percent--nitroguanidine. It can be safety concluded that reducing the ammonium perchlorate particle size, which is already known to increase the propensity of ammonium perchlorate to detonate, increases the overall detonation velocity of the ammonium perchlorate-nitroguanidine system. The effects of varying the overall bulk density, which is also known to increase detonation velocity as density increases, can be accounted for to some extent. There is no satisfactory explanation for a possible reversal in anticipated results between the coarse and medium systems. It may be attributed to the particle size distribution, which produces a greater number of fine particles on a relative basis in the coarse system than in either the medium or fine system. However, this matter can only be resolved by a more definitive study requiring both better particle size separation and perhaps an analysis of the effect of bimodal particle sizes on detonation velocity and ignition.

REFERENCES

1. M.D. Hurwitz, OSRD 5611, (1945).
2. W.H. Anderson and R.E. Pesante, Eight Int. Symp. Combust., Williams and Wilkins, (1962), pp 705-710.
3. A.J. Tulis, Sixth Int. Detonation Symp., (1976), pp 173-182.
4. A.J. Tulis, Tenth EED Symp., Proceedings in press, (1979).
5. A.J. Tulis, unpublished work.
6. A.J. Tulis, J. Hazardous Mat., 2 (1977/1978), pp 171-181.
7. C.L. Scott, Fifth Detonation Symp., ACR-184, (1970), pp 259-266.

CHEMICAL COMPATIBILITY AND SAFE STORAGE CONSIDERATIONS FOR PROCESS SYSTEMS HAZARDS ANALYSIS

C. JAMES DAHN

Safety Consulting Engineers, Inc.

(Presented 16 May 1979)

ABSTRACT

An approach to evaluating the Chemical Compatibility and Safe Storage aspects of Process Systems Hazards Analysis has been delineated.

Differential Scanning Calorimetry/Thermal Gravimetric Analysis techniques have been utilized to evaluate potential Chemical Compatibility in storage hazards with chemicals in contact with explosives and propellants. Utilization of the Frank-Kamenetski developed equations was made to determine the safe storage criteria for chemicals and chemicals in contact with contaminants. Special attention was given to Nitrocellulose materials.

INTRODUCTION

Chemical Compatibility Hazards arise in two major areas of propellants/explosives/pyrotechnic manufacturing and use. The first is in the inprocess operations of manufacture. Here the particular chemicals can come in contact with contaminants, adhesives, greases, and other foreign chemicals. The second critical area is that of storage of materials once they have been manufactured and/or placed in the item configurations.

Chemical Compatibility problems of in-process operations usually are minimized by thorough quality control and inspection methods. An upset in the Process System may create some severe Chemical Compatibility Hazards if people are not aware of the effects of various chemicals on the propellants/explosives/pyrotechnics and their intermediary configurations during the processes. Normally, these potential hazards are uncovered by Systems Hazards Analysis such as Failure Modes and Effects Analysis and Fault Tree Analysis. Through these type of Analyses, identification of critical contacts of in-process chemicals can be made. We know basically that liquids in a chemical process are of much more concern than solids because they can be contaminated very easily by gases, liquids and other solids. The chemical reactions of these contacts can range from complete inaction to very violent reactions. In some cases, an explosive mixture can be formed when the combinations of chemicals under right conditions occur.

In storage, another set of problems arise. Here we have the remote possibility of migration of chemicals (by no means as likely as in the in-process configuration). In storage, we must be concerned about the long-term effects on the explosives,propellants

and pyrotechnics. Decomposition of the materials can occur and self-heating will result. Biological degradation of the materials can also occur. Normally, sufficient information is known about the propellants, explosives and pyrotechnics to evaluate their storage capabilities. Occasionally in storage, a synergistic effect can occur when other chemicals come in contact with the basic materials. These contaminants can make contact with the materials during the in-process handling, transportation and shipment and in storage with other chemicals. Depending on the storage configurations, heating of the buildings and facilities can occur during the hot months of the summer. High relative humidities can also promote biological degradation, rusting and other actions which could contribute as catalysts to a decomposition process.

In both cases (storage and in-process), we must be concerned about the effects of chemicals and contaminants on the base materials. The incompatibilities can arise and affect the following properties of the material:

- Initiation Sensitivity
- Flame or Explosion Propagation Characteristics
- Formation of Toxic, Flammable or Carcinogenic Gases or Liquids
- Self-heating Accelerations

In some cases, the incompatibility can generate excessive corrosion and mechanical effects to create a potential handling hazard of an end item. For instance, the base of a projectile corrodes out and exposes a booster charge to the elements.

In the past, chemical compatibility with an explosive, pyrotechnic or propellant was found by using a Differential Scanning Calorimeter to monitor changes in ignition onset temperatures or lower temperature exotherm reactions.

In this Paper, we review an approach which delves much deeper into the compatibility type problem.

APPROACH

Once a number of chemicals have been identified which could potentially come in contact with a propellant, explosive or pyrotechnic, the analyst must decide which of these can be most hazardous. In our past experience, we have found that the Differential Scanning Calorimeter is a good tool for screening through the various chemicals which could come in contact with the basic materials. Here, we mix a mixture of the explosive, propellant or pyrotechnic with a contaminating chemical. After sufficient storage time, Differential Scanning Calorimetry scans are made at scanning rates normally 10 or 20 degrees centigrade per minute. If a reduction in exothermic onset temperature by greater than 10 degrees is noted, a Thermal Gravimetric Analysis plot is made on the same materials. A typical Differential Scanning Calorimeter

Exothermic Curve for Nitrocellulose is shown in Figure 1. Several tests are usually run on a chemical which could come in contact with the in-process material, so that all potential methods of contact can be explored. For instance, adding water plus the chemical plus a propellant may be done to determine the effects of water on the process.

Once an incompatibility has been identified on the Differential Scanning Calorimeter and the Thermal Gravimetric Analyser, further testing and evaluation is necessary.

The next step is that of determining the Arrhenius Kinetic Constants of the in-process material/contaminating chemical. Activation energies of first exothermic reactions plus frequency values are determined by using Differential Thermal methods. Normally, from a compatibility standpoint, we are most concerned about the early stages of decomposition and how this accelerates to yield a self-heating and a runaway reaction. At the present time, the ASTM E-27.02 Committee has drafted a test method for determining the Arrhenius Kinetic Constants. Hopefully, this Standard will be forthcoming so that everyone in the industry can utilize a common method.

Once the Arrhenius Kinetic Constants have been defined for the chemical contaminants and in-process material combination, further review must be made to be certain that the chemical reaction mechanisms observed in the Differential Scanning Calorimeter are truly indicative of those that would be expected in process. For instance, the chemical reaction may occur without presence of air. If there is a possibility that air may be present, the Differential Scanning Calorimetry tests should also utilize air and other gas combinations expected. Decisions need to be made to determine whether the materials shall be run on the Differential Scanning Calorimeter in the sealed containers or open containers.

By utilizing the Frank-Kamenetski developed equations for determining critical temperature for runaway reactions as follows:

$$T_m = \frac{E}{2.303\ R\ \log\ (\rho\ a^2 QZE / \lambda R T_m^2 \delta)} \qquad (1)$$

where:

- E - Activation Energy (Kcal/mol)
- R - Univ. Gas Constant
- ρ - Material Density (gm/cc)
- a - Slab Half Thickness, Cylinder or Sphere Radius (cm)
- Q - Heat of Reaction (cal/gm)
- Z - Arrhenius Freq. Factor (Sec^{-1})
- λ - Heat Transfer Coeff. (cal/cm-sec^{o}K)
- Tm - Critical Self-Heating Temp. (^{o}K)

δ - F-K Shape Factor
For Slab δ = 0.88
For Cylinder δ = 2.00
For Sphere δ = 3.32

We can determine the critical temperature for runaway reaction based on a configuration of the in-process or stored materials.

Recently we have evaluated Nitrocellulose configurations to determine their compatibility in in-process material handling. We have found numerous data on the reaction kinetics of Nitrocellulose. A summary of the kinetics and thermodynamics properties of Nitrocellulose, Nitroglycerine and other explosive materials are found in Table I. Since there was a wide disparity in the values of activation energy and frequency factor, we have run tests to determine the values for two Nitrocellulose type materials. A 12% Nitrogen/Nitrocellulose and a 13.35% Nitrogen/Nitrocellulose material was tested to determine the Arrhenius Kinetic Constants so that we could determine the safe storage temperatures of these in-process materials.

Critical temperature for runaway reactions for slabs of Nitrocellulose were calculated based on Equation (1) and are shown in Figure 2. In this Figure, we also list the Arrhenius rate parameters calculated at our facility. We also plotted on the same Figure, the critical temperature for runaway for Nitrocellulose using Urbanski's Rate Kinetics Constants.

Calculations of the explosion times for runaway reactions based on various surface temperatures should be calculated next. We have done this for the Nitrocellulose materials which is illustrated in Figure 3. Published data for TNT was used to determine critical temperature and time to explosion as reference. The explosion temperature was calculated by using the following equation:

$$t_{exp} = \frac{\rho C_p a^2}{\lambda} F\,(E/T_m - E/T_i)$$

where:

C_p - Specific Heat (cal/gm°K)

a - Slab Half Thickness (cm)

T_m - Critical Temp (°K)

T_i - Surface Temp (°K)

F - Function of Geometry
Ref: "Thermal Initiation of Explosives"
J. Zinn, C. Mader
J. App. Physics
Vol. 31 No. 2
Feb. 1960

After time to explosion calculations are made based on surface temperature slab, subscale tests are usually run to verify that the chemical kinetics data and time to explosion temperature data is valid. We normally run a Henkin Test (Reference: H. Henkin and R. McGill, Ind. Eng. Chem., 44, 1391 (1952). Here a known quantity of chemical is placed in a copper containment vessel and sealed against pressure. The sample is then placed in a Woods Metal Bath at a given temperature and the time is monitored until explosion occurs. As we see in Figure 3, we ran three Henkin Test Data Points to determine the time to explosion. We found that the time to explosion values came very close to the values calculated by using a slab half thickness of 0.12 centimeters (which was utilized in the Henkin Test). Actually, the Urbanski supplied information on chemical kinetics does not yield good time to explosion or critical temperature for runaway data for Nitrocellulose. After completion of the Henkin Tests, decisions are then made to determine the adequacy of analytical and test data in relation to the applications of the explosive chemical contaminent type systems.

CONCLUSIONS AND RECOMMENDATIONS

We have presented an approach to evaluate the chemical compatibility of in-process and stored materials. Calculations of safe storage temperature and sizes can be readily made on a routine basis. Verifications of the results normally should be made on subscale size quantities to be sure that scaling does apply. We did find in our testing of the Nitrocellulose materials that the Urbanski data on 13.35% Nitrocellulose did not yield accurate time to explosion and critical temperatures.

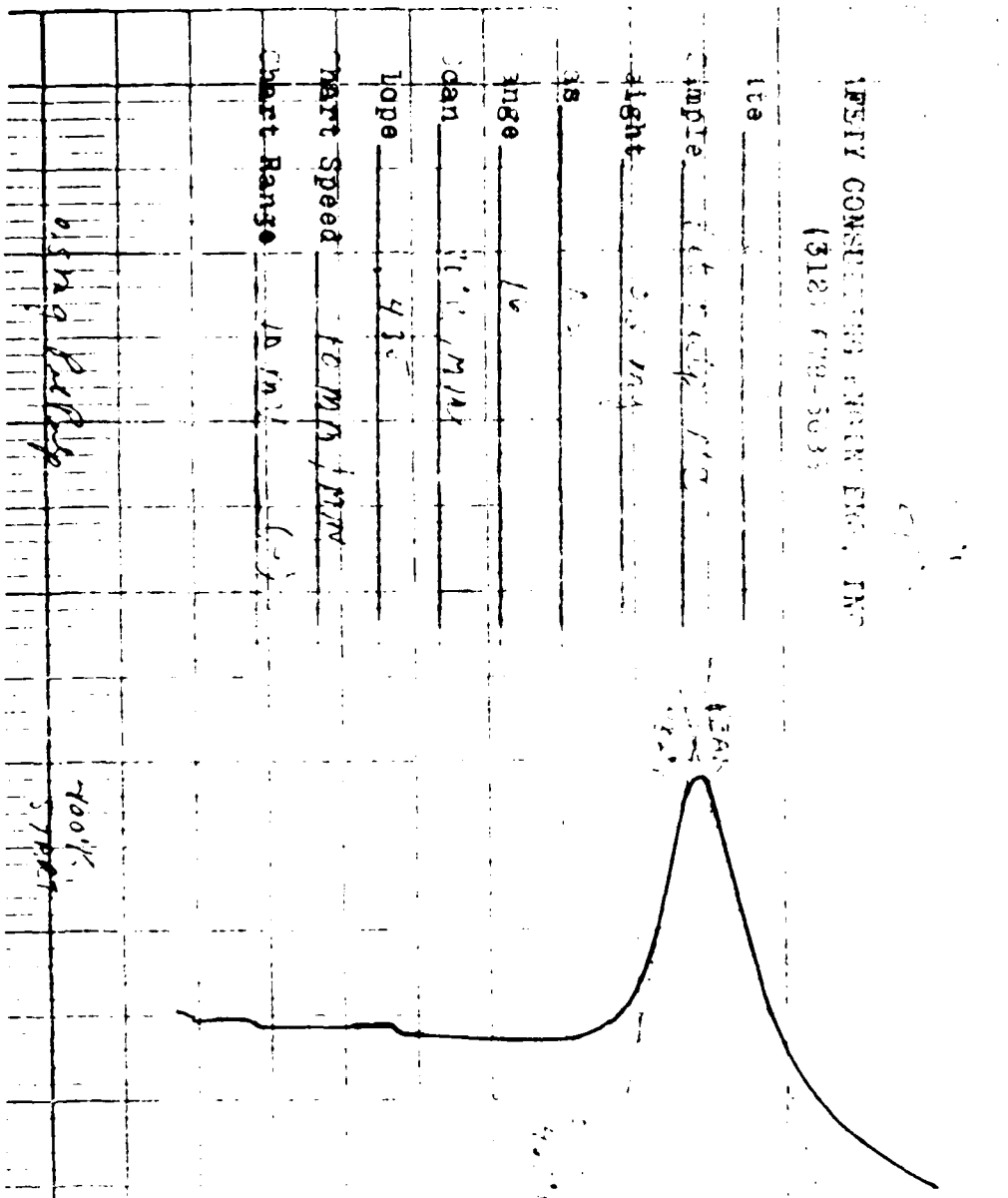

FIGURE 1 - TYPICAL DSC EXOTHERM CURVE FOR NITROCELLULOSE

TABLE I - KINETICS AND THERMODYNAMIC PROPERTIES OF PROPELLANTS AND EXPLOSIVES

MATERIAL	Activation Energy E (Kcal/mil)	Frequency Factor (1/sec)	Density (gm/cc)	Specific Heat (cal/gm°C)	Thermal Conductivity (cal/sec-cm°C)	Cns Ign Tem (°C
Nitroglycerin	$^{+}48$	$^{+}10^{20.8}$				
(20-125°C)	$^{U}42.6$		1.596	$^{+}0.30$	$^{+}0.000503$	210
(140-150°C)	$^{U}45$	$^{U}10^{20}$				
	$^{*}35$	$^{*}10^{14}$				
(90-125)	$^{s}42.6$	$^{s}10^{18}$				
(125-150)	$^{s}45.0$	$^{s}10^{19.2}$				
(150-190)	$^{s}50.0$	$^{s}10^{23.5}$				
Nitrocellulose				$^{E}0.34$	$^{E}.00051$	200
(13.1%N)	46.2	$10^{24.68}$				
(126-156°C)	$^{U}43$	$^{U}10^{18}$				
(90-135)	$^{s}49$	$^{s}10^{21}$				
(145-155)	$^{s}48$	$^{s}10^{20}$				
(155-175)	$^{s}56$	$^{s}10^{24}$				
(205-270)	$^{E}41.2$	$^{E}1.34x10^{16}$				
(130-155)	$^{E}46.7$	$^{E}10^{19}$				
PETN	$^{+}38.6$	$^{+}10^{15.3}$	$^{+}1.46$	$^{+}0.272$	$^{+}0.0006$	225
(100-120°C)	$^{s}50.9$	$^{s}10^{20.6}$	--	—		
RDX	$^{+}57.2$	$^{+}10^{21.2}$	$^{E}+1.66$	$^{E}+0.264$	$^{E}+0.00049$	260
(170-200)	$^{E}57.2$	$^{E}2.1x10^{24}$				
HMX	$^{+}57.2$	$^{+}5x10^{19}$	$^{+}1.66$	$^{+}0.315$	$^{+}.00049$	327
TNT						
(200-260)	$^{E}37.0$	$^{E}5x10^{13}$	$^{E}1.57$	$^{E}0.264$	$^{E}0.00046$	427
(257-310)	$^{*}34.4$ (L)	$^{E}10^{11.4}$(L)				
NM	*49.2	$^{*}10^{13.7}$	*1.14	0.412	.00051	370

SUPERSCRIPT SYMBOLS

* Russian Data - JPRS, 47,007- 4 Dec. 1968

\+ Picatinny Tech. RPT 3157, June 1964

s Solid Propellant Rockets, Princeton Univ. Press

U Urbanski, Chem. & Tech. of Expl.

E Erosive Burning - Solid Propellants

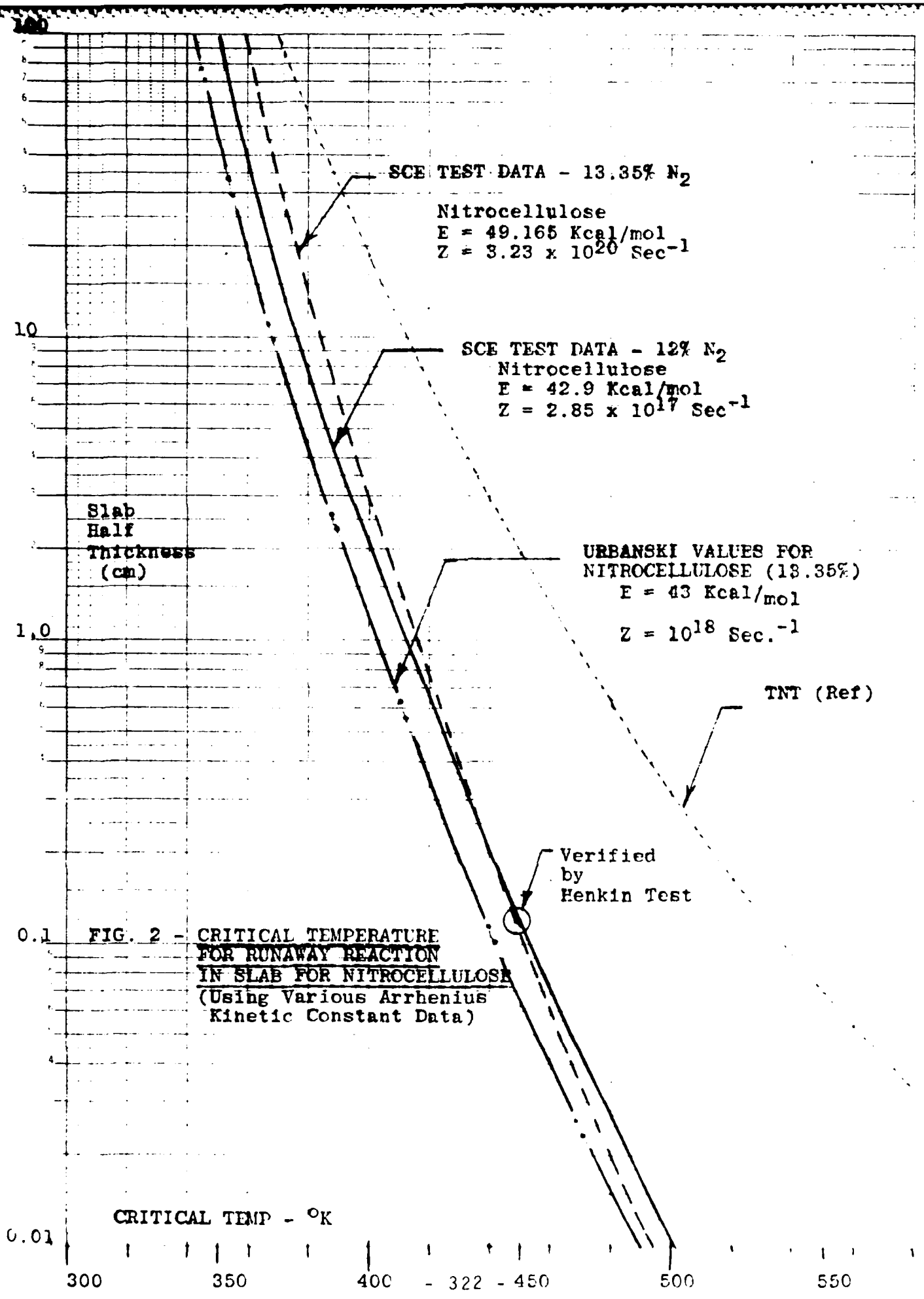

FIG. 2 - CRITICAL TEMPERATURE FOR RUNAWAY REACTION IN SLAB FOR NITROCELLULOSE (Using Various Arrhenius Kinetic Constant Data)

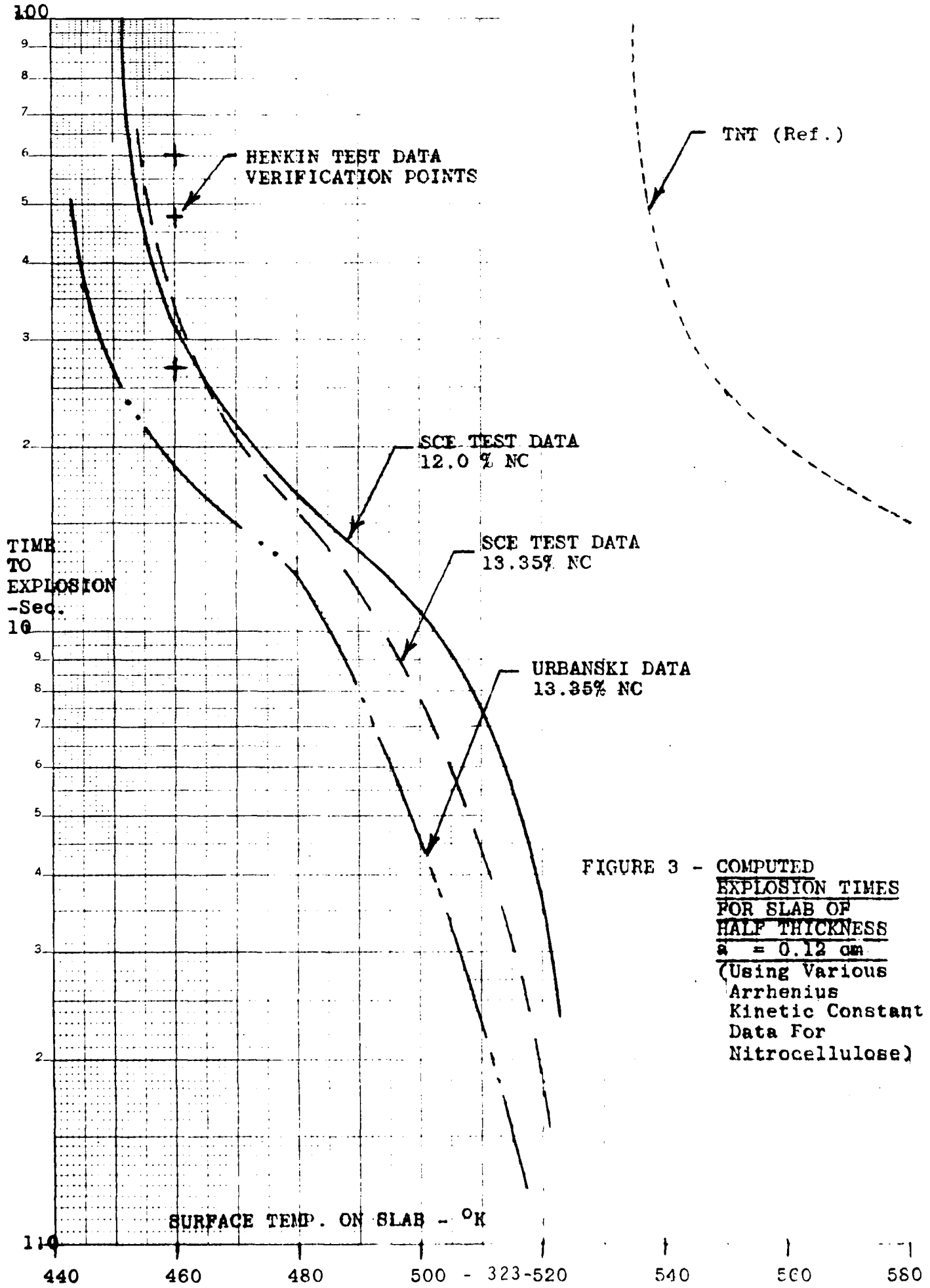

FIGURE 3 - COMPUTED EXPLOSION TIMES FOR SLAB OF HALF THICKNESS a = 0.12 cm (Using Various Arrhenius Kinetic Constant Data For Nitrocellulose)

COMPATIBILITY/PROCESSING SYMPOSIUM

15 - 17 May 1979

Sandia Laboratories

SPEAKERS ROSTER

Clyde D. Alley
Mason & Hanger-Silas Mason Co.
PO Box 30020
Amarillo, TX 79177

W. S. Anderson
United Technologies Corp.
PO Box 358
Sunnyvale, CA 94806

Theodore M. Benziger
Los Alamos Scientific Lab
WX 2 M/S 920
PO Box 1663
Los Alamos, NM 87545

Ernest P. Bergman
Southwest Research Institute
PO Drawer 28510
San Antonio, TX 78284

Dr. W. T. Bolleter
Hercules Inc.
Radford Army Ammunition Plant
Radford, VA 24141

Michael D. Coburn (Dr.)
AFATL/DLDE
Eglin AFB, FL 32542

Daniel Ellison
Naval Weapons Support Center
Code 3031
Bldg 2044
Crane, IN 47522

W. Fleming
Unidynamics, Inc.
PO Box 2990
Phoenix, AZ 85062

Arthur Fontijn (Dr.)
Aero Chem Research Labs
PO Box 12
Princeton, NJ 08540

John Fronabarger
Unidynamics, Inc.
PO Box 2990
Phoenix, AX 85062

Joel M. Goldman
ARRADCOM
Attn: DRDAR-SCM-M
Bldg 322
Dover, NJ 07801

Hyman A. Golpol
Lawrence Livermore Labs
East Avenue
LIvermore, CA 94550

J.R. Humphrey
Lawrence Livermore Labs
L-324
PO Box 808
Livermore, CA 94550

C. E. Johnson
Naval Ordnance Station
Code 2051C
Indian Head, MD 20640

D. L. Loverro
AFATL/DLDE
Eglin AFB, FL 32542

Lyle O. Malotky
Naval E.O.D. Facility
Code 5031
Indian Head, MD 20640

D. C. Mann
AFATL/DLDL
Eglin AFB, FL 32542

Thomas M. Massis
Sandia Laboratories
PO Box 5800
Albuquerque, NM 87115

V. D. McGinnis
Battelle Columbus Labs
Room 7137
505 King Avenue
Columbus, OH 43201

Lester C. Myers
Mason & Hanger-Silas Mason Co.
Pantex Plant
PO Box 30020
Amarillo, TX 79177

Natalia Petrianyk
ARRADCOM, LCWSL
Applied Sciences Division
DRDAR-LCA-OA
Dover, NJ 07801

T. V. Sachar
ARRADCOM
PM-PBMNE
Dover, NJ 07801

Albert S. Tompa (Dr.)
Naval Surface Weapons Center
Code R21
White Oak
Silver Spring, MD 20910

Allen J. Tulis
IIT Research Institute
10 W. 35th Street
Chicago, IL 60616

Dr. Herman N. Volltrauer
Aero Chem Research Lab
PO Box 12
Princeton, NJ 08540

James R. Wagener
US Naval Ordnance Station
Code 5253
Indian Head, MD 20640

J. P. Zeigler
ARRADCOM
PM-PBMNE
Dover, NJ 07801

Dr. Bernard Zeller
Societe Nationals des Poudres
et Explosifs
Centre de Recherches du
Bouchet
91710 Vert Le Petit
France

COMPATIBILITY/PROCESSING SYMPOSIUM

15 - 17 May 1979

Sandia Laboratories

ATTENDEES ROSTER

Albert F. Abbott
Boeing

Arnold A. Adams
FMC Corporation

E. W. Anderson
Naval Surface Weapons Center

Rupert D. Barefoot
Naval Sea Systems Cmd

Dr. Lester D. Bartron
E.I. du Pont de Nemours Co.

R. P. Bauman

Dr. Richard Bender
Diehl Cmbh & Co.

Jim N. Bohn
Hercules Inc.

Ernest D. Brown
Thiokol Corporation

Michael A. Bucher
Weapons Quality Eng Center

Robert J. Buxton
Sandia Laboratories

John C. B. Carlson
Naval Weapons Station

Henri R. Carpenter
US Naval Ordnance Station

Daniel C. Cicero
USA Industrial Base Eng Act

Vester D. Coffman
Naval Weapons Support Center

Carl J. Dahn
Safety Consulting Engineers

Sten-Olof Eldh
AB Bofors

Thomas G. Floyd
US Air Force

William D. Fortune
ARRCOM

Alfonzo Gillis
Naval Surface Weapons Center

Harold Gultz
US Army

Carlton L. Horine
United Technologies

David H. Huskisson
Sandia Laboratories

Michael P. Ierardi
Naval Surface Weapons Center

Normand Jerome
Canadian Arsenals Ltd

Theodore B. Johnson

R. G. Jungst
Sandia Laboratories

Harold Karp
Hi Shear Corporation

Daniel Katz
ARRADCOM

Eleonore G. Kayser
Naval Surface Weapons Center

John Kelley
Naval Ordnance Station

Robert L. Kessler
Naval Ordnance Station

Edwin Kjeldgaard
Sandia Laboratories

Robert Lantz
US Army

Dr. Sheng Y. Lee
Harry Diamond Labs

Herman R. Leider
Lawrence Livermore Labs

M. L. Lieberman
Sandia Labs

Louis Lo Fiego
Whittaker Corporation

D. M. MacLean
Valleyfield Chem Products

Peter Martin
US Army Industrial Base Eng Act

R. J. Martinelli
K & M Associates

Tore Matre
A/S Raufoss Ammunisjonsfabr

Roman M. Montoya
Naval Ordnance Station

Ralph M. Moorehead
Lawrence Livermore Labs

N. Neil Ogimachi
Teledyne McCormick Selph

W. G. Perkins
Sandia Labs

Rudolph A. Peterson
Aerojet Solid Propulsion Co.

Dr. Jean-Paul Picard
US Army

Leland B. Piper
Johns Hopkins University

Dr. R. H. Pritchard
BDM Corporation

Charles F. Reade
Reade Manfacturing Co.

Clifford G. Redden
ARRADCOM

John W. Reed
Monsanto Research Corp.

Rolf H. Renner
Naval Surface Weapons Center

Robert Robbins
Holston Defense Corp.

R. G. Sailer
Hercules Inc.

Dr. Wilhelm Schmacker
Bundesamt fur Wehretechnik

Ronald L. Simmons
Hercules, Inc.

John P. Small
Embassy of Australia

Philip J. Smith
Naval Weapons Support Center

Dr. John Stals
Embassy of Australia

D. Sutton
PERME

Frank D. Swanson
Honeywell Inc.

Robert J. Thiede
Olin Corporation

Anthony P. Trippe
IRT Corporation

Manuel G. Vigil
Sandia Labs

Roger Warner
Columbia Sci Ind Corp

John D. Warrick
ICI Americas Inc.

Robert C. Wilson
Naval Ordnance Station

Dr. Rene Yee
Naval Weapons Center

Dr. Tucker Yee
Naval Weapons Center

William C. Zeek
US Army

END

DTIC

7-86